A KINETIC THEORY APPROACH TO SHOCK STRUCTURE IN MONATOMIC GASES WITH IONIZATION

BY
MADDUR KRISHNA MURTHY

DEPARTMENT OF AERONAUTICAL ENGINEERING
INDIAN INSTITUTE OF TECHNOLOGY KANPUR
1971

A KINETIC THEORY APPROACH TO SHOCK STRUCTURE IN MONATOMIC GASES WITH IONIZATION

A Thesis Submitted
In Partial Fulfilment of the Requirements
for the Degree of
DOCTOR OF PHILOSOPHY

BY
MADDUR KRISHNA MURTHY

to the

DEPARTMENT OF AERONAUTICAL ENGINEERING
INDIAN INSTITUTE OF TECHNOLOGY KANPUR
1971

To

Lord Srinivasa

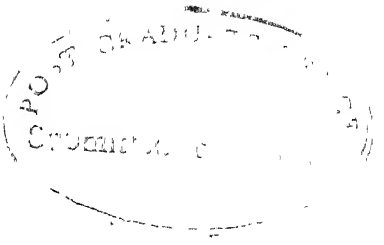

CERTIFICATE

This is to certify that the work A KINETIC THEORY APPROACH TO SHOCK STRUCTURE IN MONATOMIC GASES WITH IONIZATION has been carried out under my supervision and has not been submitted elsewhere for a degree.

S.M. Ramachandra

(S.M. Ramachandra)
Professor,
Dept. of Aeronautical Engg.
Indian Institute of Technology
Kanpur-16, India

ACKNOWLEDGEMENTS

The author takes this opportunity to express his deep sense of gratitude to Prof. S.M. Ramachandra for having suggested the problem and extended constant guidance and encouragement throughout the course of this work. The author is highly thankful to him for his concern about the author's welfare at all times.

The author wishes to place on record his appreciations and gratefulness to his colleage Mr. T. Gokuldas Pai for his invaluable and patient participation in discussions.

It is with great pleasure that the author wishes to express his sincere thanks to Prof. M.M. Oberai and Prof. R.P. Andres (from Princeton University, U.S.A., during his stay at IIT Kanpur) for their invaluable help and suggestions.

The author expresses his heartfelt and affectionate gratitudes to his sisters and brother who have been a source of inspiration all the time and also to the departed soul of his father who sacrificed everything for the welfare of the author.

The help rendered by Dr. N.G.R. Iyengar, Messers M.R. Srinath, M.S. Nagarajmurthy, B.S. Sankara, V. Raghavendra, S.V. Sachidananda and many other friends at various stages is gratefully acknowledged. The cooperation of Mr. P.K. Malhotra in preparing excellent drawings and those of Messers J.K. Misra and S.R. Gupta in typing the thesis in a nice fashion is very much appreciated.

ABSTRACT

The structure of a normal shock wave in monatomic gases at high Mach numbers when ionization becomes important is the subject of the present study. For $M \sim 30$ since the width of the relaxation zone is comparable to the gas dynamic shock width a simultaneous study of the two regions is required. Through a kinetic theory approach using the Boltzmann equation a set of equations representing the entire non-equilibrium region have been derived which are solved numerically. Radiation and multiple ionization effects have been ignored.

A trimodal distribution function has been used to represent the atom gas and Maxwellian distribution functions for ion and elect. gases. Elastic collisions between the different species have been considered through inverse-power law force models. Experimentally determined inelastic collision cross sections have been used for atom-atom and atom-electron inelastic collisions. The corresponding recombination rates have been obtained from the Saha equation. Furthermore, an additional c_x^2-moment of the Boltzmann equation has been derived.

Using the appropriate boundary conditions the resulting equations together with the Saha equation give the jump conditions across the shock wave and have been evaluated numerically. A numerical solution of the shock structure equations on the IBM 7044 computer has been obtained for the shock wave profiles for argon, krypton and xenon gases for a range of Mach numbers from 15 to 40

and for a range of initial temperatures and pressures. In addition electrical conductivity and refractive index in the shock-wave have been calculated. The shock thickness and the thickness parameter as defined by Petschek and Byron have been computed and a good agreement of the thickness parameter is found with the experimental results of Wong and Bershader.

CONTENTS

LIST OF TABLES

LIST OF FIGURES

CHAPTER 1

INTRODUCTION

1.1 General:

The structure of a shock wave is of interest for various reasons. In the beginning it attracted the attention of many scientists as a theoretical problem, the solution of which aided the understanding of the physical mechanism of shock compression, a remarkable phenomenon in gas dynamics. At very high altitudes where the density of air is very low, the mean free path may become comparable in size to the body dimensions. As the shock thickness is only of the order of a few mean free paths the variation of the macroscopic quantities like pressure, temperature, velocity etc. in this region are of great interest. When it was realised that the hydrodynamic equations of motion lose their significance in representing the phenomenon inside strong shock waves which are of the order of a few mean free paths, attention was diverted towards the kinetic theory approach to the fluid dynamical problems. The one-dimensional shock structure problem due to its simplicity and freedom from boundary effects attracted the attention of scientists working in kinetic theory of gases as a very good example for checking the validity of the approximate solutions proposed for the Boltzmann equation. Later shock waves were produced in laboratories to realise high temperatures and study the various high temperature phenomena occurring in gases like excitation of various degrees of freedom, dissociation,

chemical reactions, ionization etc. A comparison of experimental results with theory facilitated deducing much valuable information about the reaction rates of these processes. The study of shock waves of very high strength in which radiation plays an important role helps in clarifying the various interesting aspects like shock front luminosity and other optical effects observed in strong explosions in air. Shock waves of very high Mach numbers are also of interest in electro-magnetic shock tube work. With its far-from-equilibrium properties, its simple geometry and boundary conditions, the shock wave structure problem is a unique choice for testing non-equilibrium theories.

1.2 Shock Waves in a Nonreacting Gas:

The equations of conservation of mass, momentum and energy for a one-dimensional flow of an ideal gas admit a non-trivial solution which represents a possible finite jump in the flow quantities like velocity, temperature, pressure, in the absence of a characteristic length scale for the problem. Associated with this jump in pressure, velocity and temperature is an increase in entropy which indicates a dissipation of mechanical energy and an irreversible conversion of mechanical energy into heat. In order to understand this transition it is therefore necessary to include the dissipative mechanisms viz. viscosity and heat conduction attributable to the molecular structure of the fluid.

These processes give rise to additional transfer of momentum and energy resulting in nonadiabatic flow and irreversible transfer of mechanical energy into heat. With these dissipative mechanisms the discontinuities in the flow quantities appear as steep gradients. The shock wave, a plane of discontinuity for ideal fluids, becomes a wave of finite thickness. Due to the large gradients in the flow parameters existing in this region, the dissipative mechanisms are important only inside this region whereas outside the shock they are ineffective. Even though the flow parameters change strictly over the range $-\infty<x<+\infty$ a large change occurs only in a very small region of the order of a few mean free paths. Equilibrium can be assumed to exist outside this region of large gradients. Though the transport properties, viscosity and thermal diffusivity are similar in nature their relative roles in the shock wave are not alike. Viscosity plays the role of converting the directed molecular motion to random motion thus converting kinetic energy of mass motion to heat energy inside the shock wave. Conduction plays the role of redistributing the energy of random motion or heat in space and hence in heat transfer from region of higher temperature to lower temperature. The entropy change associated with viscosity is due to the generation of heat from mechanical energy and hence is positive everywhere. On the other hand the change in entropy associated with heat conduction is due to net inflow or outflow of heat at any point which can be positive or negative. Thus associated with heat

conduction a local decrease of entropy is possible. However, the overall entropy change across shock due to heat conduction is positive.

The solution of the one-dimensional hydrodynamic equations neglecting the viscosity but retaining heat conduction studied by Raleigh, revealed that a continuous solution for the flow quantities is possible for weak shocks whereas such a continuous solution may not be possible in general for strong shocks. Indeed, it is impossible to construct a continuous solution for the flow parameters for a sufficiently strong shock wave. On the other hand it is possible to construct continuous solutions of all flow parameters for all shock strengths by considering viscosity even if the heat conduction is neglected. This difficulty explains the importance of viscosity in achieving the irreversible compression of the fluid and that a strong discontinuity can disappear only through the action of viscosity but not of heat conduction. In this respect effect of conduction is secondary in the shock wave. Studies involving only thermal conduction are of interest since they illustrate the effect of other heat transfer mechanisms like radiation, electron heat conduction in plasma etc. Thus in studying the flow variables inside the shock it is necessary to include the effect of viscosity, primarily responsible for smoothening the discontinuity in flow quantities.

1.3 The Problem of Shock Structure:

The fact that the flow is almost in equilibrium both upstream and downstream of the shock and that gradients in the flow quantities are negligible in these regions implies that the flow parameters on the downstream side can be related to those of upstream side by simple hydrodynamic equations known as Rankine-Hugoniot equations for the shock front. These relations give the correct values of the downstream parameters as long as there is no change in the microscopic structure of the gas as happens at high temperatures. The problem of shock structure which does not involve a change of microscopic structure of the gas (excitation of internal degrees of freedom and a breakup of molecules) boils down to a study of the transition region in which the viscosity and thermal conductivity are active, bounded on either side by regions of equilibrium whose parameters are related by R-H relations. The fact that the flow parameters on the downstream side do not depend upon the manner in which they vary in the transition region demands that any theory proposed to explain the mechanism inside the transition region should give the downstream values as predicted by the R-H relations. When the internal degrees of freedom are excited these Rankine-Hugoniot relations have to be suitably modified to yield appropriate downstream equilibrium flow parameters.

1.4 Shock Wave Thickness:

A simple and suitable parameter is to be identified for comparing the various theories and experiments. An obvious choice of this parameter is the thickness of the transition region (if one such can be defined) due to its simplicity. The definition of such a thickness is invariably arbitrary if one wants a simple, relevant, representative parameter. Since the density, flow velocity, pressure and temperature do not vary in the same manner each can be used to define a thickness. These thicknesses need not be equal though they may be of the same order of magnitude. The arbitrariness also arises from the definition of 'a thickness' for any of these profiles, because these quantities vary continuously in $-\infty < x < +\infty$. However, as the major variations of the flow quantities are confined to a narrow region, a suitable definition of such a thickness can not be too far from reality; one such definition is, the region in which a flow variable changes by an 'accepted fraction'. But the thickness is very sensitive to the choice of this 'accepted fraction!

The most widely used definition, however avoids this ambiguity and replaces the actual profile by a linear profile with a slope equal to the maximum slope of the actual profile. The thickness is that region in which any chosen flow parameter varies linearly from the upstream value to the downstream equilibrium value. The major objection to this definition

is that it is too localized in description and fails to make sense when the profile has a point of inflexion with vertical slope. This definition is not suitable when the slopes of the actual profile at distances away from maximum slope point are very much different from maximum slope as when ionization occurs behind the shock. Nevertheless, for the description of conventional shock waves assuming that the flow parameters vary smoothly, the above definition is suitable since it can be evaluated very often without undue difficulty. Other definitions such as Grad's area rule are also often chosen. It would seem reasonable to choose that definition which agrees well with the experimental measurements; unfortunately the experimental values themselves involve a certain amount of uncertainty depending upon the type of the experimental technique.

For shock waves involving ionization, Petschek and Byron[62] and also Wong and Bershader[77] defined a thickness 'δ' as the distance behind the gasdynamic shock front to the point where the degree of ionization reaches 70% of its downstream equilibrium value. For purposes of comparison, they defined a parameter equal to the product of the upstream equilibrium pressure and the elapsed time in the laboratory reference frame between the passage of the shock front and the 70% ionization point.

1.5 Length Scale for the Shock Wave:

It is important to stress the necessity of a length unit in the problem of shock wave structure to nondimensionalise any macroscopic length scale of the problem. The absence of a body (which would have provided a characteristic length) in the problem poses considerable difficulty in identifying one such unit of length. The kinetic theory description of the gas flow suggests the 'mean free path' as a suitable parameter, suitable because the molecular collisions are responsible for the relaxation or equilibration. The mean free path has often been used as a length scale for the shock structure problem even when Navier-Stokes equations describe the motion. In the latter case mean free path is calculated based on the measured values of some macroscopic property of the gas described through the kinetics of molecular collisions. One such 'mean free path' used quite often is the viscosity mean free path. For a given viscosity a mean free path can be defined for any gas so that measurement of the viscosity is equivalent to the measurement of the viscosity mean free path for the gas. Thus in the continuum theory there is no difficulty in defining the mean free path, but the problem is where that mean free path should be measured.

The problem is a little more involved in the kinetic theory approach since the mean free path depends on the inter-molecular force law chosen. Further very often a criterion is to be chosen to define a 'collision' or a collision cross

section since in the strict sense the collision cross section is infinite in such cases. Quite often the viscosity cross section is chosen for this purpose. Further since it is not always possible to perform the calculations with the true force laws,methods have been devised to use the known viscosity-temperature dependence so that valid comparisons can be made with real gases. Even so 'where' the mean free path is to be evaluated still remains open.

In the case of the relaxation region where the effect of inelastic collisions is dominant and viscosity plays a negligible role, it is appropriate to use the mean free path corresponding to the inelastic collisions. In cases when there are more than one type of inelastic collision, as in the case of ionization due to atom-electron and atom-atom collitions, recombination collisions etc. it may be proper to choose a mean free path corresponding to the dominant collision.

As regards'where'the mean free path is to be measured, the upstream mean free path has been used very often as it is simple to calculate. The choice of the upstream mean free path makes the nondimensional shock thickness depend strongly on the choice of the inter-molecular potential at large Mach numbers. Narasimha et al[55] suggested a mean free path corresponding to the hot side as a proper choice which suppresses the sensitivity of the mean free path to the inter-molecular potential. The upstream mass velocity can also be advantageously used to

construct a length scale in place of the thermal speed. Such a length has been used by Oberai[58], even though the advantage of it has perhaps not been realised. This length scale has been used in the present investigation to nondimensionalise the equations for the entire region.

1.6 The Relaxation Phenomena in Gases:

In the case of very strong shock waves in a real gas, the high temperatures attained result in the excitation of various degrees of freedom. The state of such a gas depends on the concentration of the various components such as molecules, atoms, ions and electrons, and also on the distribution of the internal energy among the various degrees of freedom. Generally the internal energy of a gas consists of the energy of translational motion of the particles, rotational and vibrational energies, chemical energy of reactions, ionization energy, and electronic excitation energy of the molecules, atoms and ions. Associated with the excitation and reestablishment of thermodynamic equilibrium of any of these degrees of freedom there are corresponding characteristic times known as the relaxation times. Relaxation times for exciting the various degrees of freedom differ appreciably from each other so that under certain conditions it may be possible to achieve thermodynamic equilibrium for some but not all degrees of freedom. Since the kinetic energy and the momentum transferred during a collision between particles of comparable masses are

on the average of the same order as the kinetic energy and momentum of the colliding particles, the relaxation time for establishing equilibrium of translational degrees is of the order of the average time between gas kinetic collisions. Since the collision times are small compared to the flow times of macroscopic interest, it is possible to ascribe to the gas at every instant of time a 'translational' temperature, which characterizes the average kinetic energy of translational motion of the particles. Under conditions of partial thermodynamic equilibrium(thermodynamic equilibrium for the individual degrees of freedom) it is implied that the distribution of energy and concentration of the respective components of the mixture for these degrees of freedom is in equilibrium with the translational temperature of the gas. But quantities associated with nonequilibrium degrees of freedom may be arbitrary depending on many factors including the history of the gas. Such is the situation encountered in a shock front. The distribution of energy and concentrations is not determined in this case simply by the temperature, density and composition of the gas as in the case of thermodynamic equilibrium, but also by the kinetics of the physico-chemical processes leading to the reestablishment of equilibrium for the given degrees of freedom.

Normally the establishment of equilibrium of various degrees of freedom follows the following hierarchy; translational degrees, rotational degrees, vibrational degrees, dissociation

and chemical reactions, ionization and electronic excitation. Due to the pronounced difference in the various relaxation times, it is very often possible to study some relaxation processes separately, isolating them from the remaining ones.

The study of the kinetics of physico-chemical relaxation processes has two parts: the first dealing with the rates of the elementary processes leading to the excitation of one or other degree of freedom, the second dealing with the kinetics of the relaxation process itself under specific conditions. As far as the rotational degrees are concerned, it is practically always possible to assume that equilibrium is established as quickly as with the translational degrees of freedom so that they can be considered as classical type. On the other hand the problem of vibrational relaxation becomes of practical importance when the vibrational energy of the molecule is comparable to the translational energy in which case the vibration mode takes an essentially quantum character. When the translational energy is small compared to the vibrational energy of the molecule the excitation of the vibrational degree can be ignored whereas in the other limit of far classical region (the translational energy is large compared to the vibrational energy of the molecule) almost all the molecules will have dissociated and the problem loses its meaning. The dissociated gas behaves as a monatomic gas in which only ionization and electronic excitation are possible.

1.7 Ionizing Shock Wave in a Monatomic Gas:

In studying the ionization and its effect on shock structure it is interesting to deal with a monatomic gas. Due to the absence of a large number of degrees of freedom possessed by polyatomic gases it is easier to obtain higher temperatures in monatomic gases. Monatomic gases are also simpler since apart from electron state excitation ionization is the only relaxation process responsible for broadening the shock front. Most of the studies have been made with noble gases argon, krypton and xenon because their low ionization potential results in a higher degree of ionization for a given shock strength. Also their greater atomic weight (lower speed of sound) helps the production of strong shock waves. Argon has been used most often because its atomic properties are well known and the pure gas is inexpensive.

To study the physics of an ionizing shock wave, a stationary strong shock wave in a monatomic gas can be considered for simplicity. Upstream of the shock the neutral gas is in thermodynamic equilibrium. As the particles travel across the shock their ordered motion will be disturbed and a large part of the kinetic energy of the flow will be converted into thermal energy of random motion as in an inert gas shock. As a result of the high temperatures developed there will be a large number of collisions in which energies of the order I (ionization potential of the atom) will be transferred to the electrons in their orbits resulting in ionization of the atom. The

electron-atom collisional ionization is very effective due to its large cross section. However, this process needs some initial priming electrons to form an electron avalanche. One of the mechanisms which can lead to this initial ionization is through atom-atom collisions. As the cross section for this atom-atom collisional ionization process is extremely small it takes a large time for the formation of priming electrons. Consequently, significant ionization takes place only downstream of the gas dynamic shock with its structure determined by the elastic collisional dissipative mechanisms as in an inert gas. However, at Mach numbers greater than $\sim$20, when the temperature inside the gas dynamic shock is high enough to cause significant ionization by atom-atom collisions, the structure of the gas dynamic shock front is appreciably influenced by the ionization process. Hence inelastic collisional processes should be included in the study of the gas dynamic shock also. Other possible mechanisms of producing priming electrons are photoionization and ionization due to impurities.

Avalanche ionization begins when the rate of atom-electron collisional ionization becomes greater than the rate of the initiating process. Since the rate of atom-atom collisional ionization is very low, avalanche ionization begins with only a very few electrons. The point at which atom-electron ionization rate overtakes the atom-atom ionization rate is referred to as the 'take over point' or the 'onset point'.

The region downstream of the onset point is relatively insensitive to the atom-atom ionization cross section. At a constant electron temperature, the avalanche increases exponentially with time (distance) until recombination begins to balance the ionization rate leading to equilibrium. In actuality the avalanche proceeds in a much more complex manner. First, the ionization occurs through a two-step process in which an atom gets excited to its first excited level and then subsequently ionized. Further each ionization results in the electron gas losing an amount of energy I, corresponding to the thermal energy of many electrons so that the electron gas temperature is lowered. If this energy is not replenished the electron gas temperature would continue to fall very rapidly. A fall in the electron temperature in turn lowers the ionization rate which depends very strongly on the electron temperature through Boltzmann factor e^{-I/kT_e} . The electron energy loss resulting from ionization will be compensated by energy transfer from the high temperature heavy particle gas through elastic collisions. However the energy transfer between the heavy particles and electrons proceeds very slowly due to the large difference in their masses restricting the rate of electron-atom collisional ionization to a great extent. The energy an electron gains during a collision with an ion is several times more than that with an atom due to the coulombic nature of the force field between charged particles. Nevertheless in the initial stages when the ion population is very small,

the atom-electron elastic collisional energy transfer is still significant. Because of the nearly equal masses of atoms and ions and also the large elastic collision cross sections between them, energy exchange between them proceeds very rapidly. Consequently the atoms and ions have the same temperature throughout. Thus, but for an initial region, ions very efficiently supply energy to the electron gas serving as an intermediary in the energy flow from the atoms. In the electron gas the energy is very rapidly distributed through elastic collisions so that an electron temperature can be assigned which is different from the heavy particle gas temperature. In the electron-atom collisional ionization zone energy lost by the electron gas is balanced by the energy gained through elastic collisions with heavy particles so that the electron gas temperature changes very little.

Further downstream when the electron population is built up close to its equilibrium value the recombination in which ions and electrons unite to form neutral atoms becomes important. This recombination rate balances appreciably the ionization rate so that the net rate of electron production decreases. In this region the atom temperature starts falling finally approaching the electron temperature when thermal equilibrium is reached. Later, the electron density approaches its equilibrium value at which the recombination rate exactly balances the ionization rate and chemical equilibrium is reached.

1.8 Polarization in an Ionized Gas:

If an electron density gradient exists in a gas, the electrons tend to diffuse so as to smooth out the gradient, due to the high mobility of the electrons resulting from their exceedingly small mass. The ions, however, have a much lower diffusion velocity due to their large mass, and, therefore, cannot move relative to the neutral atoms. This leads to the motion of electrons relative to the ions resulting in a charge separation and creation of a strong electric field with its intensity given by Gauss equation. This electric field however prevents further polarization and inhibits the diffusion electron current.

Since the field due to a charge in a plasma is shielded within one Debye length the electrons cannot be separated from ions by more than this distance. If the Debye length is much smaller than the electron mean free path, separation is achieved very rapidly compared to the rate at which the electron density changes. As a result charge separation can always assumed to be in a steady state with no relative velocity between electrons and ions. This leads to the approximation that on a macroscopic scale the plasma is electrically neutral at every point and the electron density changes exactly equal ion density changes. In the gas dynamic shock the electrons, if present, also get compressed because of the strong electric forces exerted by the ions. With no

relative velocity, the electron pressure gradient arising from this compression cannot be supported by collisions but must be balanced by the electric field. Thus, the body force on the electron due to the electric field must equal the electron pressure gradient.

Together with the regions of increased electron concentration in the front part of the shock front, there exists a region of reduced electron concentration in the rear part. This is because, the concentration of electrons without a simultaneous concentration of positive ions in a neighbouring region would lead to the appearance of an electric field at 'infinity' requiring the expenditure of an infinite amount of energy.

1.9 Study of Ionizing Shock Waves:

Earlier investigators[50,14,62,77] have studied the relaxation zone taking the initial conditions for the atom gas obtained from Rankine-Hugoniot relations for the inert gas shock. However, the choice of initial values for the electron and ion gases are not known a priori. For low Mach numbers when little ionization occurs inside the gas dynamic shock, the downstream equilirbium state of it is determined by the Rankine-Hugoniot relations and the initial electron and ion densities are zero. However, an initial electron temperature is still required.

The first investigation of this type was carried out by Petschek and Byron[62] who ignored the effects of viscosity, heat conduction and radiation in their analysis. Collisional ionization was assumed to occur as a two-step process, the atom being excited and then ionized in a second collision. They considered only atom-electron collisional ionization and neglected recombination. The source of priming electrons was not clear from the work of Petschek and Byron. They used a steady state electron energy equation in which the energy lost by electrons in inelastic collisions is exactly balanced by the energy gained in elastic collisions with heavy particles. The energy transfer due to temperature gradients was neglected.

Their calculation of the ionization rate was verified approximately by two independent experimental measurements. The first was a measurement of the electrostatic potentials due to electron diffusion in the gas. The maximum rate of change of the diffusion potential was measured with a probe and was found to be in reasonable agreement with the calculated rate. Continuum intensity measurements also served to check the calculated ionization rate. Radiation from the recombination of ions and electrons was measured using a spectrometer and photocell with a fast response time. They also measured the time to reach equilibrium ionization.

Bond[14] has also considered theoretically the rate of approach to equilibrium ionization behind shock waves in argon and calculated the ionization time for slightly stronger shocks.

He assumed that atom-atom collisions provide the initial supply of electrons. His estimate of the electron-atom ionization rate is greater than that of Petschek and Byron but their results for the total ionization time are in agreement.

Following the work of Petschek and Byron, the experiments by Harwell and Jahn[33] and also Kelly[39] confirmed that at the Mach numbers considered the initial ionization mechanism was atom-atom collisional ionization. Morgan and Morrison[50] essentially repeated the work of Petschek and Byron but included the atom-atom collisional ionization.

Wong and Bershader[77] made a similar analysis and included atom-atom collisional ionization. They attempted to identify the dependence of the cross section on energy, for this mechanism using the available experimentally measured ionization rates. They also considered the steady state electron energy equation of the Petschek and Byron's type. They used a slightly different expression for the atom-electron collisional excitation cross section from that of Petschek and Byron and included the three body ion-electron-electron collisional recombination. Their theoretical analysis was supplemented by experiments using a Mach-Zehnder interferometer in argon. Within the realm of their experiments photoionization, precursor effects and impurities did not seem to play a significant role. Recombination was found to play a minor role in determining the electron density

profile. For Mach numbers greater than 18, the measured electron concentrations did not reach the Saha equilibrium concentration and radiation was suspected to play a significant role in cooling the gas in this region.

Hoffert and Lien[36] studied the relaxation zone by considering both atom-atom and atom-electron collisional ionization. The corresponding three body collisional recombinations were also included. They have used a complete electron energy equation which included the effect of electron temperature gradient. For an initial value for the electron temperature they chose two values, one equal to the upstream equilibrium atom temperature and the second equal to the atom temperature downstream of the atom-atom shock. Their numerical solutions showed that only the early part of the relaxation zone was affected by the choice of initial electron temperature, and that the electron temperature varies very little in the later regions so that a steady state electron energy equation was sufficient.

Chubb[19] studied the problem for larger Mach numbers ($M \sim 30$) when ionization within the gas dynamic shock becomes important. In other words the width of the relaxation zone becomes comparable to the width of the gas dynamic shock. His approach is a semi-kinetic theoretical and the regions of interest namely the gas dynamic shock and the relaxation zone are studied separately. The gas dynamic shock is described

by a Mott-Smith's[51] type of solution for atoms and included a two-step atom-atom and atom-electron collisional ionization in both the regions. The corresponding collisional recombinations have been included only in the relaxation zone. He used separate electron continuity, momentum and energy equations in addition to the plasma continuity equation and a c_x^2 - moment equation[51] for atoms. The plasma conservation equations of momentum and energy are not satisfied throughout the atom-atom shock; however, they were used to obtain jump conditions across the atom-atom shock thus satisfying momentum and energy conservation for plasma only across the atom-atom shock. In this case the quantities appearing in the structure equations for the atom-atom shock depend upon the electron density and temperature downstream of the atom-atom shock. Since these are not known a priori for starting the numerical integration of the structure equations, an iterative method was used. In the study of the relaxation zone all the three species are assumed to have Maxwellian distribution functions. The three conservation equations for the plasma and a more complete electron energy equation than that of Hoffert and Lien were used in which the velocity gradient term was included. The set of equations were solved numerically using for the initial values the downstream quantities obtained from the atom-atom shock.

As far as the gas dynamic shock is concerned for Mach numbers >20,

i) the continuum equations cannot meaningfully describe the flow and a kinetic theoretical description has to be used;

ii) the degree of ionization is large and inelastic collisional effects are to be included in addition to elastic collisional dissipative mechanisms.

For the relaxation zone earlier investigators have assumed that

iii) each species may be described by its own Maxwellian distribution. This appears reasonable as long as the average thermal energies are low compared to excitation energies, and the density is relatively high so that, a particle will experience a large number of elastic collisions between the inelastic ones which change its internal state. For the temperatures encountered in the relaxation zone behind shock waves for $M > 30$, and at low pressures the Maxwell distribution postulate for atoms is doubtful.

1.10 Scope of Present Study:

Chubb considered the aspects (i) and (ii) of section (1.9) but did not satisfy the plasma momentum and

energy conservation throughout the atom-atom shock. In the present investigation not only all the above three aspects are considered but also the plasma energy conservation explicitly satisfied throughout the entire shock front. Further the iterative proceedure of Chubb is unnecessary in the present work. In addition assuming a nonequilibrium distribution function for atoms takes into account the elastic collisional dissipative mechanisms active towards the end of the relaxation zone where gradients in velocity and temperature are not negligible. The atom-atom inelastic collisional dissipative terms that have been neglected in comparison to the elastic collisional dissipative terms in the c_x^2 - moment equation of Chubb are likely to introduce considerable error at the end of the atom-atom shock. These terms have been included in the present study. A corrected value for the atom-atom collisional excitation cross section is also used.

Furthermore, entire region of nonequilibrium is represented by a single set of equations. This study may also be looked upon as an illustration of the suitability of a trimodal distribution function[30-32] for a problem characterized by three equilibrium zones (the three zones do not really exist in a physical problem). The radiation effects, precursor effects and multiple ionization have not been considered which are, however, important at higher Mach numbers and lower initial pressures.

CHAPTER 2

COLLISION PROCESSES AND COLLISION CROSS SECTIONS

2.1 Introduction:

Ionization is a process in which sufficient energy is imparted to the electron in its orbit around the nucleus so as to leave the orbit and pass into the continuum spectrum. This energy is known as the Ionization potential of the atom. Ionization may take place in more than one step in which case the atom passes through various excited states. If sufficient energy is available, each of the elementary processes resulting in excitation of electrons in atoms can also result in ionization. Ionization is essentially a limiting case of electronic excitation.

The elementary processes which result in excitation or ionization of atoms can be broadly classified into two categories;

i) collisional process in which the required energy is transferred during the collision(s) between the atom and a high energy particle,

ii) photoprocess in which the role of the high energy particle is played by a photon.

Symbolically the two processes can be written as follows,

$$\begin{aligned} A + B &\rightleftharpoons A^{+} + B + e \\ A + h\nu &\rightleftharpoons A^{+} + e \end{aligned} \qquad (2.1)$$

where A is an atom , e an electron and A^{+} an ion. B is the secondary particle which participates in the collision. This may be an electron, which is so most often, another atom, an ion, or a foreign impurity particle (if the gas is impure) and $h\nu$ is a photon. The inverse processes represented by the reversed arrows describe the corresponding recombination processes.

Strictly speaking, all these processes occur simultaneously in a gas. However, in certain situations, some of these processes may turn out to be less significant. In general, the process may follow a more complex path than the one-step process mentioned in eq. (2.1), in which case an intermediate excited state of the atom also plays an important role. Such process can be symbolically represented as follows;

$$\begin{aligned} A + A &\rightleftharpoons A^{*} + e + A \\ A + e &\rightleftharpoons A^{*} + e \\ A + h\nu &\rightleftharpoons A^{*} \end{aligned} \qquad (2.2)$$

and

$$\begin{aligned} A^* + A &\rightleftharpoons A^+ + e + A \\ A^* + e &\rightleftharpoons A^+ + e + e \\ A^* + h\nu &\rightleftharpoons A^+ + e \end{aligned} \qquad (2.3)$$

where A^* is one of the excited states of the atom. The reactions represented by eq. (2.2) are those in which the atom is excited to one of its possible levels from the ground state, whereas those described by eq. (2.3) represent the ionization of an excited atom. Further, these processes may take place in multisteps. However, it will be shown later that the two-step process is the dominant one over the rest at such temperatures that $kT \sim I$. In what follows, the atom-atom and atom-electron two-step collisional processes are considered in detail and the relative importance of these processes over the single-step process and also the photoprocesses is established.

2.2 Atom-Atom Collisional Ionization:

This is one of the dominant mechanisms during the initial stages of ionization when the electron concentration will be very low. In the absence of other initiating mechanisms like photoionization, this mechanism determines the rate of increase of electron density in the gas[33].

Johnston and Kornegay[38], employing microwave techniques demonstrated for xenon that atom-atom collisional ionization proceeds by a two-step process in which the rate is governed by the first process of the atom getting excited to its first level from the ground state. The rate of excitation or ionization of the atoms depends on the number density of the particles that participate in the inelastic collision, the concerned collision cross section and the activation energy of the process. Harwell and Jahn[33] and recently McLaren and Hobson[48] have shown that their theoretically predicted results of the two-step model agree qualitatively with the measured ionization rates in their experiments. Assuming Maxwellian distribution for atom velocities, it can be shown that the rate at which atoms are ionized in unit volume through a one-step process is

$$\left(\frac{dn_+}{dt}\right)_1 = \frac{1}{2} n_a^2 \left(\frac{m_a}{2\pi kT_a}\right)^3 \int_0^\infty \exp\left(-\frac{m_a G^2}{kT_a}\right) 4\pi G^2 dG$$

$$\cdot \int_{g_o}^\infty e^{\left(-\frac{m_a g^2}{4kT_a}\right)} \sigma_I(g)\, 4\pi g^3\, dg \qquad (2.4)$$

where n_a, m_a and T_a are respectively atomic particle density, mass and temperature; G the center-of-mass speed of the colliding pair of atoms and g their relative speed; $g_o = \sqrt{(4I/m_a)}$; $\sigma_I(g)$ is the ionization cross section. Subscript 1 stands for one-step

process. Assuming a linear dependence of the cross section on energy in the center-of-mass system (Section 2.5) as

$$\sigma_I = C_I^{(a)} (E-I) \equiv \frac{1}{4} m_a C_I^{(a)} (g^2-g_o^2), \qquad (2.5)$$

eq. (2.4) can be written, after carrying out the integration, as

$$\left(\frac{dn_+}{dt}\right)_1 = 4 C_I^{(a)} (\pi m_a)^{-1/2} n_a^2 (k T_a)^{3/2} \left(1+ \frac{I}{2kT_a}\right) e^{-\frac{I}{kT_a}} \qquad (2.6)$$

$$= \alpha_a n_a^2 . \qquad (2.6a)$$

where $C_I^{(a)}$ is a constant and α_a is the rate constant, a function of the temperature.

The rate of excitation of atoms, per unit volume from their ground state to the first possible energy level can be written in a similar way, by replacing in eq. (2.6) $C_I^{(a)}$ and I by the corresponding constants $C_*^{(a)}$ and I_* as

$$\frac{dn_*}{dt} = 4 C_*^{(a)} (\pi m_a)^{-1/2} n_a^2 (k T_a)^{3/2} \left(1 + \frac{I_*}{2kT_a}\right) e^{-\frac{I_*}{kT_a}} \qquad (2.7)$$

An expression for the rate of ionization of the excited atoms can be similarly written as

$$\frac{dn_+}{dt} = 8 C_+^{(a)} (\pi m_a)^{-1/2} n_a n_* (kT_a)^{3/2} \left(1+ \frac{I'}{2kT_a}\right) e^{-\frac{I'}{kT_a}} \qquad (2.8)$$

where $C_+^{(a)}$ is the constant of proportionality in the cross section for ionization of the excited atoms, $\sigma_+ = C_+^{(a)} (E-I')$ and $I' = I-I_*$ is the activation energy for the process.

Since for the noble gases even the lowest excited states have energies well above half the ionization potentials, the energy increments involved in the second step, I' will be substantially less than those for the first step, I_*. Also the geometric size of an excited noble gas atom presumably exceeds that of its ground state, and a continuum of final states is available for the second step compared to a discrete level for the first. For this reason we can assume the chances of an excited atom getting ionized in a further collision to be large compared to the probability of collisional deexcitation. The process of ionization of an excited atom is faster than the process of excitation of an atom from the ground state.

The rate of ionization of excited atoms hinges on the steady state concentration of the excited atoms A^* (eq. 2.8). This, in turn depends on the relative rates of excitation and deexcitation processes. The natural life-time of a normal excited atom against radiative decay ($\sim 10^{-8}$ sec) is perhaps inadequate to support the required steady state concentration of A^*. However, in noble gases, one of the following aspects may effectively protract this life-time. In noble gases like argon at moderate pressures and temperatures the excitation collision results in the elevation of the atom from the ground state to one of the four closely spaced energy levels comprising the first excited state. Two of these are metastable states which are energitically isolated from the ground state and any

transition between these levels and ground state are forbidden by virtue of the J selection rules. Spectroscopic transitions between the other two levels and the ground state are permitted by the selection rules and give rise to so-called resonance radiation. If collisional excitation leads to one of these metastable states, the atom can remain in that state for periods of the order 10^{-4} sec.[39], because of its inability to reach the ground state by radiative decay. Consequently the chances of a second collision leading to ionization of this atom is greatly enhanced. If the atoms are collisionally excited to one of the resonance levels, which, for the noble gases studied lie less than 0.3 eV above the lowest metastable states, the life-time of the excited atoms for radiative decay is of the order of 10^{-8} sec., which is usually less than the mean collisional time. However, since the gas is optically thick for this resonance radiation, the emitted photon will be trapped in the gas, individual atoms being alternately excited collisionally or radiatively and deexcited radiatively resulting in a constant overall population of the excited atoms. Therefore, the rate of ionization of an excited atom by a collision of the second type, which depends on the population of n_*, increases with resonance radiation trapping. The role played by this resonance radiation is discussed in Section (2.42). Since the difference in the energy levels between the metastable and resonance levels is commensurate with the experimental inaccuracies it has not been

possible to experimentally verify which of the two paths the mechanism really follows. However, the experimental results of McLaren and Hobson[48] suggest that metastable states play the main role in the mechanism. This however needs further investigation. Because the activation energy for the forward reaction leading to ionization of excited atoms is considerably less than the activation energy for the deexcitation process, the ionization is more probable than the deexcitation of excited atoms. Due to the large difference between the activation energies of the excitation reaction and the ionization reaction of the second type, the former being several times the latter, the former process controls the net rate of production of electrons.

Since the energy required to excite an atom from the ground levels is less than that required to ionize an atom in one-step ($I_* < I$) and because the number of particles that have energies above I_* is much large than those having energies greater than I, the number of collisions that result in the excitation of atoms is large compared to the number that result in direct one-step ionization. Further, almost all the excited atoms get ionized by a second collision. Thus the two-step ionization process is the dominant mechanism in noble gases and the excitation collision process governs the overall rate of ionization.

Experimental measurements of the ionization rates in noble gases by Harwell and Jahn[33], Kelly[39], Margon and Morrison[50] and McLaren and Hobson[48] also suggest the choice of the two-step

ionization mechanism. Following the analysis of Harwell and Jahn[33], for a noble gas free from impurities, the possible initial two-step ionization mechanisms can be described symbolically as

$$A + A \underset{k_*'}{\overset{k_*}{\rightleftharpoons}} A^* + A$$

$$A^* \overset{\bar{k}_\nu}{\rightleftharpoons} A + h\nu \qquad (2.9)$$

$$A^* + A \xrightarrow{k^+} A^+ + e + A$$

where k_*, k_*', $\bar{k}_\nu$ and k^+ are the corresponding reaction rates, which are functions of the temperature; (2.9) represents the photoexcitation and deexcitation mechanisms.

Taking natural logarithm and differentiating the eq.(2.6) with respect to (1/kT) yields, for kT << I,

$$\frac{d\left[\ln\left(\frac{dn_+}{dt}\right)_1\right]}{d(1/kT)} \simeq -I \qquad (2.10)$$

expressing the usual Arrhenius result for one-step process.

If the ionization takes place following a two-step path then,

$$\left(\frac{dn_+}{dt}\right)_2 = \frac{dn_*}{dt} \qquad (2.11)$$

Again, from eq. (2.7) we can write the expression for the slope of the Arrhenius plot as,

$$\frac{d\left[\ln\left(\frac{dn_+}{dt}\right)_2\right]}{d(1/kT)} \simeq -I_* \qquad (2.12)$$

Measurements have shown the slopes of the ln $(\frac{dn_+}{dt})$ vs. (1/kT) curves to be closer to I_* than I, which confirms the relative importance of the activation energy I_* over I. For example, in the measurements made by Harwell and Jahn[33] using a transverse microwave detection arrangement with Ar, Kr and Xe, the activation energies deduced from the Arrhenius plots are 11.9 ± 0.5 eV, 10.4 ± 0.5 eV, and 8.6 ± 0.5 eV respectively, which are closer to the corresponding excitation energies, namely, 11.55 to 11.83 eV, 9.91 to 10.6 eV, and 8.31 to 9.55 eV for the respective gases; these activation energies differ distinctly from the respective ionization potentials 15.75 eV, 14.00 eV, and 12.13 eV. Recent experimental investigations by McLaren and Hobson[48] using double electrostatic probes in argon have revealed further aspects of the two-step process. The activation energy got from the Arrhenius plot has a value 11.4 ± 0.3 eV, which is closer to the metastable level energy of argon 11.6 eV. They were also able to measure the activation energy I' for ionization of the excited atoms and the corresponding rate constant k^+. This activation energy was found to have a value of 4.7 ± 0.4 eV, which compares closely with 4.27 eV, required to ionize an excited argon atom from its metastable level. These observations augment the model of a two-step ionization mechanism involving an intermediate metastable state of excitation. Using the values of the measured reaction rates k^* and k^+ they were able to estimate the steady state degree of excitation

n_*/n_a ($= k_*/k_+$) over the range of temperatures from 7000°K to 12000°K and at pressures from 0.2 to 3.0 torr. The concentration of excited atoms (n_*/n_a) was found to vary from 7×10^{-9} to 8.64×10^{-7} which is sufficient to keep the rate of ionization of excited atoms much greater than the rate of excitation. Ratio of the cross sections for the two processes ($C_+^{(a)}/C_*^{(a)}$) was found to be $\sim 10^3$ for argon which is of the same order as estimated by Johnston and Kornegay for xenon[38].

Harwell and Jahn[33] also highlight the relative importance of various deexcitation processes by studying the dependence of reaction rates on time and density. The rate equations for the excitation and ionization processes represented by (2.9) can be written as[33]

$$\frac{dn_*}{dt} = k_* n_a^2 - (k_+ + k_*') n_a n_* - \bar{k}_\nu n_* \qquad (2.13)$$

$$\frac{dn_+}{dt} = k_+ n_a n_*$$

Assuming n_a to be constant which is a good approximation for very low degrees of ionization, equations (2.13) can be integrated assuming n_*, $n_+ = 0$ at $t = 0$ to give,

$$n_* = k_* \tau n_a^2 (1-e^{-t/\tau}) \qquad (2.14a)$$

$$n_+ = k_* k_+ \tau n_a^3 [\, t-\tau(1-e^{-t/\tau})] \qquad (2.14b)$$

where $$\tau = (k_+ + k_*') n_a + \bar{k}_\nu \qquad (2.14c)$$

The results reproduced here for ready reference from (33) and shown in Table 2.1. give the activation energy, the density and time dependence of the electron concentration deduced from equations (2.14) for different possible cases.

Their experiments have shown that the density dependence was quadratic and the time dependence was linear, though the uncertainty about quadratic dependence on density was expressed to a certain extent. In some cases they found density dependence weaker than quadratic, which any way favours none of the alternative paths other than the second shown in the Table (2.1). So within the realm of the investigations of Harwell and Jahn, it is justifiable to neglect the collisional and radiative deexcitation processes.

McLaren and Hobson[48] also have studied the relative importance of collisional deexcitation over collisional forward ionization of excited atoms. They show from the consideration of energies involved in the two processes, that neglect of collisional deexcitation compared to forward ionization requires that,

$$\frac{g_*}{g_0} >> \frac{k_*}{k_+} e^{(I_*/kT)} \qquad (2.15)$$

where g_0 and g_* are the degeneracies of the ground and excited states. In the range of their experiments in argon it is shown that the quantity on the right hand side of the inequality (2.15) varies from 0.05 at 12000°K to 1.2 at 7000°K. For the metastable

Table 2.1

Various Ionization Routes in the Initial Regime

Process	Collisional De-excitation	Rad. decay	Phase	Density Order	Time Dep.	Activation energy
1. 2-Step	$k'_* \ll k_+$	$\bar{k}_\nu \ll k_+ n_a$	$t \ll \frac{1}{k_+ n_a}$	n_a^3	t^2	I
2.			$t \gg \frac{1}{k_+ n_a}$	n_a^2	t	I_*
3.		$\bar{k}_\nu \gg k_+ n_a$	$t \ll \frac{1}{\bar{k}_\nu}$	n_a^3	t^2	I
4.			$t \gg \frac{1}{\bar{k}_\nu}$	n_a^3	t	I
5.	$k'_* \gg k_+$	$\bar{k}_\nu \ll k'_* n_a$	$t \ll \frac{1}{k_* n_a}$	n_a^3	t^2	I
6.			$t \gg \frac{1}{k'_* n_a}$	n_a^2	t	I
7. 1-Step				n_a^2	t	I

state of the argon atom the ratio (g_*/g_o) has a minimum value of 6 which again justifies the neglect of collisional deexcitation process.

2.3 Atom-Electron Collisional Ionization:

In this process high energy electrons collide with neutral atoms resulting in transfer of energy inelastically to the atom sufficient enough to excite the atom to its first excited state. Because of the fact that the mass of an electron is several orders of magnitude less than the mass of an atom and that the energy transfer by collisions depends upon the mass ratio of the collision participants, the efficiency of this process is very much different from the atom-atom collisional process.

The condition for the probability of inelastic energy transfer during a collision to be high is that the adiabatic factor $(2\pi a\omega/v)$ should not be too great[78] compared to 1, where 'a' is Bohr radius, ω the angular frequency of an electron in orbit, and v the relative velocity of the approaching particles. Thus, in order that a collision be inelastic the impact must be sufficiently sharp, i.e. the velocities of the approaching particles must be of the same order as the velocity of the electrons in the outer orbit of the atom. In the case of an inelastic collision between two atoms with relative energy of the order of the ionization potential, say upto 10 eV, this condition is not satisfied and the inelastic cross section is very small. On the other hand when an electron approaches an atom with relative

energy of the order of I, the velocity of the electron, $\sqrt{(2I/m_e)}$, will be of comparable order to the velocity of the electron in orbit thereby making this process efficient in ionization.

Expressions similar to (2.6) can be written for the rate of generation of electrons by the atom-electron collisional process assuming a linear variation of the cross section with respect to the energy in the relative system as[62]

$$\frac{dn_+}{dt} = 4\, C_I^{(e)} \left(\frac{\pi m_e}{2} \right)^{-1/2} n_a n_e \, (kT_e)^{3/2} \left(1 + \frac{I}{2kT_e}\right) e^{-I/kT_e} \tag{2.16}$$

$$= \alpha_e \, n_a n_e \tag{2.16a}$$

where $C_I^{(e)}$ is the proportionality constant for the cross section given by,

$$\sigma_{ae}^{(i)} = C_I^{(e)} \, (E - I) \tag{2.17}$$

where m_e, n_e, T_e are the mass, density and temperature of the electrons; α_e is the rate constant, a function of the electron temperature.

Comparing α_e and α_a from (2.16) and (2.6) for the same electron and atom temperatures,

$$\frac{\alpha_e}{\alpha_a} \backsim \frac{C_I^{(e)}}{C_I^{(a)}} \sqrt{\frac{m_a}{m_e}} \frac{n_e}{n_a} \tag{2.18}$$

$\sqrt{(m_a/m_e)} \backsim 100$; and measured values of $C_I^{(e)}$ and $C_I^{(a)}$ give $C_I^{(e)}/C_I^{(a)} \backsim 10^2$.

Hence $\alpha_e >> \alpha_a$, as long as n_e/n_a is not too small (not less than 10^{-4} - 10^{-5}). Morgan et al.[50] have found that the take over degree of ionization varies from about 5×10^{-4} for temperatures of 10000°K to 5×10^{-2} at 40000°K. When T_e is much less than atom temperatures, the onset degree of ionization takes values greater than these.

For ionization fractions greater than $\sim 10^{-5}$, the electron-atom collisional ionization process dominates over the atom-atom process. In most cases, the initial building up of this electron concentration takes place through one of the priming processes. After the take over point, the electron-atom collisional process becomes dominant over the rest.

The electron-atom collisional ionization also takes place in two steps similar to atom-atom process, involving an intermediate excitation stage and the rate of ionization is again governed by the rate of excitation of the atoms from the ground state. The ratio of the characteristic time for ionization to that of excitation of atoms by electron impact for argon can be written as[78]

$$\frac{\tau_e}{\tau_e^*} \sim \frac{1}{10} \frac{n_e}{n_a} e^{I/kT} \qquad (2.19)$$

for $I/kT \sim 10$.

Close to equilibrium and with moderate degrees of ionization,

$$\frac{n_e}{n_a} \simeq \left(\frac{6 \times 10^{21}}{n_a} \right)^{1/2} T_{eV}^{3/4} \, e^{-I/2kT_e} \qquad (2.20)$$

For argon at $n_a = 1.7 \times 10^{18}$ cm^{-3} and $T_e = 13{,}000^{\circ}$K, $\tau_e/\tau_e^* \sim 5000$ indicating that the Boltzmann distribution with respect to excitation is established much faster than in ionization. The times may be comparable only at the beginning of the process when the electron density is much smaller than the equilibrium value. This along with an argument similar to that followed in Section (2.2) shows that the excitation rate is much larger than the ionization rate and that the excitation rate dictates the ionization rate in the two-step process.

2.4 Photoionization:

Photoprocesses become of considerable importance at high temperatures in determining the shock structure. The radiation emitted at the end of the relaxation zone as a result of ion-electron recombination, propagates upstream towards the cold gas. In the process it partly or completely gets absorbed by the gas. This escape of radiation from the downstream equilibrium region and its partial absorption by the gas results in (i) cooling of the downstream equilibrium gas and (ii) change of the shockwave structure due to photoexcitation and ionization of atoms.

The photoprocesses that result in the emission of radiation are

(i) free-free transitions or Bremsstrahlung radiation,

arising from the deceleration of the electron in free state in the coulomb field of the ion with the emission of a photon

$$A^+ + e \rightarrow A^+ + e + h\nu \qquad (2.21a)$$

(ii) free-bound transitions, which involve the photo recombination of the free electrons into one of the bound states of the atom, the difference in energy being released as a photon

$$A^+ + e \rightarrow A(p) + h\nu \qquad (2.21b)$$

where A(p) is an excited atom in p-th electronic state, and

(iii) bound-bound atomic transitions, in which an electron from a higher energy level moves to one of lower energy with the emission of a photon

$$A(p) \rightarrow A(q) + h\nu \qquad (2.21c)$$

Since the electrons in the free state can have a continuous distribution of energy the first two processes which involve transitions from free electronic state, result in continuum radiation while the bound-bound transition involves discrete energies and hence emits line radiation. As far as the energy loss and cooling effect are concerned, the continuum radiation makes a large contribution. Various aspects of the emission and propagation processes and the resulting cooling effects of plasma have been considered by several authors in References 20, 27,34,37,47,57,59,63,64,67,70,72. In this section, the relative importance of photoionization vis-a-vis collisional ionization, is considered and the resulting cooling effect has been ignored.

The former effect influences the entire shock structure whereas the latter effect only the tail and regions.

2.4.1 Effect of Continuum Radiation:

Assuming a one-step photoionization, the rate of production of electrons due to photoionization can be written as[78],

$$Z_{\nu 1} = n_a \int_{\nu_1}^{\infty} \frac{U(\nu)}{h\nu} \, c \, \sigma_\nu(\nu) \, d\nu \qquad (2.22)$$

where $U(\nu)$ is the radiant energy density per unit spectral interval at ν, $\sigma_\nu(\nu)$ is the photoionization cross-section for the atom from the ground state, and c is the velocity of light. Since the energy of the photon must be greater than I to ionize an atom, the lower limit for ν is ν_1 given by $h\nu_1 = I$. $\sigma_\nu(\nu)$ has a frequency dependence of ν^{-3} for hydrogen-like atoms. In complex many-electron atoms the assumption of hydrogen-like behaviour for excited states of large principal quantum numbers is reasonable, but the ground state and low lying excited states are highly nonhydrogenic. Bates and Seaton[8], through detailed quantum mechanical calculations, have established that the frequency dependence of σ_ν can differ markedly from ν^{-3} dependency for ground state photoelectric effect because of the non coulombic nature of the field between the photon absorbing electron and charges due to nucleus and the remaining electrons. Biberman et al.[9-11] developed approximate analytical expressions for free-free and bound-free transitions from excited states,

for a variety of low atomic number atoms. The expressions are valid for local thermodynamic equilibrium and resemble the well known Kramer-Unsöld expression for hydrogen. The effective nuclear charge Z has been replaced by a correction factor $\xi(\nu, T)$, that depends in general, upon both frequency and temperature. The factor $\xi(\nu, T)$ has been evaluated by Biberman and Norman using Burgess-Seaton theory[16], for a number of neutral and ionized atoms. With the crudeness of the following analysis, which is intended only to estimate the order of magnitude of the photoionization rate, an average cross section (which can be set equal to the cross section at the ionization threshold to a high degree of accuracy) can be used. The Planck equilibrium radiation energy density can be used for $U(\nu)$[78],

$$U(\nu) = \frac{8\pi h\nu^3}{c^3} \left(e^{h\nu/kT} - 1\right)^{-1} \tag{2.23}$$

Further, since $(I/kT) >> 1$, (2.23) can be approximated by the Wien's displacement expression,

$$U(\nu) \doteq \frac{8\pi h\nu^3}{c^3} e^{-h\nu/kT} \tag{2.24}$$

Using $\bar{\sigma}_\nu(\nu) = \bar{\sigma}_{\nu 1}$, and substituting from eq. (2.24) for $U(\nu)$ eq. (2.22) can be written for $Z_{\nu 1}$ as,

$$Z_{\nu 1} \approx \frac{8\pi n_a}{c^2} \bar{\sigma}_{\nu 1} \frac{kT_\nu}{h^3} \left(I^2 + 2IkT_\nu + 2k^2T_\nu^2\right) e^{-I/kT_\nu} \tag{2.25}$$

where T_ν is the equilibrium temperature for the radiation. Putting $I >> kT$ simplifies eq. (2.25) to,

$$Z_{\nu 1} \approx 8\pi n_a \sigma_{\nu 1} \frac{I^2}{c^2} \frac{kT_\nu}{h^3} e^{-I/kT_\nu} \qquad (2.26)$$

An expression similar to eq. (2.16) for the two-step atom-electron collisional ionization rate can be written for $I_* >> kT_e$,

$$Z_c \approx C_*^{(e)} \left(\frac{8kT_e}{\pi m_e} \right)^{1/2} n_a n_e I_* e^{-I_*/kT_e} \qquad (2.27)$$

where $C_*^{(e)}$ is the constant of the cross section expression for the atom-electron collisional excitation. From equations (2.26) and (2.27), for argon, using the values $I_* = 11.5$ eV and $I = 15.7$ eV,

$$\frac{Z_{\nu 1}}{Z_c} \approx \frac{1.18 \times 10^{15}}{n_e} \frac{T_\nu}{\sqrt{T_e}} \frac{\sigma_{\nu 1}}{C_*^{(e)}} \exp\left[\left(\frac{13.35}{T_e} - \frac{18.25}{T_\nu} \right) \times 10^4 \right] \qquad (2.28)$$

In the regions where electron-atom collisional ionization dominates over other collisional processes, $T_e \approx T_{eq}$ $(= T_\nu)$. Therefore eq. (2.28) can be written as,

$$\frac{Z_{\nu 1}}{Z_c} \approx \frac{1.18 \times 10^{15}}{n_e} \frac{\sigma_{\nu 1}}{C_*^{(e)}} \sqrt{T_{eq}} \exp\left[\left(- \frac{4.95}{T_{eq}} \right) \times 10^4 \right] \qquad (2.28a)$$

For an equilibrium temperature of $10^4\ ^\circ K$ (for an upstream Mach number of 30, and temperature $300^\circ K$, the equilibrium temperature is $17100^\circ K$) the ratio of photoionization to collisional ionization is,

$$\frac{Z_{\nu 1}}{Z_c} \approx \frac{2 \times 10^{16}}{n_e} \frac{\sigma_{\nu 1}}{C_*^{(e)}} . \qquad (2.29)$$

Assuming $C_*^{(e)} \sim \sigma_{v1}$, for $n_e > 10^{17}$ cm^{-3} from eq. (2.29) it is found, that photoionization is relatively less important compared to collisional processes. For lower electron densities however, the photoprocesses need to be considered.

At high Mach numbers (M > 20) there exists still quite an amount of uncertainty about the significant mechanism of ionization in the initial stages which build up the electron population to the onset value. For lower Mach numbers, it has been fairly well established[33,39,48] that atom-atom collisional process dominates over the rest. Chubb[19] estimated the ratio of photoionization rate to collisional ionization rate assuming a constant photoionization cross-section and equilibrium radiation corresponding to the downstream equilibrium. His analysis is similar to the one followed above and for σ_{v1} he has used the largest value of photoexcitation cross section quoted by Lee and Weissler[41] for argon. Chubb's expressions and calculations, which seem to be in arithmetical error* have under estimated the significance of photoionization. The corrected value of the ratio of photoionization rate to atom-atom collisional ionization rate for a Mach number of 20 is found to be 5.2, thus it seems that photoionization is important even for Mach numbers around 20 for the densities considered. However, ...

---

* Ref. 26, Eq. 50 is less by a factor 10; and the value of I_p/I_{coll} for M = 30, quoted as 5×10^{-2} is very much off the correct value of 11.2.

such a conclusion cannot be made on the basis of the crude analysis of the above type. The assumptions of constant photoionization cross section and equilibrium distribution of radiant energy are highly questionable, and the lowering of equilibrium temperature because of radiation cooling has not been considered. Since the cross section decreases for frequencies above the threshold value the constancy assumption overestimates the photoionization rate. Secondly, the effect of radiation absorption by the nonequilibrium gas as it passes through, before the radiation reaching the atom-atom zone is not considered. Nelson and Goulard[57] have considered the effect of absorption of the ground state continuum radiation for argon gas for initial pressures of 0.2, 1, and 10 cms of Hg and an initial temperature of $300^{\circ}K$ for a Mach number of 24. In their analysis the electron gas was allowed to be colder with respect to atom gas. Within the realm of their studies it is found that absorption effects are important to the extent that ground state continuum radiation does not affect the region behind the shock much and the zone is collision dominated. The absorption effect can be studied by considering the nondimensional optical thickness τ_g nondimensionalised with respect to collisional ionization mean free path, which they have calculated through-out the shock. When τ_g is large, the radiation emitted by a particle is essentially absorbed by its neighbouring particle, so that the particles just exchange equal amounts of energy and no

net loss or gain occurs; consequently, the radiation is trapped. As the optical thickness decreases below unity, the radiative energy can travel quite far before being absorbed. The results of Nelson and Goulard show that $\tau_g > 1$ in the atom-electron dominating region and $\tau_g < 1$ in the atom-atom dominating region, so that the ground state continuum radiation emitted in the atom-electron region is practically trapped and only that emitted very close to atom-atom region reaches the upstream region and participates in ionization. The radiative fluxes and optical thicknesses depend strongly on the electron temperature; thus the cool electron gas in the atom-atom region greatly curtails the magnitude of the radiation entering the atom-atom region. The assumption of equilibrium distribution of radiant energy is invalid; because the relative changes in temperature and density are large within distances equal to the penetration lengths pertinent to the radiation, nonequilibrium radiation may occur. It may also occur in optically thin regions, because the radiation emission rates are not balanced by the absorption rates.

2.4.2 Effect of Line Radiation:

The one-step radiative processes discussed above exclude the effect of resonance line radiation resulting from emission processes of the type (2.21c). This process has often been dismissed due to the strong self-absorption effect expected at the center of the line. Nevertheless, the low absorption

characteristics of the wings of the line give rise to the possibility of a substantial optical path for the escaping photons of the same frequency, until they are trapped; thus in the atom-atom region and also in the precursor region, the excited states formed by the absorption of this line radiation may get further ionized by the absorption of a second photon of continuum excited state radiation.

Biberman and Veklenko[12] and Murty[53] have theoretically investigated the importance of this two-step precursor mechanism. The experiments of Wilson and Lederman[76] in argon showed stronger precursors at higher densities which is the reverse of what any one-step ground state continuum theory would predict. Dobbins' two-step model[25] and also Murty's[54], on the other hand depict the same experimental trends, though quantitatively they are much far off. In their results the ground state continuum curves are also given which suggest that both one-step and two-step processes coexist atleast in argon gases. However, much work, particularly on the experimental side needs to be done to understand the radiation exchange process in argon and other gases. In the absence of experimentally measured photoionization cross sections, the atom-atom collisional ionization process is considered as the dominant initiating mechanism in the present investigation.

2.5 Inelastic Collision Cross Sections:

In this section the inelastic collision cross sections for the atom-electron and atom-atom collisional excitation will be considered. The first attempt to study the classical atom-electron inelastic collision cross section was made by Thomson in 1912. He described the inelastic collision on the basis of classical mechanics assuming that the collision of a free electron with an atom, takes place in a time short compared to the period of rotation of a bound electron in its orbit so that the latter acquires energy from the impact in the same manner as would a free electron. If an electron with kinetic energy E passes near a target electron, the cross section for the energy transfer to the target in the range ΔE to $\Delta E + d\Delta E$ from classical mechanics is,

$$d\sigma = \frac{\pi e^4}{E} \frac{d\Delta E}{(\Delta E)^2} \tag{2.30}$$

where e is the electron charge. The cross section for the transfer of energy E, greater than a threshold value E_o is therefore,

$$\sigma = \frac{\pi e^4}{E} \int_{E_o}^{E} \frac{d\Delta E}{(\Delta E)^2} = \frac{\pi e^4}{E^2 E_o} (E-E_o) \tag{2.31}$$

For E not far from E_o, eq. (2.31) can be written in the form,

$$\sigma \simeq C (E-E_o) \tag{2.32}$$

where C is a constant and eq. (2.32) implies linear dependence of the reaction cross section on the energy in the center-of-mass coordinate. Most often the value of C has been determined experimentally for various gases. Petschek and Byron[62] in their analysis, determined the value of this C_{ae}** for argon by making a linear approximation to the inelastic cross section data of Maier and Leibnitz[45], where as Wong and Bershader[77] used a two slope linear approximation. In the present work the value of C_{ae} reported by Petschek and Byron[62] has been used.

Experimentally measured values of cross-sections for atom-atom collisional ionization are available in the literature[33,38,39,48]. They assume a linear dependence of cross section on energy and attempt to determine the constant of proportionality using the measured reaction rates. Wong and Bershader[77] attempted to identify the relationship between the cross section and energy. However, as pointed out later by McLaren and Hobson, they seem to have erroneously assumed the constancy of a factor (C_2/p^2) in their expression for the cross section (See eq. (3) of Ref. (77)) whereas C_2/N_a^2 is, infact, found to be the constant term over their range of temperatures. With this modification incorporated, the cross section becomes temperature dependent and is, therefore, not of general applicability. Recently McLaren and Hobson[48] have considered constant, linear and quadratic dependences of the cross section on the

**Subscripts ae refer to atom-electron collisional process and aa refer to atom-atom collisional process.

energy in the center-of-mass system. They have calculated the values of C_{aa} for the three cross sections from the measured reaction rates for different temperatures. Their results show that for linear dependence, C_{aa} varies least with temperature. If the cross section for which C_{aa} changes least with temperature is taken as the criterion, this establishes the credibility of linear cross section. However, as the cross section vs. energy curve has a peak at very high energies after which the cross-section starts falling with increasing energy, the linear approximation will be in error at very high energies. In the present investigation a linear dependence of cross section with relative energy is used assuming that all the particles with energies just greater than I_* result in an inelastic collision and lose their energy and thus will seldom acquire energies much greater than I_*.

Harwell and Jahn[33] have reported a value of $C_{aa} = 7 \times 10^{-19}$ cm^2/eV for argon gas. Morgan and Morrison[50] carried out a theoretical reassessment of the ionization mechanism and later referred to the experiments of Harwell and Jahn with some equipment modification, which showed that the reaction rates reported by Harwell and Jahn were too high. They showed that values of C_{aa} should be reduced by a factor 10 to get the best fit relaxation times measured by Petschek and Byron. Later Kelly[39] from apparatus substantially the same as that of Harwell and Jahn, but with one order higher degree of purity of the gas

arrived at a value for $C_{aa} = 1.2 \times 10^{-19}$ cm^2/eV. McLaren and Hobson[48] in their experiments have incorporated corrections to allow for flow nonuniformities resulting from the effect of boundary layer growth on the shocked gas flow. As reported by McLaren and Hobson, had the appropriate corrections been made, Morgan and Morrison's result would come close to 2.5×10^{-20} cm^2/eV while that of Kelly to 4×10^{-20} cm^2/eV both in good agreement with the value measured by McLaren and Hobson namely $C_{aa} = 2.5 \times 10^{-20}$ cm^2/eV.

In the present work the value $C_{aa} = 2.5 \times 10^{-20}$ cm^2/eV has been used for argon. Since the values corrected for flow nonuniformities are not available elsewhere for other gases, the ratio of the corrected to uncorrected values of C_{aa} is assumed to be the same for all the gases and the values reported by Kelly with the correction applied are used. Since the values of C_{ae} for gases other than argon are not available elsewhere, it is assumed that the ratio C_{ae}/C_{aa} is the same as that of argon for all the gases to evaluate C_{ae} for other gases. This, however, may keep the quantitative results for gases other than Ar in error which of course will not be severe due to the fact that the shock structure is very insensitive to the value of C_{ae}.

2.6 Recombination Mechanism:

Bates, Kingston and McWhirter[7] have studied the general recombination mechanism in a plasma considering all the processes comprising electron capture, electron impact ionization, discrete transitions to distant levels, radiative capture and spontaneous radiative transitions. The collision processes predominant in a dense plasma and the radiative processes predominant in a tenuous plasma are two limiting cases of this general 'impact-radiative recombination' process. The three body collisional recombination process studied by Bates et.al.[7], can be used for gases like argon. In accordance with their model, the upper states tend to equilibrate rapidly with the unbound continuum states. Thus the net recombination rate equals the ground state atom formation by collisional deactivation and spontaneous transitions from excited states as well as by three-body and radiative recombination processes from the continuum. The principal difficulty in evaluating the impact-radiative recombination rate by an appropriate model is that the cross sections and transition probabilities of these processes are unknown. However, in a dense plasma the recombination rate is controlled mainly by collisional transitions to the ground state. In the present analysis, only three-body recombination to ground state is considered assuming all the excited states, in turn, to be in equilibrium. This recombination rate is related to the ionization rate through Saha equation. This assumes the concept of chemical

equilibrium to be preserved in the presence of thermal non-equilibrium. Strictly speaking this assumption is valid under chemical equilibrium but extension to nonequilibrium states are generally accepted. Further, as recombination is important only at the end of the relaxation zone where the electron and plasma temperatures are not very different from the equilibrium temperature, the error arising from this assumption will not be large. Thus the ratio of the recombination rate constant to ionization rate constant for the atom-atom and atom-electron processes K_{aa} and K_{ae}, can be written,

$$\begin{aligned} K_{aa} &= (2Z_+/Z_a)(2\pi m_e kT_a/h^2)^{3/2} \exp(-I/kT_a) \\ K_{ae} &= (2Z_+/Z_a)(2\pi m_e kT_e/h^2)^{3/2} \exp(-I/kT_e) \end{aligned} \qquad (2.33)$$

In the expressions (2.33), Z_+ and Z_a are the electronic partition functions of the singly ionized ion and atom respectively which can be replaced by g_+ and g_a the ground state degeneracies of the ion and atom respectively without much error. Thus eqs. (2.33) reduce to,

$$\begin{aligned} K_{aa} &= (2g_+/g_a)(2\pi m_e kT_a/h^2)^{3/2} \exp(-I/kT_a) \\ K_{ae} &= (2g_+/g_a)(2\pi m_e kT_e/h^2)^{3/2} \exp(-I/kT_e) \end{aligned} \qquad (2.34)$$

2.7 Elastic Collision Cross Sections:

2.7.1 Atom-Atom Elastic Interactions:

Several models have been proposed to represent the interaction between neutral atoms and molecules. A long-range

attractive and short-range repulsive type of force laws with experimentally determined constants have been found to be quite appropriate in describing the macroscopic transport properties of the gases. At high temperatures, what is required is precise information concerning the repulsive part of the interaction since high temperature properties are relatively insensitive to the attractive part. An inverse-power repulsive force law model would be adequate for the high temperatures encountered in shockwaves. Expressions for interaction potentials obtained by fitting curves to the experimentally measured potentials at high temperatures are reported for several gases in references 2, 3, and 4. Amdur and Mason[5] have computed the viscosity of various gases at high temperatures using the potential measurement curves of references 2, 3 and 4. Recent measurements of viscosity by Aeschliman and Cambel[1] are found to be 3 to 10 percent greater than the values reported by Amdur and Mason in the temperature range 3500° - 8500°K. Amdur and Mason also suggested that for high temperatures a more realistic model should include a factor $e^{-\xi/a}$ in the potential. But they did not use it because collision integrals for the exponential potential had not been evaluated at that time. Later computations of Devoto[24] with exponential potentials using the integrals evaluated by Monchick[49] show better agreement of viscosity with Aeschliman and Cambel's values to within 5 percent. It thus appears that the exponential potential may indeed be a more

realistic representation of the collision process. However, the complexity of the integrals involved in the shock structure problem precludes the use of these realistic models so that often simple inverse power potential laws have to be resorted to. We use an inverse-fourth power law of potential in the present work choosing the value of the constant in such a way that this law approximates the potential laws reported in references 2, 3, and 4 with least error in the range of interest. Thus the atom-atom force law is,

$$F = \frac{B_{aa}}{r^5} \tag{2.35}$$

where r is the distance between the two gas atoms during an encounter and B_{aa} is the force law constant.

2.7.2 Atom-Electron Elastic Interactions:

In order to describe the main features of the electron neutral atom interaction, the wave like nature of the electron should be introduced. This wave length called the de Broglie wave length is defined by,

$$\lambda = \frac{h}{mv} \tag{2.36}$$

where v is the total classical velocity including any variation due to the field of the atom. When this wavelength is comparable to atomic dimensions interference phenomena can occur that result in rapid variation of cross section with energy and angle. This effect is called the Ramsauer-Townsend effect. For low electron

temperatures, the long range polarization field can be used effectively. At electron energies for which Ramsauer-Townsend effect becomes important the interaction can no longer be represented by a force law of the polarization type, in which case there exists a Ramsauer minimum for the cross section.

Several investigations both experimental and theoretical have been made, e.g. ref. 28,60,65 and 66 and the cross sections over a range of electron energies are available. However, these cross sections are not easily amenable for analytical handling in such complex problems as the present one, so that approximations have to be resorted to. Since the electron-ion elastic energy transfer is dominant in heating the electron gas over the entire shock except, perhaps, in a narrow region in the beginning, (more so with the assumption of thermal equilibrium between electron and atom gases ahead of the shock) the electron temperature profile is very insensitive to the choice of the atom-electron cross section. Hence, an inverse fourth power law of polarization field is assumed. It should also be noted that in the beginning of the shock where the atom-electron collisional energy transfer is dominant, the electron temperature is low enough to justify neglecting interference effects. Thus, for argon at $T_e \backsim 300^{\circ}K$ the momentum transfer cross section from the polarization law is $\sigma_m/a_o^2 = 8.17$ which compares with the value 8.0 of Pack and Phelps[61]. (O'Malley's[60] results give a value of 14). At $T_e \backsim 1000^{\circ}K$, $\sigma_m/a_o^2 = 1.425$ whereas O'Malley's results give a value of $\backsim 1$.

Table 2.2

Various Properties and Cross Sections for the Gases

Gas	Ar	Kr	Xe
Atomic Wt.	39.948	83.7	131.3
I(eV)	15.7	13.996	12.127
I_*(eV)	11.5	10.0	8.4
*α (cm^3)	1.64×10^{-24}	2.48×10^{-24}	4.02×10^{-24}
B_{aa} (dynes cm^5)	1.124×10^{-42}	2.368×10^{-42}	4.0×10^{-42}
C_{aa} (cm^2/eV)	2.5×10^{-20}	2.92×10^{-20}	3.75×10^{-21}
C_{ae} (cm^2/eV)	7.0×10^{-18}	8.2×10^{-18}	1.0×10^{-18}
**g_a	1.0	1.003	1.043
**g_+	5.6	5.0	4.54

* Ref. 79.

** Ref. 26.

CHAPTER 3

MATHEMATICAL FORMULATION OF THE PROBLEM

3.1 Boltzmann Equation:

The Boltzmann equation is generally used for the description of problems in kinetic theory of gases. This equation involves the quantity $f(\underset{\sim}{x}, \underset{\sim}{c}, t)$, the velocity distribution function, which is the density of the particles in phase space $(\underset{\sim}{x}, \underset{\sim}{c}, t)$ such that $f(\underset{\sim}{x}, \underset{\sim}{c}, t)\ \underset{\sim}{dx}\ \underset{\sim}{dc}$ represents the number of particles at time t in the spatial volume $\underset{\sim}{dx}$ centered at $\underset{\sim}{x}$ whose velocities lie within the interval $\underset{\sim}{dc}$ centered at $\underset{\sim}{c}$. The Boltzmann equation states that Df/Dt, the rate of change of 'f' along the free trajectory of a particle is entirely the result of encounters among the particles. For a group of identical particles this may be written in the form,

$$\frac{Df}{Dt} = \frac{\partial f}{\partial t} + \underset{\sim}{c} \cdot \frac{\partial f}{\partial \underset{\sim}{x}} + \frac{\underset{\sim}{F}}{m} \cdot \frac{\partial f}{\partial \underset{\sim}{c}} = \left(\frac{\delta f}{\delta t} \right)_{coll.} \qquad (3.1)$$

where $\underset{\sim}{F}$ is the external force acting on the particle, m the mass of the particle, and $(\delta f/\delta t)_{coll.}$ represents the change in f at a point $(\underset{\sim}{x}, t)$ in space and time, due to collisions between particles evaluated on the assumption of dilute gases and binary collisions.

The validity of the Boltzmann equation thus derived rather intuitively by Boltzmann (1896) has been reconsidered by many

authors like Yvon (1935), Bogolyubov (1946), Kirkwood (1947), Born and Green (1949), Gross, Grad and Krook (1960),[40]. As long as,

(i) the gas is sufficiently rarefied, so that most of the collisions are binary, and

(ii) the accelerations of particles over macroscopic and microscopic ranges are clearly separable, there seems to be no doubt about the validity of the Boltzmann equation. In the case of a neutral and sufficiently rarefied gas, the low density and the short range forces between particles ensure the above two requirements and the Boltzmann equation is valid.

3.2 Validity of the Boltzmann Equation for Ionized Gases:

In the case of ionized gases, however due to the long range coulomb force that exists between charged particles the above conditions are not satisfied which casts doubts on the validity of the Boltzmann equation. The objection for the use of Boltzmann equation is that the assumption of binary collision does not seem plausible with long range forces and further the total cross section for collisions calculated on this assumption diverges.

To study the justification of the Boltzmann equation for a plasma it is necessary to introduce some representative lengths.

Let,

$\lambda_N = n^{-1/3}$ be the inter-particle distance,

$\lambda_L = \frac{e^2}{\frac{3}{2} kT}$ the Landau distance, and

$\lambda_D = \left(\frac{kT}{8\pi ne^2} \right)^{1/2}$ be the Debye shielding length,

where n is the particle density, e the electron charge, k the Boltzmann Constant and T the temperature of the plasma. The Landau distance gives the distance between two interacting particles, where the potential energy is of the same order as that of the mean thermal energy of a particle and can be interpreted as the mean distance of closest approach of the particles which is equivalent to the diameter of the particle. The Debye distance represents the effective range of two-particle correlations.

The interactions of particles lying within the distance λ_L can be treated as strong interactions while particles lying outside λ_L participate in weak interactions. Forces between particles separated by more than the Debye distance are statistically independent and can be taken care of by the average external force term in the Boltzmann equation. The forces arising from particles closer than λ_N can be conveniently handled by the binary collision term in the conventional Boltzmann equation. There is left the important range of distances between λ_N and λ_D (Fig. 3.1) in which the particles are correlated and yet they cannot be split into pairs for the purpose of binary

collision analysis. The number of such particles ($\sim n\lambda_D^3$) present within λ_D is large, if $n\lambda_D^3$ is large. We introduce the dimensionless parameter g frequently used in literature[40] as,

$$g = \frac{\lambda_N^3}{\lambda_D^3} = \frac{n^{-1}}{\lambda_D^3} \sim \frac{1}{n\lambda_D^3}$$

Thus g is a representative of the number of particles present in the Debye sphere. In most practical cases g is found to be small[40] so that there are a large number of particles within the Debye sphere and outside λ_N. In this case, since

$$g = \frac{\lambda_N^3}{\lambda_D^3} \sim \frac{n^{-1}}{\left(\frac{kT}{ne^2}\right)^{3/2}} \sim \frac{n^{1/2}}{\lambda_L^{-3/2}} \sim \left(\frac{\lambda_L}{\lambda_N}\right)^{3/2},$$

we have $\lambda_L < \lambda_N$ and hence weak interactions result from particles lying in $\lambda_N < \lambda < \lambda_D$. Thus the omitted range $\lambda_N < \lambda < \lambda_D$ is characterized by the super-position of many 'grazing' deflections. Treating these weak interactions as a stochastic process with many simultaneous independent small deflections, the resultant contribution to the Boltzmann equation can be shown to be the Fokker-Planck term which is a second order differential operator in addition to the integral operator which arises from strong binary collisions[21]. Making a 'grazing' collision approximation, assuming a sequence in time of the independent random 'binary' deflections, the Boltzmann collision term can be evaluated in the region $\lambda_N < \lambda < \lambda_D$, yielding exactly the same Fokker-Planck term as in the earlier method[21].

The justification that has been given for the use of Fokker-Planck equation is incomplete and any analysis which demonstrates the validity of Fokker-Planck equation also seems to justify the validity of the binary collision Boltzmann equation in this round about way. Then the simplest procedure seems to be to include in the Boltzmann term 'grazing' deflections out to the distance λ_D instead of taking a sum of Boltzmann and Fokker-Planck terms. Thus, though the validity of the Boltzmann equation for fully ionized gases is still open for investigation, the use of λ_D as a cutoff distance in evaluating the collision terms seems to be a good approximation. (In the present investigation, g evaluated in the downstream equilibrium region takes values ranging from $\sim$ 0.01 to 1 and it may however take lower values in the earlier regions of the shock where the charge densities are much less than in the equilibrium region). A simple method of obtaining convergent integrals is to use the Debye-Huckel potential instead of the coulomb potential.

3.3 Extension of the Boltzmann Equation for a Mixture:

If the gas under consideration contains m different components, the Boltzmann equation can easily be extended as follows, under the same restrictions of validity. If $f_j(\underset{\sim}{x}, \underset{\sim}{c}, t)$ represents the velocity distribution function for the j-th component (j = 1, 2, ... m) then the Boltzmann equation for a non-reacting gas mixture can be written as[15],

$$\frac{\partial f_j}{\partial t} + \underset{\sim}{c} \cdot \frac{\partial f_j}{\partial \underset{\sim}{x}} + \frac{\underset{\sim}{F}_j}{m_j} \cdot \frac{\partial f_j}{\partial \underset{\sim}{c}} = \sum_{k=1}^{n} J_{jk} \qquad (3.2)$$

where J_{jk} is the collision integral for scattering of particles of type j due to collision with particles of type k. (k = 1,2, ...m). For a reactive mixture, the inelastic collision terms are to be included in addition to the elastic terms. The Boltzmann equation can be written for the reactive case as,

$$\frac{\partial f_j}{\partial t} + \underset{\sim}{c} \cdot \frac{\partial f_j}{\partial \underset{\sim}{x}} + \frac{\underset{\sim}{F}_j}{m_j} \cdot \frac{\partial f_j}{\partial \underset{\sim}{c}} = \sum_{k=1}^{n} J^e_{jk} + J^i_{jk} \qquad (3.3)$$

where the superscripts e and i stand for elastic and inelastic collisions respectively.

3.4 Boltzman Equation for an Ionized Gas:

Let $f_a(\underset{\sim}{x}, \underset{\sim}{c}\ t)$, $f_e(\underset{\sim}{x}, \underset{\sim}{c}\ t)$ and $f_i(\underset{\sim}{x}, \underset{\sim}{c}\ t)$ represent the velocity distribution functions for atoms, electrons and ions respectively. Then the Boltzmann equations for the three species can be separately written as follows,

$$\frac{Df_a}{Dt} = \langle f_a f_a \rangle^e + \langle f_a f_e \rangle^e + \langle f_a f_i \rangle^e + \langle f_a f_a \rangle^i + \langle f_a f_e \rangle^i + \langle f_a f_i \rangle^i + \langle f_i f_e \rangle^i \qquad (3.4)$$

$$\frac{Df_e}{Dt} = \langle f_e f_a \rangle^e + \langle f_e f_e \rangle^e + \langle f_e f_i \rangle^e + \langle f_e f_a \rangle^i + \langle f_e f_i \rangle^i + \langle f_a f_a \rangle^i + \langle f_a f_i \rangle^i \qquad (3.5)$$

$$\frac{Df_i}{Dt} = \langle f_i f_a \rangle^e + \langle f_i f_e \rangle^e + \langle f_i f_i \rangle^e + \langle f_e f_a \rangle^i + \langle f_e f_i \rangle^i + \langle f_a f_a \rangle^i + \langle f_a f_i \rangle^i \qquad (3.6)$$

where the significance of each term on the right hand side is discussed in the following.

3.5 Collision Terms:

In this section the significance of the various elastic and inelastic collision terms is explained and integral forms of the various terms are given. A detailed evaluation of these integrals follows in Chapter 4.

3.5.1 Elastic Collisions:

In general, we write $\langle f_j f_k \rangle^e$ representing the rate of change of f_j, the distribution function of the particles denoted by subscripts j (at a fixed point $\underset{\sim}{x}$, along its trajectory) due to elastic encounters of j particles with particles k. k equal to j is also included. (j,k = a, e, i). Schematically the process can be described in the following manner,

$$A_j\ (\underset{\sim}{c}_j) + A_k(\underset{\sim}{c}_{k1}) \rightarrow A_j(\underset{\sim}{c}'_j) + A_k(\underset{\sim}{c}'_{k1}) \qquad (3.7)$$

where $\underset{\sim}{c}_j$ and $\underset{\sim}{c}_k$ are the pre-collision velocities of the j-particles and k-particles respectively before the encounter and $\underset{\sim}{c}'_j$ and $\underset{\sim}{c}'_{k1}$ represent the corresponding velocities after the elastic interaction. The symbol 'A' represents the particle.

A general expression for any elastic collision comprises of both loss and gain terms, because during encounters some j-particles disappear from the volume $d\underset{\sim}{c}_j$ centered at $\underset{\sim}{c}_j$, (in phase space) and some other particles of j type reenter this volume. For a process such as the one described above schematically in (3.7) the general collision term can be

written as

$$\langle f_j f_k \rangle^e = \int [f_j(\underset{\sim}{c}_j') f_k(\underset{\sim}{c}_{k1}') - f_j(\underset{\sim}{c}_j) f_k(\underset{\sim}{c}_{k1})] \sigma_{jk}^e g \, d\underset{\sim}{c}_{k1} \quad ..(3.8)$$

where σ_{jk}^e is the elastic collision cross section for the j-k encounter. In general σ_{jk}^e is a function of $\underset{\sim}{c}_j$, $\underset{\sim}{c}_{k1}$ and the parameters that describe the encounter in the physical space, viz. the impact parameter b and the azimuthal angle ϵ of the encounter; it also depends upon the interaction force law; $g = |\underset{\sim}{c}_j - \underset{\sim}{c}_{k1}|$ is the relative speed of the pair of incoming particles j, k. For an elastic collision, as there is no exchange of energy between various degrees of freedom, the kinetic energy of the particles in the center-of-mass coordinates remains invariant during a collision. Consequently, the relative speed of the particles after the encounter is equal to their relative speed before the encounter. Thus,

$$g = |\underset{\sim}{c}_j - \underset{\sim}{c}_{k1}| = |\underset{\sim}{c}_j' - \underset{\sim}{c}_{k1}'| \quad (3.9)$$

Subscript 1 in $\underset{\sim}{c}_{k1}$ is used for convenience. The variable with this subscript 1 is a dummy variable and disappears after the integration is performed.

3.5.2 Inelastic Collision Terms:

(1) $\langle f_a f_a \rangle^i$: Represents the rate at which f_a decreases as a result of loss of atoms in an inelastic atom-atom collision of this type. When two atoms collide with sufficient energy, they may give rise

to ionization of one of the atoms resulting in the creation of an ion and an electron so that one atom is effectively lost. Schematically we can represent this type of collision as follows,

$$A(\underset{\sim}{c}_a) + A(\underset{\sim}{c}_{a1}) \rightarrow A^+(\underset{\sim}{c}'_i) + A(\underset{\sim}{c}'_{a1}) + e(\underset{\sim}{c}'_{e1})$$

where $\underset{\sim}{c}_a$ and $\underset{\sim}{c}_{a1}$ are the velocities of atoms before encounter and $\underset{\sim}{c}'_i$, $\underset{\sim}{c}'_{a1}$, $\underset{\sim}{c}'_{e1}$ are the velocities after encounter of the ion, atom and the electron respectively. The expression for the collision integral can be written as,

$$\langle f_a f_a \rangle^i = - \int f_a(\underset{\sim}{c}_a) f_a(\underset{\sim}{c}_{a1}) \sigma^i_{aa} g \, d\underset{\sim}{c}_{a1} \; ; \; g \geq g_{oa} \qquad \ldots (3.10)$$

where σ^i_{aa} is the cross section relevant to atom-atom collisional ionization, and $g = |\underset{\sim}{c}_a - \underset{\sim}{c}_{a1}|$; g_{oa} is the threshold value given by $\frac{1}{2} \mu_{aa} g^2_{oa} = I$. I is the ionization potential of the atom (more appropriately the excitation potential to the first excited state of the atom) and $\mu_{aa} = \frac{m_1 m_2}{m_1 + m_2}$ reduced mass of the system ($= \frac{1}{2} m_a$ since $m_1 = m_2 = m_a$).

(2) $\langle f_a f_e \rangle^i$: Represents the rate at which f_a decreases resulting from the loss of atoms as they get ionized by electron impacts. When an electron bombards an atom with sufficient kinetic energy there is a

possibility of the atom getting ionized resulting in an ion and an electron. The consequent disappearance of the atom is described by this loss term. This type of collision may be schematically represented by,

$$A(\underset{\sim}{c}_a) + e_1(\underset{\sim}{c}_{e1}) \rightarrow A^+(\underset{\sim}{c}_i') + e_1(\underset{\sim}{c}_{e1}') + e_2(\underset{\sim}{c}_{e2}')$$

where $\underset{\sim}{c}_a$ and $\underset{\sim}{c}_{e1}$ are the precollision velocities of the atom and electron respectively and $\underset{\sim}{c}_i'$, $\underset{\sim}{c}_{e1}'$, $\underset{\sim}{c}_{e2}'$ are the post collision velocities of the resulting particles viz. ion and the two electrons respectively. One electron plays a sort of dummy role in the process similar to that of an atom in $\langle f_a f_a \rangle^i$. The expression for the collision integral describing this process can be written as,

$$\langle f_a f_e \rangle^i = -\int f_a(\underset{\sim}{c}_a) f_e(\underset{\sim}{c}_{e1}) \sigma_{ae}^i \; g \; d\underset{\sim}{c}_{e1}; \; g \geq g_{oe} \qquad (3.11)$$

where σ_{ae}^i is the collision cross section for the atom-electron collision resulting in ionization of the atom and $g = |\underset{\sim}{c}_1 - \underset{\sim}{c}_{e1}|$; g_{oe} is the threshold value given by $\frac{1}{2}\mu_{ae} g_{oe}^2 = I$, $\mu_{ae} = \left(\frac{m_a m_e}{m_a + m_e}\right)$ being the reduced mass of the system; $\mu_{ae} \simeq m_e$ since $m_e << m_a$; m_a and m_e mentioned above are the masses of atom and electron respectively.

(3) $\langle f_a f_i \rangle^i$: Represents the rate at which f_a changes due to collisions between atoms and ions resulting in

the ionization of the atom. Schematically this process can be represented by,

$$A(\underset{\sim}{c}_a) + A^+(\underset{\sim}{c}_{i1}) \rightarrow A^+(\underset{\sim}{c}'_i) + A^+(\underset{\sim}{c}'_{i1}) + e(\underset{\sim}{c}'_e)$$

where $\underset{\sim}{c}_a$ and $\underset{\sim}{c}_{i1}$ are the precollision velocities of the atom and ion respectively and $\underset{\sim}{c}'_i$, $\underset{\sim}{c}'_e$, are the post-collision velocities of the newly born ion and electron respectively and $\underset{\sim}{c}'_{i1}$ is the post collision velocity of the dummy ion which participated in the collision. This term has been neglected in the present studies; (see Section 4.4.1).

(4) $\langle f_i f_e \rangle^i$: This represents the rate at which f_a increases due to the recombination collisions between ions and electrons, resulting in the formation of new atoms. This process is the inverse process of (2) above in which three bodies participate. A third dummy particle, an electron in most cases, serves the purpose of transferring the required energy in the process. Schematically the process may be represented as follows,

$$A^+(\underset{\sim}{c}'_i) + e_1(\underset{\sim}{c}'_e) + e_2(\underset{\sim}{c}'_{e1}) \rightarrow A(\underset{\sim}{c}_a) + e_2(\underset{\sim}{c}_{e1})$$

where $\underset{\sim}{c}_a$ and $\underset{\sim}{c}_{e1}$ are the velocities after collision of the resulting atom and the dummy electron respectively; $\underset{\sim}{c}'_i$, $\underset{\sim}{c}'_e$, $\underset{\sim}{c}'_{e1}$ are the velocities before

collision of the incoming ion, the electron to be captured and the dummy electron respectively. Only those combinations of $\underset{\sim}{c}'_i$, $\underset{\sim}{c}'_e$ and $\underset{\sim}{c}'_{e1}$ that result in $\underset{\sim}{c}_a$ for the final atom are considered. The contributions arising from the recombination processes can be obtained from the corresponding ionization processes (see Section 2.6).

(5) $\langle f_e f_a \rangle^i$: Represents the rate at which f_e changes due to collisions between atoms and electrons resulting in the ionization of the atom. In this case there are loss as well as gain terms. If the electrons having velocities in $d\underset{\sim}{c}_e$ around $\underset{\sim}{c}_e$ participate in this type of collision, they will be scattered out of their original phase volume causing in effect a loss term for f_e. On the other hand, a few of the electrons created in this process may have velocities lying in $d\underset{\sim}{c}_e$ around $\underset{\sim}{c}_e$ appearing as a gain term for f_e. The process may be schematically represented as follows,

a) gain: $A(\underset{\sim}{c}'_{a1}) + e_1(\underset{\sim}{c}'_{e1}) \rightarrow A^+(\underset{\sim}{c}_{i1}) + e_1(\underset{\sim}{c}_{e1}) + e_2($

b) loss: $A(\underset{\sim}{c}_{a1}) + e_1(\underset{\sim}{c}_e) \rightarrow A^+(\underset{\sim}{c}'_{i1}) + e_1(\underset{\sim}{c}'_e) + e_2(\underset{\sim}{c}'_e$

In (a) $\underset{\sim}{c}'_{a1}$ and $\underset{\sim}{c}'_{e1}$ are the velocities of atom and electron before collision which result in the creation of a new electron whose velocity lies in $d\underset{\sim}{c}_e$ around $\underset{\sim}{c}_e$; $\underset{\sim}{c}_{i1}$ and $\underset{\sim}{c}_{e1}$ are the velocities after

the collision of the ion and the dummy electron respectively. In (b) $\underset{\sim}{c}_{a1}$ and $\underset{\sim}{c}_e$ are the velocities of the atom and the electron before collision and $\underset{\sim}{c}'_{i1}$, $\underset{\sim}{c}'_e$ and $\underset{\sim}{c}'_{e1}$ are the velocities of the ion, the dummy electron and the newly born electron, respectively, after the collision. The collision integrals may be written separately for gain and loss cases as follows,

$$\langle f_e f_a \rangle^i_{gain} = \int f_a(\underset{\sim}{c}'_{a1}) f_e(\underset{\sim}{c}'_{e1}) \sigma^i_{ae}\, g' \underset{\sim}{dc}'_{e1}; \qquad g' \geq g_{oe} \tag{3.12a}$$

$$\langle f_e f_a \rangle^i_{loss} = -\int f_e(\underset{\sim}{c}_e) f_a(\underset{\sim}{c}_{a1}) \sigma^i_{ae}\, g\, \underset{\sim}{dc}_{a1}; \qquad g \geq g_{oe} \tag{3.12b}$$

where σ^i_{ae} is the cross-section for atom-electron collisional ionization and g', g the relative speed of the incoming particles.

(6) $\langle f_e f_i \rangle^i$: Represents the rate of change of f_e due to electrons participating in the ion-electron recombination process. This contains both gain and loss terms. The loss term appears because an electron disappears in each such collision. If the dummy electron which participates in the collision has a velocity before collision lying in $\underset{\sim}{dc}_e$ around $\underset{\sim}{c}_e$, then this can also be counted for the loss term. If the dummy electron acquires a

velocity lying in $\underset{\sim}{dc}_e$ at $\underset{\sim}{c}_e$ after the collision it is to be treated as a gain term. The process is schematically represented as follows;

(a) gain: $A^+(\underset{\sim}{c}'_{i1})+e_1(\underset{\sim}{c}'_{e1})+e_2(\underset{\sim}{c}'_e) \rightarrow A(\underset{\sim}{c}_{a1})+e_2(\underset{\sim}{c}_e)$

(b) loss: $A^+(\underset{\sim}{c}_{i1})+e_1(\underset{\sim}{c}_e)+e_2(\underset{\sim}{c}_{e1}) \rightarrow A(\underset{\sim}{c}'_{a1})+e_2(\underset{\sim}{c}'_{e1})$

$A^+(\underset{\sim}{c}_{i1})+e_1(\underset{\sim}{c}_{e1})+e_2(\underset{\sim}{c}_e) \rightarrow A(\underset{\sim}{c}'_{a1})+e_2(\underset{\sim}{c}'_e)$

where in (a) $\underset{\sim}{c}'_{i1}$, $\underset{\sim}{c}'_{e1}$ and $\underset{\sim}{c}'_e$ are the velocities before collision of the ion, the electron to be captured and the dummy electron respectively; $\underset{\sim}{c}_{a1}$ and $\underset{\sim}{c}_e$ are the velocities after collision of the atom and the dummy electron respectively; in (b) $\underset{\sim}{c}_{i1}$, $\underset{\sim}{c}_e$ and $\underset{\sim}{c}_{e1}$ are the velocities before collision of the ion, the electron to be captured and the dummy electron respectively where as $\underset{\sim}{c}'_{a1}$ and $\underset{\sim}{c}'_{e1}$ are the velocities after the collision of the atom and the dummy electron; in the second equation of (b), $\underset{\sim}{c}_{i1}$, $\underset{\sim}{c}_{e1}$ and $\underset{\sim}{c}_e$ stand for the velocities before collision of the ion, the electron to be captured and the dummy electron respectively; $\underset{\sim}{c}'_{a1}$, $\underset{\sim}{c}'_e$ represent the post collision velocities of the atom and the dummy electron respectively.

(7) $\langle f_a f_a \rangle^i$: Represents the rate at which f_e increases following creation of new electrons during an atom-atom collision resulting in ionization. The process can

be schematically represented as follows,

$$A(\underset{\sim}{c}'_a)+A(\underset{\sim}{c}'_{a1}) \rightarrow A^+(\underset{\sim}{c}_i)+A(\underset{\sim}{c}_{a1})+e(\underset{\sim}{c}_e),$$

where $\underset{\sim}{c}'_a$ and $\underset{\sim}{c}'_{a1}$ are the velocities before collision of the two incoming atoms; $\underset{\sim}{c}_i$, $\underset{\sim}{c}_{a1}$, $\underset{\sim}{c}_e$ are the velocities after collision of the ion, the dummy atom and the newly born electron respectively. The expression for the collision integral can be written as

$$\langle f_a f_a \rangle^i = \int f_a(\underset{\sim}{c}'_a) f_a(\underset{\sim}{c}'_{a1}) \sigma^i_{aa}\, g' d\underset{\sim}{c}'_{a1}; \quad g' \geq g_{oa} \qquad (3.13)$$

where σ^i_{aa} is the cross section for atom-atom collision that results in ionization and $g' = |\underset{\sim}{c}'_a - \underset{\sim}{c}'_{a1}|$.

(8) $\langle f_a f_i \rangle^i$: Represents the rate at which f_e changes due to generation of electrons followed by atom-ion collision resulting in ionization. This term is ignored following the arguments given in Section (4.4.1).

(9) $\langle f_e f_a \rangle^i$: Represents the rate of increase of f_i due to ions being created in the atom-electron collisional ionization process. Schematically this process can be represented as follows,

$$A(\underset{\sim}{c}'_a)+e_1(\underset{\sim}{c}'_{e1}) \rightarrow A^+(\underset{\sim}{c}_i)+e_1(\underset{\sim}{c}_{e1})+e_2(\underset{\sim}{c}_{e2})$$

where $\underset{\sim}{c}'_a$ and $\underset{\sim}{c}'_{e1}$ are the velocities of the atom

and the electron before the collision and $\underset{\sim}{c}_i$, $\underset{\sim}{c}_{e1}$, $\underset{\sim}{c}_{e2}$ are the velocities of the ion, and the two electrons after the impact respectively. The expression for the collision integral may be written as

$$\langle f_e f_a \rangle^i = \int f_a(\underset{\sim}{c}'_a) f_e(\underset{\sim}{c}'_{e1}) \sigma^i_{ae} \, g' \, d\underset{\sim}{c}'_{e1} \; ; \quad g' \geq g_{oe} \qquad (3.14)$$

where σ^i_{ae} is the cross section defined in (2) above, and $g' = |\underset{\sim}{c}'_a - \underset{\sim}{c}'_{e1}|$.

(10)$\langle f_e f_i \rangle^i$: Represents the rate at which f_i decreases due to the disappearance of ions in the ion-electron recombination process resulting in a neutral atom. This is the three body interaction process described in (4). Schematically the process can be represented as,

$A^+(\underset{\sim}{c}_i) + e(\underset{\sim}{c}_{e1}) + e(\underset{\sim}{c}_{e2}) \rightarrow A(\underset{\sim}{c}'_{a1}) + e(\underset{\sim}{c}'_{e1})$

where $\underset{\sim}{c}_i$, $\underset{\sim}{c}_{e1}$ and $\underset{\sim}{c}_{e2}$ are the velocities before collision of the ion and the two electrons; $\underset{\sim}{c}'_{a1}$ and $\underset{\sim}{c}'_{e1}$ are the velocities of the newly formed atom and the dummy electron respectively.

(11)$\langle f_a f_a \rangle^i$: Represents the rate of increase of f_i due to the creation of ions in atom-atom collisional ionization. Schematically this process may be represented by

$$A(\underset{\sim}{c}'_a)+A(\underset{\sim}{c}'_{a1}) \rightarrow A^+(\underset{\sim}{c}_i)+A(\underset{\sim}{c}_{a1})+e(\underset{\sim}{c}_{e1})$$

where $\underset{\sim}{c}'_a$ and $\underset{\sim}{c}'_{a1}$ are the velocities before impact of the two incoming atoms; $\underset{\sim}{c}_i$, $\underset{\sim}{c}_{a1}$, $\underset{\sim}{c}_{e1}$ are the velocities after collision of the ion, the dummy atom and the electron created respectively. The collision integral may be written as follows,

$$\langle f_a f_a \rangle^i = \int f_a(\underset{\sim}{c}'_a) f_a(\underset{\sim}{c}'_{a1}) \sigma^i_{aa}\, g' d\underset{\sim}{c}'_{a1};$$

$$g' \geq g_{oa} \qquad (3.15)$$

where σ^i_{aa} is the cross section defined in (1) and $g' = |\underset{\sim}{c}'_a - \underset{\sim}{c}'_{a1}|$.

(12) $\langle f_a f_i \rangle^i$: Represents the rate at which f_i changes due to any possible creation of ions in the atom-ion collisional ionization process. Following the arguments of Section (4.4.1) this term is neglected.

CHAPTER 4

GOVERNING DIFFERENTIAL EQUATIONS

In this chapter suitable functional forms for the distribution functions referred to in Chapter 3 for the three species and the appropriate moment functions are chosen. For the choice of these and the collision cross sections from Chapter 2, the collision integrals of the integro-differential moment equations are evaluated analytically so that the system of equations reduces to a set of nonlinear first order ordinary differential equations. The boundary conditions relevant to the problem are also discussed.

4.1 Distribution Function for the Atom Gas:

It is well known that a bimodal distribution function of Mott-Smith type can adequately describe the nonequilibrium region inside a strong shock wave even though it does not represent an exact solution of the Boltzmann equation even at infinite Mach number[55]. Apart from its simplicity there are other reasons to continue the bimodal ansatz for the description of the shockwave. The exact solutions of the B-G-K model equation[17] suggest that the true distribution function does resemble the Mott-Smith's ansatz although later detailed asymptotic studies show that it is unlikely to be an exact solution.

Ananthasayanam and Narasimha[6] have shown for the B-G-K model that the bimodal ansatz can give reliable estimates of the density-slope shock thickness provided suitable criteria are employed. Recently Bird[13] employed a direct computer simulation Monte-Carlo technique to study the structure of strong shock waves. The velocity distribution function within the shock wave has been illustrated by computer display photographs with the molecules represented as dots in the velocity space. This result of Bird gives qualitative support to the bimodal model. However, Bird's results predict a certain degree of asymmetry in the density profiles contrary to the bimodal prediction, though the ansatz can predict reasonably the maximum-density shock thickness profiles.

The bimodal ansatz is more general than that originally given by Mott-Smith[51] in as much as the parameters describing the two Maxwellians are functions of x. It can be shown that in an inert gas problem, in which the collision terms of the differential forms of the equation of continuity, momentum and energy are zero, the choice of these parameters is not completely arbitrary; and if the parameters of one of the Maxwellians are considered as constants, then it is imperative that the other two also should be constants for consistency. However, when the inelastic collisions present make the collision terms of the conservation equations nonzero, it will be possible to consider the parameters of one of the Maxwellians as constants

corresponding to the upstream equilibrium conditions, keeping the parameters of the other Maxwellians as functions of x.

The original physical idea of Mott-Smith namely, that the state of a point within the shock wave can be described by considering the point to be characterised by a certain number of molecules of upstream equilibrium region and a certain number of the downstream equilibrium region has been extended by Haight and Lundgren[30-32] to the study of shock wave structure in diatomic gases taking the excitation of rotational degrees of freedom into account. Haight and Lundgren considered a trimodal distribution function, two Maxwellians of the three being characterised by one upstream and one downstream equilibrium regions; the third Maxwellian is characterised by an intermediate equilibrium state defined by permitting only the excitation of the translational degrees of freedom, while the energy in the rotational degrees is unchanged. The trimodal distribution function is then a sum of three Maxwellians with weighting functions dependent on x, and the parameters characterising the Maxwellians being constants. The hypothesis of a trimodal distribution function is essentially an extension of Mott-Smith's bimodal theory for a monatomic gas and consequently is most applicable to strong shock waves. So far the trimodal ansatz has only been sporadically accepted. In what follows, a trimodal distribution function for the atom gas is assumed where the two Maxwellians are characterised by the two equilibrium

regions upstream and downstream, and the third is characterised by an inert gas equilibrium state where only translational degrees would be excited. The atom distribution function can be written as,

$$f_a = \sum_j n_j(x)\, f_j \; ; \qquad j = 1, 2, 3. \tag{4.1}$$

where $n_j(x)$'s are the weight functions, and

$$f_j = (\pi\beta_j)^{-3/2} \exp\left[-(\underset{\sim}{c}_a - U_j \hat{i})^2/\beta_j\right] \; ; \tag{4.2}$$

$\underset{\sim}{c}_a$ is the molecular velocity for the atoms, and β_j is defined by,

$$\beta_j = 2kT_j/m_a \; . \tag{4.3}$$

In eq. (4.3), m_a is the mass of an atom and k the Boltzmann constant. U_j and T_j in the above expressions represent the mass velocities and temperatures of the atom gas.

Subscripts 1 represent the quantities corresponding to upstream equilibrium condition,

2 correspond to intermediate fictitious state where only the translational degrees get completely excited (corresponding to the downstream equilibrium in an inert monatomic gas) and

3 correspond to the downstream equilibrium state;

$\hat{i}$ is a unit vector in x-direction, representing the direction of the flow.

4.2 Electron and Ion Distribution Functions:

Petschek and Byron[62] have argued that a Maxwellian distribution can be assumed to exist in an electron gas if an electron has appreciably more than one collision with another electron for every 10^5 collisions with atoms; this requires a degree of ionization greater than 10^{-8}. Within the realm of the present work the electron gas as well as the ion gas are each assumed to have Maxwellian distribution functions, which can be written as,

$$f_e = n_e(x)\,(\pi\beta_e(x))^{-3/2} \exp\left[-(\underset{\sim}{c}_e - U_e(x)\hat{i})^2/\beta_e\right] \quad (4.4)$$

and

$$f_i = n_i(x)\,(\pi\beta_i(x))^{-3/2} \exp\left[-(\underset{\sim}{c}_i - U_i(x)\hat{i})^2/\beta_i\right], \quad (4.5)$$

where $\underset{\sim}{c}_e$ and $\underset{\sim}{c}_i$ are the absolute velocity vectors of the electrons and ions respectively; β is defined by

$$\beta_p = 2kT_p/m_p \quad , \qquad p = e, i \quad . \quad (4.6)$$

Subscripts e and i stand for electron and ion respectively; $n_p(x)$, $U_p(x)$ and $T_p(x)$ are the number density, mass velocity and temperature of the p species respectively and m_p is the mass of the p particle.

4.3 Moment Functions:

It has seldom been possible to solve the Boltzmann equation for the distribution function f, and most often only a set of moment equations obtained by taking moments with suitable functions $\phi(\underset{\sim}{c})$, of the Boltzmann equation have been solved to

describe the unknown parameters in the assumed form of distribution function. Amongst the choice of moment functions $\phi(\underset{\sim}{c})$, $\phi(\underset{\sim}{c}) = 1$, c_x and c^2 result in the familiar conservation equations of mass, momentum and energy. The difficulty that has been faced todate right from Mott-Smith's work is the insufficiency of the number of equations to determine all the unknowns of the problem with these moments. Mott-Smith used an additional $\phi(\underset{\sim}{c})$ to complete the solution by choosing c_x^2 and c_x^3 in his analysis. Attempts by Sakurai[71], Rosen[69] and others did not yield much so far as eliminating this ambiguity is concerned,as pointed out by Gustafson[29] and Narasimha[56]. Nevertheless it is felt that the choice of c_x^2 seems to give closer estimates of the density profile shock thicknesses, though there is no rigorous justification for the choice of c_x^2. Narasimha and Deshpande[55] from their minimum error solutions have recently concluded that c_x^3 results should be better than c_x^2 particularly for higher Mach numbers. However, their method is not free from certain arbitrariness either, since the definition of the 'error' itself is not unique. The present work continues with the choice of c_x^2, from the point of view of simplicity over the minimum error methods. Bird's results[13] also seem to support to the choice of c_x^2. It should be noticed, as highlighted by Rode and Tanenbaum[68] that the solution is highly sensitive to the choice of $\phi(\underset{\sim}{c})$.

4.4 Governing Differential Equations:

Expressions (4.1), (4.4) and (4.5) can be substituted in the equations (3.4), (3.5) and (3.6). Using the linear cross sections from Sections (2.5), (2.6) and (2.7) various moment equations can be derived.

4.4.1 Number Conservation Equation for Atoms:

As the elastic collisions do not result in any change in the number of particles of any species, the elastic collision contribution is zero. The atom-ion collisional ionization is neglected through out, though, this cross section is of the same order as atom-atom collisional ionization cross section. This is justifiable because in the atom-electron collision dominated region it is as insignificant as atom-atom collisional process and in the atom-atom collision dominated region the ion population is too far less to compete with the atom-atom process.

Integrating equation (3.4) over the $\underset{\sim}{c}_a$ space, we get,

$$\frac{d}{dx}\left[\sum_j n_j U_j\right] = \sum_{k=1}^{4} \Delta\phi_k \qquad (4.7)$$

where the $\Delta\phi_k$'s are as given below,

$\Delta\phi_1$ = rate at which atoms are lost due to atom-atom inelastic collisions,

$$= -\frac{1}{2}\int f_a f_{a1} \sigma^{i}_{aa}\, g\, d\underset{\sim}{c}_a\, d\underset{\sim}{c}_{a1} \; ; \quad g \geq g_{oa} .$$

The factor 1/2 is included to account for the duplication of collisions. Using,

$$\sigma^{i}_{aa} = \frac{1}{2}\mu_{aa}\, C_{aa}\,(g^2-g_{oa}^2) = \frac{1}{4}\, m_a\, C_{aa}\,(g^2-g_{oa}^2)\,, \quad (4.8)$$

$$\Delta\phi_1 = -\frac{1}{8}\, m_a\, C_{aa} \int \left\{ \sum_j n_j(\pi\beta_j)^{-3/2} \exp\left[-(\underset{\sim}{c}_a - U_j\hat{i})^2/\beta_j\right]\right\}$$
$$\cdot \left\{\sum_k n_k(\pi\beta_k)^{-3/2} \exp\left[-(\underset{\sim}{c}_{a1}-U_k\hat{i})^2/\beta_k\right]\right\} (g^2-g_{oa}^2)\, g\, \underset{\sim}{dc}_a \underset{\sim}{dc}_a$$

Using the results of Appendix A-I,

$$\Delta\phi_1 = -\frac{1}{16\sqrt{\pi}}\, m_a\, C_{aa} \sum_j \sum_k n_j n_k\, \beta_{jk}^{3/2}\, F_1\left(\frac{U_{jk}}{\sqrt{\beta_{jk}}}\,,\ \frac{g_{oa}}{\sqrt{\beta_{jk}}}\right) \quad (4.9)$$

where,

$$F_1(U,V) = \sqrt{\pi}\left\{\mathrm{Erf}(V+U)-\mathrm{Erf}(V-U)\right\}\left[U^3+(3-V^2)U + \left(\frac{3}{4}-\frac{V^2}{2}\right)\frac{1}{U}\right]$$
$$+ \exp\left[-(U^2+V^2)\right]\left[(2U^2+5)\cosh 2UV + (2U^2+3)\,\frac{V}{U}\sinh 2UV\right] \quad (4.10)$$

and,

$$F_1(0, V) = 4(2+V^2)\exp(-V^2)\ ;$$
$$U_{jk} = U_j - U_k \quad \text{and} \quad \beta_{jk} = \beta_j + \beta_k \quad (4.11)$$
$$\Delta\phi_2 = \text{rate at which atoms are lost due to atom-electron inelastic collisions,}$$
$$= -\int f_a f_e\, \sigma^{i}_{ae}\, g\, \underset{\sim}{dc}_e \underset{\sim}{dc}_a;\quad g \geq g_{oe}\,.$$

Using

$$\sigma^{i}_{ae} = \frac{1}{2}\mu_{ae}\, C_{ae}\,(g^2-g_{oe}^2) \doteq \frac{1}{2}\, m_e\, C_{ae}\,(g^2-g_{oe}^2), \quad (4.12)$$
$$\Delta\phi_2 = -\frac{1}{2}\, m_e\, C_{ae} \int \left\{\sum_j n_j(\pi\beta_j)^{-3/2} \exp\left[-(\underset{\sim}{c}_a - U_j\hat{i})^2/\beta_j\right]\right\}$$
$$\cdot\ n_e(\pi\beta_e)^{-3/2} \exp\left[-(\underset{\sim}{c}_e - U_e\hat{i})^2/\beta_e\right]$$
$$\cdot\ (g^2-g_{oe}^2)\, g\, \underset{\sim}{dc}_a \underset{\sim}{dc}_e\,.$$

Using the results from Appendix A-I for the integrals, the expression for $\Delta\phi_2$ can be written as,

$$\Delta\phi_2 = -\frac{1}{4\sqrt{\pi}} m_e C_{ae} n_e \sum_j n_j \beta_{je}^{3/2} F_1 \left(\frac{U_{je}}{\sqrt{\beta_{je}}}, \frac{g_{oe}}{\sqrt{\beta_{je}}}\right) \quad (4.13)$$

where,

$$U_{je} = U_j - U_e \text{ and } \beta_{jc} = \beta_j + \beta_e . \quad (4.14)$$

$\Delta\phi_3$ = rate at which atoms are created as a result of recombination between atom-ion-electron, and can written from eqs. (2.34) as,

$$= -\Delta\phi_1 \left[4\pi^{3/2} \frac{g_a}{g_+} \frac{\hbar^3}{m_e^3} \varepsilon^{3/2} \frac{1}{\beta_a^{3/2}} \exp\left(g_{oa}^2/2\beta_a\right) \cdot \frac{n_i n_e}{n_a}\right] \quad (4.15)$$

$\Delta\phi_4$ = rate at which atoms are created as a result of ion-electron-electron recombination, from eq. (2.34),

$$= -\Delta\phi_2 \left[4\pi^{3/2} \frac{g_a}{g_+} \frac{\hbar^3}{m_e^3} \frac{1}{\beta_c^{3/2}} \exp\left(g_{oe}^2/\beta_e\right) \cdot \frac{n_i n_e}{n_a}\right] \quad (4.16)$$

In the eqs. (4.15) and (4.16),

$$n_a = \sum_j n_j ; \quad \beta_a = \frac{2kT_a}{m_a} ; \quad \varepsilon = \frac{m_e}{m_a}$$

and T_a is the atom temperature defined in eq. (5.21).

Substituting expressions (4.8), (4.13), (4.15) and (4.16) in

eq. (4.7), the atom conservation equation can be written as

$$\frac{d}{dx}\left(\sum_j n_j U_j\right) = -\frac{1}{16\sqrt{\pi}}\, n_a C_{aa} \cdot \left[1-4\pi^{3/2}\frac{g_a}{g_+}\frac{\hbar^3}{m_e^3}\epsilon^{3/2}\frac{1}{\beta_a^{3/2}}\exp\left(\frac{g_{oa}^2}{2\beta_a}\right)\frac{n_i n_e}{n_a}\right] \cdot \sum_j \sum_k n_j n_k \beta_{jk}^{3/2} F_1\left(\frac{U_{jk}}{\sqrt{\beta_{jk}}}, \frac{g_{oa}}{\sqrt{\beta_{jk}}}\right) - \frac{1}{4\sqrt{\pi}}\, n_e C_{ae} n_e \cdot \left[1-4\pi^{3/2}\frac{g_a}{g_+}\frac{\hbar^3}{m_e^3}\frac{1}{\beta_e^{3/2}}\exp\left(\frac{g_{oe}^2}{\beta_e}\right)\frac{n_i n_e}{n_a}\right] \cdot \sum_j n_j \beta_{je}^{3/2} F_1\left(\frac{U_{je}}{\sqrt{\beta_{je}}}, \frac{g_{oe}}{\sqrt{\beta_{je}}}\right) \qquad (4.17)$$

4.4.2 c_x^2-Moment Equation for the Atom Gas:

Multiplying eq. (3.4) by c_x^2 and integrating, we get,

$$\sum_j n_j U_j \left(U_j^2 + \frac{3}{2}\beta_j\right) = \sum_{k=1}^{6} \Delta\theta_k , \qquad (4.18)$$

where $\Delta\theta_k$'s are described below.

$$\Delta\theta_1 = \frac{1}{2}\int c_{ax}^2 \left(f_a' f_{a1}' - f_a f_{a1}\right) g\, b\,db\, d\epsilon\, \underset{\sim}{dc}_a \underset{\sim}{dc}_{a1} \qquad (4.19)$$

where b is the impact parameter and ϵ the azimuthal angle. Using the results from reference 18, (4.19) can be written as,

$$\Delta\theta_1 = \frac{1}{2}\int \left(c_{ax}'^2 - c_{ax}^2\right) f_a f_{a1}\, g\, b\,db\, d\epsilon\, \underset{\sim}{dc}_a \underset{\sim}{dc}_{a1} \qquad (4.20)$$

Substituting for f_a from eq. (4.1), and using the results from Appendix A-V, eq. (4.20) reduces to,

$$\Delta\theta_1 = -\frac{\pi}{2\sqrt{2}}\left(\frac{B_{aa}}{m_a}\right)^{1/2} A_2(5) \sum_j \sum_k n_j n_k U_{jk}^2 \qquad (4.21)$$

where B_{aa} is the force law constant for the atom-atom interaction.

$$\Delta\theta_2 = \int c_{ax}^2 (f_a' f_e' - f_a f_e)\, g\, b\,db\, d\epsilon\, d\underset{\sim}{c}_a\, d\underset{\sim}{c}_e$$
$$= \int (c_{ax}'^2 - c_{ax}^2) f_a f_e\, g\, bdb\, d\epsilon\, d\underset{\sim}{c}_a\, d\underset{\sim}{c}_e \qquad (4.22)$$

from the results of reference 18.

Inserting the expressions from (4.1) and (4.4) for f_a and f_e, $\Delta\theta_2$ can be written as

$$\Delta\theta_2 = \int \left\{\sum_j n_j(\pi\beta_j)^{-3/2} \exp\left[-(\underset{\sim}{c}_a - U_j\hat{i})^2/\beta_j\right]\right\} n_e(\pi\beta_e)^{-3/2}$$
$$\cdot \exp\left[-(\underset{\sim}{c}_e - U_e\hat{i})^2/\beta_e\right] (c_{ax}'^2 - c_{ax}^2)\, g\, bdb\, d\epsilon\, d\underset{\sim}{c}_a\, d\underset{\sim}{c}_e \qquad (4.23)$$

Evaluating the integrals using the results of Appendix (A-V), $\Delta\theta_2$ can be shown to be equal to,

$$\Delta\theta_2 = 2\pi\left(\frac{B_{ae}}{m_e}\right)^{1/2} \epsilon\, n_e \sum_j n_j \beta_{je} P_1\left(\frac{U_j}{\sqrt{\beta_{je}}}, \frac{\beta_j}{\beta_{je}}, \frac{U_{je}}{\sqrt{\beta_{je}}}, \epsilon\right) \qquad (4.24)$$

where,

$$P_1(U,V,X,W) = (A_1(5) - A_2(5))\, WX^2$$
$$- 2A_1(5)\, UX + A_1(5)\,(W-V); \qquad (4.25)$$

$A_1(5)$ and $A_2(5)$ are defined in Appendix.

$$\Delta\theta_3 = \int c_{ax}^2 (f_a' f_i' - f_a f_i)\, g\, bdb\, d\epsilon\, d\underset{\sim}{c}_a\, d\underset{\sim}{c}_i \qquad (4.26)$$
$$= \int (c_{ax}'^2 - c_{ax}^2) f_a f_i\, g\, bdb\, d\epsilon\, d\underset{\sim}{c}_a\, d\underset{\sim}{c}_i.$$

Using the expressions from (4.1) and (4.5) for f_a and f_e, $\Delta\theta_3$ can be written as,

$$\Delta\theta_3 = \int\left\{\sum_j n_j(\pi\beta_j)^{-3/2}\exp\left[-(\underset{\sim}{c}_a-U_j\hat{i})^2/\beta_j\right]\right\} n_i(\pi\beta_i)^{-3/2}$$
$$\exp\left[-(\underset{\sim}{c}_i-U_i\hat{i})^2/\beta_i\right](c_{ax}'^2-c_{ax}^2)\, g\, bdb\, d\varepsilon\, d\underset{\sim}{c}_a\, d\underset{\sim}{c}_i \qquad (4.27)$$

which, after using the integrals from Appendix (A-V) reduces to the form,

$$\Delta\theta_3 = \sqrt{2\pi}\left(\frac{B_{ai}}{m_a}\right)^{1/2} n_i \sum_j n_j\, \beta_{ji}\, P_1\left(\frac{U_j}{\sqrt{\beta_{ji}}}, \frac{\beta_j}{\beta_{ji}}, \frac{U_{ji}}{\sqrt{\beta_{ji}}}, \frac{1}{2}\right) \qquad (4.28)$$

In obtaining the elastic collisional expressions (4.21), (4.24) and (4.28) the inverse-fifth-power laws of force described in Section (2.7) have been used,

$$\Delta\theta_4 = -\frac{1}{2}\int c_{ax}^2\, f_a\, f_{a1}\, \sigma_{aa}^i\, g\, d\underset{\sim}{c}_a\, d\underset{\sim}{c}_{a1}\ ;\ g \geq g_{oa} \qquad (4.29)$$

Using the distribution function described in (4.1) and σ_{aa}^i from (4.9), eq. (4.29) can be written in the form,

$$\Delta\theta_4 = -\frac{1}{8} m_a C_{aa}\int\left\{\sum_j n_j(\pi\beta_j)^{-3/2}\exp\left[-(\underset{\sim}{c}_a-U_j\hat{i})^2/\beta_j\right]\right\}$$
$$\cdot\left\{\sum_k n_k(\pi\beta_k)^{-3/2}\exp\left[-(\underset{\sim}{c}_{a1}-U_k\hat{i})^2/\beta_k\right]\right\}$$
$$\cdot (g^2-g_{oa}^2)\, c_{ax}^2\, g\, d\underset{\sim}{c}_a\, d\underset{\sim}{c}_{a1} \qquad (4.30)$$

$$= -\frac{1}{8\sqrt{\pi}} m_a C_{aa} \sum_j \sum_k n_j\, n_k\, \beta_{jk}^{5/2}$$
$$\cdot F_2\left(\frac{U_j}{\sqrt{\beta_{jk}}}, \frac{\beta_j}{\beta_{jk}}, \frac{U_{jk}}{\sqrt{\beta_{jk}}}, \frac{g_{oa}}{\sqrt{\beta_{jk}}}\right). \qquad (4.31)$$

after using the results from Appendix (A-II), where,

$$F_2(U,V,X,W) = \sqrt{\pi}\left\{\mathrm{Erf}(W+X)-\mathrm{Erf}(W-X)\right\}\left[\frac{1}{2}\left(\frac{1}{2}V+U^2\right)X^3 + \frac{3}{2}UVX^2\right.$$
$$+\left\{\frac{3}{4}V^2 + \frac{1}{2}(3-W^2)\left(\frac{1}{2}V+U^2\right)\right\}X + \frac{1}{2}UV(3-W^2) +$$
$$+\frac{1}{8}\left(\frac{1}{2}V+U^2\right)(3-2W^2)\frac{1}{X} - \frac{1}{8}UV(3-2W^2)\frac{1}{X^2}$$
$$\left.+\frac{1}{16}V^2(3-2W^2)\frac{1}{X^3}\right] + \exp\left[-(W^2+X^2)\right]$$
$$\cdot\left[\left\{\left(\frac{1}{2}V+U^2\right)X^2 + 3UVX + \frac{5}{2}\left(\frac{1}{2}V+U^2\right) + \frac{3}{2}V^2\right.\right.$$
$$+\frac{1}{2}UV(3+4W^2)\frac{1}{X} - \frac{1}{4}V^2(3+4W^2)\frac{1}{X^2}\Big\}\cosh 2WX$$
$$+\left\{\left(\frac{1}{2}V+U^2\right)X^2 + 3UVX + \frac{1}{2}V^2(3+2W^2) + \frac{3}{2}\left(\frac{1}{2}V+U^2\right)\right.$$
$$\left.\left.-\frac{3}{2}UV\frac{1}{X} + \frac{3}{4}V^2\frac{1}{X^2}\right\}\frac{W}{X}\sinh 2WX\right]$$

and,

$$F_2(U, \tfrac{1}{2}, 0, W) = \frac{1}{4}\left[16U^2 + 8U^2W^2 + \frac{11}{3}W^2 + \frac{2}{3}W^4 + 6\right]\exp(-W^2) \qquad (4.32)$$

$$\Delta\theta_5 = -\int f_a\, f_e\, \sigma^i_{ae}\, c^2_{ax}\, g\, \underset{\sim}{dc}_a\, \underset{\sim}{dc}_e \quad ; \quad g \geq g_{oe}. \qquad (4.33)$$

Substituting for f_a and f_e from eqs. (4.1) and (4.4) and using σ^i_{ae} defined earlier,

$$\Delta\theta_5 = -\frac{1}{2}m_e\, C_{ae}\int\left\{\sum_j n_j(\pi\beta_j)^{-3/2}\exp\left[-(\underset{\sim}{c}_a-U_j\hat{i})^2/\beta_j\right]\right\}$$
$$\cdot\, n_e(\pi\beta_e)^{-3/2}\exp\left[-(\underset{\sim}{c}_e-U_e\hat{i})^2/\beta_e\right]$$
$$\cdot\,(g^2-g^2_{oe})\, g\, c^2_{ax}\, \underset{\sim}{dc}_a\, \underset{\sim}{dc}_e \quad ,$$

$$= -\frac{1}{2\sqrt{\pi}}m_e\, C_{ae}\, n_e \sum_j n_j\, \beta_{je}^{5/2}$$
$$\cdot\, F_2\left(\frac{U_j}{\sqrt{\beta_{je}}}, \frac{\beta_j}{\beta_{je}}, \frac{U_{je}}{\sqrt{\beta_{je}}}, \frac{g_{oe}}{\sqrt{\beta_{je}}}\right) \qquad (4.34)$$

after evaluating the integrals using the results from Appendix (A-II) .

$$\Delta\theta_6 = \int \left(\frac{\delta f_a}{\delta t}\right)_{rec.} c_{ax}^2 \, \underset{\sim}{dc}_a,$$

which can be shown to be approximately equal to $(U_i^2 + \frac{\beta_i}{2})$ times the recombination rate. Therefore,

$$\Delta\theta_6 = 4\pi \frac{g_a}{g_+} \frac{\hbar^3}{m_e^2} C_{ae} n_i n_e^2 (U_i^2 + \frac{\beta_i}{2})(2 + \frac{g_{oe}^2}{\beta_e}) \qquad (4.35)$$

The contribution from atom-electron-ion recombination is neglected.

Substituting for $\Delta\theta_k$'s, eq. (4.18) reduces to,

$$\begin{aligned}
\sum_j n_j U_j (U_j^2 + \tfrac{3}{2}\beta_j) = &- \frac{\pi}{2\sqrt{2}} \left(\frac{B_{aa}}{m_a}\right)^{1/2} A_2(5) \sum_j \sum_k n_j n_k U_{jk}^2 \\
&+ 2\pi \left(\frac{B_{ae}}{m_e}\right)^{1/2} \epsilon n_e \sum_j n_j \beta_{je} P_1\left(\frac{U_j}{\sqrt{\beta_{je}}}, \frac{\beta_j}{\beta_{je}}, \frac{U_{je}}{\sqrt{\beta_{je}}}, \epsilon\right) \\
&+ \sqrt{2\pi}\left(\frac{B_{ai}}{m_a}\right)^{1/2} n_i \sum_j n_j \beta_{ji} P_1\left(\frac{U_j}{\sqrt{\beta_{ji}}}, \frac{\beta_j}{\beta_{ji}}, \frac{U_{ji}}{\sqrt{\beta_{ji}}}, \frac{1}{2}\right) \\
&- \frac{1}{8\sqrt{\pi}} m_a C_{aa} \sum_j \sum_k n_j n_k \beta_{jk}^{5/2} F_2\left(\frac{U_j}{\sqrt{\beta_{jk}}}, \frac{\beta_j}{\beta_{jk}}, \frac{U_{jk}}{\sqrt{\beta_{jk}}}, \frac{g_{oa}}{\sqrt{\beta_{jk}}}\right) \\
&- \frac{1}{2\sqrt{\pi}} m_e C_{ae} n_e \sum_j n_j \beta_{je}^{5/2} F_2\left(\frac{U_j}{\sqrt{\beta_{je}}}, \frac{\beta_j}{\beta_{je}}, \frac{U_{je}}{\sqrt{\beta_{je}}}, \frac{g_{oe}}{\sqrt{\beta_{je}}}\right) \\
&+ 4\pi \frac{g_a}{g_+} \frac{\hbar^3}{m_e^2} C_{ae} n_i n_e^2 (U_i^2 + \tfrac{\beta_i}{2})(2 + \frac{g_{oe}^2}{\beta_e}) \qquad (4.36)
\end{aligned}$$

4.4.3 Number Conservation Equation for Electrons:

Integrating eq (3.5) over the $\underset{\sim}{c}_e$ space, gives,

$$\frac{d}{dx}(n_e U_e) = - \sum_{k=1}^{4} \Delta\phi_k \qquad (4.37)$$

where the right hand side of eq. (4.37) is the negative of that of eq. (4.7), since for each atom lost or gained there exists an electron gained or lost irrespective of what the velocities are.

4.4.4 Momentum Equation for the Electron Gas:

The electron momentum equation can be got by multiplying equation (3.5) by c_{ex} and integrating over $\underset{\sim}{c}_e$. The left hand side of eq. (3.5) for x-direction for steady case is,

$$= c_{ex} \frac{\partial f_e}{\partial x} + \frac{F_x}{m_e} \frac{\partial f_e}{\partial c_{ex}} \qquad (4.38)$$

where F_x is the product of the electric field in x-direction and electron charge = Ee. Multiplying (4.38) by c_{ex} and integrating over c_e yields that the left hand side of the momentum equation

$$= \frac{d}{dx}\left[n_e(U_e^2 + \frac{\beta_e}{2})\right] + \frac{Ee}{m_e} \int c_{ex} \frac{\partial f_e}{\partial c_{ex}} \underset{\sim}{dc}_e$$

$$= \frac{d}{dx}\left[n_e(U_e^2 + \frac{\beta_e}{2})\right] + \frac{Een_e}{m_e} \qquad (4.39)$$

since $(f_e)_{\pm \infty} = 0$.

Momentum equation is given by,

$$\frac{d}{dx}\left[n_e (U_e^2 + \frac{\beta_e}{2})\right] + \frac{Een_e}{m_e} = \sum_k \Delta\psi_k .$$

The electron-electron elastic interaction can be assumed to result in no net change of momentum.

$$\Delta\psi_1 = \int (c'_{ex} - c_{ex})\, f_a\, f_e\, g\, b\,db\, d\epsilon\, \underset{\sim}{dc}_e\, \underset{\sim}{dc}_a . \qquad (4.40)$$

Using the results from Appendix (A-III), after substituting for

f_a and f_e from (4.1) and (4.4), eq. (4.40) can be written as,

$$\Delta\psi_1 = 2\pi \left(\frac{B_{ae}}{m_e}\right)^{1/2} A_1(5)\, n_e \sum_j n_j\, U_{je}\,. \qquad (4.41)$$

$$\Delta\psi_2 = \int (c'_{ex}-c_{ex})\, f_e f_i\, g\, b\,db\, d\varepsilon\, \underset{\sim}{dc}_e\, \underset{\sim}{dc}_i \qquad (4.42)$$

which can be shown using the results from Appendix (A-III) after substituting for f_i and f_e from eqs. (4.4) and (4.5) to be equal to,

$$\Delta\psi_2 = 4\sqrt{\pi} \left(\frac{B_{ie}}{m_e}\right)^2 A_1(2)\, n_i n_e \frac{1}{\sqrt{\beta_{ei}}\, U_{ei}} \cdot \left[\exp\left[-(U_{ei}^2/\beta_{ei})\right] - \frac{\sqrt{\pi}}{2} \frac{\sqrt{\beta_{ei}}}{U_{ei}} \mathrm{Erf}\left(\frac{U_{ei}}{\sqrt{\beta_{ei}}}\right)\right], \qquad (4.43)$$

where $\beta_{ei} = \beta_e + \beta_i$, $U_{ei} = U_e - U_i$ and $A_1(2)$ is defined in Appendix.

Each electron produced or lost in inelastic collisions can be assumed to have an average local mean speed U_e and a random speed corresponding to the local electron temperature T_e. Under this assumption the contribution to momentum by inelastic collisions, per electron is unaltered and hence these terms can be omitted. A detailed quantitative estimate of these terms made but not included here justifies the assumption of negligible contribution to the momentum equation from inelastic collisions.

Hence the electron momentum equation can be written as,

$$\frac{d}{dx}\left[n_e(U_e^2+\frac{\beta_e}{2})\right] = -\frac{Een_e}{m_e} + 2\pi\left(\frac{B_{ae}}{m_e}\right)^{1/2} n_e A_1(5) \sum_j n_j U_{je}$$
$$+ 4\sqrt{\pi}\left(\frac{B_{ie}}{m_e}\right)^2 A_1(2)\, n_i\, n_e \frac{1}{\sqrt{\beta_{ie}}\, U_{ei}}$$
$$\cdot \left[\exp\left(-\left(\frac{U_{ei}^2}{\beta_{ei}}\right)\right) - \frac{\sqrt{\pi}}{2}\frac{\sqrt{\beta_{ei}}}{U_{ei}} \operatorname{Erf}\left(\frac{U_{ei}}{\sqrt{\beta_{ei}}}\right)\right] \tag{4.44}$$

4.4.5 Electron Energy Equation:

The electron energy equation can be obtained by taking c_e^2-moment of equation (3.5) which can be written as

$$\frac{d}{dx}\left[n_e U_e (U_e^2 + \frac{5}{2}\beta_e)\right] + \frac{2n_e U_e Ee}{m_e} = \sum_{k=1}^{3} \Delta\chi_k . \tag{4.45}$$

The elastic collisions between electrons do not contribute to the net change of energy of the electron gas,

$$\Delta\chi_1 = \int (c_e'^2 - c_e^2)\, f_e f_a\, g\, bdb\, d\varepsilon\, \underset{\sim}{dc}_e\, \underset{\sim}{dc}_a . \tag{4.46}$$

which, after using f_a and f_ε from (4.1) and (4.4) and using the results from Appendix (A-IV) reduces to,

$$\Delta\chi_1 = 2\pi\left(\frac{B_{ae}}{m_e}\right)^{1/2} A_1(5)\, n_e \sum_j n_j \beta_{je} P_2\left(\frac{U_e}{\sqrt{\beta_{je}}}, \frac{\beta_e}{\beta_{je}}, \frac{U_{ej}}{\sqrt{\beta_{je}}}, \frac{1}{1+\epsilon}\right.$$

(4.47)

where,

$$P_2(U,V,X,W) = 3(W-V) + 2WX^2 - 2UX . \tag{4.48}$$

$$\Delta\chi_2 = \int (c_e'^2 - c_e^2)\, f_e\, f_i\, g\, bdb\, d\varepsilon\, \underset{\sim}{dc}_e\, \underset{\sim}{dc}_i \tag{4.49}$$

which reduces, after using the results of Appendix (A-IV) to,

$$\Delta\chi_2 = 4\pi \left(\frac{B_{ie}}{m_e}\right)^2 A_1(2)\, n_i n_e \frac{1}{\sqrt{\beta_{ei}}} \cdot P_3\left(\frac{U_e}{\sqrt{\beta_{ei}}}, \frac{\beta_e}{\beta_{ei}}, \frac{U_{ei}}{\sqrt{\beta_{ei}}}, 1-\epsilon\right) \qquad (4.50)$$

where,

$$P_3(U,V,X,W) = \frac{1}{X}\,\mathrm{Erf}(X)\left(W - \frac{U}{X}\right) + \frac{2}{\sqrt{\pi}} \exp(-X^2)\left(\frac{U}{X} - V\right) \qquad (4.51)$$

With the same argument as given in deriving the electron momentum equation, it can be assumed that the change in electron energy due to processes (5) and (6) of Chapter 3 is mainly due to the energy I, being lost from the electron during ionization or being gained by the electron in recombination, and hence it can be written that,

$$\Delta\chi_3 = g_I^2 \,(\text{Recombination rate} - \text{Ionization rate}) \qquad (4.52)$$

where, $g_I^2 = 2I/m_e$.

Thus the electron energy equation can be written in the form,

$$\begin{aligned}\frac{d}{dx}\left[n_e U_e\left(U_e^2 + \frac{5}{2}\beta_e\right)\right] = &-\frac{2n_e U_e E_e}{m_e} + 2\pi\left(\frac{B_{ae}}{m_e}\right)^{1/2} A_1(5)\, n_e \\ &\cdot \sum_j n_j \beta_{je} P_2\left(\frac{U_e}{\sqrt{\beta_{ej}}}, \frac{\beta_e}{\beta_{ej}}, \frac{U_{ej}}{\sqrt{\beta_{ej}}}, 1-\epsilon\right) \\ &+ 4\pi\left(\frac{B_{ie}}{m_e}\right)^2 A_1(2)\, n_i n_e \frac{1}{\sqrt{\beta_{ie}}} P_3\left(\frac{U_e}{\sqrt{\beta_{ei}}}, \frac{\beta_e}{\beta_{ei}}, \frac{U_{ei}}{\sqrt{\beta_{ei}}}, 1-\epsilon\right) \\ &- \frac{1}{4\sqrt{\pi}} m_e\, C_{ae}\, g_I^2\, n_e \left(1 - 4\pi^{3/2} \frac{g_a}{g_+} \frac{\hbar^3}{m_e^3} \cdot \frac{1}{\beta_e^{3/2}} \exp(g_{oe}^2/\beta_e) \frac{n_i n_e}{n_a}\right) \\ &\cdot \sum_j n_j \beta_{je}^{3/2} F_1\left(\frac{U_{je}}{\sqrt{\beta_{je}}}, \frac{g_{oe}}{\sqrt{\beta_{je}}}\right). \end{aligned} \qquad (4.53)$$

4.4.6 Conservation Equations for the Plasma:

Conservation equations for the plasma are obtained by the addition of the conservation equations for the three species. The overall conservation equations of mass, momentum and energy will be almost exact since the approximation errors in the collision integrals of the component equations are nullified by the addition of the component equations.

Multiplying the number conservation equations for atoms, electrons and ions by their respective masses and adding yields,

$$\frac{d}{dx}\left[m_a \sum_j n_j U_j + m_i n_i U_i + m_e n_e U_e \right] = 0 \quad (4.54)$$

which represents the conservation of mass for the plasma.

The momentum equation for the plasma can be obtained by multiplying eqs. (3.4), (3.5) and (3.6) by $m_a c_{ax}$, $m_e c_{ex}$ and $m_i c_{ix}$ respectively, integrating over $\underset{\sim}{c}_a$, $\underset{\sim}{c}_e$ and $\underset{\sim}{c}_i$ and adding. During a collision, elastic or inelastic the total momentum of the participant particles is conserved in the absence of any external force. The only external force present, namely, electric field arising from possible polarization has already been included in the force term of the Boltzman equation. The resultant change in momentum of the entire gas due to collisions is therefore zero so that the momentum equation is,

$$\frac{d}{dx}\left[m_a \sum_j n_j\left(U_j^2 + \frac{\beta_j}{2}\right) + m_i n_i\left(U_i^2 + \frac{\beta_i}{2}\right) + m_e n_e\left(U_e^2 + \frac{\beta_e}{2}\right)\right] + Ee(n_e - n_i) = 0 \quad (4.56)$$

where the last term in (4.56) arises from charge separation.

The energy equation can be obtained by evaluating $\frac{1}{2} m_a c_a^2$, $\frac{1}{2} m_e c_e^2$ and $\frac{1}{2} m_i c_i^2$ moments respectively of the equations (3.4), (3.5) and (3.6) and adding. The elastic collision terms disappear, since the total energy is conserved during every elastic collision. In the inelastic collision an amount of energy equal to I is effectively lost or gained according as the process results in ionization or recombination, and the rate at which energy is gained can be written as

$$\Delta E = I \text{ (Recombination rate - Ionization rate)} \quad (4.57)$$

Substituting in the right hand side of eq. (4.57) from eqs. (4.37) and (4.7) for the net rate of production of charge, eq. (4.57) reduces to,

$$\Delta E = - I \frac{d}{dx} (n_e U_e) = - \frac{1}{2} m_e g_I^2 \frac{d}{dx} (n_e U_e).$$

Using this, the energy equation for the plasma can be written as

$$\frac{d}{dx} \left[\frac{1}{2} m_a \sum_j n_j U_j (U_j^2 + \frac{5}{2} \beta_j) + \frac{1}{2} m_e n_e U_e (U_e^2 + \frac{5}{2} \beta_e) + \frac{1}{2} m_i n_i U_i (U_i^2 + \frac{5}{2} \beta_i)\right] + eE(n_e U_e - n_i U_i) + \frac{1}{2} m_e g_I^2 \cdot \frac{d}{dx} (n_e U_e) = 0. \quad (4.58)$$

Subtracting the electron conservation equation from ion conservation equation yields,

$$\frac{d}{dx} \left[n_i U_i - n_e U_e\right] = 0, \quad (4.59)$$

since the rates of production of ions and electrons are same.

Integrating (4.59) and using the condition that,

$x \to -\infty$, $n_e = n_i = 0$, yields,

$$n_i U_i - n_e U_e = 0 \qquad (4.60)$$

Equation (4.60) also implies that the net current flux is zero at every point when there is no externally applied electric field.

Using eq. (4.60), eq.(4.58) can be written as,

$$\frac{d}{dx}\left[m_a \sum_j n_i U_j (U_j^2 + \frac{5}{2}\beta_j) + m_e n_e U_e (U_e^2 + \frac{5}{2}\beta_e + g_I^2) + m_i n_i U_i (U_i^2 + \frac{5}{2}\beta_i)\right] = 0, \qquad (4.61)$$

from which it is seen that the electric field term does not affect the energy equation. This is because in the absence of external fields, the sum of kinetic and potential energies remains unaltered.

4.4.7 Gauss Equation:

Lastly, the electric field E is described by the Gauss equation,

$$\nabla \cdot \underset{\sim}{E} = 4\pi e (n_i - n_e)$$

which for a one-dimensional problem reduces to,

$$\frac{dE}{dx} = 4\pi e (n_i - n_e) \qquad (4.62)$$

.5 Nondimensionalization of the Equations:

The various physical quantities of the problem can be nondimensionalised by using the upstream n_o and β_1 as follows,

$$N_j = \frac{n_j}{n_o}, \quad U_j = \frac{U_j}{\sqrt{\beta_1}}, \quad \bar{\beta}_j = \frac{\beta_j}{\beta_1}, \quad j = 1,2,3,e,i.$$

$$\bar{E} = \frac{E}{E_o}, \quad \bar{x} = \frac{x}{L} \qquad (4.63)$$

$$E_o = \sqrt{2\pi}\left(\frac{B_{aa}}{m_a}\right)^{\frac{1}{2}} \frac{n_o m_e \sqrt{\beta_1}}{e},$$

where L is a suitably chosen length scale.

Frequently the mean free path λ, corresponding to the cold side of the gas has been used for nondimensionalising the shock thickness and the equations. This mean free path, unfortunately is very sensitive to the intermolecular potential law chosen in the kinetic theory model or equivalently to the viscosity-temperature law chosen in the continuum model. For values of s, the power in the force law $F = B/r^s$, > 1, $\lambda \to \infty$ for $M_1 \to \infty$ and hence makes the nondimensional shock thickness go to zero though the actual thickness of the shock remains finite. From time to time, the need for a more appropriate length scale insensitive to the choice of the force law has been stressed. Lighthill[43] has recognized in the solution of Navier-Stokes equations for the shock wave thickness, that the downstream mean free path does not go to infinity as $M_1 \to \infty$ for any value of s. Leipmann et.al.[42] have shown that the use of the mean free-path at the sonic point inside the shock is particularly appropriate for the Navier-Stokes solutions. Mukenfuss[52] from a

study of Mott-Smith type solutions suggested the mean free path corresponding to a point inside the shock, where $\nu = \frac{1}{2}$ (Ref.51, $\nu = n_1/n_0$). The latter lengths, where a knowledge of the conditions at an interior point in the shock is required are difficult to use in practice. Narasimha and Deshpande[55] suggest the mean free-path λ_2 of the hot side of the gas in their study on minimum error solutions of the Boltzmann equation for shockwave structure. λ_2 always remains finite both in the continuum and kinetic theories. Further, they show that the temperature variation inside the shock after the point where $\nu = \frac{1}{2}$ is not significant for large Mach numbers so that the mean free path on the hot side of the shock is of the same order of magnitude as that at $\nu = \frac{1}{2}$. This also means that the effective diameter of the molecules change very little in the shock region for $\nu > \frac{1}{2}$ and the molecules behave very nearly as rigid spheres for strong shocks. The work on B-G-K model by Ananthasayanam and Narasimha[6] also suggests the choice of λ_2.

Quite often a mean free path based on a collisional process in the region of interest has been used, e.g. in the atom-atom collisional ionization dominated region, the atom-atom collisional ionization mean free path[57] and so on. Chubb[19] in his studies has used the atom-electron inelastic collision mean free path for nondimensionalising the relaxation zone. This length tends to infinity in the region where the gas is fully ionized since the atom density is zero. Also, for certain

gases e.g. Xenon[19], this length becomes too large because of the very small collisional cross-section and hence cannot be used as an appropriate scaling length. Nevertheless, the choice of the length scale is not serious because results from one length to another can always be transformed without undue difficulty. In the present study an altogether different length scale is used. We construct a length scale here which in some sense is not a 'mean free path'. We take the upstream mass flow velocity U_1 instead of the upstream thermal speed of the gas for constructing the length. This length is defined as follows,

$$L = \frac{U_1}{\pi n_o} \left(\frac{m_a}{2F_{aa}}\right)^{1/2} . \qquad (4.64)$$

We can show that L is proportional to the mean free path on the hot side of the gas for large Mach numbers and hence is finite for infinite Mach numbers. From reference 35,

$$\lambda_2 = \frac{1}{\sqrt{2}\pi\sigma^2 n_2} , \qquad (4.65)$$

$$\sigma = \sqrt{\frac{2}{A_2(5)\Gamma(3/2)}} \left(\frac{2k}{B_{aa}}\right)^{1/4} T^{1/4} \text{ for } s = 5,$$

where σ is the effective diameter of the molecule.

Then,

$$\lambda_2 = \frac{1}{\sqrt{2}\pi n_2} \frac{2}{A_2(5)\Gamma(3/2)} \left(\frac{2k}{B_{aa}}\right)^{1/2} T_2^{1/2} . \qquad (4.66)$$

Now from the R-H relations for a normal shock, as $M_1 \to \infty$,

$$\frac{n_2}{n_1} \to \frac{\gamma+1}{\gamma-1} \quad ; \quad \frac{T_2}{T_1} \to M_1^2 \sim \frac{U_1^2}{T_1}$$

where γ is the ratio of specific heats.

Thus from eq. (4.66),

$$\lambda_2 \sim T_2^{1/2} \sim M_1 T_1^{1/2} \sim U_1.$$

$$\therefore \lambda_2 \sim L \quad \text{for large } M_1$$

The same length has also been used by Oberai[58]. This length L has all the advantages of the downstream mean free path but still denotes the upstream flow which is known before hand both in experimental and theoretical investigations.

4.6 Nondimensional Equations:

The equations described in the Section (4.4) have been nondimensionalized using the parameters discussed in the Section (4.5) and the resulting equations are given below.

4.6.1 Atom Equations:

$$\frac{d}{d\bar{x}} \left[\sum_j N_j \bar{U}_j \right] = -\frac{1}{4} D_1 \bar{U}_1 \sum_j \left[\frac{1}{4\epsilon} \frac{C_{aa}}{C_{ae}} \right.$$

$$\cdot (1 - D_2 \epsilon^{3/2} \bar{\beta}_a^{-3/2} \exp(g_{oa}^2 / 2\beta_1 \bar{\beta}_a) \frac{N_i N_e}{N_a})$$

$$\cdot \sum_k N_j N_k \bar{\beta}_{jk}^{3/2} F_1 \left(\frac{U_{jk}}{\sqrt{\beta_{jk}}}, \frac{g_{oa}}{\sqrt{\beta_{jk}}} \right)$$

$$+ N_e (1 - D_2 \bar{\beta}_e^{-3/2} \exp(\frac{g_{oe}^2}{\beta_1 \bar{\beta}_e}) \frac{N_i N_e}{N_a})$$

$$\left. \cdot N_j \bar{\beta}_{je}^{3/2} F_1 \left(\frac{U_{je}}{\sqrt{\beta_{je}}}, \frac{g_{oe}}{\sqrt{\beta_{je}}} \right) \right] \qquad (4.67)$$

where

$$D_1 = \frac{1}{\sqrt{2}\pi^{3/2}} m_e m_a^{1/2} \frac{C_{ae}}{\sqrt{B_{aa}}} \beta_1^{3/2}$$

and

$$D_2 = 4\pi^{3/2} \frac{g_a}{g_+} \left(\frac{\hbar}{m_e}\right)^3 \cdot \frac{n_o}{\beta_1^{3/2}} \cdot \qquad (4.68)$$

$$\frac{d}{d\bar{x}} \left[\sum_j N_j \bar{U}_j (\bar{U}_j^2 + \frac{3}{2} \bar{\beta}_j) \right] =$$

$$\bar{U}_1 \sum_j \left[-\frac{1}{4} A_2(5) \sum_k N_j N_k \bar{U}_{jk}^2 + \sqrt{2} \left(\frac{B_{ae}}{B_{aa}}\right)^{1/2} \epsilon^{1/2} N_e N_j \bar{\beta}_{je} \right.$$

$$\cdot P_1 \left(\frac{U_j}{\sqrt{\beta_{je}}}, \frac{\beta_j}{\beta_{je}}, \frac{U_{je}}{\sqrt{\beta_{je}}}, \epsilon\right) + \left(\frac{B_{ai}}{B_{aa}}\right)^{1/2} N_i N_j \bar{\beta}_{ji}$$

$$\cdot P_1 \left(\frac{U_j}{\sqrt{\beta_{ji}}}, \frac{\beta_j}{\beta_{ji}}, \frac{U_{ji}}{\sqrt{\beta_{ji}}}, \frac{1}{2}\right) - D_1 \left\{ \frac{1}{8} \frac{1}{\epsilon} \frac{C_{aa}}{C_{ae}} \sum_k N_j N_k \bar{\beta}_{jk}^{5/2} \right.$$

$$\cdot F_2 \left(\frac{U_j}{\sqrt{\beta_{jk}}}, \frac{\beta_j}{\beta_{jk}}, \frac{U_{jk}}{\sqrt{\beta_{jk}}}, \frac{g_{oa}}{\sqrt{\beta_{jk}}}\right) + \frac{1}{2} N_e N_j \bar{\beta}_{je}^{5/2}$$

$$\cdot F_2 \left(\frac{U_j}{\sqrt{\beta_{je}}}, \frac{\beta_j}{\beta_{je}}, \frac{U_{je}}{\sqrt{\beta_{je}}}, \frac{g_{oe}}{\sqrt{\beta_{je}}}\right) - \frac{D_2}{3} N_i N_e^2$$

$$\left. \left. \cdot (\bar{U}_i^2 + \frac{1}{2} \bar{\beta}_i)(2 + \frac{g_{oe}^2}{\beta_e}) \right\} \right] \qquad (4.69)$$

4.6.2 Electron Equations:

$$\frac{d}{d\bar{x}} [N_e \bar{U}_e] = -\frac{d}{d\bar{x}} [\sum_j N_j \bar{U}_j] \qquad (4.70)$$

$$\frac{d}{d\bar{x}} [N_e (\bar{U}_e^2 + \frac{1}{2} \bar{\beta}_e)] = \bar{U}_1 \left[-\bar{E} N_e + D_3 N_e \sum_j N_j \bar{U}_{je} + D_4 A_1(2) \frac{N_i N_e}{\bar{\beta}_{ie}} \right.$$

$$\left. \frac{\sqrt{\beta_{ie}}}{\bar{U}_{ei}} \left\{ \exp(-U_{ei}^2/\beta_{ei}) - \frac{\sqrt{\pi}}{2} \frac{\sqrt{\beta_{ie}}}{U_{ei}} \operatorname{Erf} \left(\frac{U_{ei}}{\sqrt{\beta_{ie}}}\right) \right\} \right] \qquad (4.71)$$

where

$$D_3 = \sqrt{2}\,\left(\frac{B_{ae}}{B_{aa}}\right)^{1/2}\,\frac{A_1(5)}{\sqrt{\epsilon}}$$

and,

$$D_4 = \frac{2\sqrt{2}}{\sqrt{\pi}}\,\left(\frac{B_{ie}}{m_e}\right)^2\,\left(\frac{m_a}{B_{aa}}\right)^{1/2}\,\frac{1}{\beta_1^{3/2}}\,. \qquad (4.72)$$

$$\frac{d}{dx}\left[N_e U_e\left(\bar{U}_e^2 + \frac{5}{2}\bar{\rho}_e\right)\right] = \bar{U}_1\Big[-2N_e\bar{U}_e\bar{E} + D_3\,N_e\,\sum_j N_j\,\bar{\beta}_{je}$$

$$\cdot\,P_2\left(\frac{U_e}{\sqrt{\beta_{ej}}},\ \frac{\beta_e}{\rho_{ej}},\ \frac{U_{ej}}{\sqrt{\beta_{ej}}},\ 1-\epsilon\right) + \sqrt{\pi}\,D_4\,A_1(2)N_iN_e\,\frac{1}{\sqrt{\rho_{ie}}}$$

$$\cdot\,P_3\left(\frac{U_e}{\sqrt{\beta_{ie}}},\ \frac{\beta_e}{\beta_{ie}},\ \frac{U_{ie}}{\sqrt{\beta_{ie}}},\ 1-\epsilon\right) - \frac{1}{4}D_1^2\,\bar{g}_I^2$$

$$\cdot\,N_e\left(1-D_2\,\bar{\beta}_e^{-3/2}\,\exp\left(\frac{g_{oe}^2}{\beta_1}/\bar{\beta}_e\right)\right)\frac{N_iN_e}{T_a}$$

$$\cdot\,\sum_j N_j\,\bar{\beta}_{je}^{3/2}\,F_1\left(\frac{U_{je}}{\sqrt{\beta_{je}}},\ \frac{g_{oe}}{\sqrt{\beta_{je}}}\right)\Big] \qquad (4.73)$$

where,

$$\bar{g}_I^2 = \frac{g_I^2}{\beta_1}\,.$$

4.6.3 Plasma Equations:

$$\frac{d}{d\bar{x}}\left[\sum_j N_j\bar{U}_j + (1-\epsilon)\,N_i\bar{U}_i + \epsilon N_e\bar{U}_e\right] = 0.$$

which can be written using eq. (4.59) as

$$\frac{d}{d\bar{x}}\left[\sum_j N_j\bar{U}_j + N_e\bar{U}_e\right] = 0 \qquad (4.74)$$

Eqn. (4.56) after substituting for $(n_e - n_i)$ from (4.62) and using eq. (4.63), reduces to,

$$\frac{d}{d\bar{x}} \left[\sum_j N_j (\bar{U}_j^2 + \frac{1}{2} \bar{\beta}_j) + (1-\epsilon) N_i (\bar{U}_i^2 + \frac{1}{2} \bar{\beta}_i) + \epsilon N_e (\bar{U}_e^2 + \frac{1}{2} \bar{\beta}_e) - \frac{\pi}{4} \epsilon^2 n_o \frac{B_{aa}}{e^2} \bar{E}^2 \right] = 0 \qquad (4.75)$$

and eq. (4.61) reduces to

$$\frac{d}{d\bar{x}} \left[\sum_j N_j \bar{U}_j (\bar{U}_j^2 + \frac{5}{2} \bar{\beta}_j) + (1-\epsilon) N_e \bar{U}_e (\bar{U}_i^2 + \frac{5}{2} \bar{\beta}_i) + \epsilon N_e \bar{U}_e (\bar{U}_e^2 + \frac{5}{2} \bar{\beta}_e + \bar{g}_I^2) \right] = 0 \qquad (4.76)$$

4.7 Boundary Conditions:

The boundary conditions governing the various parameters in the distribution function are;

$$\bar{x} \to -\infty; \qquad N_1 \to 1, \qquad N_j \to 0, \quad (j = 2,3,i,e), \quad \bar{E} \to 0, \qquad (4.77a)$$

and

$$\bar{x} \to +\infty; \qquad N_1 \to 0, \qquad N_2 \to 0, \qquad \bar{E} \to 0$$
$$U_e, U_i \to U^*(=U_3); \quad T_e, T_i \to T^*(=T_3) \qquad (4.77b)$$

4.8 Plasma Equations:

Equations (4.74) to (4.76) can be integrated and the boundary conditions (4.77a) if introduced, yields,

$$\sum_j N_j \bar{U}_j + N_e \bar{U}_e = \bar{U}_1 \qquad (4.78)$$

$$\sum_j N_j(\bar{U}_j^2 + \frac{1}{2}\bar{\beta}_j) + (1-\epsilon) N_i(\bar{U}_i^2 + \frac{1}{2}\bar{\beta}_i) + \epsilon N_e(\bar{U}_e^2 + \frac{1}{2}\bar{\beta}_e)$$

$$- \frac{\pi}{4}\epsilon^2 n_o \frac{B_{aa}}{e^2} \bar{E}^2 = (\bar{U}_1^2 + \frac{1}{2}) \qquad (4.79)$$

and

$$\sum_j N_j\bar{U}_j(\bar{U}_j^2 + \frac{5}{2}\bar{\beta}_j) + N_e\bar{U}_e \{(1-\epsilon)(\bar{U}_i^2 + \frac{5}{2}\bar{\beta}_i)$$

$$+ \epsilon(\bar{U}_e^2 + \frac{5}{2}\bar{\beta}_e + \bar{g}_I^2)\} = \bar{U}_1(\bar{U}_1^2 + \frac{5}{2}) \qquad (4.80)$$

Equations (4.78) to (4.80) represent the plasma equations of conservation of mass, momentum and energy within the shockwave.

CHAPTER 5

METHOD OF SOLUTION AND PHYSICAL PARAMETERS

5.1 General:

In this chapter the nondimensional equations derived in Chapter 4 will be simplified to describe the flow in the downstream equilibrium region by introducing appropriate boundary conditions and the resulting equations will be numerically solved for the jump quantities across the shock. The structure equations also will be solved to get the shock structure profiles for a given set of initial conditions till the final equilibrium values are reached. Various physical parameters of interest are computed.

5.2 Equations Representing the Jump Conditions:

Introducing the boundary condition (4.77b) in the equations (4.78) to (4.80), denoting the values of $\bar{N}_3$, N_e, N_i, $\bar{U}_3$, $\bar{\beta}_3$ for $\bar{x} \to +\infty$, by N^*, N_e^*, N_i^*, $\bar{U}^*$, $\bar{\beta}^*$ and using,

$$\bar{\beta}_e^* = \bar{\beta}^*/\epsilon \quad , \quad \text{and} \quad \bar{\beta}_i^* = \bar{\beta}^*/(1-\epsilon)$$

yields,

$$(N^* + N_e^*)\,\bar{U}^* = \bar{U}_1 \tag{5.1}$$

$$N^*\left(\bar{U}^{*2} + \frac{1}{2}\,\bar{\beta}^*\right) + (1-\epsilon)\,N_i^*\left(\bar{U}^{*2} + \frac{1}{1-\epsilon}\,\frac{\bar{\beta}^*}{2}\right)$$

$$+ \epsilon\, N_e^*\left(\bar{U}^{*2} + \frac{1}{2\epsilon}\,\bar{\beta}^*\right) = \left(\bar{U}_1^2 + \frac{1}{2}\right) \tag{5.2}$$

and

$$N^* \bar{U}^*(\bar{U}^{*2} + \frac{5}{2}\bar{\beta}^*) + N_e^* \bar{U}^* \left\{(1-\epsilon)(\bar{U}^{*2} + \frac{5}{2(1-\epsilon)}\bar{\beta}^*) + \epsilon\,(\bar{U}^{*2} + \frac{5}{2\epsilon}\bar{\beta}^* + \bar{g}_I^2)\right\} = \bar{U}_1(\bar{U}_1^2 + \frac{5}{2}). \quad (5.3)$$

Introducing α, the degree of ionization, defined by

$$\alpha = = N_e/(N_e+N_a) , \quad \text{and} \quad \alpha^* = N_e^*/(N_e^*+N^*) \quad (5.4)$$

equations (5.1) to (5.3) can be rewritten as

$$N^* \bar{U}^* = \bar{U}_1(1-\alpha^*) \quad (5.5)$$

$$N^*[\bar{U}^{*2} + \frac{\bar{\beta}^*}{2}(1+\alpha^*)] = (1-\alpha^*)(\bar{U}_1^2 + \frac{1}{2}) \quad (5.6)$$

and,

$$N^* \bar{U}^* [\bar{U}^{*2} + \frac{5}{2}\bar{\beta}^*(1+\alpha^*) + \epsilon\alpha^* g_I^2] = (1-\alpha^*)\bar{U}_1(\bar{U}_1^2 + \frac{5}{2}) \quad (5.7)$$

The Saha equation for equilibrium, is

$$\frac{\alpha^{*2}}{1-\alpha^*} = \frac{1}{n_o}\frac{U^*}{U_1}\bar{\beta}^{*3/2} \exp\left(-\frac{I}{kT_1\bar{\beta}^*}\right) \quad (5.8)$$

where,

$$K = \frac{2g_+}{g_a}\left(\frac{2\pi m_e kT_1}{h^2}\right)^{3/2}$$

Eliminating $\bar{\beta}^*$ between equations (5.6) and (5.7) and substituting from eq. (5.5), yields.

$$\frac{U^*}{U_1} = \frac{5}{8}\left[\left(\frac{5}{3} + \frac{1}{M_1^2}\right) - \sqrt{\left(1 - \frac{1}{M_1^2}\right)^2 + \frac{32}{15}\frac{\alpha^*}{M_1^2}\left(\frac{I}{kT_1}\right)}\right] \quad (5.9)$$

where M_1 is defined by,

$$\frac{5}{6} M_1^2 = \frac{U_1^2}{\beta_1}$$

The positive sign behind the radical sign in eq.(5.9) has been omitted as it corresponds to a trivial solution when $\alpha^* = 0$. From eqs. (5.5) and (5.9), it can be written that,

$$N^* = \frac{8}{3}(1-\alpha^*)/\left[\left(\frac{5}{3}+\frac{1}{M_1^2}\right)-\sqrt{\left(1-\frac{1}{M_1^2}\right)^2+\frac{32}{15}\frac{\alpha^*}{M_1^2}\left(\frac{I}{kT_1}\right)}\right] \tag{5.10}$$

From equations (5.5), (5.6) and (5.7), $\bar{\beta}^*$ can be solved. Using eq. (5.9), $\bar{\beta}^*$ can be written as

$$\bar{\beta}^* = \frac{1}{2(1+\alpha^*)}\left[\frac{5}{2}\left(1+\frac{1}{3}M_1^2\right)-\frac{3}{16}\left(1+\frac{5}{3}M_1^2\right)\left\{\left(\frac{5}{3}+\frac{1}{M_1^2}\right)-\sqrt{\left(1-\frac{1}{M_1^2}\right)^2+\frac{32}{15}\frac{\alpha^*}{M_1^2}\left(\frac{I}{kT_1}\right)}\right\}-\frac{I}{kT_1}\cdot\alpha^*\right] \tag{5.11}$$

Equations (5.9), (5.10) and (5.11) give explicit expressions for the velocity, density and temperature across the shock in terms of the initial Mach number and equilibrium degree of ionization.

Equation (5.8) can be written using eq. (5.10), as

$$\frac{\alpha^{*2}}{1-\alpha^*} = \frac{3}{8}\frac{K}{n_o}\bar{\beta}^{*3/2}\left[\left(\frac{5}{3}+\frac{1}{M_1^2}\right)-\sqrt{\left(1-\frac{1}{M_1^2}\right)^2+\frac{32}{15}\frac{\alpha^*}{M_1^2}\left(\frac{I}{kT_1}\right)}\right]\exp\left(-I/kT_1\bar{\beta}^*\right) \tag{5.12}$$

Equations (5.9) to (5.12) constitute the expressions for the jump conditions across an ionizing shockwave.

Equations (5.11) and (5.12) have been simultaneously solved for $\bar{\rho}^*$ and α^* numerically using Newton-Raphson method with double precision on IBM 7044 Computer for argon, krypton and xenon for initial pressures of 0.1 to 100 torrs with initial temperature $T_1 = 300^{\circ}K$ and Mach numbers ranging from 10 to 40. The velocity ratio and the density ratio have been calculated from eqs. (5.9) and (5.10). The Mach number for complete ionization of atoms has also been computed. The various physical parameters that will be discussed in Section (5.4) have been computed and the results presented in tables (5.1 - 5.6).

5.3 Shock Structure Profiles:

The set of equations (4.67) to (4.76) and (4.62) can be solved simultaneously subject to the initial conditions (4.77a). Equations (4.62) will be dropped and the quasi-neutrality assumption $N_e = N_i$ is made everywhere. Using equation (4.60), this yields $\bar{U}_e = \bar{U}_i$ for all $\bar{x}$. Since $m_i \simeq m_a$ and the atom-ion collision cross section is very high, the atom and ion temperatures can be assumed to be same and hence everywhere $\bar{T}_a = \bar{T}_i$. Also it can be assumed that $U_i = U_a$. This gives,

$$\bar{U}_e = \bar{U}_i = \bar{U}_a$$

and (5.13)

$$\bar{T}_a = \bar{T}_i$$

With these approximations, the momentum conservation for plasma is approximately satisfied and hence equation (4.75) can be ignored. Further $m_e << m_a$, $\bar{U}_e << \bar{\beta}_e$ and hence the kinetic energy of mass motion of electrons can be neglected compared to its thermal energy. With these assumptions, we have the following equations,

$$\frac{d}{d\bar{x}}\left[N_e \bar{U}_e\right] = \frac{1}{4} D_1 \bar{U}_1 \sum_j \left[\frac{1}{4\epsilon}\frac{C_{aa}}{C_{ae}}(1-R_1)\sum_k N_j N_k \bar{\beta}_{jk}^{3/2} \cdot F_1\left(\frac{U_{jk}}{\sqrt{\beta_{jk}}}, \frac{g_{oa}}{\sqrt{\beta_{jk}}}\right) + (1-R_2) N_e N_j \bar{\beta}_{je}^{3/2} F_1\left(\frac{U_{je}}{\sqrt{\beta_{je}}}, \frac{g_{oe}}{\sqrt{\beta_{je}}}\right)\right] \tag{5.14}$$

where

$$R_1 = D_2 \epsilon^{3/2} \bar{\beta}_a^{-3/2} \exp\left(\frac{g_{oa}^2}{2\beta_1}/\bar{\beta}_a\right) \frac{N_i N_e}{N_a}, \tag{5.15}$$

and

$$R_2 = D_2 \bar{\beta}_e^{-3/2} \exp\left(\frac{g_{oe}^2}{\beta_1}/\bar{\beta}_e\right) \frac{N_i N_e}{N_a} \cdot$$

$$\bar{E} = -\frac{1}{2N_e \bar{U}_1}\frac{d}{d\bar{x}}(N_e \bar{\beta}_e) \tag{5.16}$$

and

$$\frac{5}{2}\frac{d}{d\bar{x}}\left[N_e \bar{U}_e \bar{\beta}_e\right] = \bar{U}_1\left[-2N_e \bar{U}_e + D_3 N_e \sum_j N_j \left\{3(\bar{\beta}_j - \epsilon\bar{\beta}_e) + 2\bar{U}_j(\bar{U}_j - \bar{U}_e)\right\} + 2D_4 A_1(2)\frac{N_i N_e}{\bar{\beta}_{ie}^{3/2}}(\bar{\beta}_i - \epsilon\bar{\beta}_e) - \frac{1}{4} D_1 \bar{g}_I^2 N_e (1-R_2) \sum_j N_j \bar{\beta}_{je}^{3/2} F_1\left(\frac{U_j}{\sqrt{\beta_{je}}}, \frac{g_{oe}}{\sqrt{\beta_{je}}}\right)\right]$$

which after using equation (5.16) can be rewritten as

$$\frac{3}{2} N_e \bar{U}_e \frac{d\bar{\beta}_e}{d\bar{x}} = \bar{U}_1 \Big[D_3 N_e \sum_j N_j \Big\{ 3(\bar{\beta}_j - \epsilon\bar{\beta}_e) + 2\bar{U}_j(\bar{U}_j - \bar{U}_e) \Big\}$$

$$+ 2D_4 A_1(2) \frac{N_i N_e}{\bar{\beta}_{ie}^{3/2}} (\bar{\beta}_i - \epsilon\bar{\beta}_e)$$

$$- \frac{1}{4} D_1 \bar{g}_I^2 N_e (1-R_2) \sum_j N_j \bar{\beta}_{je}^{3/2} F_1\left(\frac{U_j}{\sqrt{\beta_{je}}}, \frac{g_{oe}}{\sqrt{\beta_{je}}}\right) \Big]$$

$$- N_e \bar{\beta}_e \frac{d\bar{U}_e}{d\bar{x}} - \frac{3}{2} \bar{\beta}_e \frac{d}{d\bar{x}} (N_e \bar{U}_e) \qquad (5.17)$$

In eq. (5.17) the last term on the right hand side represents the average energy the electron gas has to spare for every newly born electron to raise it to the local electron gas temperature. If the newly born electrons are assumed to have already attained the local temperature of the electron gas, the last term drops out. Hoffert and Lin[36] have shown that the last term in eq. (5.17) can be ignored in view of the argument that this term gets cancelled with a similar term arising from the time derivative term of Boltzmann equation on left hand side. In the present work this term has been omitted.

The c_x^2 - moment equation for atoms is,

$$\frac{d}{d\bar{x}}\left[\sum_j N_j \bar{U}_j(\bar{U}_j^2+\frac{3}{2}\bar{\beta}_j)\right]=\bar{U}_1\sum_j\left[-\frac{1}{4}\sigma_2(5)\sum_k N_j N_k \bar{U}_{jk}^2\right.$$
$$+\sqrt{2}\left(\frac{B_{ae}}{B_{aa}}\right)^{1/2}\epsilon^{1/2}N_e N_j\bar{\beta}_{je}P_1\left(\frac{U_j}{\sqrt{\beta_{je}}},\frac{\beta_j}{\beta_{je}},\frac{U_{je}}{\sqrt{\beta_{je}}},\epsilon\right)$$
$$+\left(\frac{B_{ai}}{B_{aa}}\right)^{1/2}N_i N_j\bar{\beta}_{ji}P_1\left(\frac{U_j}{\sqrt{\beta_{ji}}},\frac{\beta_j}{\beta_{ji}},\frac{U_{ji}}{\sqrt{\beta_{ji}}},\frac{1}{2}\right)$$
$$-D_1\left\{\frac{1}{8\epsilon}\frac{C_{aa}}{C_{ae}}\sum_k N_j N_k\bar{\beta}_{jk}^{5/2}F_2\left(\frac{U_j}{\sqrt{\beta_{jk}}},\frac{\beta_j}{\beta_{jk}},\frac{U_{jk}}{\sqrt{\beta_{jk}}},\frac{g_{oa}}{\sqrt{\beta_{jk}}}\right)\right.$$
$$+\frac{1}{2}N_e N_j\bar{\beta}_{je}^{5/2}F_2\left(\frac{U_j}{\sqrt{\beta_{je}}},\frac{\beta_j}{\beta_{je}},\frac{U_{je}}{\sqrt{\beta_{je}}},\frac{g_{oa}}{\sqrt{\beta_{je}}}\right)$$
$$\left.\left.-\frac{D_2}{3}N_i N_e^2(\bar{U}_i^2+\frac{1}{2}\bar{\beta}_i)(2+\frac{g_{oe}^2}{\rho_e})\right\}\right] \qquad (5.18)$$

The plasma conservation equations can be written from equations (4.74) and (4.76) after introducing the boundary conditions (4.77a), as

$$\sum_j N_j\bar{U}_j=\bar{U}_1-N_e\bar{U}_e \qquad (5.19)$$

and

$$\sum_j N_j\bar{U}_j(\bar{U}_j^2+\frac{5}{2}\bar{\beta}_j)=\bar{U}_1(\bar{U}_1^2+\frac{5}{2})$$
$$-N_e U_e\left\{\epsilon(\frac{5}{2}\bar{\beta}_e+\bar{g}_I^2)+(\bar{U}_i^2+\frac{5}{2}\bar{\beta}_i)\right\} \qquad (5.20)$$

The set of equations (5.14) to (5.20) have been solved numerically for the variables N_e, $\bar{\beta}_e$, $\bar{E}$, N_1, N_2 and N_3 using Runge-Kutta-Gill's method on the IBM 7044 Computer. To initiate the integration process a value of 0.99 for N_1 and the corresponding value of N_2 given by the inert gas shock profiles from

Mott-Smith's solution have been used and this initial point has been arbitrarily taken as the origin for the shock coordinate. It is to be recalled that the position of a normal shockwave in one dimensional flow is indeterminate and hence the choice of the origin for the shock coordinate is immaterial. The structure profile for negative $\bar{x}$ will be little different from that of inert gas profiles as the degree of ionization is negligibly small in this region if the effect of precursor is neglected. In the present work the precursor effect is neglected and an initial value of 10^{-6} for the degree of ionization at the starting point has been used. This value has little influence on the structure profiles as reported by Chubb and also checked in the present studies for the range of Mach numbers studied. The initial electron temperature has been taken to be the same as the initial atom temperature in the upstream equilibrium region. The electron temperature however, increases very fast initially and remains constant over a large part of the shock, and the value of initial electron temperature assumed affects the shock structure negligibly[36]. However, the position of the onset point varies considerably.

The following definitions of density, velocity and temperatures are used.

$$n = \int f \, \underset{\sim}{dc}, \quad U = \frac{1}{n} \int f \, c.\hat{i} \, \underset{\sim}{dc}, \quad \frac{3}{2} kT = \frac{1}{2} m \int f \, c^2 \, \underset{\sim}{dc}, \qquad (5.21)$$

The parameters of interest namely, temperatures of atom, ion and electrons, their velocity, pressure, densities, degree of

ionization, electrical conductivity, the electric field and potential and refractive index have been computed at every point within the shockwave. The integration is continued till N_1, N_2 reach values less than 10^{-4}. At this stage the various quantities will have reached their equilibrium values to the third digit accuracy. These results are discussed in Chapter 6.

5.4 Physical Parameters:

1) Pressure:

The pressure in an ionized gas can be written as

$$p = \sum_i p_i + \Delta p_c$$

where p_i is the partial pressure due to i-th species and Δp_c is the pressure correction term arising from the coulomb interaction between charged particles. Δp_c is negligible since the mean coulomb potential energy e^2/r_o, is much less than the mean thermal energy $\frac{3}{2} kT_e$, where $r_o = n_e^{-1/3}$, within the range of present interest. Substituting

$$p_i = n_i k T_i,$$

the ratio of the local pressure to the free-stream pressure can be written as,

$$\bar{p} = N_a \bar{T}_a + N_i \bar{T}_i + N_e \bar{T}_e .$$

Since $T_a = T_i$ and $N_e = N_i$ everywhere,

$$\bar{p} = \bar{\rho}\, \bar{T}_a \,(1 + \alpha\, \bar{T}_e/\bar{T}_a) \qquad (5.22)$$

where $\bar{\rho}$ is the dimensionless mass density. At equilibrium, $\bar{T}_e - \bar{T}_a$ and hence eq. (5.22) reduces to

$$\bar{p} = \bar{\rho}\, \bar{T}_a\, (1 + \alpha^*). \tag{5.23}$$

2) Downstream Mach Number:

The Mach number in the downstream equilibrium region is

$$M_2 = \frac{U^*}{a}$$

where 'a' is the speed of sound in the equilibrium region. An expression for 'a' can be obtained from the isentropic equation, the equation of state and the internal energy expression for an ionized gas. The equation of state and the internal energy are given by

$$p = f_1(\rho, T) = \rho \frac{k}{m_a} T\, (1 + \alpha^*(\rho, T)) \tag{5.24}$$

and

$$\mathcal{E} = f_2(\rho, T) = \frac{3}{2} \frac{k}{m_a} T\, (1 + \alpha^*(\rho, T)) + \frac{I}{m_a} \alpha^*(\rho, T) \tag{5.25}$$

where $\mathcal{E}$ is the internal energy per unit mass of the gas.

Eqs. (5.24), (5.25) and the isentropic expressions in the differential forms are;

$$dp = \frac{\partial f_1}{\partial \rho} d\rho + \frac{\partial f_1}{\partial T} dT \tag{5.26}$$

$$d\mathcal{E} = \frac{\partial f_2}{\partial \rho} d\rho + \frac{\partial f_2}{\partial T} dT \tag{5.27}$$

$$d\mathcal{E} + p\, d\left(\frac{1}{\rho}\right) = T dS \equiv 0 \tag{5.28}$$

From eqs. (5.26) - (5.28) it can be written that,

$$a^2 \equiv \left(\frac{\partial p}{\partial \rho}\right)_S = \frac{\partial f_1}{\partial \rho} + \left(\frac{p}{\rho^2} - \frac{\partial f_2}{\partial \rho}\right) \frac{\partial f_1/\partial T}{\partial f_2/\partial T} \qquad (5.29)$$

Using expressions for f_1 and f_2 from eqs. (5.24) and (5.25), and for α^* from eq. (5.8), it can be shown that

$$a^2 = \frac{k}{m_a} T \left\{ \frac{5(4+9\alpha^*-5\alpha^{*3})\theta^2 + 4\alpha^*(1-\alpha^{*2})(5\theta+1)}{3(4+5\alpha^*-5\alpha^{*2})\theta^2+4\alpha^*(1-\alpha^*)(3\theta+1)} \right\} \qquad (5.30)$$

where,

$$\theta = (I/kT)^{-1}$$

We shall define an adiabatic index γ for an ionized gas by the expression.

$$\gamma = \frac{a^2}{p/\rho} = \frac{a^2}{\frac{kT}{m_a}(1+\alpha^*)}$$

which reduces to

$$\gamma = \left\{ \frac{5(4+9\alpha^*-5\alpha^{*3})\theta^2 + 4\alpha^*(1-\alpha^{*2})(5\theta+1)}{3(4+5\alpha^*-5\alpha^{*2})\theta^2+4\alpha^*(1-\alpha^*)(3\theta+1)} \right\} \frac{1}{(1+\alpha^*)} \qquad (5.31)$$

$\gamma \to 5/3$, as $\alpha^* \to 0, 1$.

3. Electrical Conductivity:

The contribution to electrical conductivity of an ionized gas arises from the close encounters between the electrons and neutral particles, and from the long range interactions between electrons and ions. Lin et al.[44] have pointed out that for a high degree of ionization ($\alpha > 10^{-3}$ for Ar), the diffusion of electrons is primarily limited by long range coulomb interaction of the gas and the contribution arising from the electron interaction with neutral particles is negligible.

Often the Chapmann-Enskog method of solving the Maxwell-Boltzmann equation has been used to get the electrical conductivity of completely ionized gases to various degrees of approximation. Spitzer et al.[74] solved the problem in a different way by considering the effect of electron ion encounters as a problem of diffusion in the velocity space and their results agree closely with that of Chapmann and Cowling.

According to Spitzer and Harm[74] the electrical conductivity of a fully ionized gas is

$$\sigma = \frac{0.591\ (kT_e)^{3/2}}{m_e^{1/2}\ e^2\ \ln\ (\lambda_D/\lambda_L)} \qquad (5.32)$$

where, $\lambda_D = \left(\frac{kT_e}{8\pi n_e\ e^2}\right)^{1/2}$, the Debye shielding length, and $\lambda_L = \frac{e^2}{3kT_e}$, the Landau distance.

Equation (5.32) has a relative inaccuracy of the order of $\ln\ (\lambda_D/\lambda_L)$ arising from the uncertainty in the choice of the cut-off distance.

In the present case $\alpha > 10^{-3}$ over a large part of the shock and the electrical conductivity calculated from equation (5.32) is fairly accurate.

4. Refractive Index:

For a partially ionized gas composed of ground state atoms, ions and free electrons the expression for the refractive

index can be written as[77]

$$\mu = 1 + 2\pi (\xi_a n_a + \xi_i n_i) - \frac{1}{2} \left(\frac{\omega_p}{\omega} \right)^2 \qquad (5.33)$$

where ω_p = the plasma frequency, $(4\pi n_e e^2/m_e)^{1/2}$; ω = impressed frequency; ξ_a, ξ_i are the polarizabilities of the ground state atom and ion respectively, and μ the refractive index. The expression (5.33) is valid when the plasma frequency is much smaller than the applied frequency and when the number density of the excited atoms is small compared to the ground state atom number density. The refractive index has been calculated for Sodium yellow line (λ = 5890 Å).

5. Electric Potential:

The electric potential due to the field $\mathbb{E}$ can be written as

$$V = - \int_0^x \mathbb{E} \, dx$$

which can be suitably nondimensionalised and written as

$$\bar{V} = \frac{eV}{kT_1} = 2\bar{U}_1 \in \int_0^{\bar{x}} \bar{\mathbb{E}} \, d\bar{x} \qquad (5.34).$$

CHAPTER 6

DISCUSSIONS AND CONCLUSIONS

6.1 Equilibrium Properties:

The downstream equilibrium properties computed numerically for Mach numbers from 10 to 40 for argon, krypton and xenon for initial pressures of 0.1, 1.0, 10 and 100 torrs are presented in tables 5.1 to 5.6 for an initial temperature of 300°K. Results for argon are also plotted in Figs.(6.16.1) to (6.21.1) for different initial pressures and temperatures. It is seen that the equilibrium degree of ionization is higher for higher initial Mach numbers and temperatures and lower initial pressures. The equilibrium temperature ratio increases with Mach number but takes much lower values than in the inert gas case. For low initial pressures due to the high degree of equilibrium ionization the downstream temperature will be lower than that for higher pressures. The density vs M_1 curves exhibit a peak where the density attains a maximum which can be explained by eq. (5.9) where U^*/U_1 is the reciprocal of the density ratio. The second term under the radical sign in eq. (5.9) causes this type of

behaviour. At low** Mach numbers α^* increases faster than M_1^2 so that α^*/M_1^2 increases whereby an increase in the Mach number results in an increase of the density ratio. At higher Mach numbers α^* will be close to its upper bound value of 1 and increases very slowly so that α^*/M_1^2 decreases with increase of M_1 causing the density ratio to decrease. For very large Mach numbers when $\alpha^*/M_1^2 \to 0$ the density ratio reaches a value of 4 corresponding to that for a monatomic gas as may be expected. The Mach number for which the equilibrium density is maximum increases with increase of upstream pressure. The equivalent $\gamma < 1.67$ (its value for inert monatomic gas) over a range of Mach numbers depending upon the initial pressure. At low Mach numbers when ionization is insignificant its value is $\gamma = 1.67$; again for high Mach numbers when the gas is fully ionized and can be considered as a mixture of monatomic gases of different species it attains the value $\gamma = 1.67$. For low initial pressures the variation of γ is very sudden exhibiting a bucket type of behaviour (Fig. 6.20.1) and as the initial pressure increases the variations become less steep. The lowest value

---

** In the following the words 'high' and 'low' are used in a restricted sense. Low corresponds to the region towards the lower end of the range of parameter studied and high corresponds to the region towards the upper end of it.

of γ reached depends upon the initial pressure and increases with increase of the initial pressure. In Fig.(6.21.1) it is seen that the curve of the Mach number for $\alpha_{eq} > 99\%$ versus upstream pressure for different initial temperatures shows that the Mach number increases with pressure, the variation becoming less as the initial temperature increases. Further, the Mach number for $\alpha_{eq} > 99\%$ increases with decrease of initial temperature because as may be expected an increase in either the initial temperature or the initial Mach number is required to produce the high temperature behind the shockwave.

6.2 Shock Structure Profiles:

The structure profiles for various parameters of interest are plotted in Figs.(6.1.1) to (6.15.1) for argon, krypton and xenon for different initial conditions. On the whole the structure profiles show a similar behaviour for different initial conditions. Over almost the entire part of the gasdynamic shock region the structure profiles are independent of the initial pressure and temperature and are also independent of the gas. The length of the relaxation zone, however, does depend upon the initial conditions like pressure, temperature and also the gas. This is pronounced at high initial Mach numbers. The intermediate zones do not depend

upon the initial conditions for low Mach numbers whereas for higher Mach numbers they do show a weak dependence.

Curves in Figs. (6.6.1) to (6.6.3) show typical variations of the weight functions N_1, N_2 and N_3 used in the trimodal distribution function for the atom gas. In the region of the gasdynamic shock, N_1 decreases monotonically to zero and N_2 increases monotonically from zero as in the case of Mott-Smith's study. Towards the end of the gasdynamic shock region N_2 reaches a maximum and starts decreasing when N_3 will have started building up. N_1 reaches zero quite early, particularly, for low Mach numbers; N_2 and N_3 will be active throughout the relaxation zone. Towards the end of the relaxation zone $N_2 \to 0$ while N_3 approaches the equilibrium atom density value, the downstream equilibrium region being characterized by N_3 alone. When either N_1 alone or N_3 alone is present alongwith N_2 the gasdynamic shock region and the relaxation zone are clearly separable, at least conceptually. For high Mach numbers, particularly with the choice of a larger value of C_{aa} (as used by earlier investigators) such a separation does not seem to be a good approximation and a trimodal representation of the present type is perhaps better.

The atom and ion temperatures increase very rapidly within the gasdynamic shock and starts drooping in the relaxation zone with large gradients towards the end. The maximum atom and ion temperatures reached will be less than the inert gas equilibrium value. The electron temperature rises rapidly from its upstream equilibrium value to around its downstream equilibrium value remaining almost constant over the rest of the flow region where the electron gas loses energy in inelastic collisions at just the same rate as it gains energy through elastic collisions with heavy particles. The initial rise in the electron temperature results from a continuous supply of energy through elastic collisions from the heavy particles in the absence of inelastic collisions. This energy transfer rate depends upon the mass ratio ϵ and the difference between atom and electron temperatures. For high Mach numbers the heavy particle temperatures attained within the gasdynamic shock are very high. Consequently the electron temperature rises rapidly and reaches a constant value almost by the end of the gasdynamic shock region. But for low Mach numbers, because of the relatively lower heavy particle temperatures developed within the shock the region of electron temperature rise extends much beyond the atom-atom shock as can be seen from Fig.(6.2.1). For argon due to its relatively larger mass ratio, the electron temperature rises

fast and attains an almost constant value, whereas for xenon due to its much lower mass ratio the electron temperature not only rises slowly but also attains a lower constant value. Over a large part of the relaxation zone the electron temperature rises very slowly and reaches the atom temperature towards the end of the relaxation zone and finally both the temperatures together go to the equilibrium temperature. Similar qualitative behaviour of the electron temperature has been reported by earlier investigations also neglecting radiation cooling effects. For $M = 40$, nearly half the electron temperature rise takes place in a narrow region towards the end of the relaxation zone. This is possibly due to the very low inelastic energy loss in this region since recombination almost balances the ionization rate. For lower Mach numbers however the recombination rates were found to be less then the ionization rate when the two temperatures get equalised. For low Mach numbers it was found[77] that recombination plays a minor role over the entire relaxation zone and, hence, could be neglected. For high Mach numbers, however, the recombination is important in determining the electron temperature profiles and, perhaps, radiation cooling also may have considerable influence. This aspect however needs further experimental investigation.

The density profiles are practically unaffected by the presence of ionization in the gasdynamic shock but for a slight rise in density towards the end of the gasdynamic shock noticeable only for high Mach numbers. Apart from the gasdynamic shock, a large part of the density changes occur only towards the end of the relaxation zone where a major part of the equilibrium electron density is built up. In this region both the total density and ionization degree increase to their equilibrium value rapidly.

The computed electrical conductivity σ has been plotted for only that part of the shock where $\alpha > 10^{-3}$ since, as already mentioned, the present calculations of the electrical conductivity are reliable only for a degree of ionization greater than $\sim 10^{-3}$. Qualitatively the behaviour of σ is mainly decided by the shape of the electron temperature profiles; the electron density influences through a logarithmic term. In the earlier parts of the shock σ increases very fast due to a similar increase in the electron temperature. In a large part of the relaxation zone where the electron temperature changes very little the electrical conductivity continues to increase slowly due to an increase in the electron density. Towards the end

of the relaxation zone once again a fall in electron temperature, if any, influences the electrical conductivity so that the σ profiles show a peak towards the end before attaining the equilibrium value. From Figs. (6.2.4) and (6.4.4) it can be observed that for initial pressures of 1.0 and 10 torrs. the fall in electron temperature is sufficient enough to produce a peak in the σ curves. But for an initial pressure of 0.1 torr. since the electron temperature gradient is small no peak is seen in the σ curves. For M = 40, associated with a steep rise in electron temperature towards the end of the relaxation zone there is also seen a corresponding rapid increase in the electrical conductivity.

The refractive index(μ) profiles within the shock for argon have been obtained using a value of $\xi_+ / \xi_a = 0.67$ [37]. In the earlier region of the shock when the lectron density is very small the contribution to μ arises only from the second term of the eq. (5.33) and increases as the density increases. Towards the downstream end where the electron density is sufficient enough so that the third term of eq. (5.33) becomes comparable to the second, μ ceases to

increase and starts decreasing further downstream. The refractive index profiles are in qualitative agreement with those obtained from the observed fringe shifts in the experiments.[37,77]

Amongst the other parameters of interest the profiles of electric field and the electric potential are also presented. Thus, Fig.(6.11.1)shows a typical variation of electric field with two peaks. At first, because of the large electron temperature gradients present a thermal diffusion of electrons takes place giving rise to a steep rise in the electric field. As the electron temperature gradient decreases to a very low value the electric field also decreases and then slowly increases because of the electron diffusion resulting from the electron density gradient, over a large part of the relaxation zone. Towards the end of the relaxation zone because of very large electron density gradients causing strong electron diffusion the electric field again increases rapidly and ultimately decreases to zero at the downstream end where no gradients are present. The electric potential (Figs. 6.7.1 to 6.7.3) is positive every where which indicates that the electrons move upstream relative to the ions to smoothout the gradients. The other parameters of interest namely the pressure, velocity etc. are also presented and need no explanation.

6.3 Onset-degree of Ionization:

The onset-degree of ionization is of interest as it helps to identify the region of atom-electron collisional ionization dominance. The region downstream of the onset point is practically independent of the priming mechanisms. The onset-α and the onset point for different shock Mach numbers are given in tables (6.1) to (6.6). The onset-α is also plotted against Mach number in Fig. (6.22.1). It can be seen that the onset degree of ionization increases with increase of Mach number and seems to reach an asymptotic value for large Mach numbers. However, at such high Mach numbers it is doubtful if the atom-atom collisional ionization is the appropriate initiating mechanism. The onset-α strongly depends on the value of C_{aa}, has a higher value for krypton and a relatively lower value for xenon. The onset degree of ionization has a slight dependence on the initial pressure.

6.4 Shock Thickness:

The shock thickness and the thickness parameter have been computed for each case and are presented in tables 6.1 to 6.6 for the three gases. Since collisional ionization is predominantly binary the relaxation time will exhibit an inverse initial pressure dependence. Consequently, $p_1 \tau$ is

independent of the initial pressure and has been recommended as a suitable parameter for comparison purposes. The shock thickness δ decreases with increase of Mach number. Since the nondimensional shock thickness increases very slowly with pressure, the actual shock thickness decreases almost inversely with pressure. The shock thickness also depends upon the excitation and ionization potentials and the cross section for the atom-atom collisional ionization. It increases with decrease of the atom-atom collisional ionization cross section. The shock thickness is less sensitive to C_{ae} because the rate of atom-electron collision ionization is decided by the rate of energy transfer to the electron gas from ion gas, which in turn depends upon the mass ratio ϵ. It may be seen that krypton has the smallest shock thickness and xenon has the largest amongst the three gases studied. The smaller shock thickness in krypton is due to its lower excitation and ionization potentials and also its larger atom-atom collisional excitation cross section. Since argon has a slightly lower value of this cross section and comparatively larger activation energies it has shock thicknesses larger than those of krypton gas. On the other hand though xenon has the lowest values of activation potentials compared to argon and krypton, its atom-atom collisional excitation cross section

is nearly 10 times smaller. This in addition to its relatively larger atomic weight causes much broader shocks in xenon compared to the other two gases.

The thickness parameter $p_1 \tau$ is plotted against Mach number for the three gases in Fig. (6.23.1). The results of Chubb and also the results from the present investigation for argon with $C_{aa} = 1.2 \times 10^{-19} cm^2/eV$ have been included for comparison. The qualitative behaviour is in general agreement with Chubb's results and the quantitative discrepancy is mainly due to a different value of C_{aa} chosen. The curve for argon with $C_{aa} = 1.2 \times 10^{-19} cm^2/eV$ lies very close to the corresponding curve of Chubb but has a faster asymptotic variation with Mach number than the other. In Fig. (6.24.1) the thickness parameter $p_1 \tau$ is plotted against the reciprocal of the maximum atom temperature within the shock to compare the present results with earlier theories and experiments. Some of the results of Wong and Bershader[77], and Petschek and Byron[62] are also reproduced here. The results of Hoffert and Lien[36] and also Morgan and Morrison[50] have been given. Results of the present investigation seem to show a close agreement with the measurements of Wong and Bershader at lower Mach numbers. Lack of availability of experimental results in the high Mach number range precludes any better comparison than

this. The high Mach number results of Hoffert and Lien, and those of Petschek and Byron for higher degree of purity extrapolated to larger Mach numbers, seem to agree with the present studies.

6.5 Conclusions:

For large Mach numbers ($M \sim 30$) it is necessary to consider the gasdynamic shock and the relaxation zone simultaneously since it is difficult to assign a definite plane of demarcation between the two regions. It is still worse when a relatively larger value of the atom-atom collisional excitation cross section is used for which there does not exist an intermediate plateau in the shock structure profiles. A trimodal distribution function model of the atom gas on the other hand overcomes this difficulty and the entire region of nonequilibrium can be studied uniformly without resorting to identifying the two regions. However, no justification for a trimodal distribution postulate has been given.

The good agreement of the results of the present work with those of Wong and Bershader is mainly attributable to the better choice of the atom-atom collisional excitation

cross section used. The shock thickness and the onset point depend strongly upon the value of this cross section whereas they are less sensitive to the choice of the atom-electron collisional excitation cross section. Further a steady state electron energy equation seems to be a good approximation for a large part of the relaxation zone and the electron temperature variations are significant only in the gasdynamic shock and towards the end of the relaxation zone.

The effect of radiation on initial ionization and cooling of the downstream equilibrium region along with absorption and emission of the radiation by the gas is to be included for a more meaningful study. More reliable experimental cross sections for the photoprocesses still remain for investigation before a general study of this type can be carried through. The effect of second ionization is to be included in large Mach number studies.

18. Champman, S. and Cowling, T.G., 'The Mathematical Theory of Non-Uniform Gases', Cambridge University Press (1964)

19. Chubb, D.L., Phys. Fluids 11, 2363 (1968)

20. Clarke, J.H. and Ferrari, C., Phys. Fluids 8, 2121 (1965)

21. Clauser, F.H., 'Symposium of Plasma Dynamics', Addison-Wesley Reading, Massachusetts (1960)

22. Cottrell, T.L., Discussions Faraday Soc., 22, 10 (1956)

23. Daniel, P.A. and Ali, B.C., Phys. Fluids 13, 2466 (1970)

24. Devoto, R.S., Phys. Fluids 10, 354 (1967)

25. Dobbins, R.A., AIAA Fluid and Plasma Dynamics Conference, Preprint 68, 666 (1968)

26. Drawn, H.W., and Felenbok, P., 'Data for Plasmas in Local Thermodynamic Equilibrium', (Garthier-Villars, Paris) (1965)

27. Dronov, A .P., Sviridov, A.G. and Sobolev, N.N., Optics and Spectroscopy 12, 383 (1962)

28. Frost, L.S. and Phelps, A.V., Phys. Rev. 136, A1538 (1964)

29. Gustafson, W.A., Phys. Fluids 3, 732 (1960)

30. Haight, C.H., 'Shock Structure in Gas of Rigid Non-central Particles' Ph.D. thesis, Univ. of Minnesota (1965)

31. Haight, C.H., and Lundgren, T.S., Phys. Fluids 10, 786 (1967)

32. Haight, C.H., and Lundgren, T.S., 'Trimodal Solutions for Shock Structure in A Gas of Spherocylinders' Report No. O-71000/8R-1, LTV Research Center, January (1968)

33. Harwell, K.E. and Jahn, R.G., Phys. Fluids 7, 214 (1964)

34. Heaslet, N.H. and Baldwin, B.S., Phys. Fluids 6, 781 (1963)

35. Hirschfelder, J.O., Curtiss, C.F., and Bird, R.V., 'Molecular Theory of Gases and Liquids', Wiley and Sons Inc., N.Y. (1954)

36. Hoffert, M.I. and Lien, H., Phys. Fluids 10, 1769 (1967)

37. Horn, K.P., Wong, H. and Bershader, D., J. Plasma Phys. 1, 157 (1967)

38. Johnston, N.S. and Kornegay, W., Trans. Faraday Soc. 57, 1563 (1961)

39. Kelly, A.J., J. Chem. Phys. 45, 1723 (1966)

40. Koga, T. 'Rarefied Gas Dynamics' 1, Academic Press, New York, London (1963)

41. Lee, P. and Weissler, G.L., Phys. Rev. 99, 540 (1955)

42. Liepmann, H.W., Narasimha, R. and Chahine, M.T., Phys. Fluids 5, 1313 (1962)

43. Lighthill, M.J., 'Surveys in Mechanics' Cambridge University Press (1956)

44. Lin, S.C., Resler, E.L. and Kantrowitz, A., J. Appl. Phys. 26. 95 (1955)

45. Maier Leibnitz, V.H., Z. Phys. 95, 499 (1935)

46. Massey, H.S.W. and Burhop, E.H.S., 'Electronic and Ionic Impact Phenomena', Oxford University Press, London (1952)

47. McChesney, M. and Al-Attar, Z., JQSRT. 5, 553 (1965)

48. McLaren, T.I. and Hobson, R.M., Phys. Fluids 11, 2162 (1968)

49. Monchik, L., Phys. Fluids 2, 695 (1959)

50. Morgan, E.J. and Morrison, R.D., Phys. Fluids 8, 1608 (1965)

51. Mott-Smith, H.M., Phys. Rev. 82, 885 (1951)

52. Muckenfuss, C., Phys. Fluids 5, 1325 (1962)

53. Murty, S.S.R., JQSRT. 8, 531 (1968)

54. Murty, S.S.R., Aeronautical Soc. of India and Indian Institute of Science Joint Technical Sessions, May (1968), Bangalore

55. Narasimha, R. and Deshpande, S.M., J. Fluid Mech. 36, 555 (1969)

56. Narasimha, R., Phys. Fluids 9, 2524 (1966)

57. Nelson, H.F. and Goulard, R., Phys. Fluids 12, 1605 (1969)

58. Oberai M.M., Phys. Fluids 8, 826 (1965)

59. Oettinger, P.E. and Bershader, D., AIAA Journal 5, 1625 (1967)

60. O'Malley, T.F., Phys. Rev. 130, 1020 (1963)

61. Pack, J.L. and Phelps, A.V., Phys. Rev. 121, 798 (1961)

62. Petschek, H.E. and Byron, S.R., Ann. Phys. 1, 270 (1957)

63. Petschek, H.E., Rose, P.H., Glick, H.S., Kane, A. and Kantrowitz, A., J. Appl. Phys. 26, 83 (1955)

64. Pomerantz, J., JQSRT. 1, 185 (1961)

65. Ramsauer, C. and Kollath, R., Ann. Physik 3, 536 (1929)

66. Ramsauer, C. and Kollath, R., Ann. Physik 12, 529 and 837 (1932)

67. Redkoborodyi, Y.N. and Fedulov, V.I., Soviet Phys. - Tech. Phys 10, 1275 (1966)

68. Rode, D.L. and Tanenbaum, B.S., Phys. Fluids 10, 1352 (1967)

69. Rosen, P., J. Chem. Phys 22, 1045 (1954)

70. Rutowski, R.W. and Bershader, D., Phys. Fluids 7, 568 (1964)

71. Sakurai, A., J. Fluid Mech. 3, 255 (1957)

72. Sevastyaneko, V.G. and Yakubov, I.T., Optics and Spectroscopy 16, 1 (1964)

73. Spitzer, L. Jr., 'Physics of Fully Ionized Gases', John Wiley and Sons, Inc. New York (1962)

74. Spitzer, L. Jr. and Härm, R., Phys. Rev. 89, 977 (1953)

75. Wannier, G.H., Phys. Rev. 96, 831 (1954)

76. Wilson, D.S. and Lederman, S., Polytechnic Institute of Brooklyn, PBIAL Report No. 1033 (1967)

77. Wong, H. and Bershader, D., J. Fluid Mech. 26, 459 (1966)

78. Zel' dovich, Y.B. and Raizer, Y.P., 'Physics of Shock Waves and High-Temperature Hydrodynamic Phenomena', Academic Press, New York and London, Parts I and II (1967)

79. Rothe, E.W. and Bernstein, R.B., J. Chem. Phys. 31, 1619 (1959)

80. Jeans, J.H., 'The Dynamical Theory of Gases' Dover Publications, Inc. (1925)

Table-5.1:Equilibrium Properties Across Ionizing Shock in Ar. ,T_1=300°K.

	p_1 = 0.1 torr.				p_1 = 1.0 torr.			
M_1	M_2	α^*	$\bar{\rho}^*$	$\bar{T}^*$	M_2	α^*	$\bar{\rho}^*$	$\bar{T}^*$
10	0.4793	0.0192	4.696	27.61	0.4791	0.0123	4.375	29.26
11	0.3996	0.0382	5.390	29.53	0.4148	0.0285	4.939	31.06
12	0.3417	0.0608	6.127	31.05	0.3573	0.0490	5.568	33.86
13	0.2959	0.0864	6.873	32.35	0.3107	0.0729	6.219	35.53
14	0.2594	0.1147	7.627	33.50	0.2729	0.0995	6.872	37.28
15	0.2299	0.1454	8.364	34.56	0.2423	0.1287	7.515	38.44
16	0.2059	0.1786	9.084	35.56	0.2171	0.1603	8.142	39.72
17	0.1860	0.2141	9.781	36.50	0.1959	0.1943	8.749	40.93
18	0.1693	0.2518	10.450	37.41	0.1786	0.2304	9.332	42.09
19	0.1552	0.2918	11.089	38.29	0.1640	0.2687	9.892	43.22
20	0.1431	0.3339	11.692	39.15	0.1513	0.3090	10.404	44.32
21	0.1327	0.3782	12.260	40.01	0.1404	0.3515	10.893	45.41
22	0.1237	0.4245	12.790	40.87	0.1309	0.3958	11.347	46.50
23	0.1158	0.4728	13.279	41.74	0.1226	0.4421	11.756	47.61
24	0.1089	0.5230	13.725	42.63	0.1153	0.4902	12.147	48.73
25	0.1028	0.5750	14.126	43.55	0.1089	0.5399	12.483	49.86
26	0.0973	0.6287	14.479	44.52	0.1031	0.5913	12.787	51.09
27	0.0923	0.6839	14.774	45.57	0.0980	0.6440	13.041	52.37
28	0.0881	0.7402	15.007	46.74	0.0934	0.6979	13.243	53.77
29	0.0842	0.7972	15.161	48.09	0.0893	0.7525	13.387	55.32
30	0.0807	0.8547	15.208	49.73	0.0855	0.8072	13.459	57.13
31	0.0773	0.9087	15.093	51.95	0.0821	0.8603	13.424	59.34
32	0.0736	0.9566	14.689	55.37	0.0787	0.9113	13.270	62.26
33	0.0647	1.0000	14.195	59.62	0.0753	0.9542	13.807	66.52
34	0.0669	1.0000	12.591	70.47	0.0718	0.9826	13.203	73.15
35	0.0680	1.0000	11.417	81.62	0.0686	1.0000	11.417	81.62
36	0.0698	1.0000	10.505	93.07	0.0698	1.0000	10.505	93.07
37	0.0706	1.0000	9.777	104.80	0.0706	1.0000	9.777	104.80
38	0.0712	1.0000	9.182	116.84	0.0712	1.0000	9.182	116.84
39	0.0716	1.0000	8.687	129.16	0.0716	1.0000	8.687	129.16
40	0.0718	1.0000	8.270	141.79	0.0718	1.0000	8.270	141.79

Table-5.2: Equilibrium Properties Across Ionizing Shock in Ar., T_1=300°K.

	p_1 = 10.0 torrs				p_1 = 100.0 torrs			
M_1	M_2	α^*	$\bar{\rho}^*$	$\bar{T}^*$	M_2	α^*	$\bar{\rho}^*$	$\bar{T}^*$
10	0.4786	0.0065	4.135	30.60	0.4702	0.0023	3.930	31.47
11	0.4263	0.0189	4.550	34.16	0.4304	0.0105	4.248	36.15
12	0.3727	0.0363	5.059	36.91	0.3846	0.0241	4.622	39.95
13	0.3261	0.0579	5.604	39.20	0.3428	0.0421	5.053	43.09
14	0.2876	0.0824	6.159	41.20	0.3036	0.0635	5.502	45.93
15	0.2559	0.1090	6.708	43.01	0.2704	0.0874	5.953	48.42
16	0.2297	0.1391	7.244	44.69	0.2434	0.1143	6.405	50.57
17	0.2079	0.1716	7.762	46.28	0.2208	0.1439	6.836	52.71
18	0.1896	0.2056	8.257	47.80	0.2016	0.1752	7.247	54.77
19	0.1740	0.2412	8.727	49.28	0.1853	0.2083	7.637	56.76
20	0.1607	0.2795	9.169	50.72	0.1712	0.2433	8.004	58.72
21	0.1491	0.3194	9.582	52.13	0.1591	0.2800	8.345	60.67
22	0.1391	0.3613	9.965	53.57	0.1485	0.3197	8.660	62.52
23	0.1304	0.4050	10.317	55.03	0.1393	0.3602	8.949	64.42
24	0.1227	0.4504	10.635	56.45	0.1311	0.4021	9.210	66.25
25	0.1159	0.4974	10.921	57.93	0.1239	0.4456	9.443	68.09
26	0.1098	0.5458	11.171	59.46	0.1174	0.4903	9.648	70.01
27	0.1044	0.5955	11.384	61.07	0.1117	0.5360	9.822	72.00
28	0.0995	0.6460	11.558	62.78	0.1066	0.5823	9.969	74.05
29	0.0951	0.6975	11.693	64.64	0.1019	0.6288	10.092	76.15
30	0.0911	0.7496	11.788	66.71	0.0976	0.6748	10.192	78.33
31	0.0875	0.8016	11.790	69.08	0.0937	0.7263	10.285	82.74
32	0.0842	0.8519	11.738	71.91	0.0902	0.7743	10.206	85.60
33	0.0810	0.8977	11.582	75.46	0.0870	0.8173	10.160	88.53
34	0.0778	0.9381	11.308	80.19	0.0839	0.8563	10.057	92.62
35	0.0749	0.9681	10.868	86.71	0.0811	0.9032	9.836	97.59
36	0.0727	0.9857	10.300	95.41	0.0784	0.9352	9.641	103.77
37	0.0718	0.9937	9.701	105.86	0.0761	0.9613	9.323	111.47
38	0.0717	0.9971	9.152	117.34	0.0744	0.9774	8.955	120.79
39	0.0718	0.9985	8.674	129.43	0.0733	0.9871	8.574	131.49
40	0.0719	0.9992	8.264	141.94	0.0727	0.9925	8.212	143.19

Table-5.3: Equilibrium Properties Across Ionizing Shock in Kr., T_1=300°K.

	p_1 = 0.1 torr				p_1 = 1.0 torr			
M_1	M_2	α^*	$\bar{\rho}^*$	$\bar{T}^*$	M_2	α^*	$\bar{\rho}^*$	$\bar{T}^*$
10	0.4545	0.0292	5.041	25.94	0.4687	0.0203	4.646	27.10
11	0.3839	0.0516	5.796	27.54	0.4007	0.0403	5.279	29.95
12	0.3281	0.0775	6.576	28.86	0.3445	0.0643	5.950	31.69
13	0.2847	0.1066	7.358	30.02	0.2995	0.0919	6.629	33.19
14	0.2510	0.1384	8.130	31.06	0.2635	0.1217	7.291	34.55
15	0.2221	0.1730	8.882	32.04	0.2344	0.1546	7.930	35.84
16	0.1993	0.2102	9.610	32.96	0.2105	0.1901	8.545	37.09
17	0.1804	0.2499	10.307	33.84	0.1906	0.2283	9.132	38.32
18	0.1646	0.2921	10.970	34.69	0.1740	0.2693	9.686	39.52
19	0.1512	0.3368	11.595	35.53	0.1599	0.3131	10.206	40.69
20	0.1397	0.3837	12.180	36.37	0.1479	0.3596	10.690	41.86
21	0.1298	0.4330	12.722	37.20	0.1374	0.4087	11.140	43.02
22	0.1212	0.4845	13.219	38.05	0.1284	0.4603	11.557	44.19
23	0.1137	0.5380	13.667	38.92	0.1205	0.5142	11.941	45.37
24	0.1071	0.5935	14.064	39.83	0.1135	0.5703	12.293	46.57
25	0.1013	0.6509	14.405	40.81	0.1074	0.6285	12.614	47.80
26	0.0961	0.7097	14.691	41.87	0.1019	0.6885	12.906	49.08
27	0.0915	0.7695	14.879	43.08	0.0970	0.7502	13.170	50.41
28	0.0873	0.8296	14.978	44.53	0.0926	0.8132	13.408	51.80
29	0.0836	0.8884	14.930	36.42	0.0886	0.8765	13.618	53.26
30	0.0795	0.9420	14.631	49.22	0.0849	0.9338	13.812	55.09
31	0.0749	0.9809	13.871	54.13	0.0811	0.9719	13.808	59.41
32	0.0727	1.0000	12.727	61.82	0.0772	0.9769	12.195	65.04
33	0.0726	1.0000	11.459	72.33	0.0726	1.0000	11.459	72.33
34	0.0739	1.0000	10.490	83.12	0.0739	1.0000	10.490	83.12
35	0.0749	1.0000	9.726	94.22	0.0749	1.0000	9.726	94.22
36	0.0755	1.0000	9.109	105.60	0.0755	1.0000	9.109	105.60
37	0.0759	1.0000	8.600	117.29	0.0759	1.0000	8.600	117.29
38	0.0761	1.0000	8.174	129.27	0.0761	1.0000	8.174	129.27
39	0.0761	1.0000	7.811	131.55	0.0761	1.0000	7.811	141.55
40	0.0759	1.0000	7.500	154.13	0.0759	1.0000	7.500	154.13

Table-5.4: Equilibrium Properties Across Ionizing Shock in Kr., T_1=300°K.

	p_1 = 10.0 torrs				p_1 = 100.0 torrs			
M_1	M_2	α^*	$\bar{\rho}^*$	$\bar{T}^*$	M_2	α^*	$\bar{\rho}^*$	$\bar{T}^*$
10	0.4762	0.0124	4.322	29.51	0.4742	0.0052	4.094	30.82
11	0.4158	0.0287	4.616	32.45	0.4256	0.0177	4.434	34.85
12	0.3669	0.0498	5.372	34.81	0.3757	0.0349	4.861	38.09
13	0.3154	0.0746	5.943	36.83	0.3313	0.0553	5.323	40.86
14	0.2733	0.1025	6.516	38.63	0.2932	0.0790	5.792	43.35
15	0.2480	0.1332	7.074	39.29	0.2627	0.1036	6.253	45.53
16	0.2250	0.1664	7.613	41.85	0.2368	0.1290	6.700	47.70
17	0.2032	0.2021	8.126	43.54	0.2151	0.1717	7.125	49.71
18	0.1847	0.2401	8.612	44.79	0.1968	0.2056	7.527	51.67
19	0.1699	0.2804	9.067	46.29	0.1812	0.2437	7.903	53.57
20	0.1572	0.3227	9.490	47.59	0.1678	0.2832	8.251	55.45
21	0.1462	0.3672	9.880	48.98	0.1562	0.3238	8.571	57.31
22	0.1366	0.4136	10.234	50.38	0.1461	0.3656	8.860	59.18
23	0.1283	0.4618	10.553	51.80	0.1372	0.4111	9.120	61.03
24	0.1209	0.5117	10.833	53.27	0.1294	0.4571	9.349	63.01
25	0.1144	0.5632	11.075	54.79	0.1225	0.5042	9.547	65.00
26	0.1086	0.6160	11.276	56.40	0.1165	0.5531	9.713	67.07
27	0.1034	0.6698	11.431	58.14	0.1108	0.6026	9.845	69.25
28	0.0988	0.7241	11.536	60.05	0.1059	0.6524	9.944	71.58
29	0.0945	0.7784	11.583	62.22	0.1013	0.7031	10.001	74.12
30	0.0907	0.8316	11.557	64.78	0.0972	0.7532	10.018	76.94
31	0.0871	0.8819	11.438	67.95	0.0935	0.8020	9.986	80.15
32	0.0836	0.9265	11.192	72.13	0.0901	0.8453	9.899	83.91
33	0.0802	0.9616	10.788	77.89	0.0869	0.8808	9.745	88.44
34	0.0770	0.9823	10.237	85.72	0.0839	0.9271	9.516	94.[illegible]
35	0.0764	0.9929	9.635	95.37	0.0813	0.9556	9.212	101.12
36	0.0761	0.9965	9.074	106.15	0.0792	0.9738	8.852	109.72
37	0.0762	0.9983	8.585	117.57	0.0779	0.9851	8.473	119.70
38	0.0762	0.9991	8.167	129.43	0.0771	0.9914	8.109	130.72
39	0.0761	0.9995	7.808	141.65	0.0766	0.9948	7.777	142.45
40	0.0760	0.9997	7.498	154.19	0.0762	0.9967	7.481	154.72

Table-5.5:Equilibrium Properties Across Ionizing Shock in Xe., T_1=300°K.

	p_1 = 0.1 torr				p_1 = 1.0 torr			
M_1	M_2	α^*	$\bar{\rho}^*$	$\bar{T}^*$	M_2	α^*	$\bar{\rho}^*$	$\bar{T}^*$
10	0.4332	0.0444	5.517	23.86	0.4510	0.0363	5.036	25.85
11	0.3652	0.0712	6.334	25.18	0.3829	0.0581	5.754	27.61
12	0.3128	0.1017	7.158	26.31	0.3291	0.0865	6.446	29.09
13	0.2719	0.1355	7.972	27.32	0.2856	0.1184	7.152	30.41
14	0.2395	0.1724	8.764	28.26	0.2520	0.1534	7.840	31.63
15	0.2133	0.2123	9.527	29.15	0.2254	0.1914	8.501	32.77
16	0.1920	0.2551	10.255	29.99	0.2039	0.2323	9.130	33.86
17	0.1742	0.3003	10.944	30.81	0.1844	0.2758	9.722	34.91
18	0.1594	0.3492	11.588	31.62	0.1687	0.3221	10.270	35.93
19	0.1467	0.4003	12.186	32.42	0.1555	0.3709	10.767	36.90
20	0.1360	0.4543	12.734	33.23	0.1441	0.4221	11.214	38.01
21	0.1267	0.5101	13.229	34.06	0.1343	0.4756	11.613	39.07
22	0.1186	0.5665	13.668	34.92	0.1258	0.5315	12.046	40.15
23	0.1115	0.6291	14.044	35.83	0.1183	0.5892	12.306	41.25
24	0.1053	0.6915	14.352	36.83	0.1115	0.6486	12.619	42.31
25	0.0998	0.7552	14.578	37.96	0.1060	0.7097	12.826	43.35
26	0.0949	0.8195	14.697	39.30	0.1008	0.7707	12.951	45.38
27	0.0905	0.8824	14.663	41.05	0.0961	0.8316	12.976	47.22
28	0.0860	0.9398	14.365	43.66	0.0918	0.8839	12.865	49.61
29	0.0807	0.9811	13.577	48.31	0.0875	0.9411	12.540	53.14
30	0.0765	1.0000	12.389	55.69	0.0831	0.9770	11.901	58.44
31	0.0785	1.0000	11.128	65.54	0.0785	1.0000	11.128	65.54
32	0.0799	1.0000	10.173	75.69	0.0749	1.0000	10.173	75.69
33	0.0818	1.0000	9.425	86.13	0.0808	1.0000	9.425	86.13
34	0.0814	1.0000	8.824	96.86	0.0814	1.0000	8.824	96.86
35	0.0817	1.0000	8.330	107.89	0.0817	1.0000	8.330	107.89
36	0.0818	1.0000	7.919	119.22	0.0818	1.0000	7.919	119.22
37	0.0817	1.0000	7.571	130.85	0.0817	1.0000	7.571	130.85
38	0.0814	1.0000	7.272	142.78	0.0814	1.0000	7.272	142.78
39	0.0810	1.0000	7.014	155.02	0.0810	1.0000	7.014	155.02
40	0.0805	1.0000	6.789	167.55	0.0805	1.0000	6.789	167.55

Table-5.6: Equilibrium Properties Across Ionizing Shock in Xe., T_1=300°K.

	p_1 = 10.0 torrs				p_1 = 100.0 torrs			
M_1	M_2	α^*	$\bar{\rho}^*$	$\bar{T}^*$	M_2	α^*	$\bar{\rho}^*$	$\bar{T}^*$
10	0.4655	0.0227	4.615	27.87	0.4724	0.0131	4.283	29.67
11	.4005	0.0439	5.183	30.26	0.4153	0.0258	4.707	32.93
12	.3464	0.0696	5.781	32.26	0.3683	0.0413	5.181	35.74
13	.3027	0.0989	6.379	34.03	0.3296	0.0774	5.666	38.26
14	.2676	0.1314	6.962	35.64	0.2826	0.1063	6.148	40.56
15	0.2390	0.1669	7.524	37.15	0.2539	0.1435	6.611	42.42
16	.2155	0.2052	8.056	38.59	0.2294	0.1784	7.041	44.37
17	.1959	0.2461	8.557	39.99	0.2088	0.2189	7.464	46.26
18	.1794	0.2896	9.023	41.35	0.1915	0.2567	7.846	48.13
19	.1654	0.3355	9.452	42.70	0.1767	0.2942	8.187	49.94
20	.1534	0.3837	9.842	44.05	0.1641	0.3372	8.525	51.70
21	.1430	0.4340	10.192	45.42	0.1531	0.3835	8.800	53.59
22	0.1340	0.4864	10.501	36.82	0.1435	0.4315	9.051	55.46
23	.1261	0.5405	10.767	38.28	0.1351	0.4814	9.268	57.37
24	.1192	0.5963	10.987	49.81	0.1277	0.5328	9.449	59.36
25	.1130	0.6532	11.159	51.46	0.1211	0.5846	9.592	61.45
26	0.1075	0.7110	11.277	53.27	0.1153	0.6370	9.700	63.66
27	.1026	0.7687	11.331	55.32	0.1100	0.6890	9.765	66.11
28	.0981	0.8253	11.309	57.75	0.1053	0.7440	9.785	68.89
29	0.0940	0.8788	11.188	60.77	0.1010	0.7957	9.754	71.88
30	0.0901	0.9258	10.933	64.77	0.0971	0.8446	9.664	75.46
31	0.0868	0.9617	10.512	70.33	0.0934	0.8894	9.505	79.80
32	0.0835	0.9829	9.947	77.88	0.0901	0.9271	9.268	85.30
33	0.0823	0.9927	9.345	87.09	0.0872	0.9556	8.956	92.14
34	0.0820	0.9967	8.793	97.32	0.0850	0.9744	8.592	100.41
35	.0820	0.9983	8.317	108.13	0.0836	0.9855	8.217	109.98
36	0.0819	0.9991	7.913	119.36	0.0828	0.9915	7.861	120.46
37	0.0817	0.9995	7.567	130.94	0.0822	0.9949	7.540	131.64
38	0.0814	0.9997	7.270	142.84	0.0817	0.9967	7.255	143.30
39	0.0810	0.9998	7.013	155.05	0.0811	0.9975	7.004	155.37
40	0.0805	0.9998	6.788	167.58	0.0806	0.9985	6.782	167.81

Table 6.1

Characteristics of Ionizing Shock

Argon: $p_1 = 0.1$ torr. $T_1 = 300^{\circ}K$

M_1	L(cms)	α-Onset $x10^{2}$	$\bar{x}$-Onset $x10^{-2}$	δ(cms) $x10^{-2}$	τ (secs.) $x10^{4}$	δ/L $x10^{-2}$
15	0.2753	0.0919	1.3600	1.4636	3.0241	5.3159
20	0.3671	0.4923	0.3482	0.3282	0.5086	0.8940
25	0.4589	1.0175	0.1612	0.1565	0.1940	0.3410
30	0.5506	1.5298	0.1031	0.1065	0.1100	0.1934
35	0.6424	2.0033	0.0789	0.0892	0.0790	0.1388
40	0.7342	2.4384	0.0664	0.0772	0.0599	0.1052

Table 6.2

Characteristics of Ionizing Shock

Argon: p_1 = 1.0 torr. T_1 = 300°K

M_1	L(cms) x10	α-Onset $x10^2$	$\bar{x}$-Onset $x10^{-2}$	δ(cms) $x10^{-1}$	τ(secs.) $x10^5$	δ/L $x10^{-2}$
15	0.2753	0.0940	1.4000	1.4831	3.0645	5.3869
20	0.3671	0.5173	0.3630	0.3449	0.5342	0.9396
25	0.4589	1.0790	0.1684	0.1664	0.2063	0.3626
30	0.5506	1.6303	0.1073	0.1122	0.1159	0.2037
35	0.6424	2.1377	0.0815	0.0936	0.0829	0.1457
40	0.7342	2.6075	0.0683	0.0809	0.0627	0.1102

Table 6.3

Characteristics of Ionizing Shock

Argon: $p_1 = 10.0$ torrs. $T_1 = 300^{\circ}K$

M_1	L(cms) $\times 10^{2}$	α-Onset $\times 10^{2}$	$\bar{x}$-Onset $\times 10^{-2}$	δ(cms)	τ (secs.) $\times 10^{6}$	δ/L $\times 10^{-2}$
15	0.2753	0.0956	1.4100	1.5233	3.1476	5.533
20	0.3671	0.5469	0.3805	0.3682	0.5706	1.0030
25	0.4589	1.1577	0.1775	0.1796	0.2226	0.3913
30	0.5506	1.7578	0.1126	0.1211	0.1251	0.2199
35	0.6424	2.3111	0.8490	0.0998	0.0883	0.1553
40	0.7342	2.8083	0.7060	0.0859	0.0666	0.1170

Table 6.4

Characteristics of Ionizing Shock

Argon: $p_1 = 1.0$ torr. $T_1 = 300^{\circ}K$

$C_{aa} = 1.2 \times 10^{-19}$ cm^2/eV

M_1	L(cms) x10	α-Onset $\times 10^{2}$	$\ddot{x}$-Onset $\times 10^{-2}$	δ(cms) $\times 10^{-1}$	τ(secs.) $\times 10^{5}$	δ/L $\times 10^{-2}$
15	0.2753	0.3283	1.0620	0.9017	1.8631	3.2750
20	0.3670	1.4235	0.2355	0.1920	0.2975	0.5230
25	0.4589	2,7642	0.1119	0.0941	0.1167	0.2051
30	0.5506	4.0581	0.0762	0.0672	0.0695	0.1221
35	0.6424	5.2386	0.0619	0.0614	0.0543	0.0955
40	0.7342	6.3761	0.0548	0.0601	0.0466	0.0819

Table 6.5

Characteristics of Ionizing Shock

Krypton: p_1 = 1.0 torr. T_1 = 300°K

M_1	L(cms) x10	α-Onset $x10^2$	$\bar{x}$-Onset $x10^{-2}$	δ(cms) $x10^{-1}$	τ(secs) $x10^5$	δ/L $x10^{-2}$
15	0.1788	0.1707	1.6470	0.9770	2.9222	5.4650
20	0.2384	0.7159	0.4497	0.2650	0.5945	1.1117
25	0.2980	1.3563	0.2111	0.1359	0.2439	0.4561
30	0.3575	1.9586	0.1328	0.0935	0.1398	0.2615
35	0.4175	2.5073	0.0987	0.0780	0.1000	0.1870
40	0.4767	3.0032	0.0806	0.0697	0.0782	0.1463

Table 6.6

Characteristics of Ionizing Shock

Xenon: p_1 = 1.0 torr. T_1 = 300°K

M_1	L(cms) x10	α-Onset $x10^{2}$	$\bar{x}$-Onset $x10^{-2}$	δ(cms) $x10^{-1}$	τ (secs.) $x10^{5}$	δ/L $x10^{-2}$
15	0.1377	0.0521	2.3240	1.5118	5.6634	10.9820
20	0.1835	0.2092	0.8192	0.5080	1.4274	2.7680
25	0.2980	0.3982	0.3340	0.2854	0.6414	0.9577
30	0.2753	0.5775	0.2662	0.1975	0.3700	0.7175
35	0.3212	0.7429	0.1904	0.1558	0.2501	0.4850
40	0.4767	0.8918	0.1222	0.1382	0.1942	0.2900

APPENDIX

1. Inelastic Collision Integrals:

All the integrals encountered in the evaluation of inelastic collision terms come under the general form,

$$I = \int \exp\left[- \frac{(\underset{\sim}{\xi} - U\hat{i})^2}{\beta} - \frac{(\underset{\sim}{\eta} - (U-\zeta)\hat{i})^2}{1-\beta} \right] [g^2 - g_o^2]\, g\, \phi(\underset{\sim}{\xi})\, d\underset{\sim}{\xi}\, d\underset{\sim}{\eta} \qquad (A-1)$$

where all the variables are dimensionless and the domain of integration is that part of $\underset{\sim}{\xi} - \underset{\sim}{\eta}$ space in which,

$$g \geq g_o \qquad (A-2)$$

where $\underset{\sim}{g}$ is defined by,

$$\underset{\sim}{g} = \underset{\sim}{\xi} - \underset{\sim}{\eta} \ .$$

$\phi(\underset{\sim}{\xi})$ is the moment function and $\hat{i}$ is the unit vector along x-direction. $\underset{\sim}{\xi}$ and $\underset{\sim}{\eta}$ have components (ξ_x, ξ_y, ξ_z) and (η_x, η_y, η_z) along x, y, z directions.

Integral (A-1) is evaluated for different $\phi(\underset{\sim}{\xi})$.

(a) Transformations:

Introducing the following transformations which simplify the terms in the exponent of eq. (A-1),

$$\underset{\sim}{\xi} - U\hat{i} = \underset{\sim}{F} - \beta \underset{\sim}{G} \qquad (A-3)$$

and

$$\underset{\sim}{\eta} - (U-\zeta)\hat{i} = \underset{\sim}{F} + (1-\beta)\, \underset{\sim}{G},$$

it can be shown that,

$$\frac{(\underset{\sim}{\xi} - U\hat{i})^2}{\beta} + \frac{(\underset{\sim}{\eta} - (U-\zeta)\hat{i})^2}{(1-\beta)} = \frac{F^2}{\beta(1-\beta)} + G^2 \quad , \tag{A-4}$$

$$\underset{\sim}{g} = \underset{\sim}{\xi} - \underset{\sim}{\eta} = \zeta\hat{i} - \underset{\sim}{G} \tag{A-5}$$

and

$$\phi(\underset{\sim}{\xi}) = \phi_1(U, \beta, \underset{\sim}{F}, \underset{\sim}{G}). \tag{A-6}$$

Integral (A-1) can be written as

$$I = \int_{\underset{\sim}{F},\underset{\sim}{G}} \exp\left[-\left(\frac{F^2}{\beta(1-\beta)} + G^2\right)\right] (g^2 - g_c^2)\, g\, \phi_1(U, \beta, \underset{\sim}{F}, \underset{\sim}{G}) J\, d\underset{\sim}{G} \tag{A-7}$$

where J is the Jacobian of transformation. From eqs. (A-3)

$$J \equiv \frac{\partial(\underset{\sim}{\xi}, \underset{\sim}{\eta})}{\partial(\underset{\sim}{F}, \underset{\sim}{G})} = 1.$$

Introducing the spherical coordinates for $\underset{\sim}{F}$ and $\underset{\sim}{G}$ as,

$$\underset{\sim}{F} \equiv (F, \theta_F, \phi_F)$$

and (A-8)

$$\underset{\sim}{G} \equiv (G, \theta_G, \phi_G)$$

the elemental volumes $d\underset{\sim}{F}$ and $d\underset{\sim}{G}$ can be written as

$$\begin{aligned} d\underset{\sim}{F} &= F^2 \sin\theta_F\, dF\, d\theta_F\, d\phi_F \,, \\ d\underset{\sim}{G} &= G^2 \sin\theta_G\, dG\, d\theta_G\, d\phi_G \end{aligned} \tag{A-9}$$

and the relative speed g is given by

$$g^2 = \zeta^2 + G^2 - 2\zeta G \cos\theta_G \tag{A-10}$$

since $\underset{\sim}{G} \cdot \hat{i} = G \cos\theta_G$.

b) Limits of Integration:

From eq. (A-10) it can be seen that $\underset{\sim}{g}$ is independent of $\underset{\sim}{F}$ and hence the constraint (A-2) is a constraint only on $\underset{\sim}{G}$. Therefore the limits of $\underset{\sim}{F}$ are,

$$F \sim 0 \text{ to } \infty, \quad \theta_F \sim 0 \text{ to } \pi, \quad \phi_F \sim 0 \text{ to } 2\pi \ . \tag{A-11}$$

Limits of $\underset{\sim}{G}$ should satisfy (A-2). The minimum value of g is g_o, so that for every θ_G, there is a lower limit for $G = G_o(\theta_G)$ given by,

$$g_o^2 = \zeta^2 + G_o^2 - 2\zeta G_o \cos\theta_G \ . \tag{A-12}$$

Curve represented by eq. (A-12) is shown in Fig. (A-1) which divides the $G - \theta_G$ domain into two regions, in one $g < g_o$ and in the other $g > g_o$. Eq. (A-12) can be solved for G_o to give,

$$G_o = \zeta \cos\theta_G \pm \sqrt{g_o^2 - \zeta^2 \sin\theta_G} \ . \tag{A-13}$$

where $\zeta \geq 0$ and $g_o \geq \zeta$, for G_o to be positive it can be shown that positive sign is the proper choice in (A-13).

It will be shown later that $\zeta \geq 0$ is not a limitation however, and $g_o \geq \zeta$ is satisfied in the range of speeds of interest in the present studies.

In Fig. (A-1) is shown the region of integration in $G - \theta_G$ plane denoted by R, which can be divided into R_1 and R_2 as shown, so that,

$$\int_R = \int_{R_1} + \int_{R_2} \tag{A-14}$$

and the limits of integration for R_1 and R_2 are appropriately denoted by,

$$\int_{R_1} = \int_{g_o+\zeta}^{\infty} dG \int_{0}^{\pi} d\theta_G$$

and

$$\int_{R_2} = \int_{g_o-\zeta}^{g_o+\zeta} dG \int_{\theta_{GO}}^{\pi} d\theta_G \qquad \text{(A-15)}$$

where θ_{GO} is given by,

$$g_o^2 = \zeta^2 + G^2 - 2\zeta G \cos\theta_{GO} \; . \qquad \text{(A-16)}$$

Finally ϕ_G varies from 0 to 2π.

c) Evaluation of the Integral:

Introducing eqs. (A-8) and (A-9) into eq. (A-7) and using the limits defined earlier, eq. (A-7) can be shown to be equal to,

$$I = \int_{F=0}^{\infty} \int_{\theta_F=0}^{\pi} \int_{\phi_F,\, \phi_G=0}^{2\pi} \left[\int_{R_1} + \int_{R_2} \right] \exp\left[-\left(\frac{F^2}{\beta(1-\beta)} + G^2\right)\right] (g^2-g_o^2)\, g\, \phi_1\, F^2 G^2 \sin\theta_F \sin\theta_G \; dF\, dG$$

$$d\theta_F\, d\theta_G\, d\phi_F\, d\phi_G \; . \qquad \text{(A-17)}$$

Since $\underset{\sim}{F}$ and $\underset{\sim}{G}$ are independent vectors, integration over $\underset{\sim}{F}$ and $\underset{\sim}{G}$ can be performed independently. In the following, I is evaluated for different moment functions of interest.

A-I $\phi(\underset{\sim}{\xi}) = 1$:

From eq. (A-17),

$$I = \int_{F=0}^{\infty} \int_{\theta_F=0}^{\pi} \int_{\phi_F=0}^{2\pi} \int_{\phi_G=0}^{2\pi} \int_{R_1+R_2} \left\{ \exp\left[-\left(\frac{F^2}{\beta(1-\beta)} + G^2\right)\right] (g^2-g_o^2)\, g\, F^2 G^2 \sin\theta_F \sin\theta_G \right\}$$

$$dF\, dG\, d\theta_F\, d\theta_G\, d\phi_F\, d\phi_G \qquad \text{(A-18)}$$

Integrating over $\underset{\sim}{F}$ and ϕ_G, and using the results,

$$\int_0^{\pi} \sin\theta\, d\theta = 2, \quad \int_0^{2\pi} d\phi = 2\pi, \quad \text{and} \quad \int_0^{\infty} \exp(-x^2)\, x^2\, dx = \sqrt{\pi}/4$$

eq. (A-18) can be written as

$$1 = 2\pi^{5/2}\, \beta^{3/2}\, (1-\beta)^{3/2} \int_{R_1+R_2} \exp(-G^2)\, (g^2-g_o^2)\, gG^2 \sin\theta_G\, d\theta_G\, dG \,. \qquad \text{(A-19)}$$

Evaluation of the Integral Over R_1:

$$\int_{R_1} \exp(-G^2)\, (g^2-g_o^2)\, gG^2 \sin\theta_G\, d\theta_G\, dG = \int_{g_o+\zeta}^{\infty} \exp(-G^2)\, x\, G^2 \left[\int_0^{\pi} (g^2-g_o^2)\, g \sin\theta_G\, d\theta_G\right] dG. \qquad \text{(A-20)}$$

From eq. (A-10),

$$\zeta\, G \sin\theta_G\, d\theta_G = g\, dg \qquad \text{(A-21)}$$

and when $\theta_G = 0$; $g = \zeta - G$, $\theta_G = \pi$; $g = \zeta + G$.

Using (A-21) in eq. (A-20), it can be written that,

$$\int_0^{\pi} (g^2-g_o^2)\, g \sin\theta_G \, d\theta_G = \frac{1}{\zeta G}\int_{\zeta-G}^{\zeta+G} (g^2-g_o^2)\, g^2 \, dg,$$

which after integration reduces to

$$\int_0^{\pi} (g^2-g_o^2)\, g \sin\theta_G \, d\theta_G = \frac{2}{G}\left[G^4+(2\zeta^2-g_o^2)G^2 + \zeta^2\left(\frac{1}{5}\zeta^2 - \frac{1}{3} g_o^2\right)\right] . \qquad (A-22)$$

Introducing eq. (A-22) in eq. (A-20),

$$\int_{R_1} \exp(-G^2)(g^2-g_o^2)\, gG^2 \sin\theta_G \, d\theta_G \, dG = 2\int_{g_o+\zeta}^{\infty} \exp(-G^2)\, G\left[G^4 + (2\zeta^2-g_o^2)\, G^2 + \zeta^2\left(\frac{1}{5}\zeta^2 - \frac{1}{3} g_o^2\right)\right] dG$$

which reduces to,

$$\int_{R_1} = \exp\left[-(g_o+\zeta)^2\right]\left[\frac{16}{5}\zeta^4 + 8g_o\,\zeta^3 + \left(\frac{20}{3} g_o^2 + 4\right)\zeta^2 + 2g_o\,(g_o^2+2)\zeta + (g_o^2+2)\right] . \qquad (A-23)$$

Evaluation of Integral Over R_2:

$$\int_{R_2} \exp(-G^2)\,(g^2-g_o^2)\, gG^2 \sin\theta_G \, d\theta_G \, dG = \int_{g_o-\zeta}^{g_o+\zeta} \exp(-G^2) \times G^2\left[\int_{\theta_{GO}}^{\pi} (g^2-g_o^2)\, g \sin\theta_G \, d\theta_G\right] dG \qquad (A-24)$$

From eqs. (A-10) and (A-16),

$$\sin\theta_G \, d\theta_G = \frac{g\,dg}{G\zeta} \; ; \qquad (A-25)$$

and when $\theta_G = \theta_{GO}$, $g = g_o$; $\theta_G = \pi$, $g = \zeta + G$.

Using (A-25), it can be written that

$$\int_{\theta_{GO}}^{\pi} (g^2-g_o^2)\, g \sin\theta_G \, d\theta_G = \frac{1}{\zeta G} \int_{g_o}^{\zeta+G} (g^2-g_o^2)\, g^2 \, dg$$

which after integrating reduces to

$$\int_{\theta_{GO}}^{\pi} (g^2-g_o^2)\, g \sin\theta_G \, d\theta_G = \frac{1}{\zeta G} \left[\frac{1}{5} G^5 + \zeta G^4 + (2\zeta^2 - \frac{1}{3} g_o^2) G^3 \right.$$

$$+ (2\zeta^3 - g_o^2\zeta) G^2 + (\zeta^4 - \zeta^2 g_o^2) G$$

$$\left. + (\frac{1}{5}\zeta^5 - \frac{1}{3}\zeta^3 g_o^2 + \frac{2}{15} g_o^5)\right] \qquad (A-26)$$

Inserting (A-26) in (A-24) and integrating over G yields,

$$\int_{R_2} \exp(-G^2)\,(g^2-g_o^2)\, gG^2 \sin\theta_G \, d\theta_G \, dG$$

$$= \frac{\sqrt{\pi}}{16} \frac{1}{\zeta} \cdot \left\{\mathrm{Erf}(g_o+\zeta) - \mathrm{Erf}(g_o-\zeta)\right\} \left[4\zeta^4 + 4(3-g_o^2)\zeta^2 \right.$$

$$\left. + (3-2g_o^2)\right] + \frac{1}{2\zeta} \exp\left\{-(g_o-\zeta)^2\right\} \left[\frac{1}{2}\zeta^3 + \frac{1}{2} g_o\zeta^2 + \frac{5}{4}\zeta + \frac{3}{4} g_o\right]$$

$$- \frac{1}{2\zeta} \exp\left\{-(g_o+\zeta)^2\right\} \left[\frac{32}{5}\zeta^5 + 16 g_o \zeta^4 + (\frac{15}{2} + \frac{40}{3} g_o^2)\zeta^3 \right.$$

$$\left. + (4g_o^3 + \frac{17}{2} g_o)\zeta^2 + (\frac{11}{4} + 2g_o^2)\zeta + \frac{3}{4} g_o\right] \qquad (A-27)$$

Adding eqs. (A-23) and (A-27), and introducing the resulting expression in eq. (A-19) yields finally,

$$I = \frac{\pi^{5/2}}{2} \beta^{3/2} (1-\beta)^{3/2} F_1(\zeta, g_o), \qquad (A-28)$$

where,

$$F_1(\zeta, g_o) = \sqrt{\pi}\left\{ \text{Erf}\,(g_o+\zeta) - \text{Erf}\,(g_o-\zeta)\right\}$$
$$\times\left[\zeta^3 + (3-g_o^2)\,\zeta + (\frac{3}{4} - \frac{1}{2}\,g_o^2)\,\frac{1}{\zeta}\right] + \exp\left\{-(g_o^2+\zeta^2)\right\}$$
$$\times\left[(2\zeta^2+5)\cosh 2g_o\,\zeta + (2\zeta^2+3)\,\frac{g_o}{\zeta}\sinh 2g_o\,\zeta\right], \quad (A-29)$$

and

$$F_1(0, g_o) = 4(2 + g_o^2)\exp(-g_o^2) \quad (A-30)$$

Case when $\zeta < 0$:

The transformation similar to (A-3) is chosen as,

$$\underset{\sim}{\xi} - U\hat{i} = \underset{\sim}{F} + \beta\underset{\sim}{G}$$

and (A-31)

$$\underset{\sim}{\eta} - (U-\zeta)\hat{i} = \underset{\sim}{F} - (1-\beta)\,\underset{\sim}{G}$$

so that eq. (A-4) is unaltered but (A-5) becomes,

$$\underset{\sim}{\varepsilon} = \zeta\hat{i} + \underset{\sim}{G}$$

and hence eq. (A-10) is,

$$g^2 = \zeta^2 + G^2 + 2G\zeta$$
$$= \zeta'^2 + G^2 - 2G\zeta' \quad (A-32)$$

where,

$$\zeta' \quad (= -\zeta) > 0.$$

Therefore eq. (A-7) reduces to

$$I = \int_{\underset{\sim}{F},\underset{\sim}{G}} \exp\left(-\frac{F^2}{\beta(1-\beta)} - G^2\right)$$
$$\times (g^2-g_o^2)\; g\; \phi_1(U, \beta, \underset{\sim}{F}, \underset{\sim}{G})\; J\; d\underset{\sim}{G}\; d\underset{\sim}{F} \quad (A-33)$$

where $\zeta' > 0$.

Thus the result for $\zeta < 0$ can be obtained by substituting $\zeta'(= -\zeta)$ in (A-29) and hence (A-29) is valid for $\zeta \gtrless 0$.

A-II $\phi(\underset{\sim}{\xi}) = \xi_x^2$:

From eqs. (A-3),

$$\xi_x \equiv \underset{\sim}{\xi} \cdot \hat{i} = U + F \cos\theta_F - \beta G \cos\theta_G$$

and

$$\phi_1(U,\beta,\underset{\sim}{F},\underset{\sim}{G}) = U^2 + F^2 \cos^2\theta_F + \beta^2 G^2 \cos^2\theta_G + 2UF \cos\theta_F - 2U\beta G \cos\theta_G - 2F\beta G \cos\theta_F \cos\theta_G . \quad (A-34)$$

Using eq. (A-34) in (A-17) and following a similar procedure as in A-I, it can be shown that,

$$1 = \pi^{5/2} \beta^{3/2} (1-\beta)^{3/2} F_2(U, \beta, \zeta, g_o), \quad (A-35)$$

where

$$F_2(U,\beta,\zeta,g_o) = \frac{\sqrt{\pi}}{2}\left\{\mathrm{Erf}(g_o+\zeta) - \mathrm{Erf}(g_o-\zeta)\right\} \times \left[(U^2 + \tfrac{1}{2}\beta)\zeta^3 + 3U\beta\zeta^2 + \left\{\tfrac{3}{2}\beta^2 + (3-g_o^2)(U^2+\tfrac{\beta}{2})\right\}\zeta + U\beta(3-g_o^2) + \tfrac{1}{4}(U^2+\tfrac{1}{2}\beta)(3-2g_o^2)\tfrac{1}{\zeta} - \tfrac{1}{4}U\beta(3-2g_o^2)\tfrac{1}{\zeta^2} + \tfrac{1}{8}\beta^2(3-2g_o^2)\tfrac{1}{\zeta^3}\right] + \exp(U^2+g_o^2)\left[\left\{(U^2+\tfrac{1}{2}\beta)\zeta^2 + 3U\beta\zeta + \tfrac{5}{2}(U^2+\tfrac{1}{2}\beta) + \tfrac{3}{2}\beta^2 + \tfrac{1}{2}U\beta(3+4g_o^2)\tfrac{1}{\zeta} - \tfrac{1}{4}\beta^2(3+4g_o^2)\tfrac{1}{\zeta^2}\right\}\cosh 2g_o\zeta + \left\{(U^2+\tfrac{1}{2}\beta)\zeta^2 + 3U\beta\zeta + \tfrac{1}{2}\beta^2(3+2g_o^2) + \tfrac{3}{2}(U^2+\tfrac{1}{2}\beta) - \tfrac{3}{2}U\beta\tfrac{1}{\zeta} + \tfrac{3}{4}\beta^2\tfrac{1}{\zeta^2}\right\}\frac{g_o}{\zeta}\sinh 2g_o\zeta\right] . \quad (A-36)$$

Eq. (A-36) is valid for $\zeta \gtrless 0$, and

$$F_2(U,\beta,0,g_o) = \exp(-g_o^2)\left[\tfrac{2}{3}\beta^2 g_o^4 + (2U^2 + \tfrac{5}{3}\beta^2 + \beta) g_o^2 + (4U^2 + 2\beta^2 + 2\beta)\right] . \quad (A-37)$$

2. Elastic Collision Integrals:

All the integrals encountered in the evaluation of elastic collision terms come under the general form,

$$I = \int \exp\left[-\frac{(\underset{\sim}{\xi} - U\hat{i})^2}{\beta} - \frac{(\underset{\sim}{\eta} - (U-\zeta)\hat{i})^2}{1-\beta}\right] \sigma(\xi,\eta)\, d\underset{\sim}{\xi}\, d\underset{\sim}{\eta} \qquad (A\text{-}38)$$

where σ depends upon the force law of interaction and the moment function. $\hat{i}$ is the unit vector along x-direction. $\underset{\sim}{\xi}$ and $\underset{\sim}{\eta}$ have components (ξ_x, ξ_y, ξ_z) and (η_x, η_y, η_z).

a) Transformations:

Introducing the transformations (A-3) we get,

$$\frac{(\underset{\sim}{\xi} - U\hat{i})^2}{\beta} + \frac{(\underset{\sim}{\eta} - (U-\zeta)\hat{i})^2}{(1-\beta)} = \frac{F^2}{\beta(1-\beta)} + G^2, \qquad (A\text{-}39)$$

$$\underset{\sim}{g} = \underset{\sim}{\xi} - \underset{\sim}{\eta} = \zeta\hat{i} - \underset{\sim}{G} \qquad (A\text{-}40)$$

and

$$\sigma(\underset{\sim}{\xi}, \underset{\sim}{\eta}) = \sigma_1(U, \beta, \zeta, \underset{\sim}{F}, \underset{\sim}{G}). \qquad (A\text{-}41)$$

Integral (A-38) can be written as

$$I = \int_{\underset{\sim}{F},\underset{\sim}{G}} \exp\left(-\frac{F^2}{\beta(1-\beta)} - G^2\right) \sigma_1(U,\beta,\zeta,\underset{\sim}{F},\underset{\sim}{G})\, d\underset{\sim}{G}\, d\underset{\sim}{F} \qquad (A\text{-}42$$

Further, spherical coordinates can be introduced for $\underset{\sim}{F}$ and $\underset{\sim}{G}$ from eqs. (A-8) to (A-10).

b) Limits of Integration:

Integral (A-42) is to be evaluated subject to $g \geq 0$. It can be recalled from Section 1 of Appendix that integration over

$\underset{\sim}{F}$ can be performed independent of this constraint. Therefore the limits on $\underset{\sim}{F}$ are the same as given by (A-11).

Proceeding in a similar way as in Section 1, it can be shown that the limits on $\underset{\sim}{G}$ are such that,

$$\begin{aligned} &\phi_G \backsim 0 \text{ to } 2\pi, \quad G \backsim 0 \text{ to } \infty, \\ &g \backsim G - \zeta \text{ to } G + \zeta \quad \text{for } G \geq \zeta \\ &g \backsim \zeta - G \text{ to } \zeta + G \quad \text{for } G \leq \zeta . \end{aligned} \tag{A-43}$$

Thus the integral over R, the region in G-g space is

$$\int_R = \int_{R_1} + \int_{R_2} , \tag{A-44}$$

where

$$\int_{R_1} = \int_{\zeta}^{\infty} dG \int_{G-\zeta}^{G+\zeta} dg$$

and (A-45)

$$\int_{R_2} = \int_{0}^{\zeta} dG \int_{\zeta-G}^{\zeta+G} dg .$$

Finally the integral (A-38) can be written as

$$\begin{aligned} I = \int_{F=0}^{\infty} \int_{\theta_F=0}^{\pi} \int_{\phi_F,\, \phi_G=0}^{2\pi} \left(\int_{R_1} + \int_{R_2} \right) \\ \left[\exp\left(-\frac{F^2}{\beta(1-\beta)} - G^2\right) \sigma_1(U, \beta, \zeta, \underset{\sim}{F}, \underset{\sim}{G})\, G^2 F^2 \sin\theta_F \right. \\ \left. \sin\theta_G \right] dF\, dG\, d\theta_F\, d\theta_G\, d\phi_F\, d\phi_G \quad . \end{aligned} \tag{A-46}$$

c) Collision Dyanmics and Evaluation of $\sigma(\underset{\sim}{\xi}, \underset{\sim}{\eta})$

Fig. (A-2) gives the details of a two body encounter in the center-of-mass system where $\underset{\sim}{g}_{12} = -\underset{\sim}{g}_{21} = \underset{\sim}{\xi} - \underset{\sim}{\eta}$; $\hat{i}$ is the unit vector along x-direction; $\hat{k}$ is the apseline vector; scattering angle $\chi = \pi - 2\psi$ defines ψ, and ϵ is the azimuthal angle. θ is the angle made by the relative velocity vector with x-direction.

If m_1 and m_2 are the masses of the particles whose velocities are respectively $\underset{\sim}{\xi}$ and $\underset{\sim}{\eta}$ the following quantities can be defined.

$$M_1 = \frac{m_1}{m_1+m_2}, \quad M_2 = \frac{m_2}{m_1+m_2} \quad \text{and} \quad \mu_{12} = \frac{m_1 m_2}{m_1+m_2} \qquad \text{(A-47)}$$

If $\underset{\sim}{\xi}'$ is the velocity of the particle 1 after encounter, then from conservation of momentum and energy we can write,

$$\underset{\sim}{\xi}' = \underset{\sim}{\xi} + 2M_2\, g \cos\psi\, \hat{k} \quad . \qquad \text{(A-48)}$$

Also from spherical trigonometry we have the result

$$\hat{k} \cdot \hat{i} = \cos\theta \cos\psi + \sin\theta \sin\psi \cos\epsilon \quad . \qquad \text{(A-49)}$$

σ is defined by,

$$\sigma = \int_b \int_\epsilon (\phi_1' - \phi_1)\, g_{21}\, b\, db\, d\epsilon \qquad \text{(A-50)}$$

where b is the impact parameter and ϵ is the azimuthal angle in an encounter. $\phi_1 = \phi_1(\underset{\sim}{\xi})$ is the moment function and $\phi_1' = \phi_1(\underset{\sim}{\xi}')$.

We also use the results from ref. 18 that for a force law of the form,

$$F = B_{12}/r^s \quad ,$$

we can define

$$\Phi_{12}^{(l)} = \left(\frac{B_{12}}{\mu_{12}}\right)^{\frac{2}{s-1}} g^{\frac{s-5}{s-1}} A_l(s) \qquad (A-51)$$

where

$$A_l(s) = \int_0^\infty (1 - \cos^l \chi)\, v_o\, dv_o \qquad (A-52)$$

and

$$v_o = b \left(\frac{\mu g^2}{B_{aa}}\right)^{\frac{1}{s-1}} .$$

$A_l(s)$ is a pure number depending only on l and s. For s = 2, the integrals $\Phi_{12}^{(1)}$ and $\Phi_{12}^{(2)}$ diverage and hence a cut-off is required in evaluating these integrals. If v_{o1} is the cut off value of v_o, then from ref. 18 we have,

$$A_1(5) = 0.422, \quad A_2(5) = 0.36 \qquad (A-53)$$

$$A_1(2) = \ln (1+v_{o1}^2);$$

$$A_2(2) = 2\left[\ln (1+v_{o1}^2) - \frac{v_{o1}^2}{1+v_{o1}^2}\right] . \qquad (A-53)$$

In the present analysis Debye radius is chosen as the cut off distance so that

$$v_{o1}^2 = \frac{9k T_e^3}{4\pi e^6 n_e} .$$

A-III $\phi_1(\xi) = \xi_x$:

From eq. (A-48) it can be written that

$$\xi_x' - \xi_x = 2M_2 \, g \cos\psi \, \hat{k}.\hat{i} \qquad (A\text{-}54)$$

Introducing eq. (A-54) in the eq. (A-50) and after using the result (A-49), eq. (A-50) can be integrated and from eqs.(A-51) and (A-52) it may be written that

$$\sigma = 2\pi \, M_2 \, g \cos\theta \; \Phi_{12}^{(1)}(g) \; . \qquad (A\text{-}55)$$

a) $s = 5$:

From eq. (A-51), eq. (A-55) can be written as

$$\sigma = 2\pi \, M_2 \, (\underset{\sim}{g}_{21}.\hat{i}) \, \left(\frac{B_{12}}{\mu_{12}}\right)^{1/2} \; A_1(5). \qquad (A\text{-}56)$$

From eq. (A-40) one can write that,

$$\sigma_1 = 2\pi \, M_2 \, \left(\frac{B_{12}}{\mu_{12}}\right)^{1/2} \; A_1(5) \, (G \cos\theta_G - \zeta). \qquad (A\text{-}57)$$

From eq. (A-57), integral (A-46) can be written as

$$I = \int_{F=0}^{\infty} \int_{\theta_F=0}^{\pi} \int_{\phi_F,\phi_G=0}^{2\pi} \left(\int_{R_1} + \int_{R_2} \right)$$

$$\left[\exp\left(- \frac{F^2}{\beta(1-\beta)} - G^2 \right) (G \cos\theta_G - \zeta) \; G^2 F^2 \sin\theta_G \; \sin\theta_F \right]$$

$$\cdot dG\,dF \; d\theta_G \; d\theta_F \; d\phi_G \; d\phi_F \qquad (A\text{-}58)$$

Using the limits for R_1 and R_2 from (A-45) and integrating (A-58) it reduces to,

$$I = -2\pi^4 M_2 \left(\frac{B_{12}}{\mu_{12}}\right)^{1/2} {}_{-1}(5)\ \beta^{3/2}(1-\beta)^{3/2}\ \zeta\ . \qquad (A-59)$$

b) $s = 2$:

From eq. (A-51), expression for σ from eq. (A-55) can be written as

$$\sigma = 2\pi\ M_2\ (\underset{\sim}{g}_{21}\cdot\hat{i})\ \left(\frac{B_{12}}{\mu_{12}}\right)^2\ g^{-3}\ A_1(2).$$

Hence from eq. (A-40),

$$\sigma_1 = 2\pi\ M_2\ \left(\frac{B_{12}}{\mu_{12}}\right)^2\ A_1(2)\ g^{-3}(G\cos\theta_G - \zeta). \qquad (A-60)$$

Using this value of σ_1, and using the results (A-45), the integral (A-58) can be evaluated and can be shown to be equal to

$$I = 2\pi^{7/2}\ M_2\ \left(\frac{B_{12}}{\mu_{12}}\right)^2\ A_1(2)\ \beta^{3/2}\ (1-\beta)^{3/2}$$

$$\cdot\left[\frac{2}{\zeta}\ \exp(-\zeta^2) - \frac{\sqrt{\pi}}{\zeta^2}\ \mathrm{Erf}(\zeta)\right]\ . \qquad (A-61)$$

$I = 0$, when $\zeta = 0$.

A-IV $\phi(\xi) = \xi^2$:

From ref. 80, the components of post collision velocity of one of the particles can be written as,

$$\begin{aligned}
\xi_x' &= \xi_x + M_2 \left[2(\eta_x-\xi_x)\cos^2\psi + \sqrt{g^2-(\eta_x-\xi_x)^2}\right. \\
&\qquad \left.\sin 2\psi \cos(\varepsilon-\omega_1)\right] \\
\xi_y' &= \xi_y + M_2 \left[2(\eta_y-\xi_y)\cos^2\psi + \sqrt{g^2-(\eta_y-\xi_y)^2}\right. \\
&\qquad \left.\sin 2\psi \cos(\varepsilon-\omega_2)\right] \qquad (A\text{-}62) \\
\xi_z' &= \xi_z + M_2 \left[2(\eta_z-\xi_z)\cos^2\psi + \sqrt{g^2-(\eta_z-\xi_z)^2}\right. \\
&\qquad \left.\sin 2\psi \cos(\varepsilon-\omega_3)\right],
\end{aligned}$$

where

$$\begin{aligned}
\omega_1 &= 0, \\
\omega_2 &= \frac{(\eta_x-\xi_x)(\eta_y-\xi_y)}{\sqrt{\left[g^2-(\eta_x-\xi_x)^2\right]\left[g^2-(\eta_y-\xi_y)^2\right]}}, \qquad (A\text{-}63) \\
\omega_3 &= \frac{(\eta_y-\xi_y)(\eta_z-\xi_z)}{\sqrt{\left[g^2-(\eta_y-\xi_y)^2\right]\left[g^2-(\eta_z-\xi_z)^2\right]}}.
\end{aligned}$$

Introducing the expressions (A-62) and (A-63) in eq. (A-50), and using in addition to the results (A-51) and (A-52), also the integrals

$$\int_0^{2\pi} \cos(\varepsilon-\omega)\,d\varepsilon = 0, \qquad \int_0^{2\pi} \cos^2(\varepsilon-\omega)\,d\varepsilon = \pi,$$

it can be shown that,

$$\sigma = 2\pi M_2 \Phi_{12}^{(1)}(\xi)\left[\eta^2-\xi^2 + (2M_2-1)\zeta^2\right] . \qquad (A-64)$$

From eq. (A-40) and (A-8) to (A-10), it can be written that,

$$\sigma_1 = 2\pi M_2 \Phi_{12}^{(1)}(\xi)\left[(2M_2-1)g^2-U^2+(U-\zeta)^2+(1-2\beta)G^2-2\zeta F\cos\theta\right.$$
$$\left. + 2\left\{U\beta + (U-\zeta)(1-\beta)\right\} G\cos\theta_G+2\underset{\sim}{F}.\underset{\sim}{G}\right] \qquad (A-65)$$

s=5:

Using the results from (A-51) and (A-52) in (A-65) and introducing the resulting expression in the integral (A-46), the integral can be evaluated and shown to be equal to

$$I = 2\pi^4 M_2 \left(\frac{B_{12}}{\mu_{12}}\right)^{1/2} A_1(5)\ \beta^{3/2}(1-\beta)^{3/2}$$
$$\cdot\left[3(M_2-\beta) + 2M_2\zeta^2 - 2U\zeta\right] . \qquad (A-66)$$

s=2:

Using the results from (A-51) in (A-65) and substituting the resulting expression for σ_1 in the integral (A-46), the integral can be evaluated and shown to be equal to,

$$I = 4\pi^4 M_2 \left(\frac{B_{12}}{\mu_{12}}\right)^2 A_1(2)\ \beta^{3/2}\ (1-\beta)^{3/2}$$
$$\cdot\left[\frac{1}{\zeta}\ \mathrm{Erf}\ (\zeta)\ \left(M_2 - \frac{U}{\zeta}\right) + \frac{2}{\sqrt{\pi}}\exp\ (-\zeta^2)\ \left(\frac{U}{\zeta} - \beta\right)\right] . \qquad (A-67)$$

A-V $\phi(\xi) = \xi_x^2$;

From a procedure similar to that in (A-III), expressio for σ can be written as

$$\sigma = 4\pi M_2 \Big[\xi_x (\underset{\sim}{g}_{21}\cdot\hat{i})\ \Phi_{12}^{(1)} + M_2 (\underset{\sim}{g}_{21}\cdot\hat{i})^2 \left(\Phi_{12}^{(1)} - \tfrac{1}{2}\Phi_{12}^{(2)}\right) + \tfrac{1}{4} M_2 \left\{ g_{21}^2 - (\underset{\sim}{g}_{21}\cdot\hat{k})^2 \right\} \Phi_{12}^{(2)} \Big] .$$

Using the results of (A-39) and (A-40) and also (A-8) to (A-10), expression for σ_1 comes out to be,

$$\sigma_1 = 4\pi M_2 \Big[(U + F\cos\theta_F - \beta G\cos\theta_G)(G\cos\theta_G - \zeta)\ \Phi_{12}^{(1)} + M_2 (G\cos\theta_G - \zeta)^2 \left(\Phi_{12}^{(1)} - \tfrac{1}{2}\Phi_{12}^{(2)}\right) + \tfrac{1}{4} M_2 \left\{ g^2 - (G\cos\theta_G - \zeta)^2 \right\} \Phi_{12}^{(2)} \Big] . \qquad \text{(A-68)}$$

Using this expression for σ_1, the integral (A-46) can be evaluat in a similar way as done earlier for $s = 5$ and 2; the results are,

<u>$s = 5$</u>

$$I = 2\pi^4 M_2 \left(\frac{B_{12}}{\mu_{12}}\right)^{1/2} \beta^{3/2} (1-\beta)^{3/2} \Big[\left(2A_1(5) - A_2(5)\right) \cdot M_2 \zeta^2 - 2A_1(5)\, U\zeta + A_1(5)\ (M_2 - \beta) \Big] . \qquad \text{(A-69)}$$

s=2

$$I = 4\pi^{7/2} M_2 \left(\frac{B_{12}}{\mu_{12}}\right)^2 \beta^{3/2} (1-\beta)^{3/2} \Big[\exp(-\zeta^2) \Big\{ -2\beta A_1(2) + 2A_1(2) \frac{U}{\zeta} + (-2\beta A_1(2) + 2M_2 A_1(2) - \frac{3}{2} M_2 A_2(2)) \frac{1}{\zeta^2} \Big\} + \frac{\sqrt{\pi}}{2} \mathrm{Erf}(\zeta) \Big\{ \Big[2M_2 A_1(2) - M_2 A_2(2) \Big] \frac{1}{\zeta} - 2A_1(2) \frac{U}{\zeta^2} + (2\beta A_1(2) - 2M_2 A_1(2) + \frac{3}{2} M_2 A_2(2)) \frac{1}{\zeta^3} \Big\} \Big] . \qquad (A-70)$$

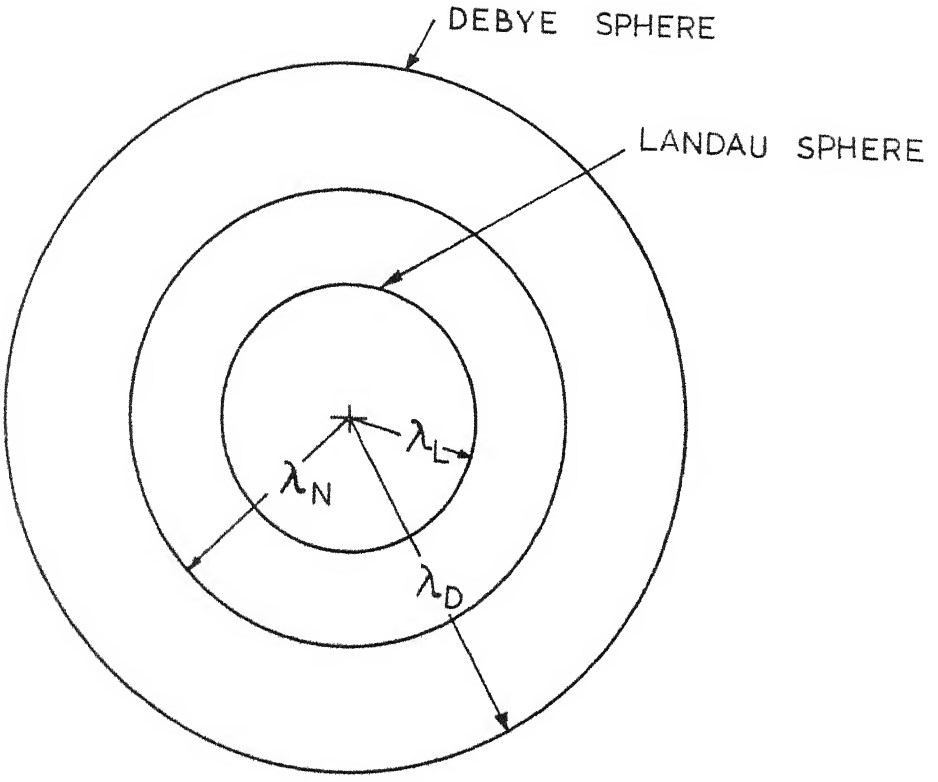

FIG. 3.1 _ VARIOUS LENGTHS

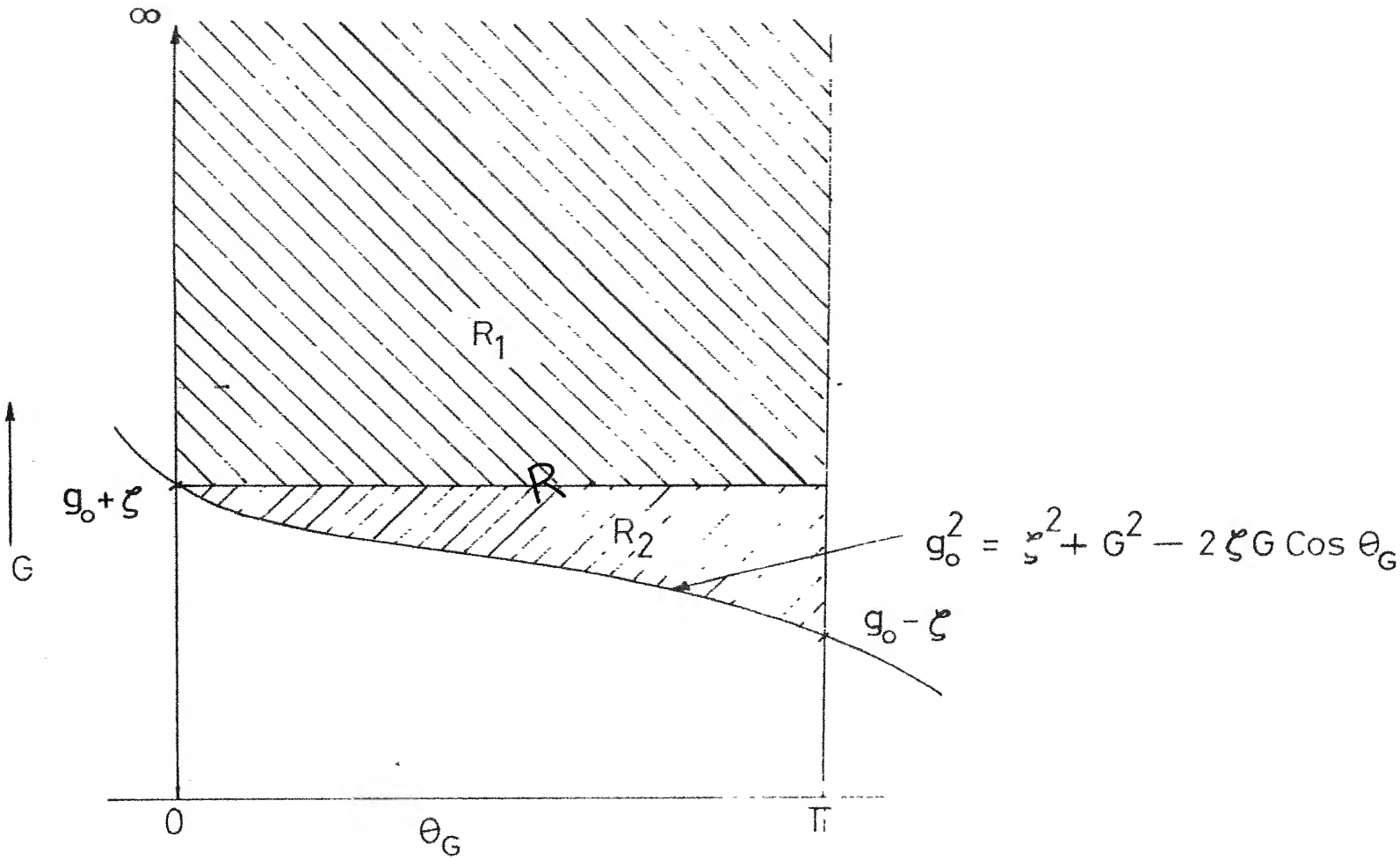

FIG. A_1_ REGION OF INTEGRATION

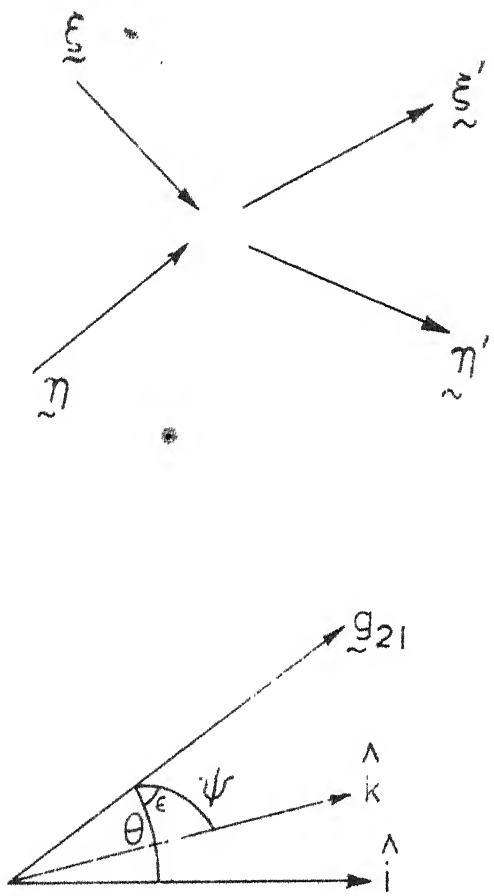

FIG. A_2 ..ELASTIC COLLISION DYNAMICS

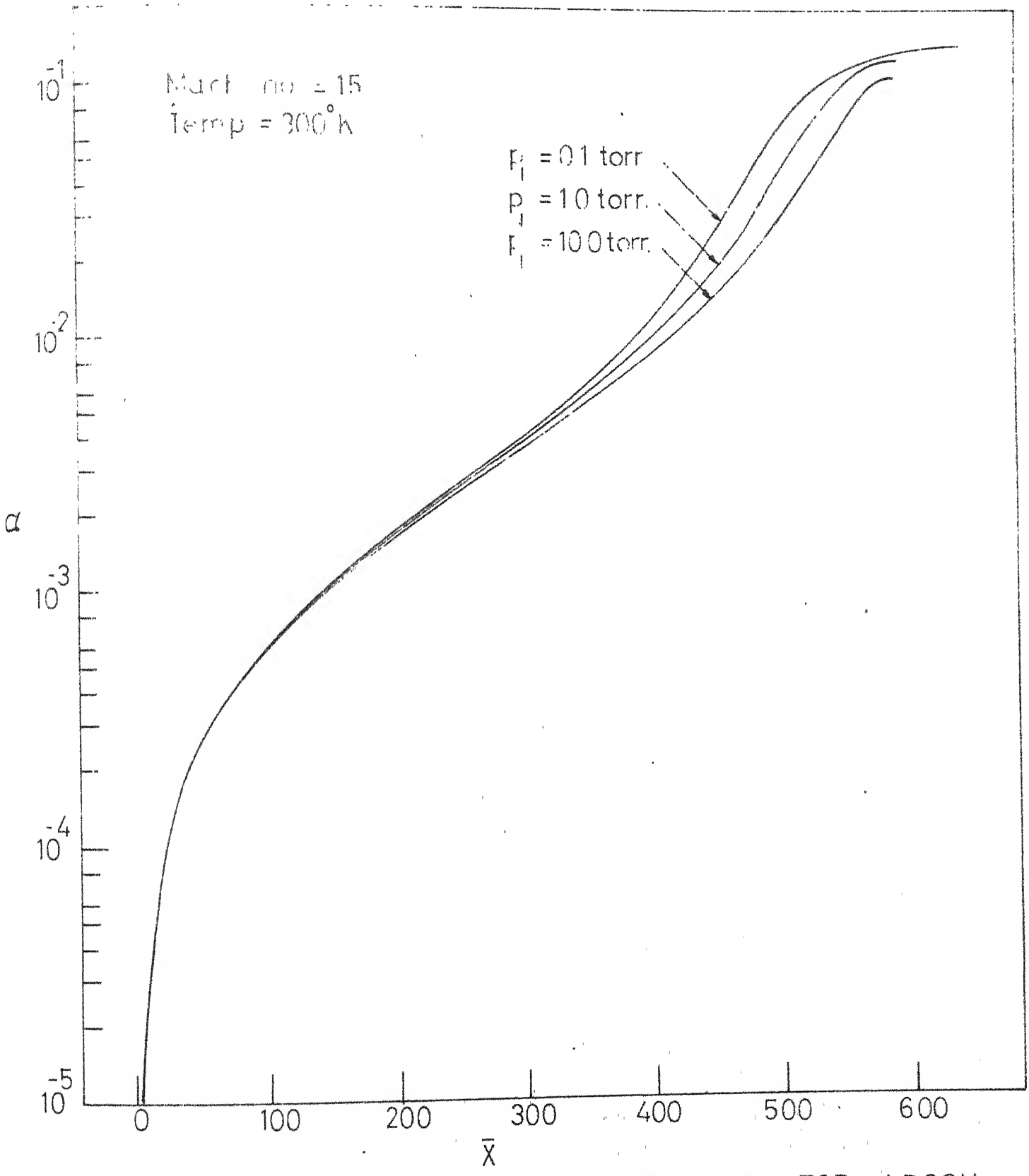

FIG. 6.1.1_ DEGREE OF IONIZATION PROFILES FOR ARGON

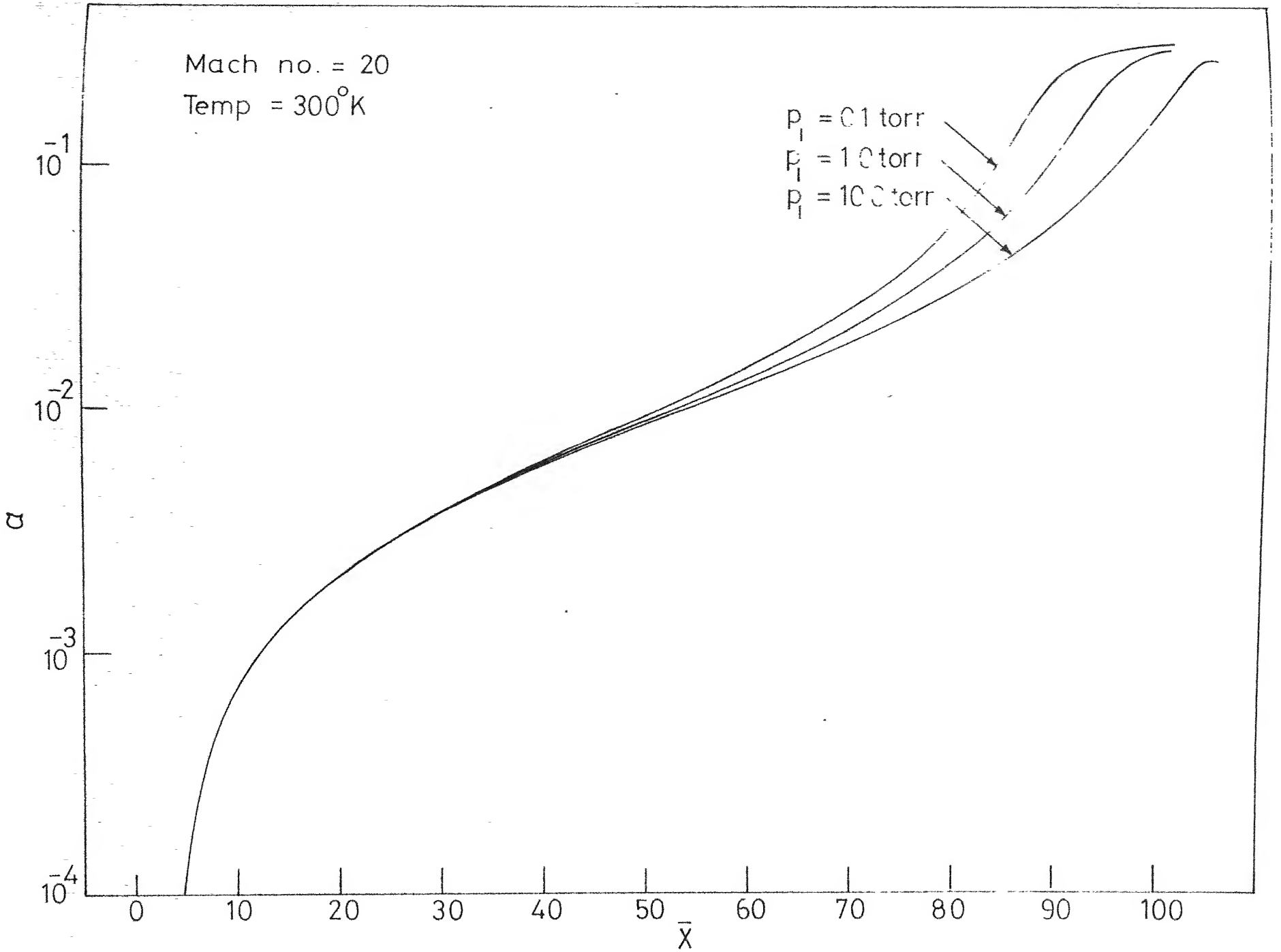

FIG. 6.1.2_ DEGREE OF IONIZATION PROFILES FOR ARGON

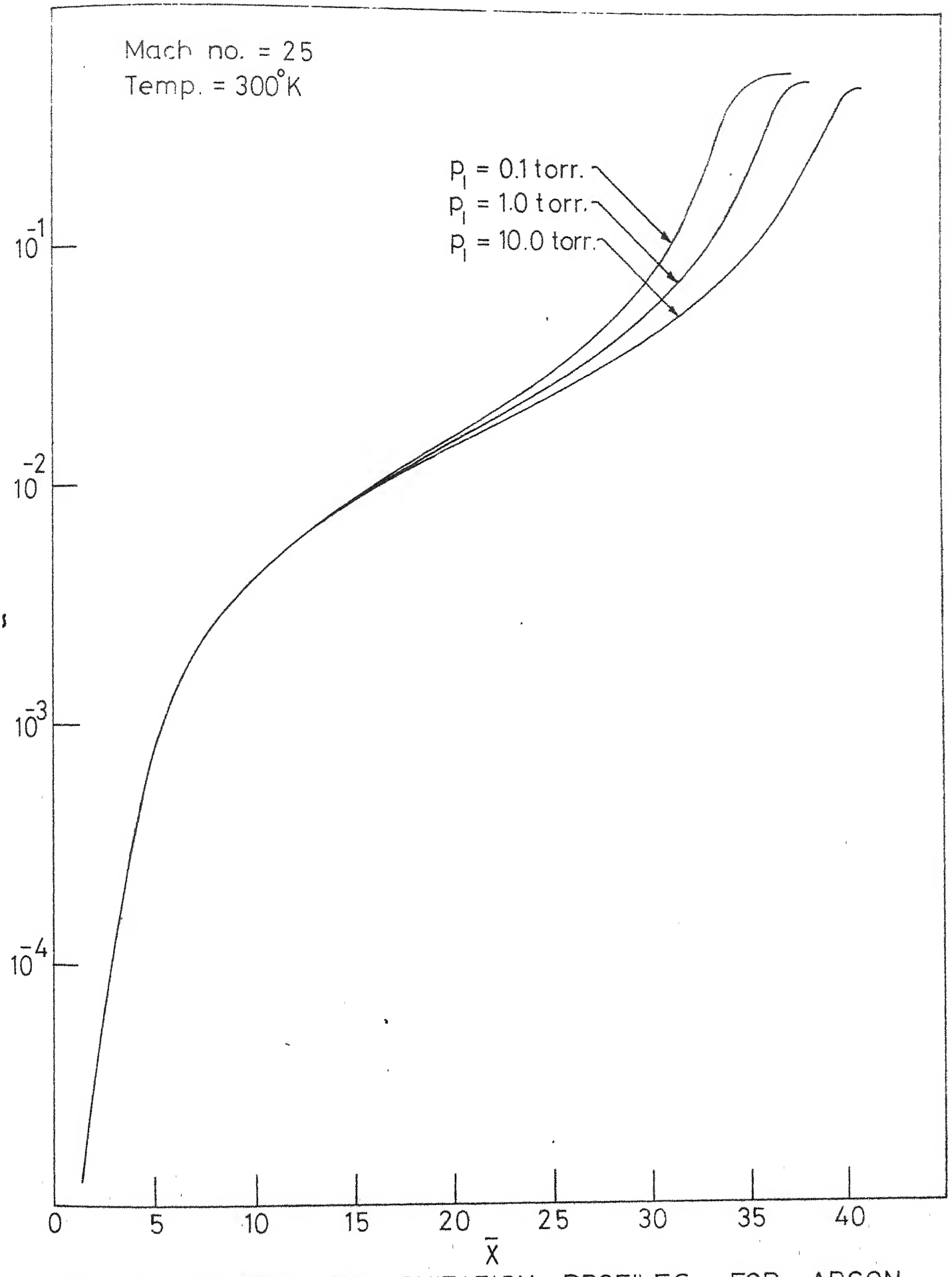

FIG. 6.1.3 _ DEGREE OF IONIZATION PROFILES FOR ARGON

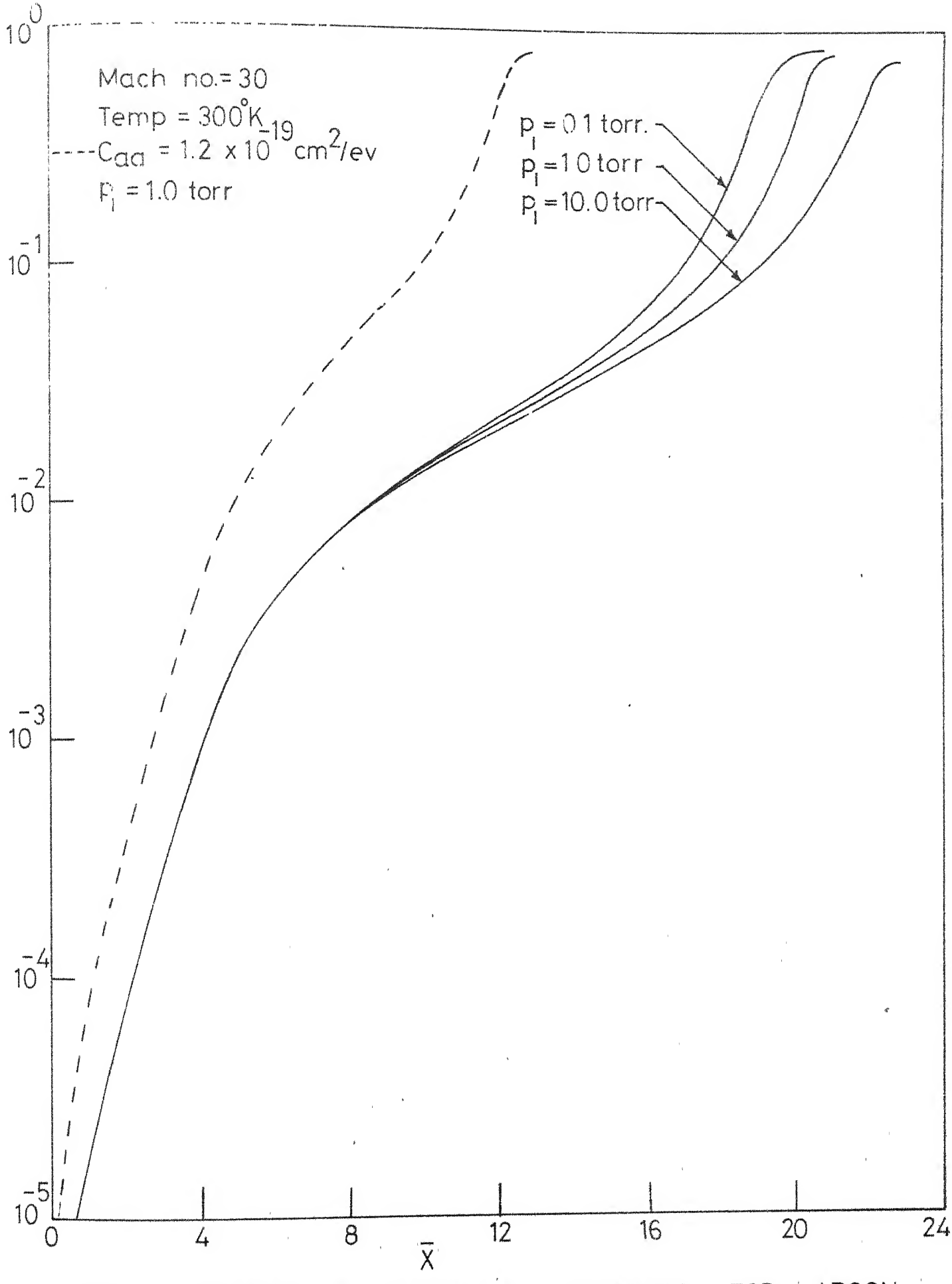

FIG.6.1.4_DEGREE OF IONIZATION PROFILES FOR ARGON

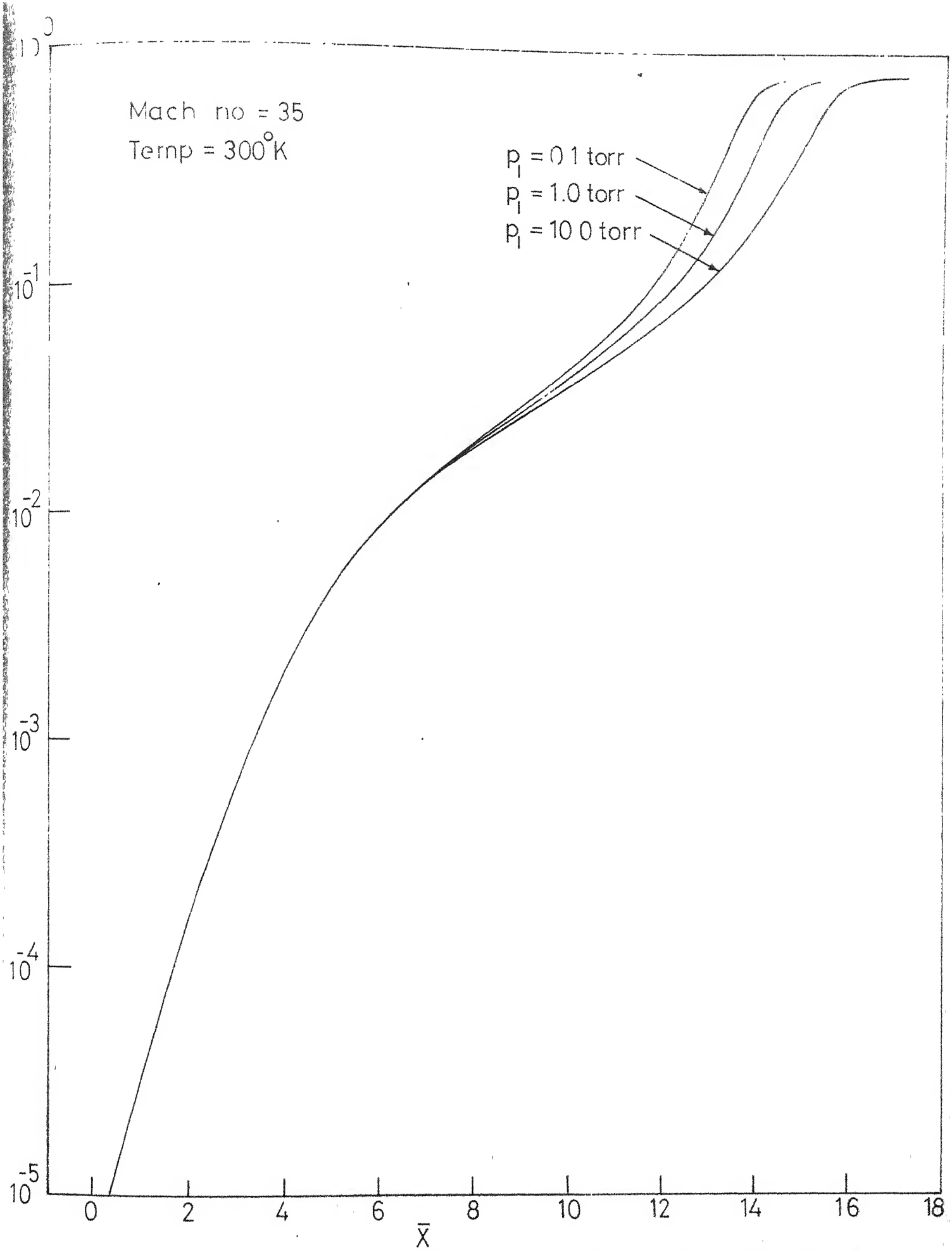

FIG. 6.1.5 _ DEGREE OF IONIZATION PROFILES FOR ARGON

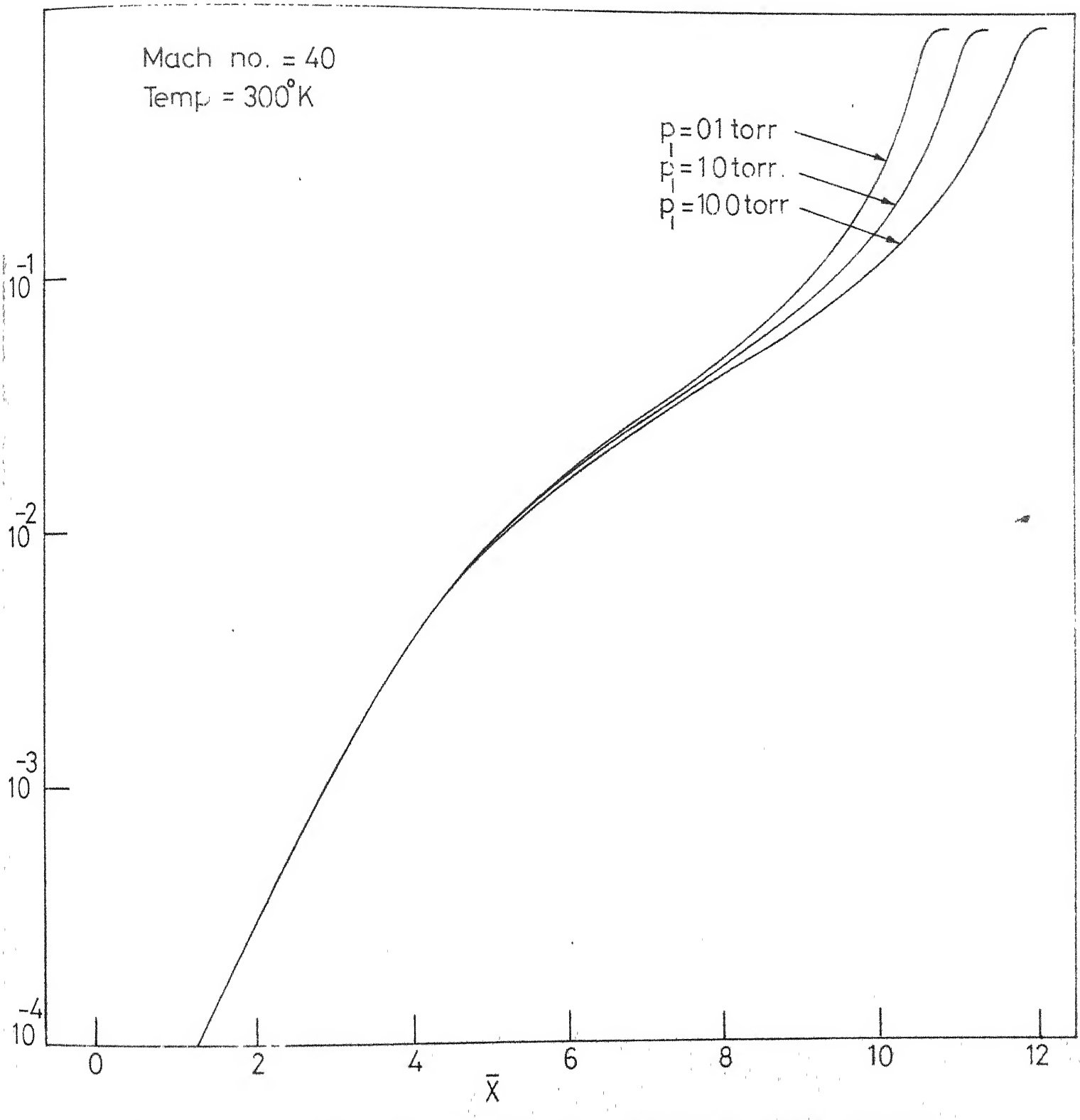

FIG.6.1.6_DEGREE OF IONIZATION PROFILES FOR ARGON

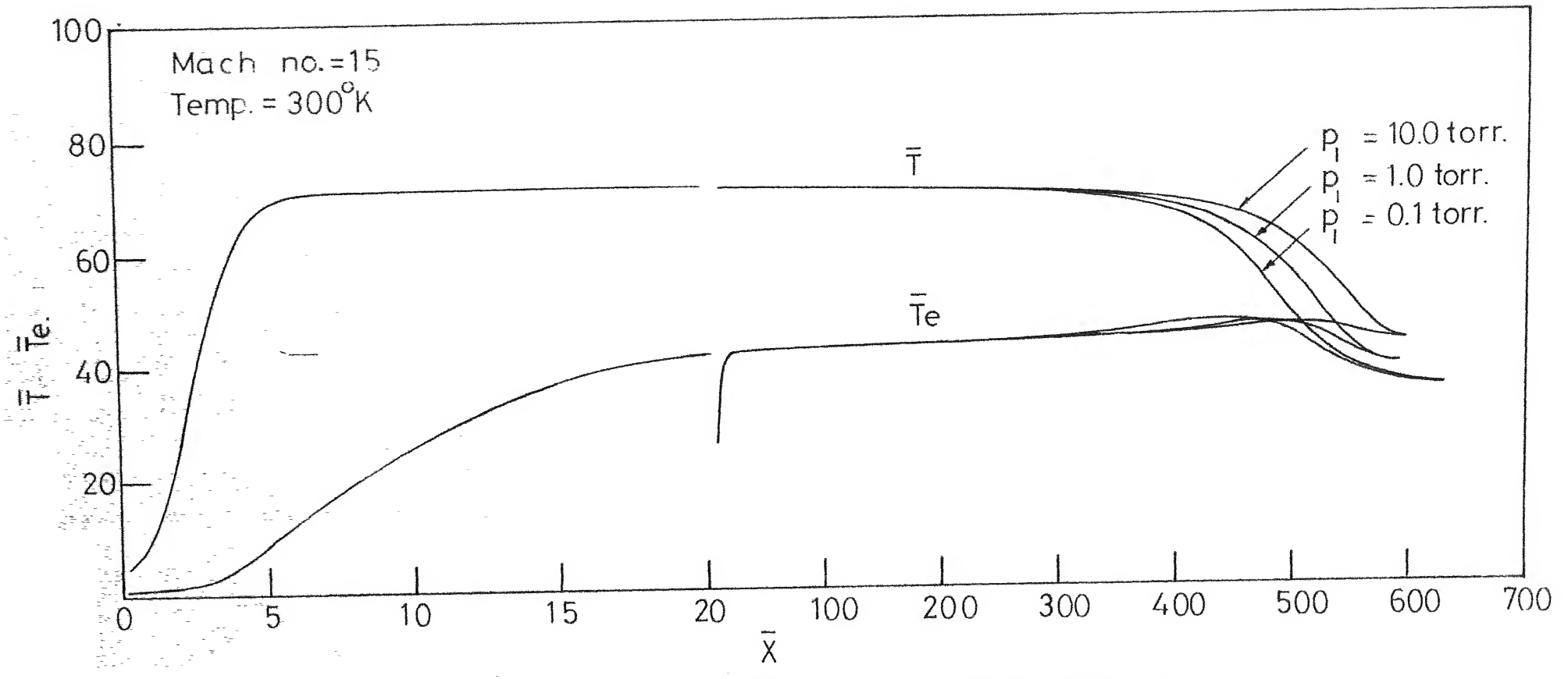

FIG.6.2.1_TEMPERATURE PROFILES FOR ARGON

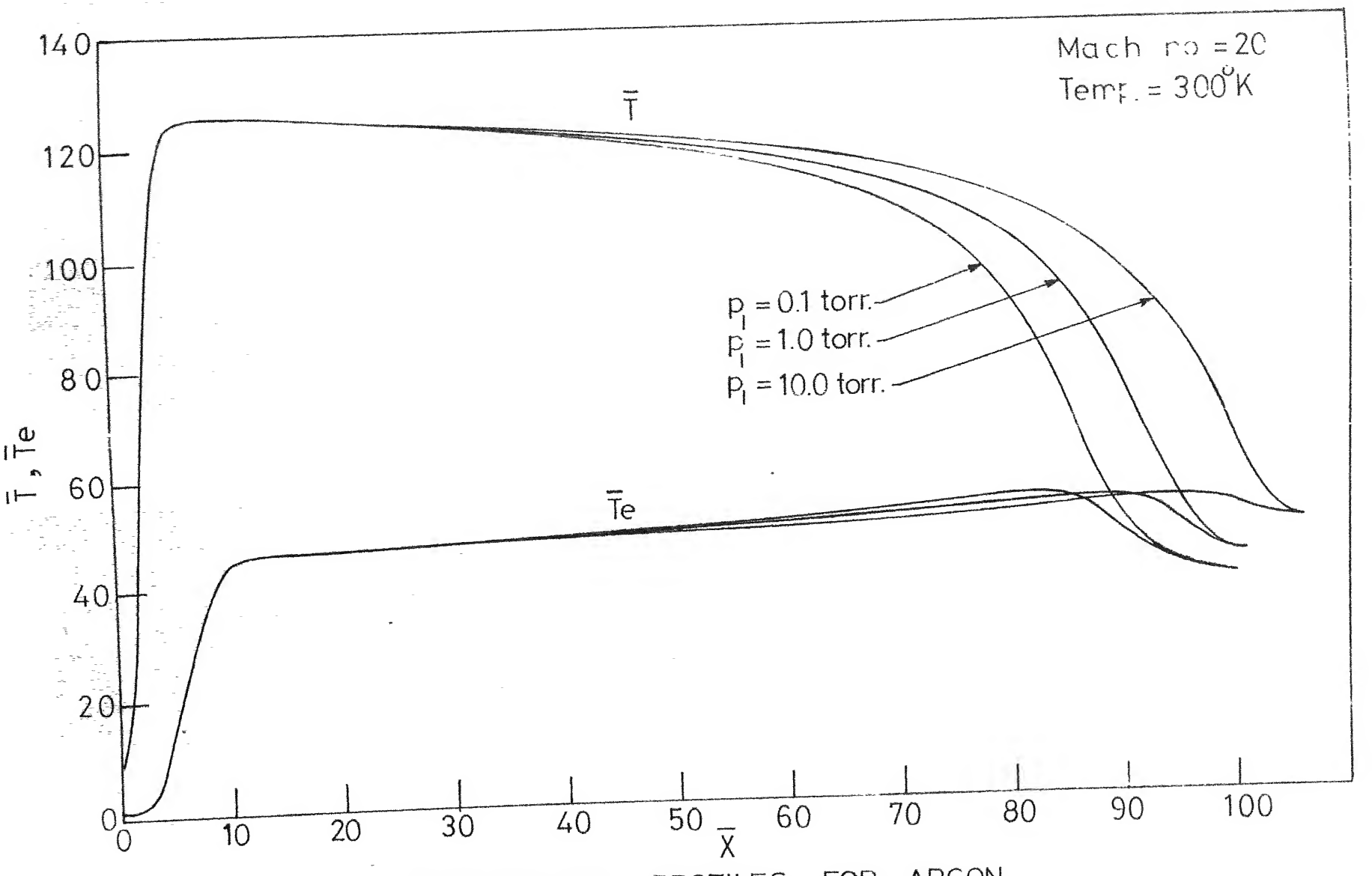

FIG. 6.2.2 – TEMPERATURE PROFILES FOR ARGON

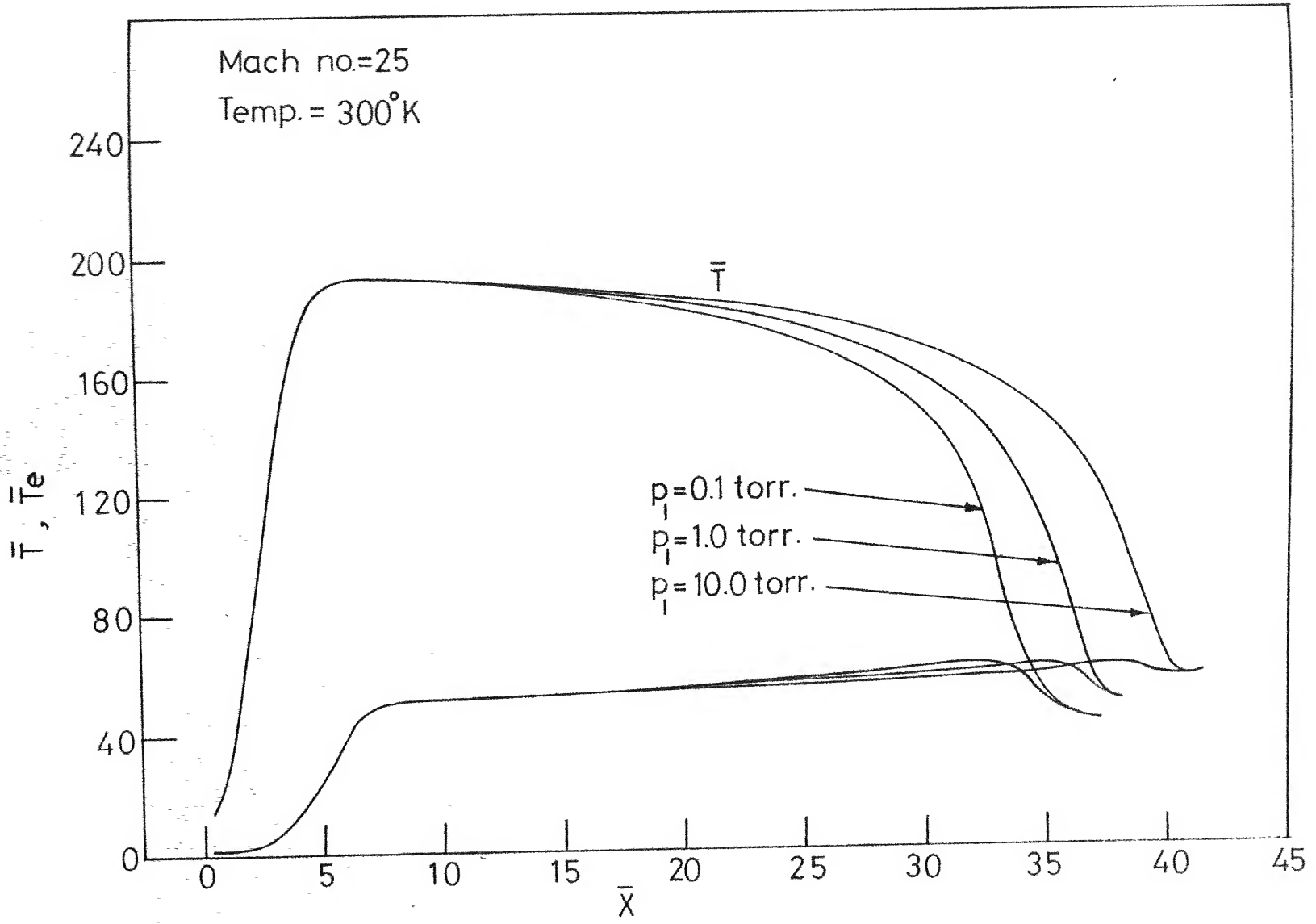

FIG.6.2.3_TEMPERATURE PROFILES FOR ARGON

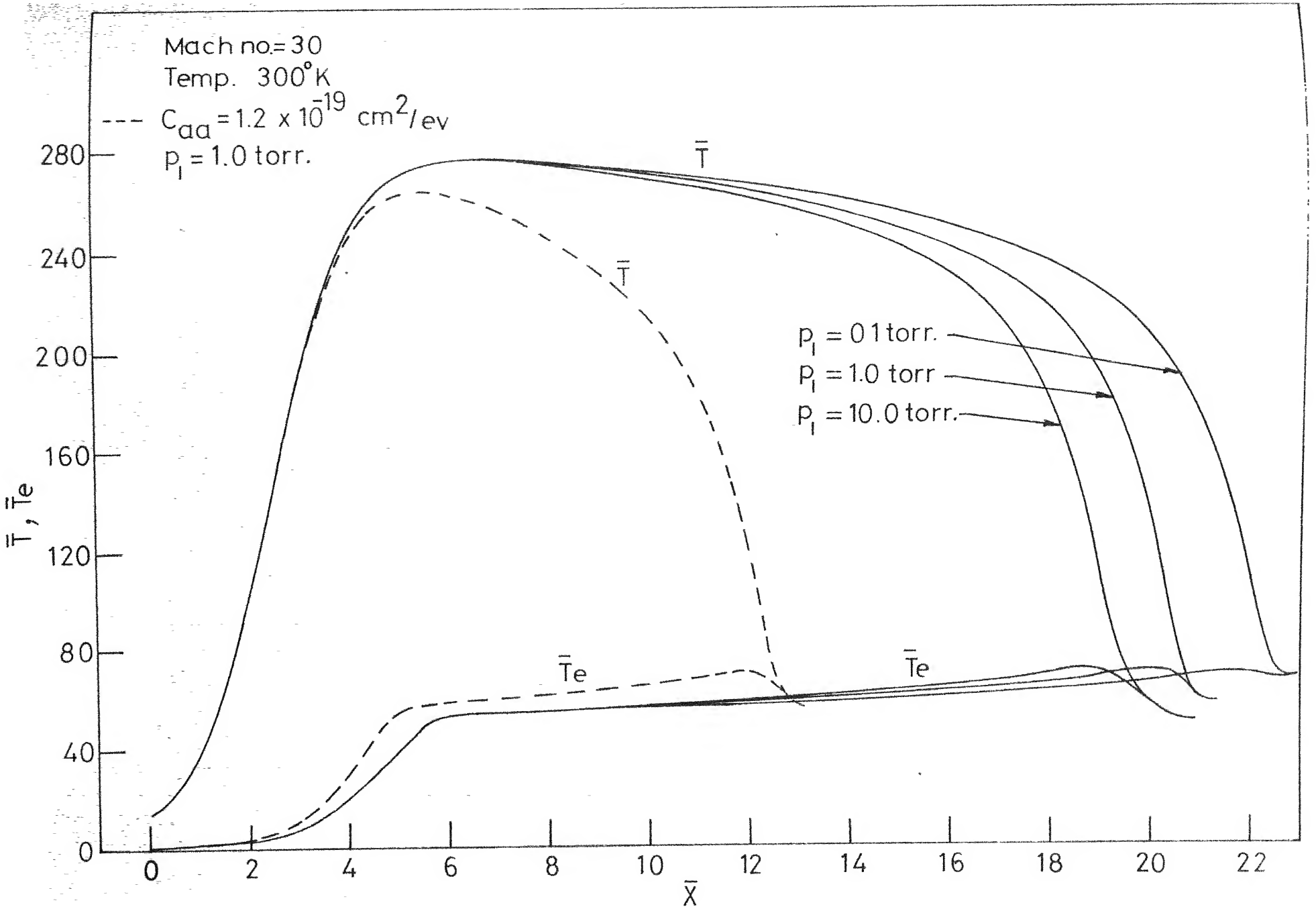

FIG.6.2.4_TEMPERATURE PROFILES FOR ARGON

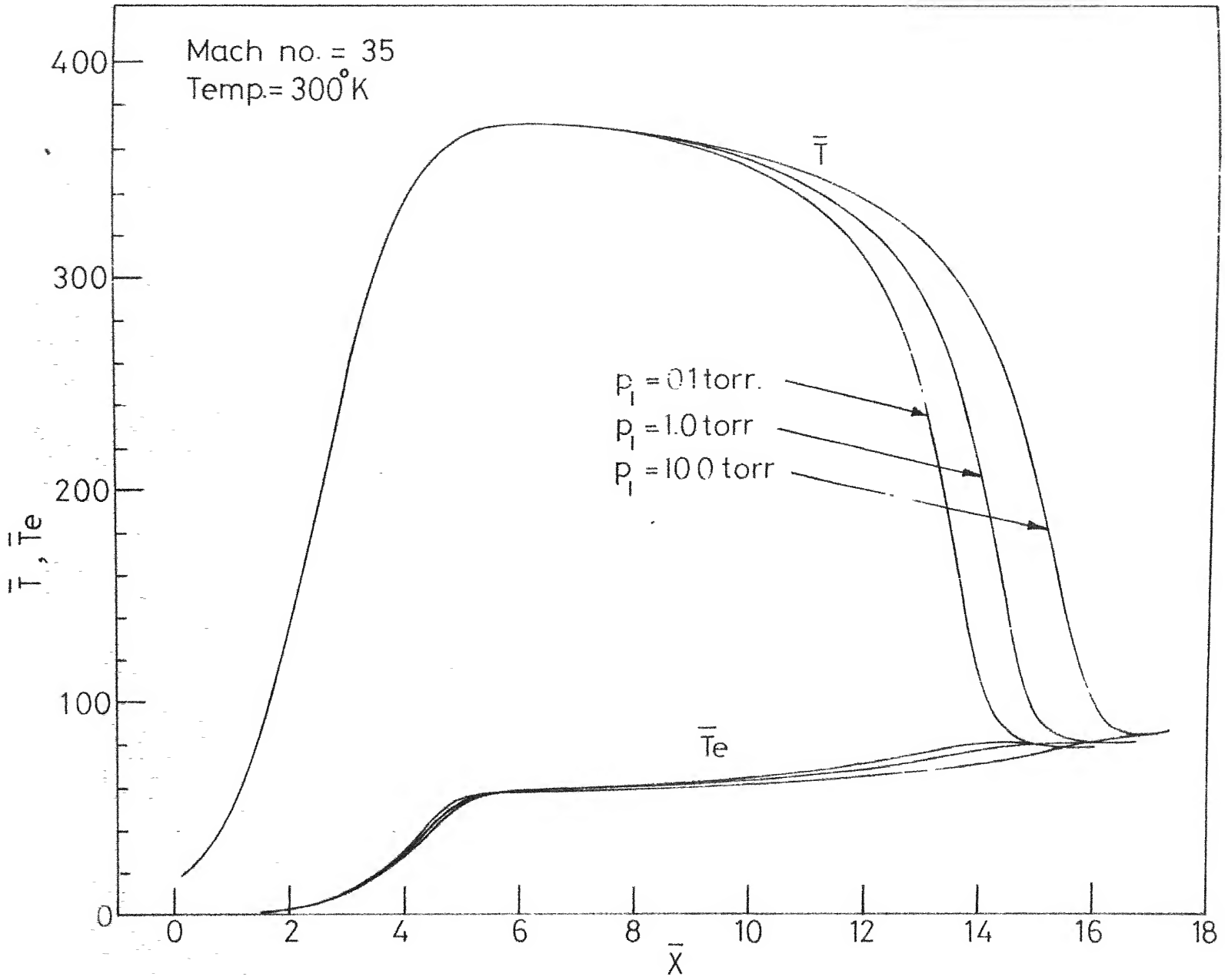

FIG. 6.2.5_TEMPERATURE PROFILES FOR ARGON

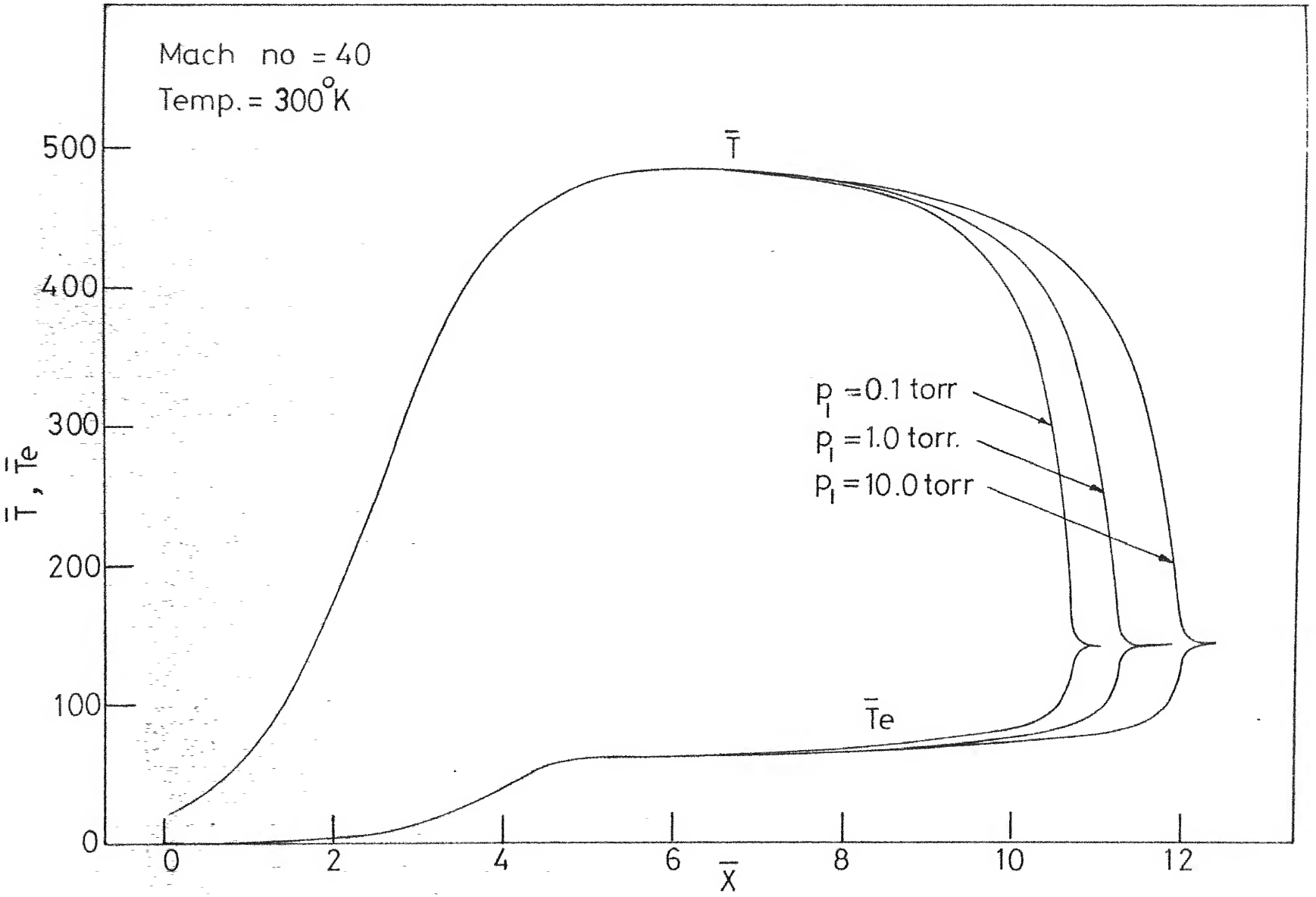

FIG. 6.2.6_TEMPERATURE PROFILES FOR ARGON

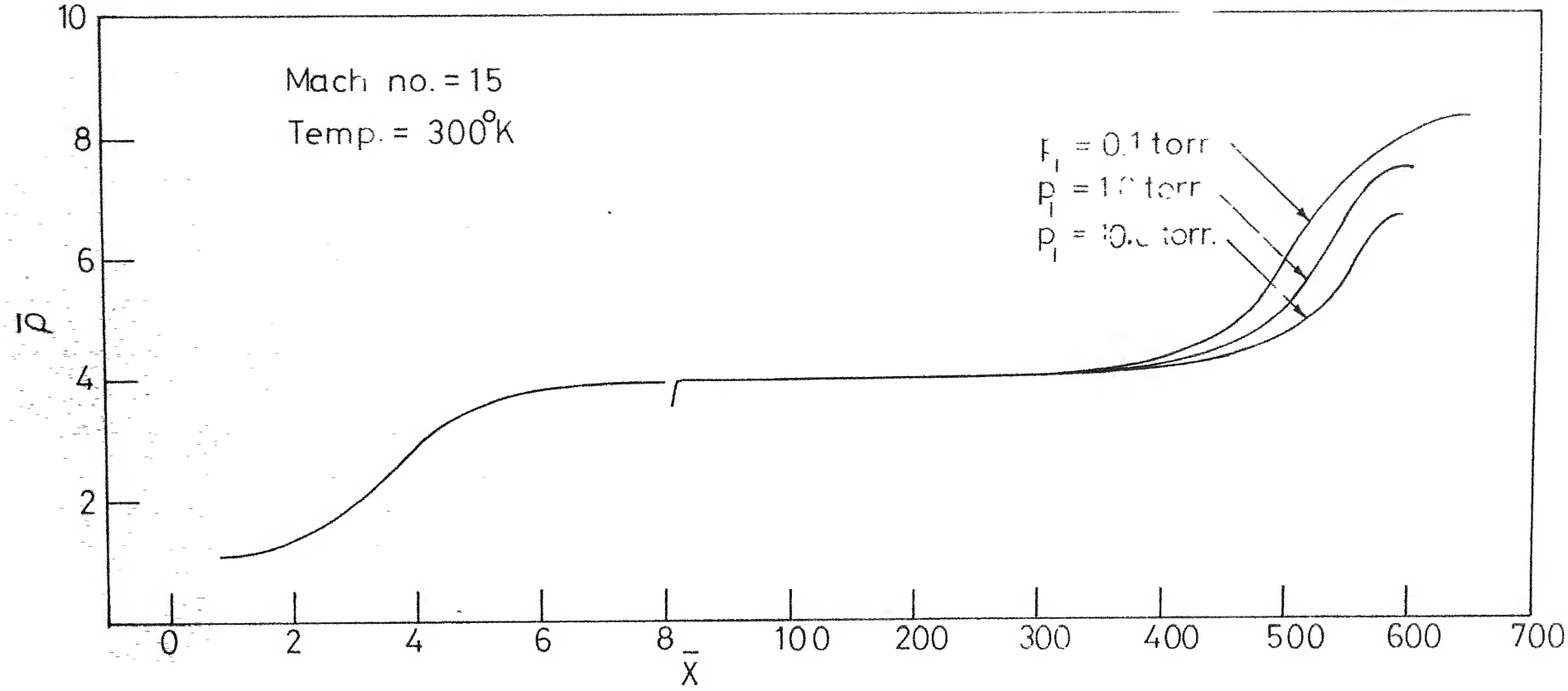

FIG.6.3.1_ DENSITY PROFILES FOR ARGON

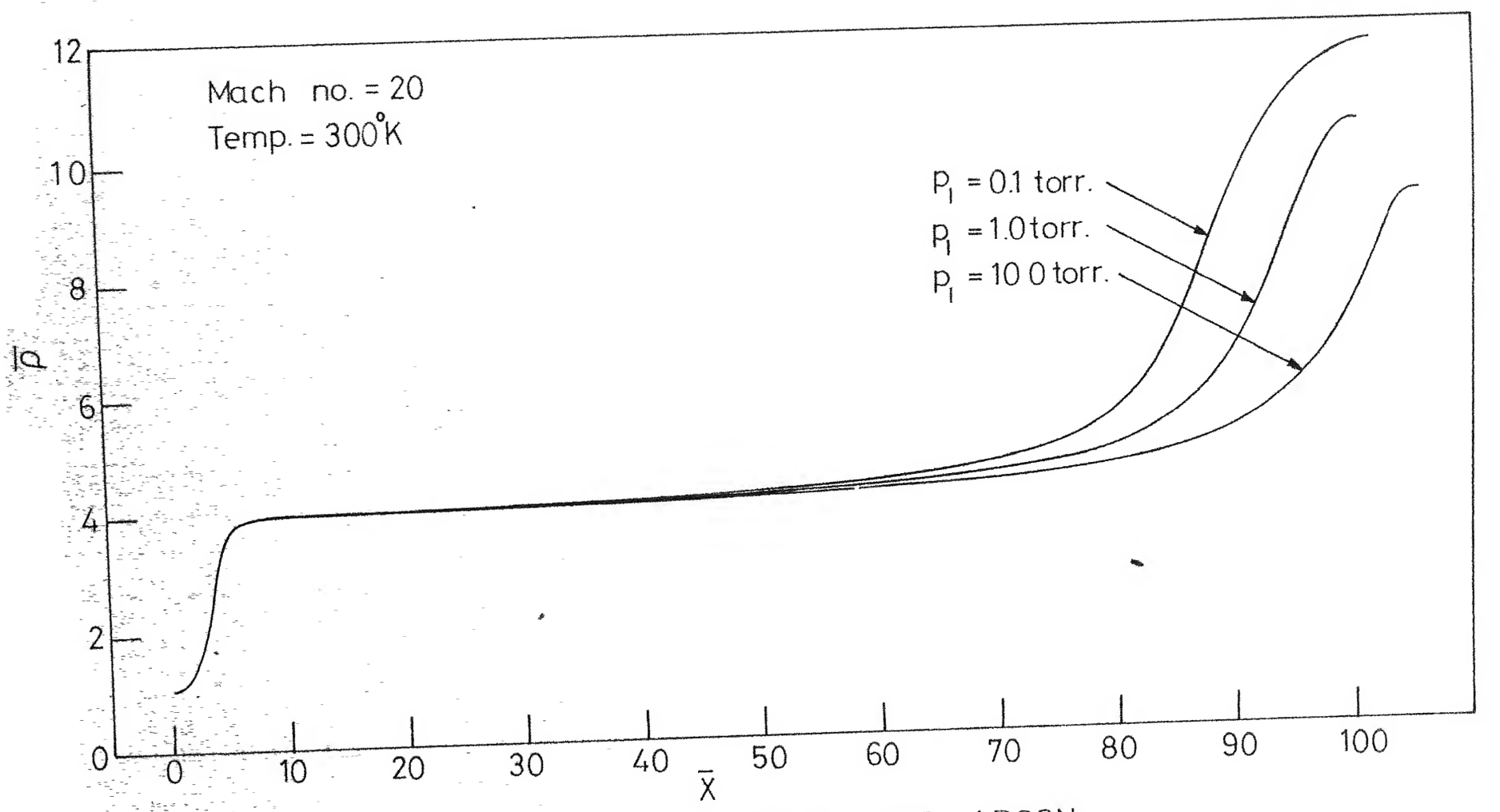

FIG.6.3.2._DENSITY PROFILES FOR ARGON

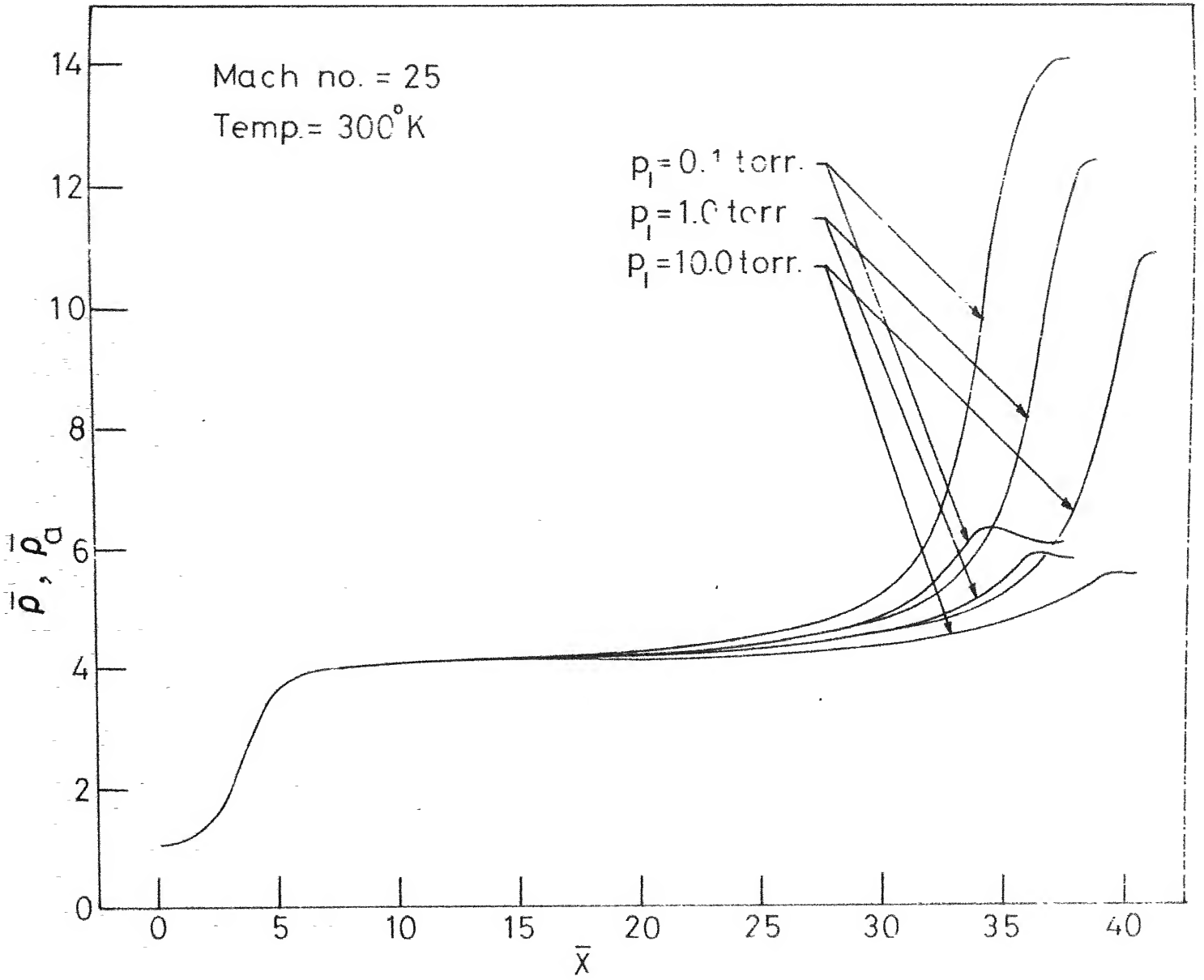

FIG.6.3.3._DENSITY PROFILES FOR ARGON

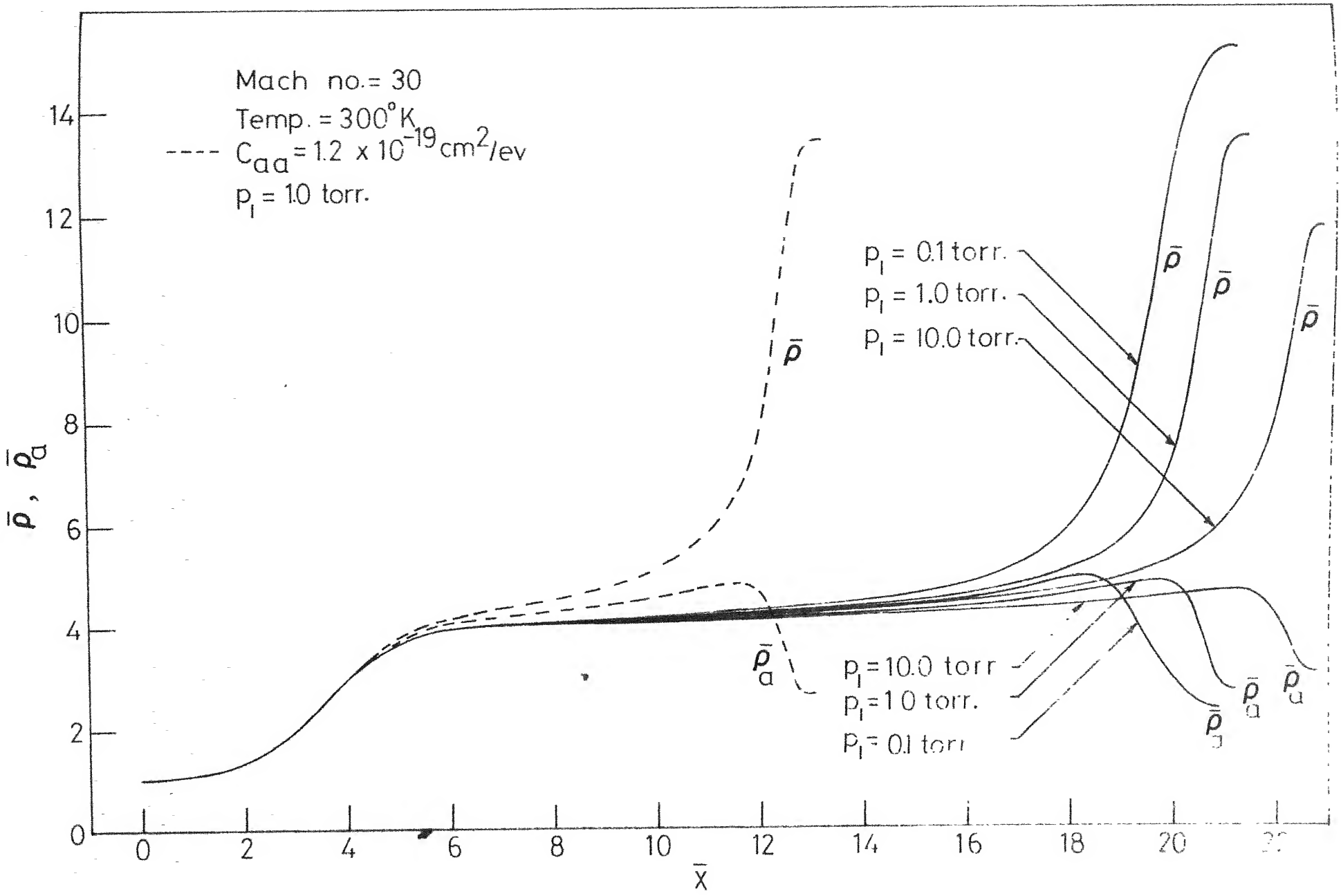

FIG.6.3.4_DENSITY PROFILES FOR AGON

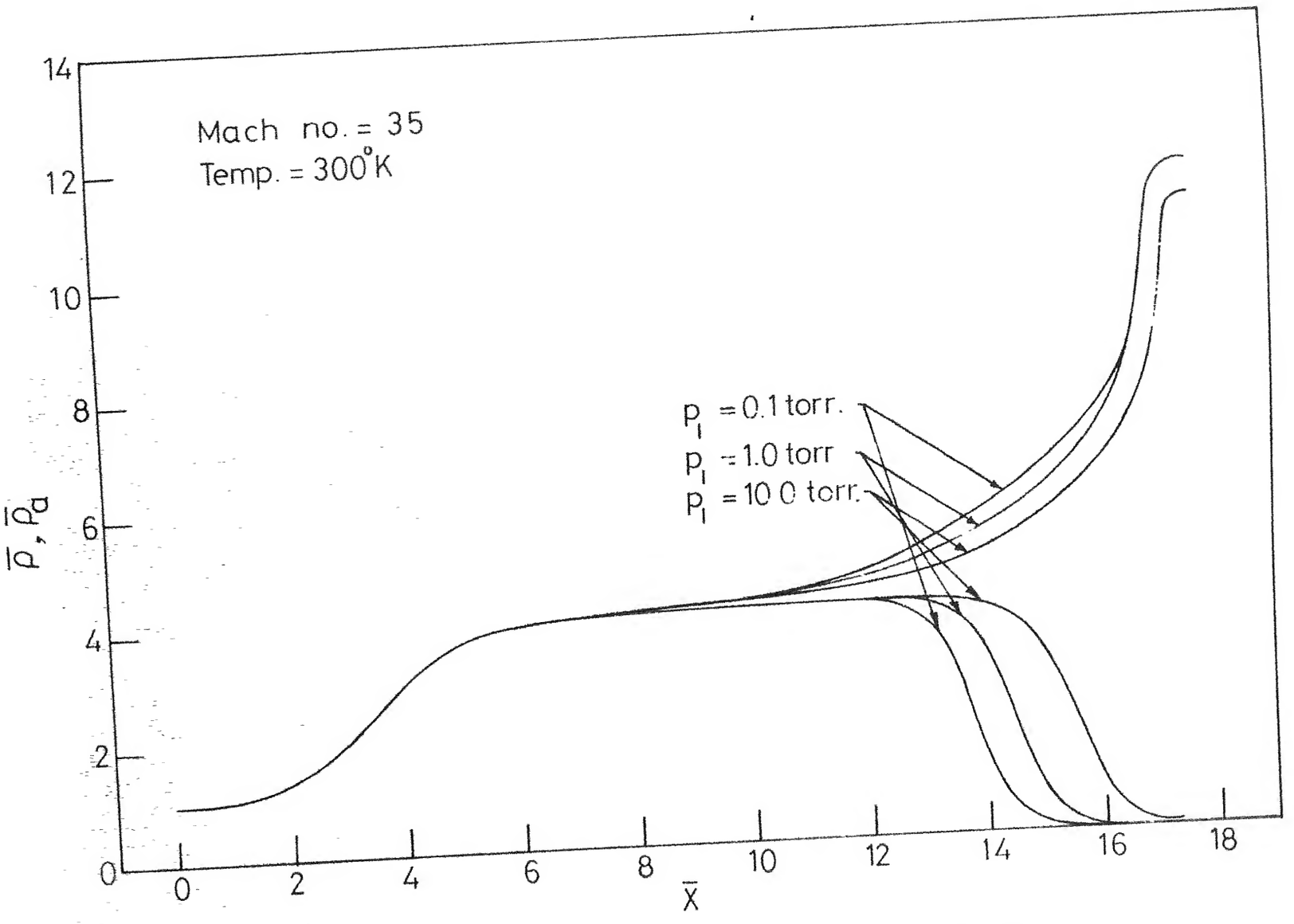

FIG. 6.3.5_DENSITY PROFILES FOR ARGON

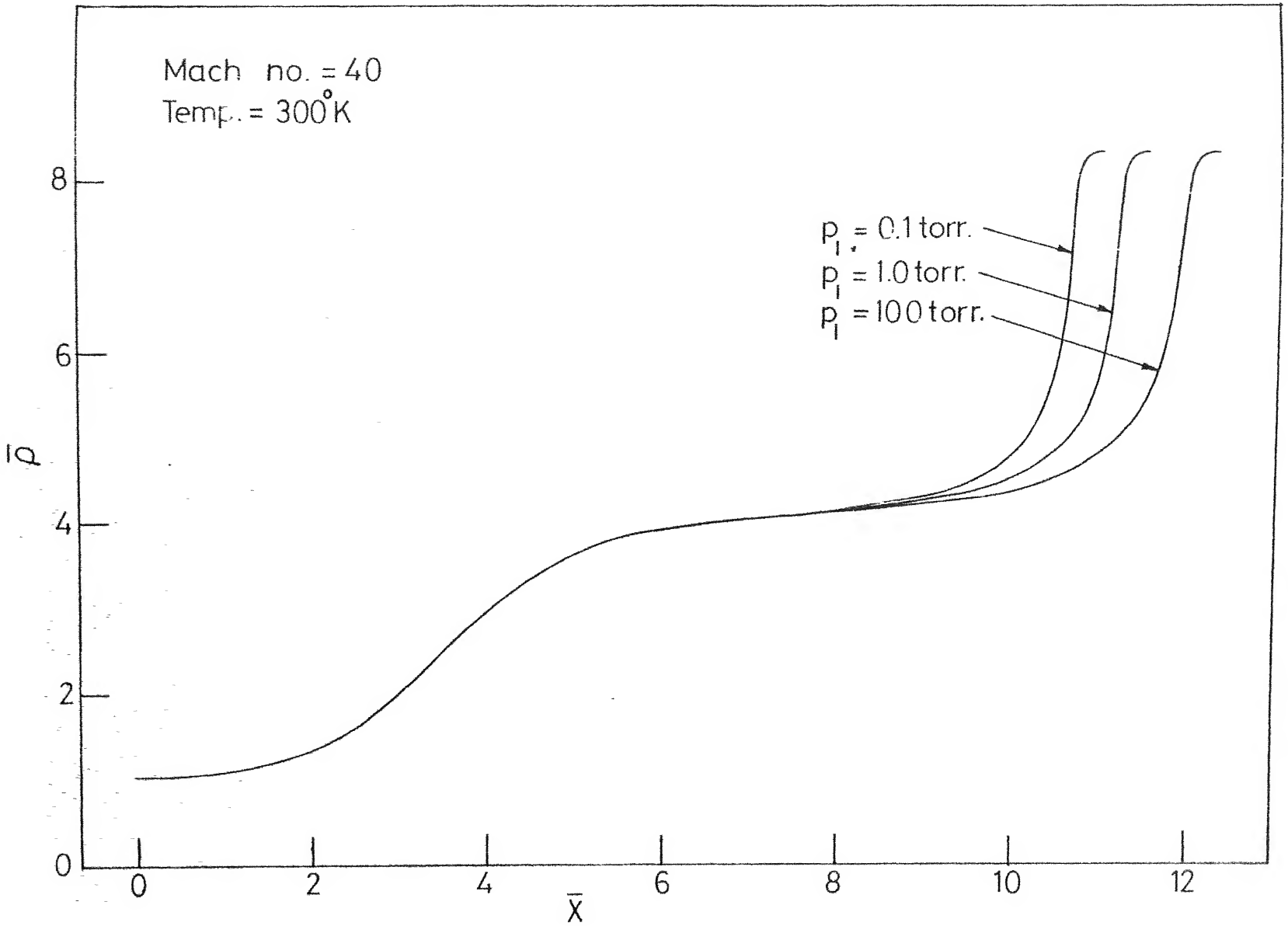

FIG.6.3.6_DENSITY PROFILES FOR ARGON

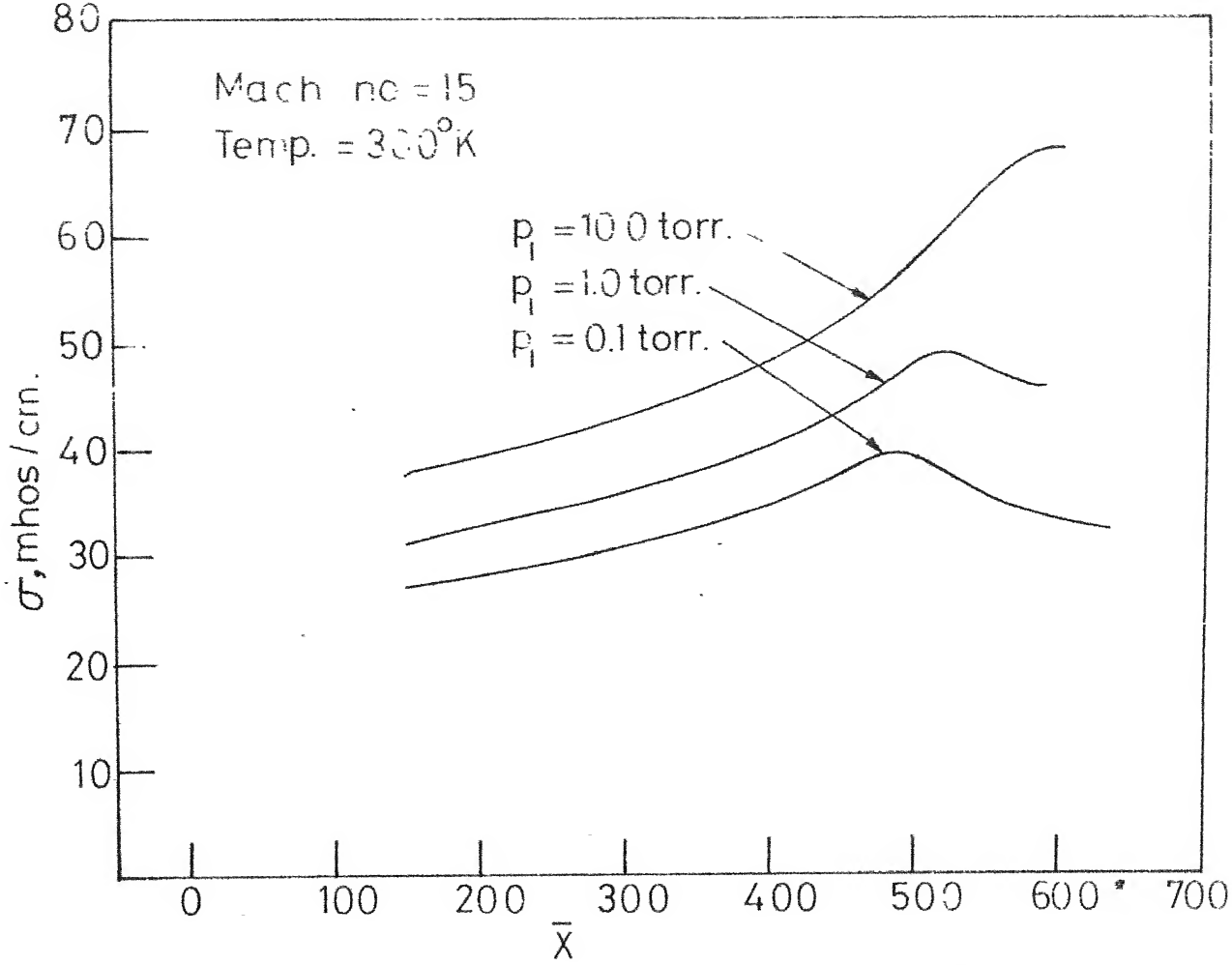

FIG. 6.4.1_ELECTRICAL CONDUCTIVITY PROFILES FOR ARGON

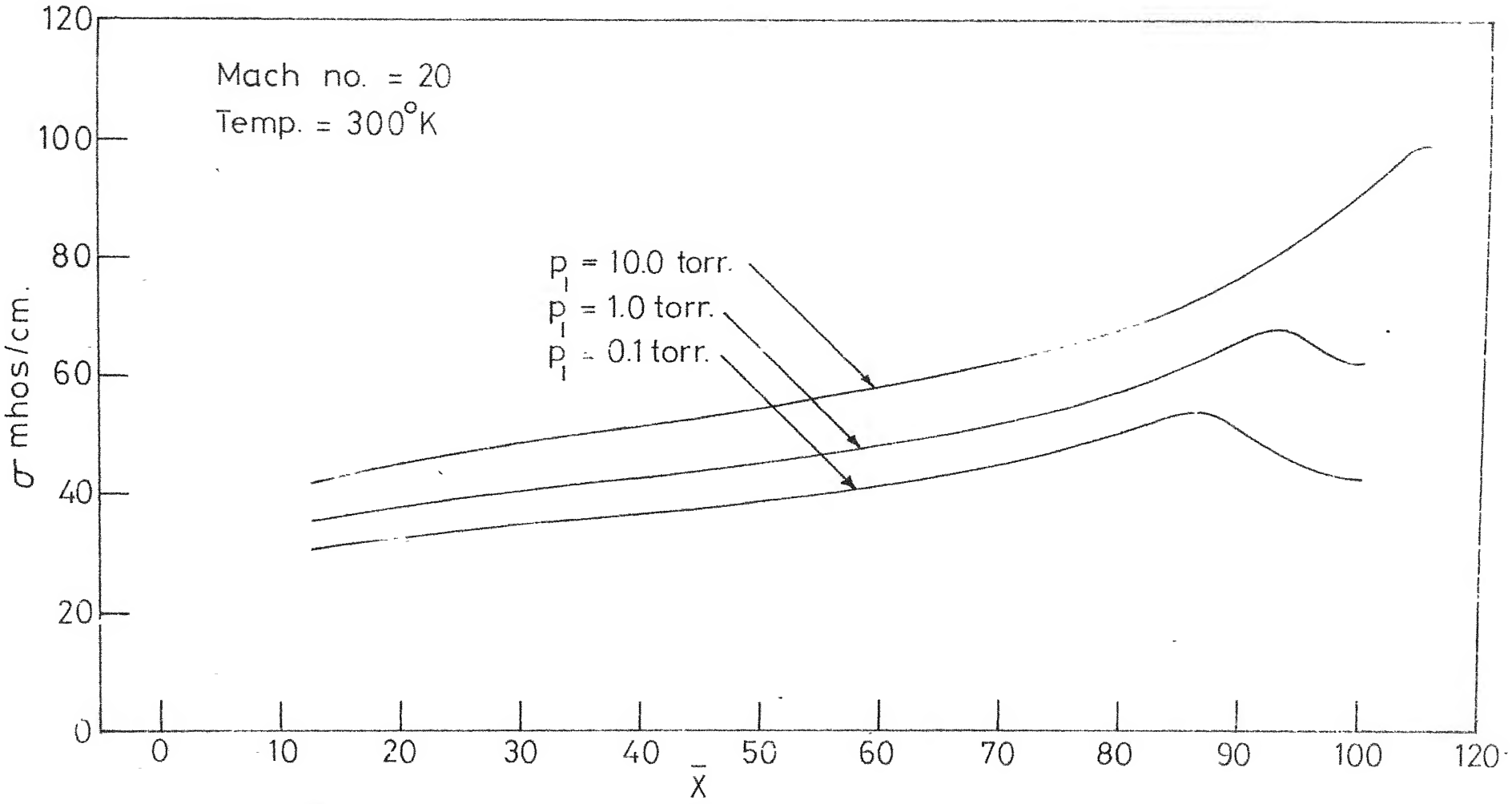

FIG.6.4.2 _ELECTRICAL CONDUCTIVITY PROFILES FOR ARGON

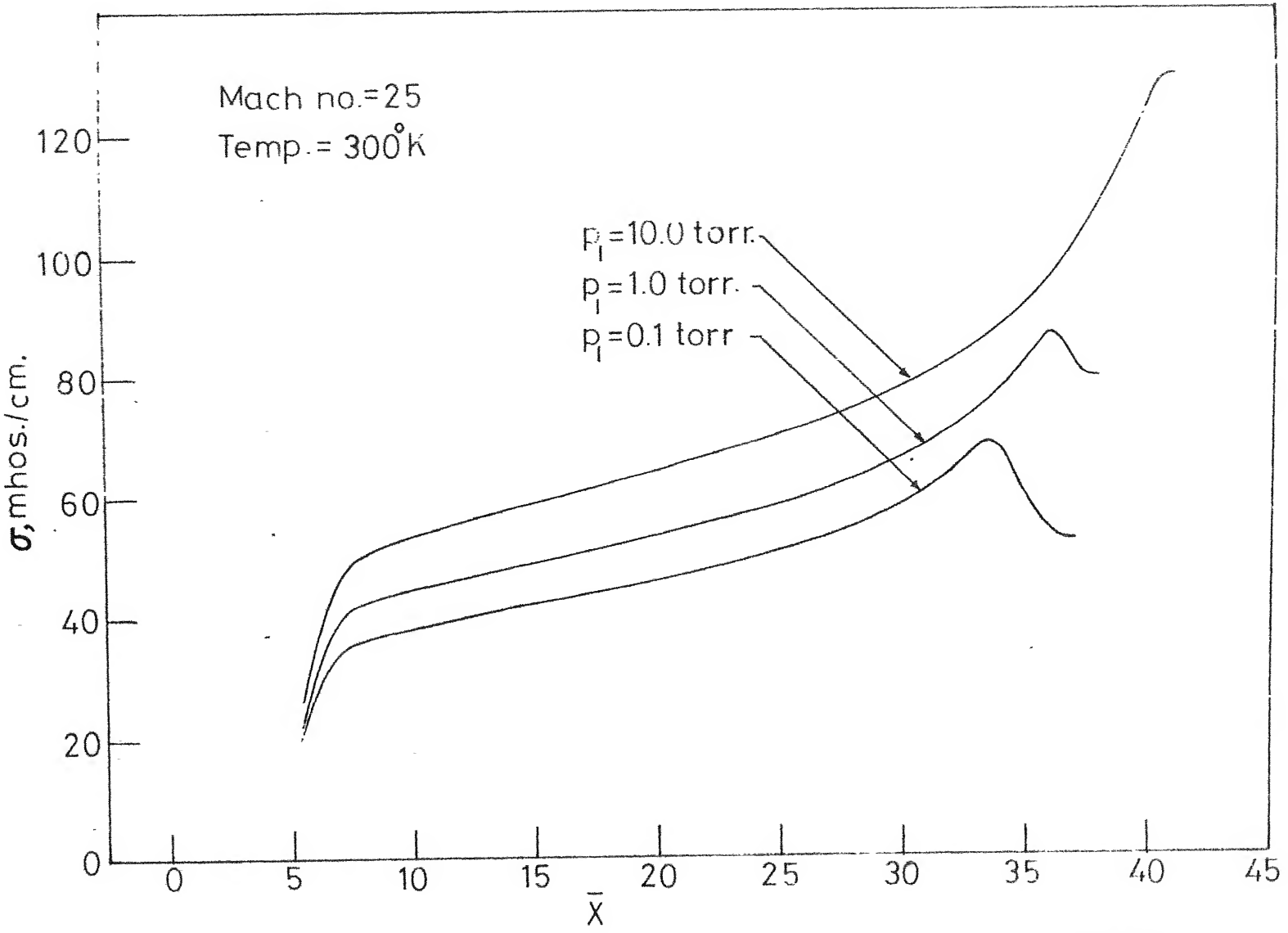

FIG.6.4.3. ELECTRICAL CONDUCTIVITY PROFILES FOR ARGON

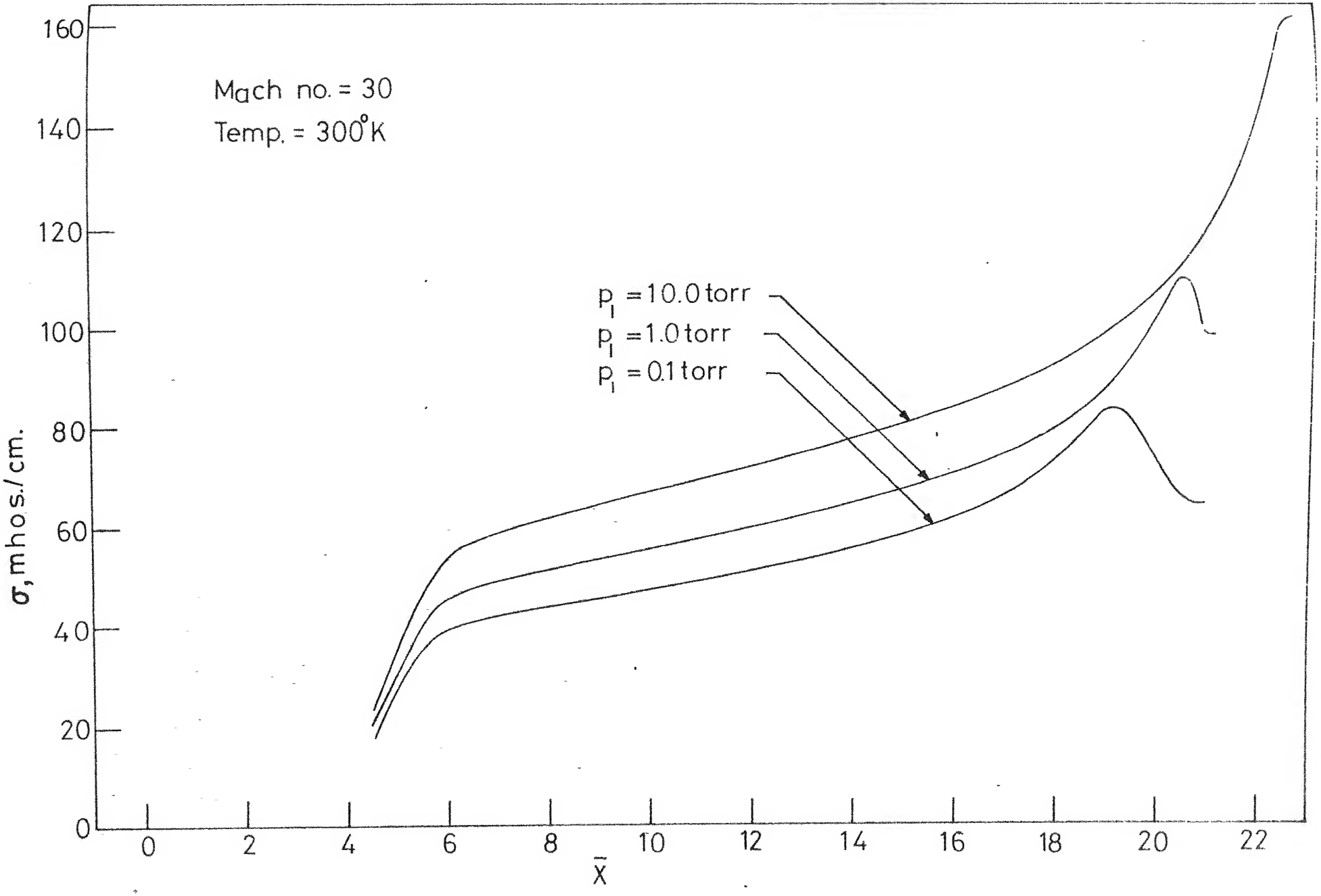

FIG.6.4.4.-ELECTRICAL CONDUCTIVITY PROFILES FOR ARGON

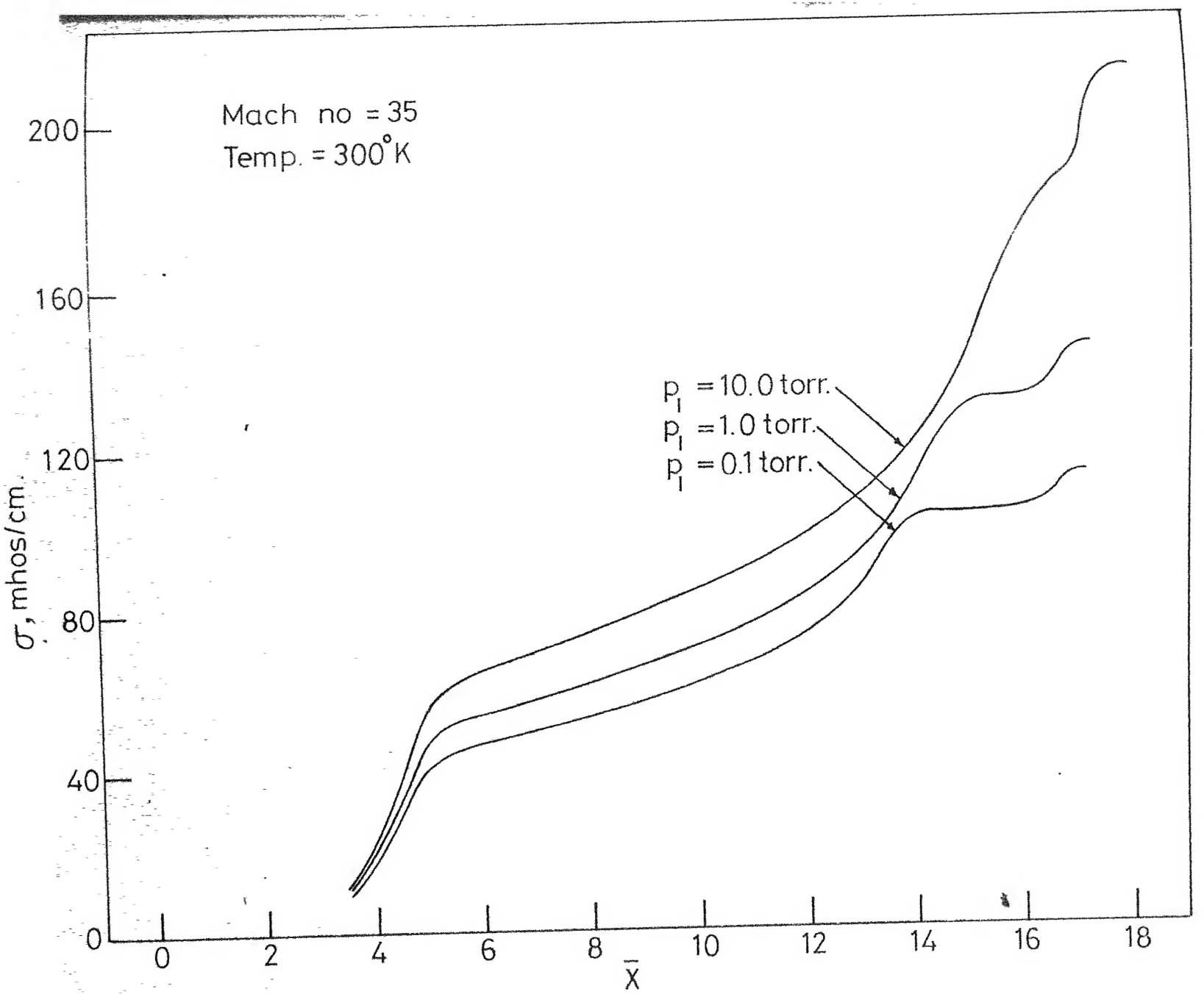

FIG.6.4.5_ELECTRICAL CONDUCTIVITY PROFILES FOR ARGON

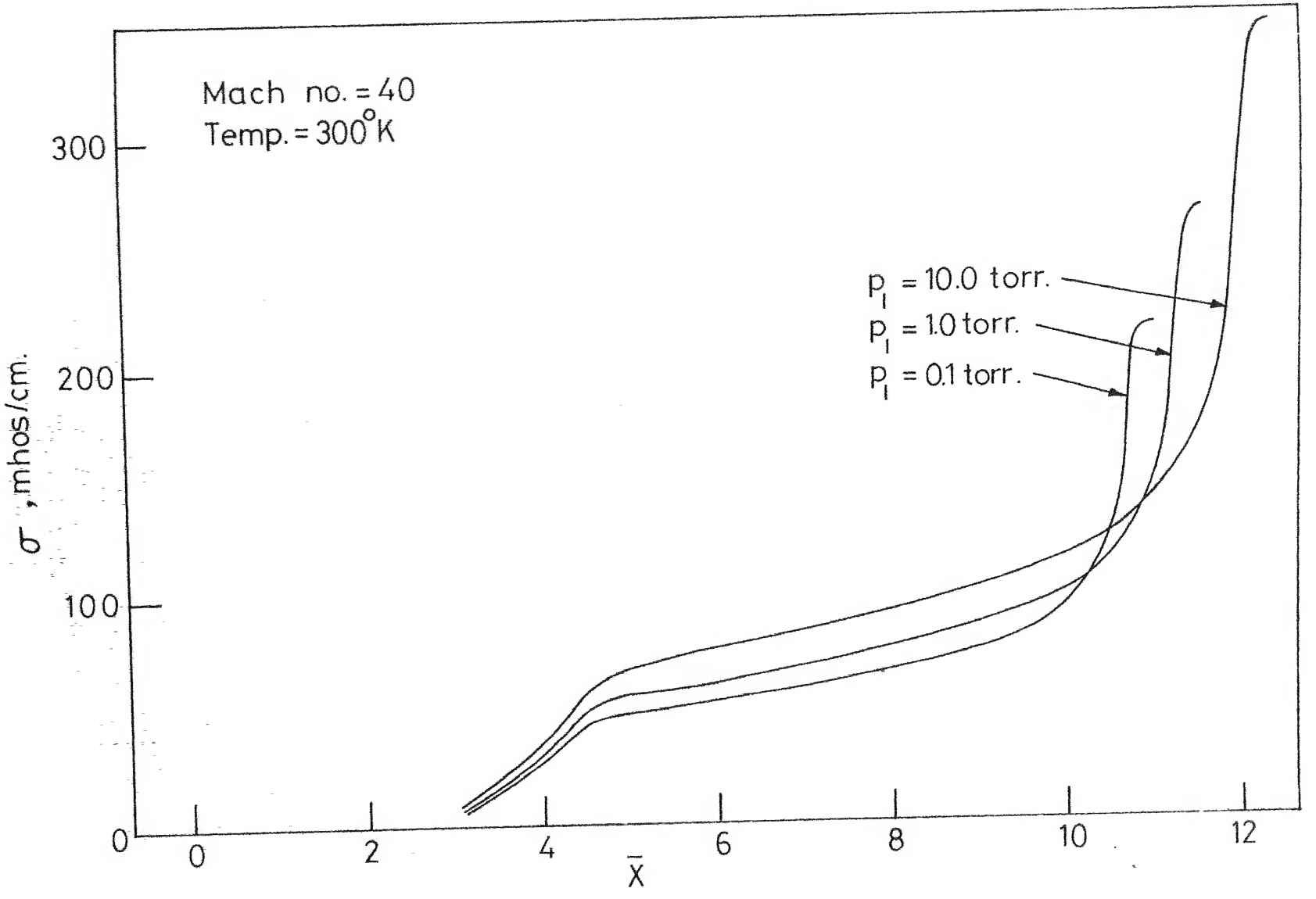

FIG.6.4.6_ELECTRICAL CONDUCTIVITY PROFILES FOR ARGON

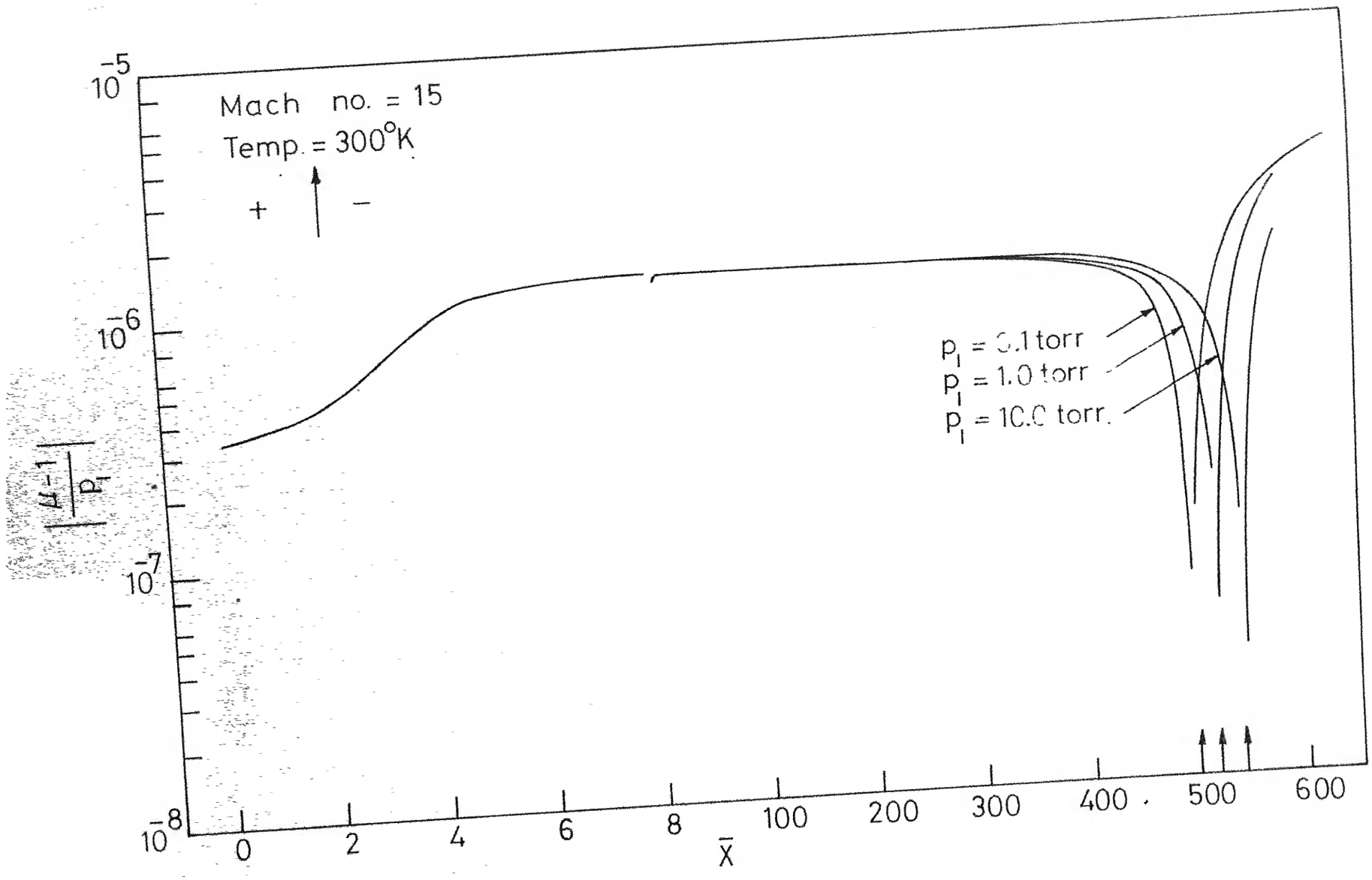

FIG.6.5.1_REFRACTIVE INDEX PROFILES FOR ARGON

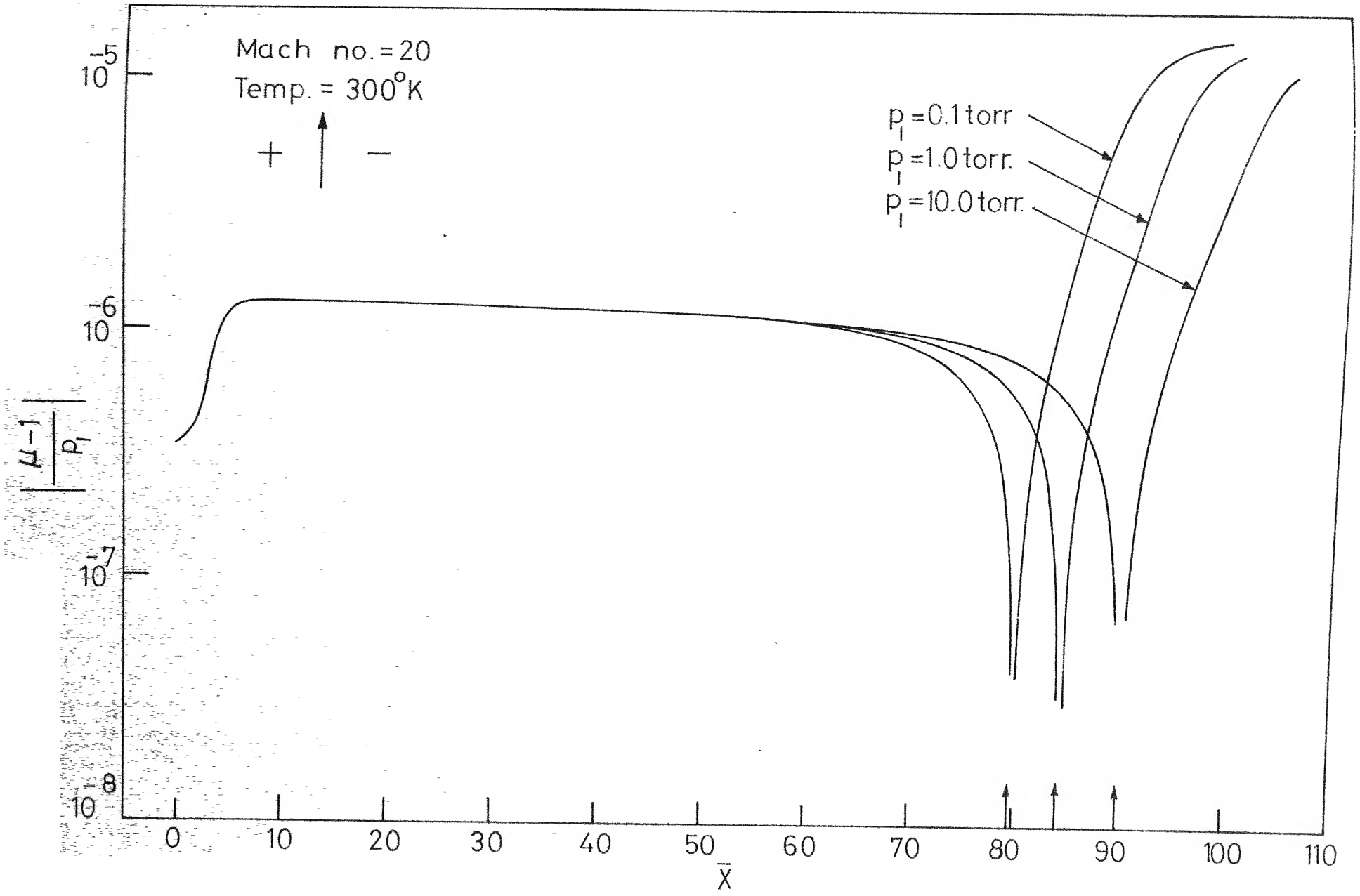

FIG. 6.5.2_REFRACTIVE INDEX PROFILES FOR ARGON

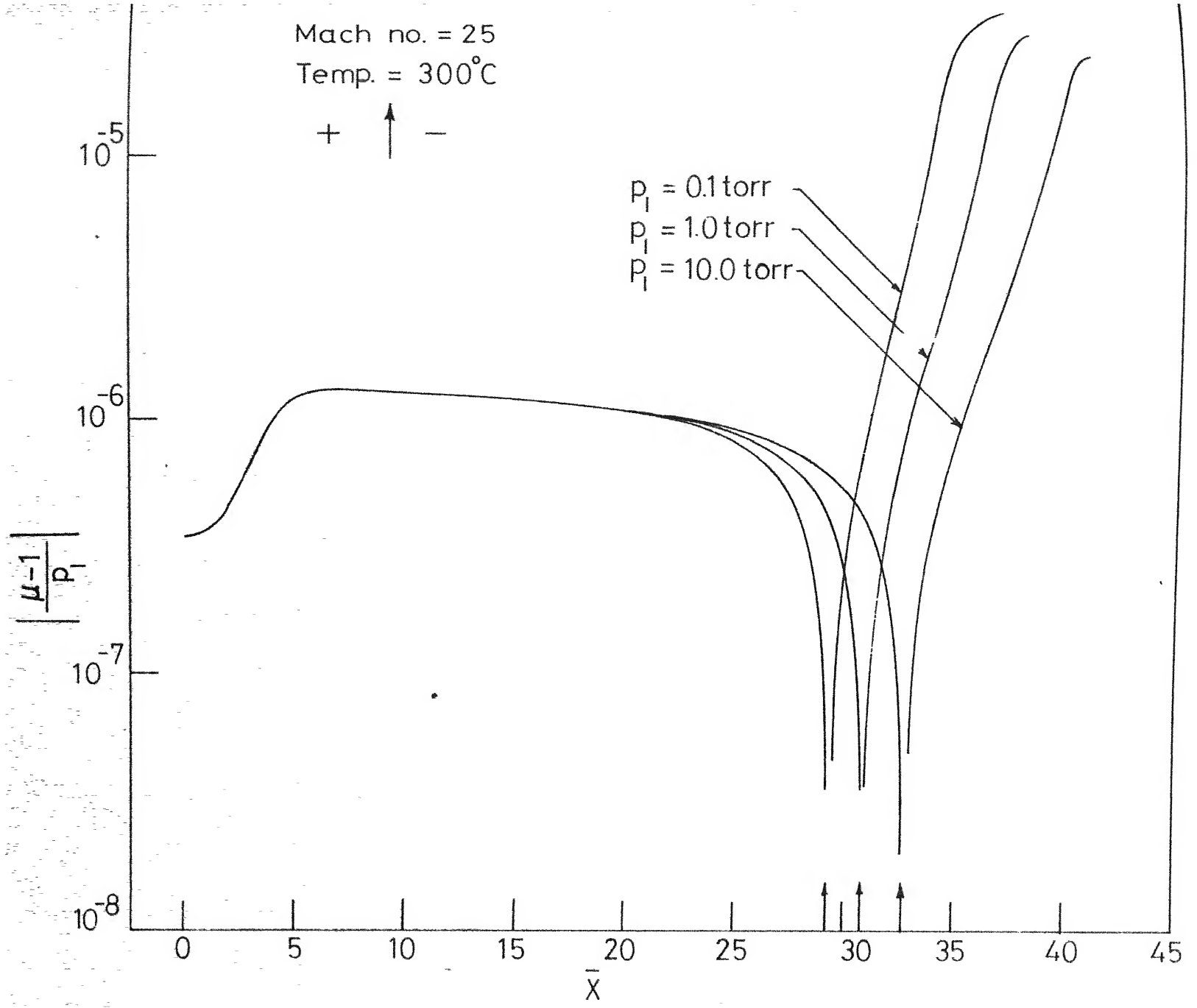

FIG. 6.5.3_REFRACTIVE INDEX PROFILES FOR ARGON

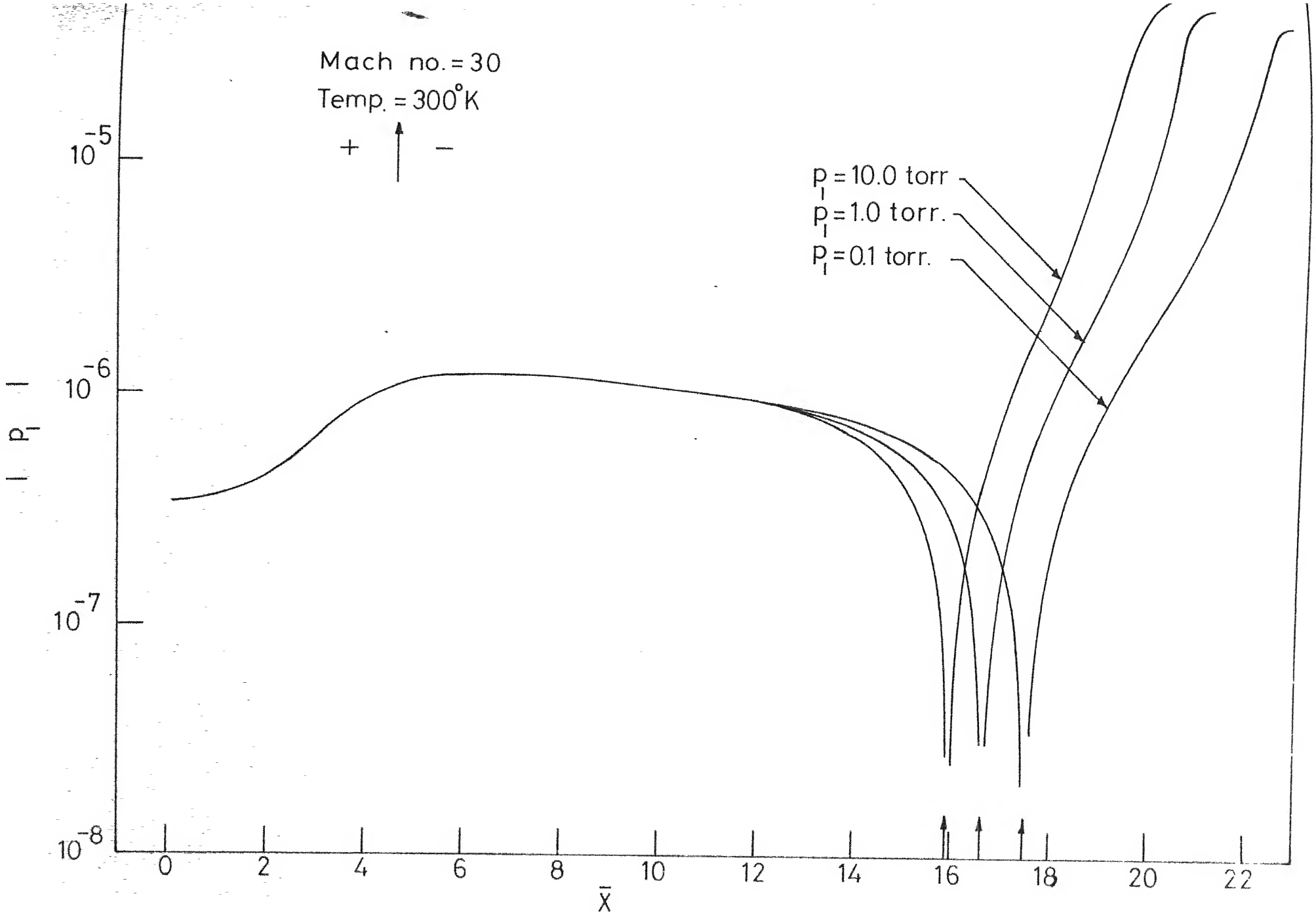

FIG. 6.5.4 – REFRACTIVE INDEX PROFILES FOR ARGON

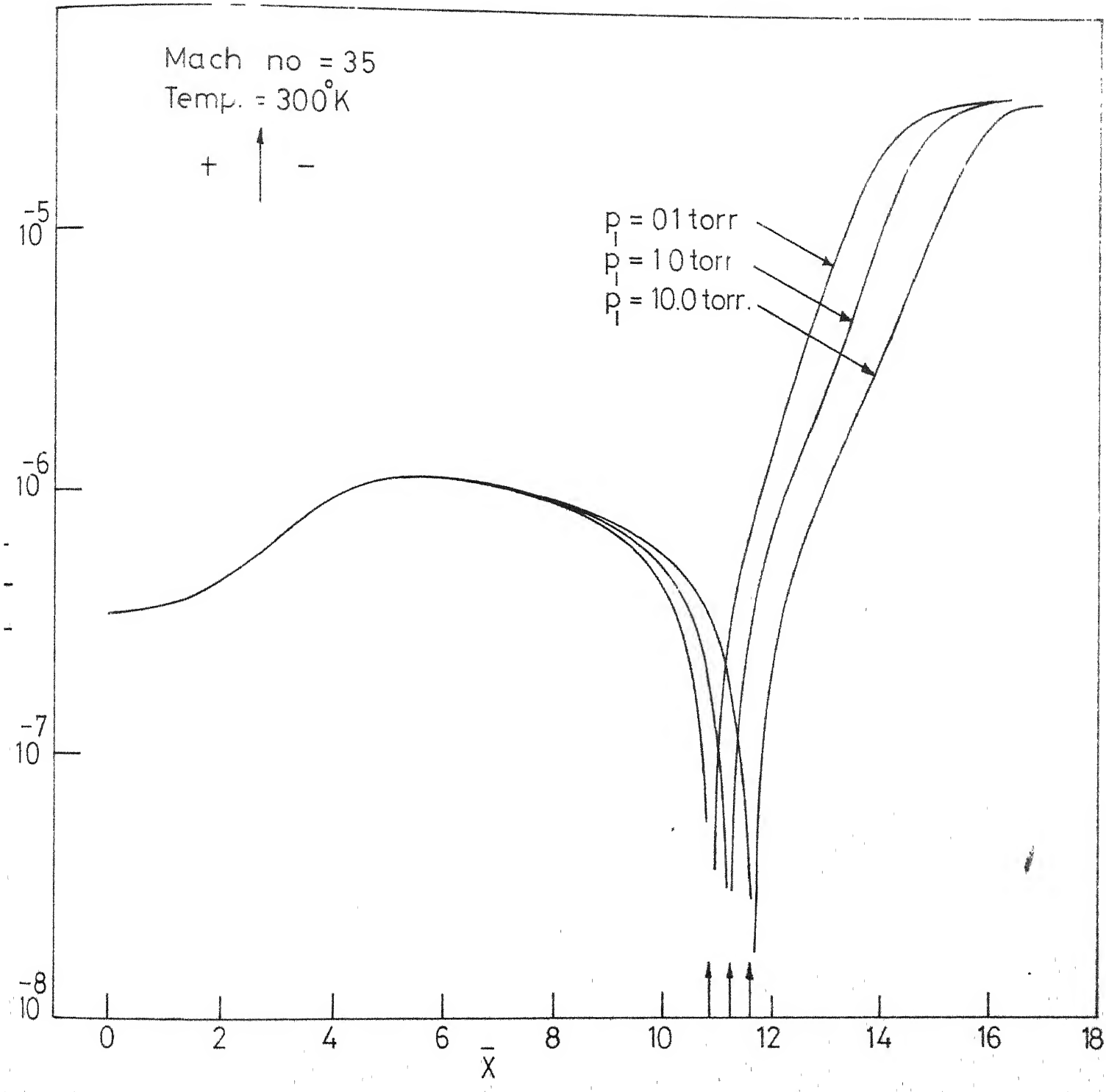

FIG.6.5.5_REFRACTIVE INDEX PROFILES FOR ARGON

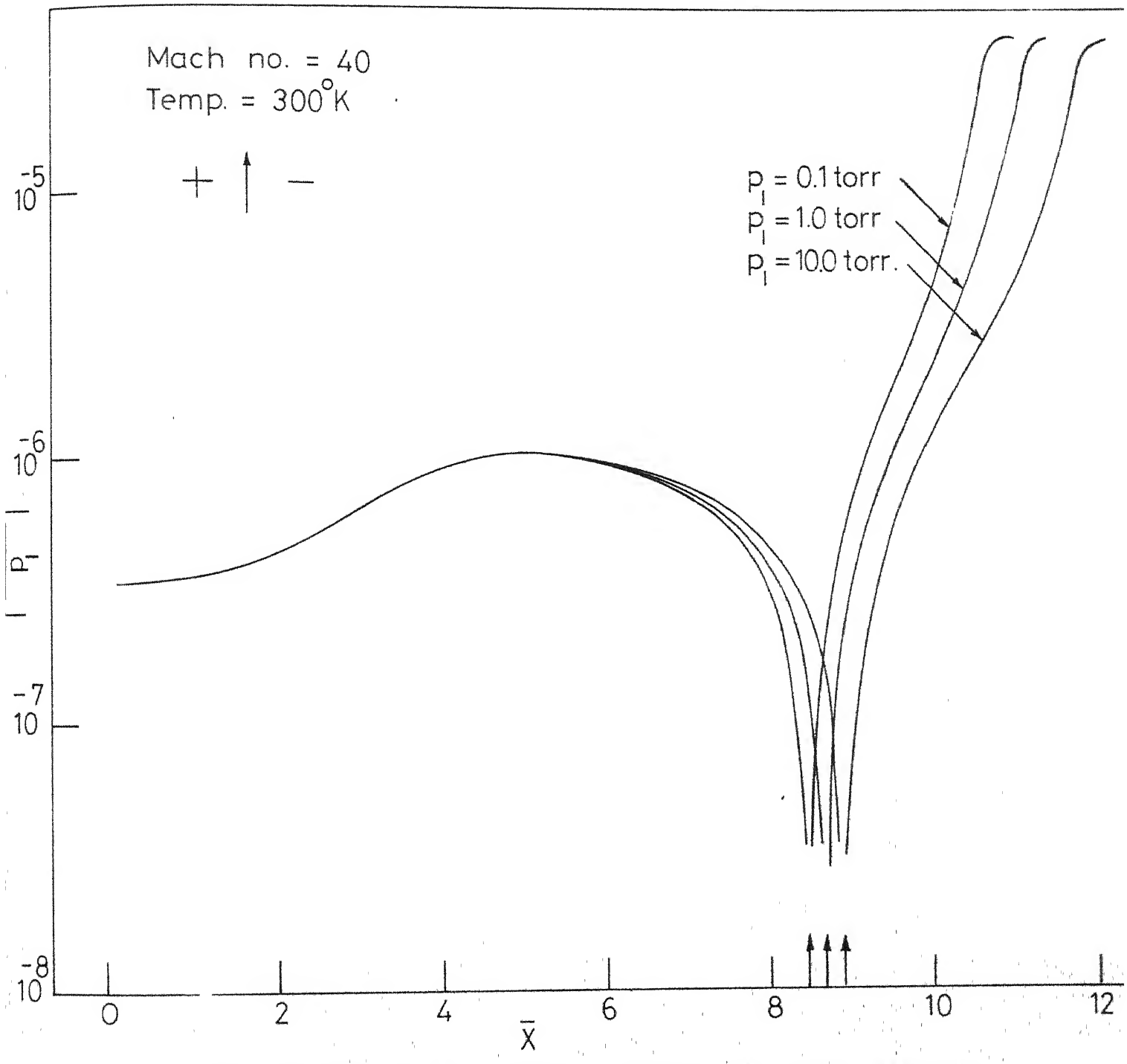

FIG.6.5.6_REFRACTIVE INDEX PROFILES FOR ARGON

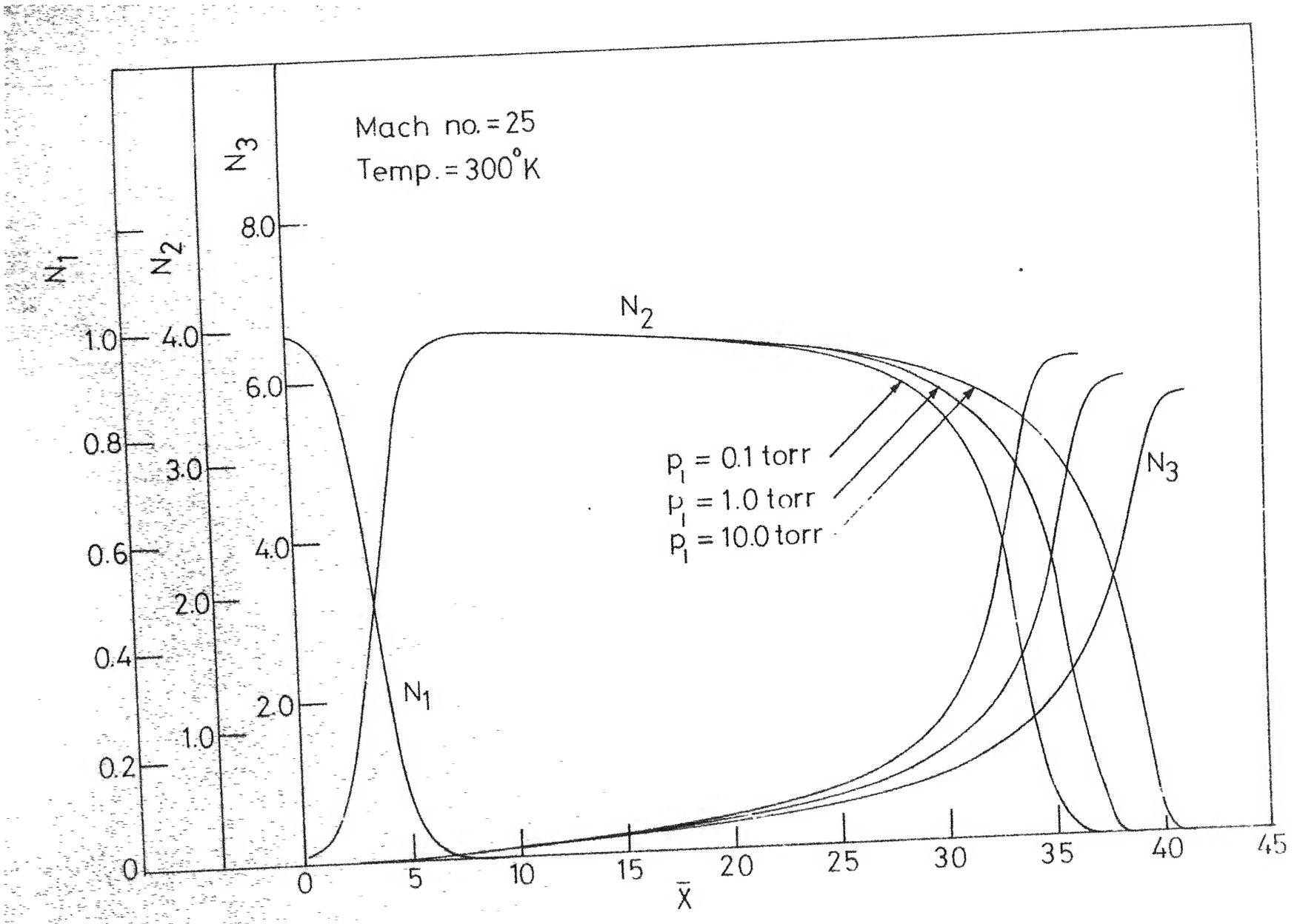

FIG. 6.61_TYPICAL PROFILES OF N_1, N_2, N_3 FOR ARGON

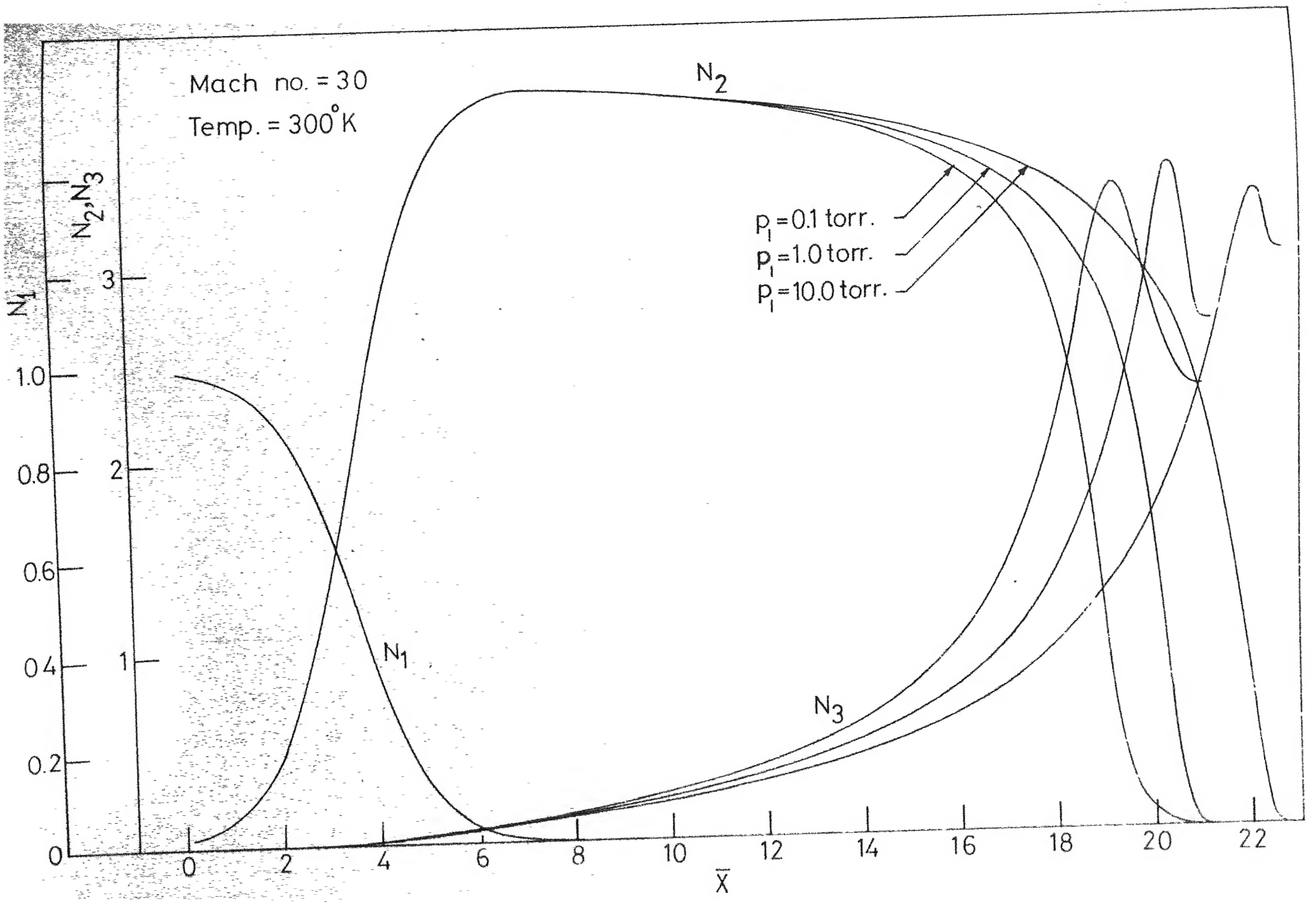

FIG. 6.6.2_TYPICAL PROFILES OF N_1, N_2, N_3, FOR ARGON

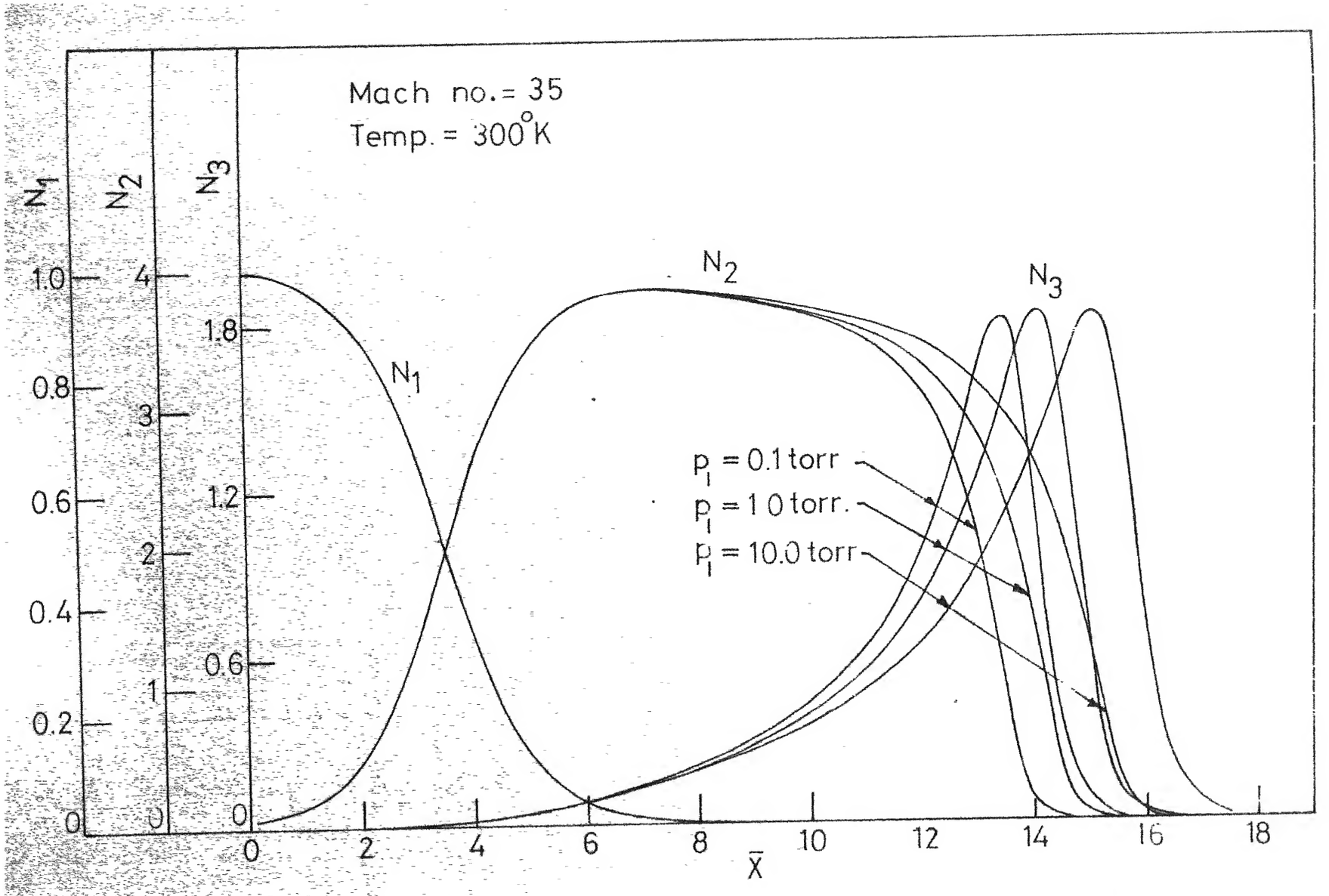

FIG.6.6.3_TYPICAL PROFILES OF N_1, N_2, N_3, FOR ARGON

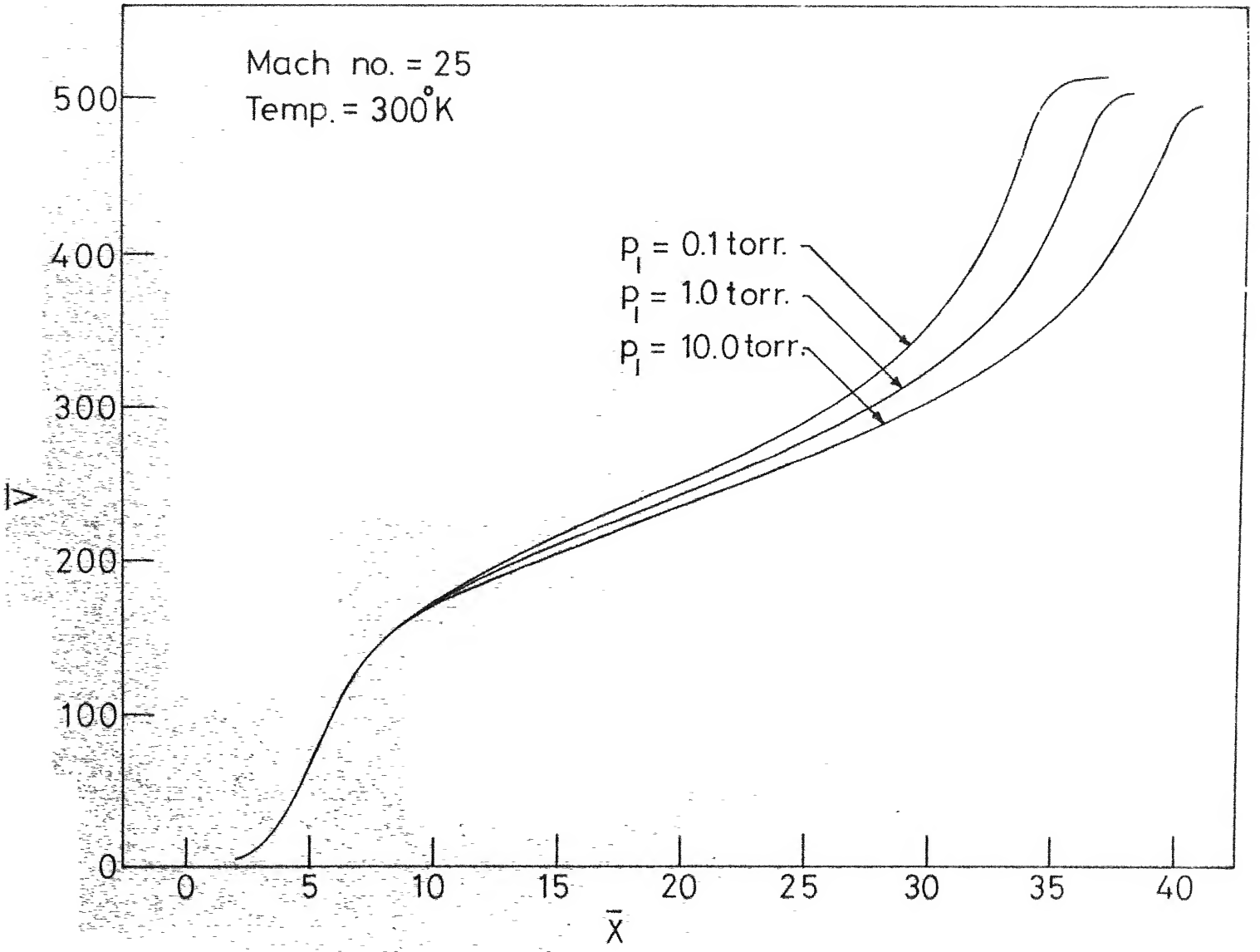

FIG. 6.7.1 ELECTRIC POTENTIAL PROFILES FOR ARGON.

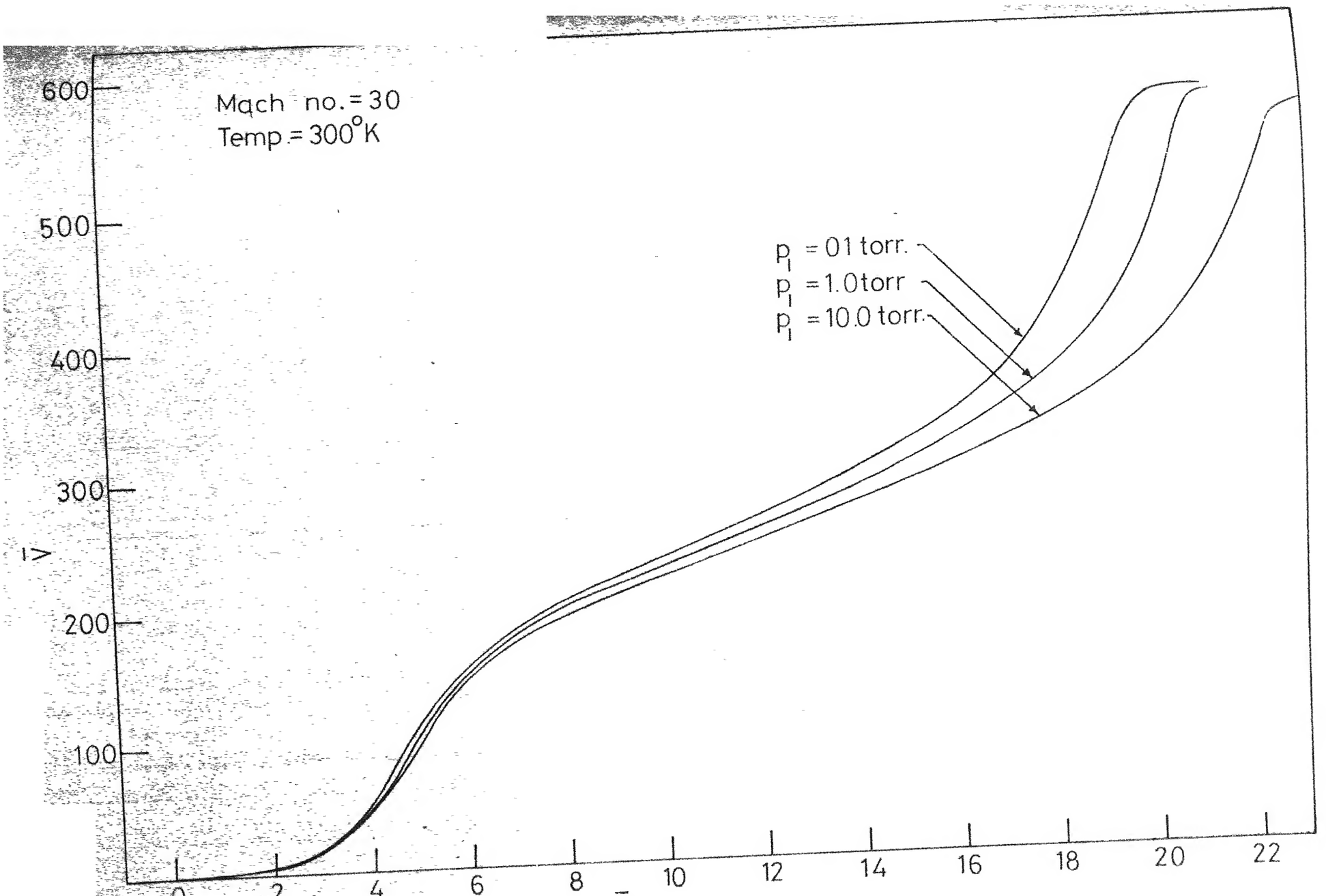

FIG. 6.7.2 ELECTRIC POTENTIAL PROFILES FOR ARGON

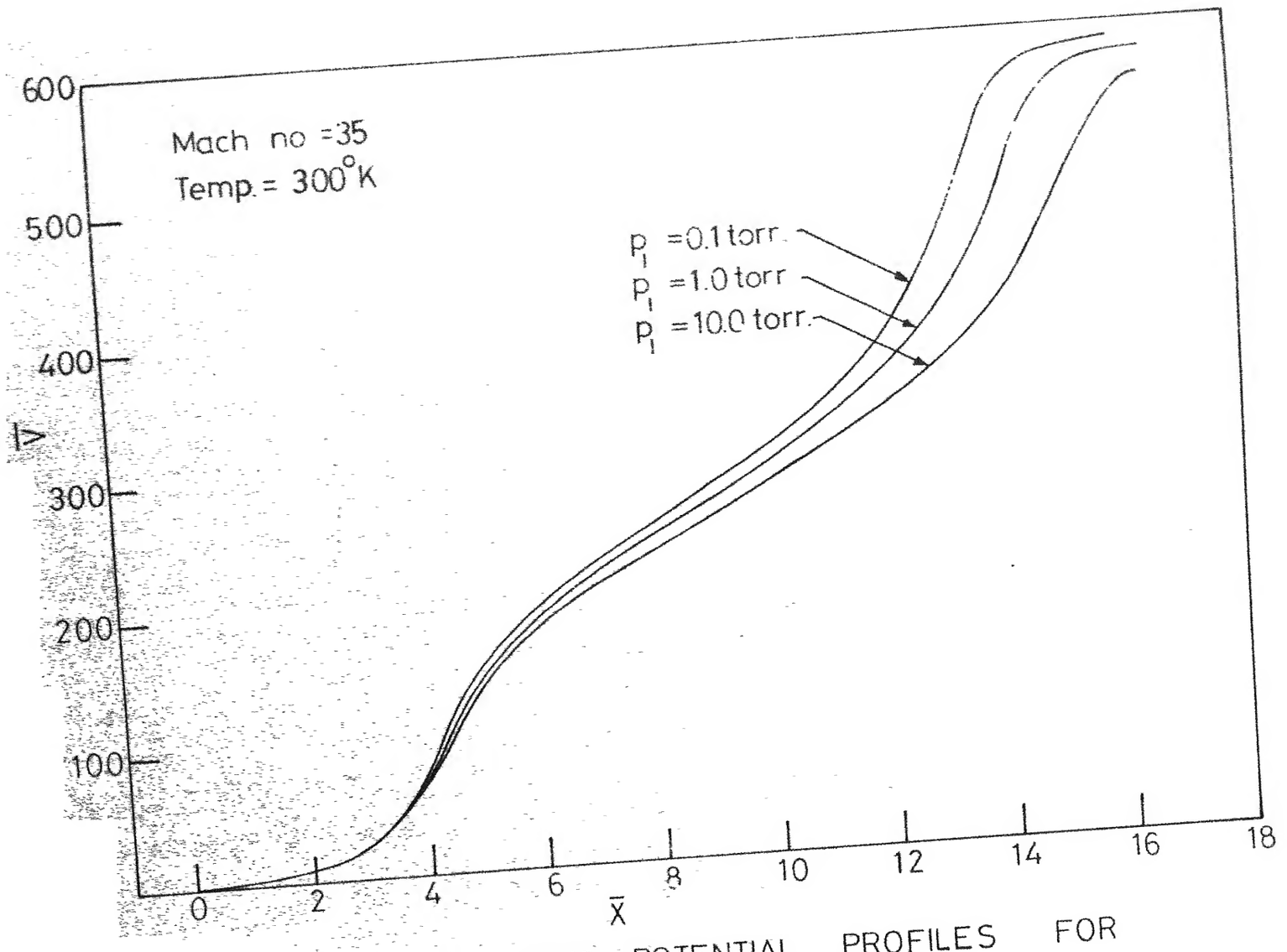

FIG.6.7.3_ELECTRIC POTENTIAL PROFILES FOR ARGON

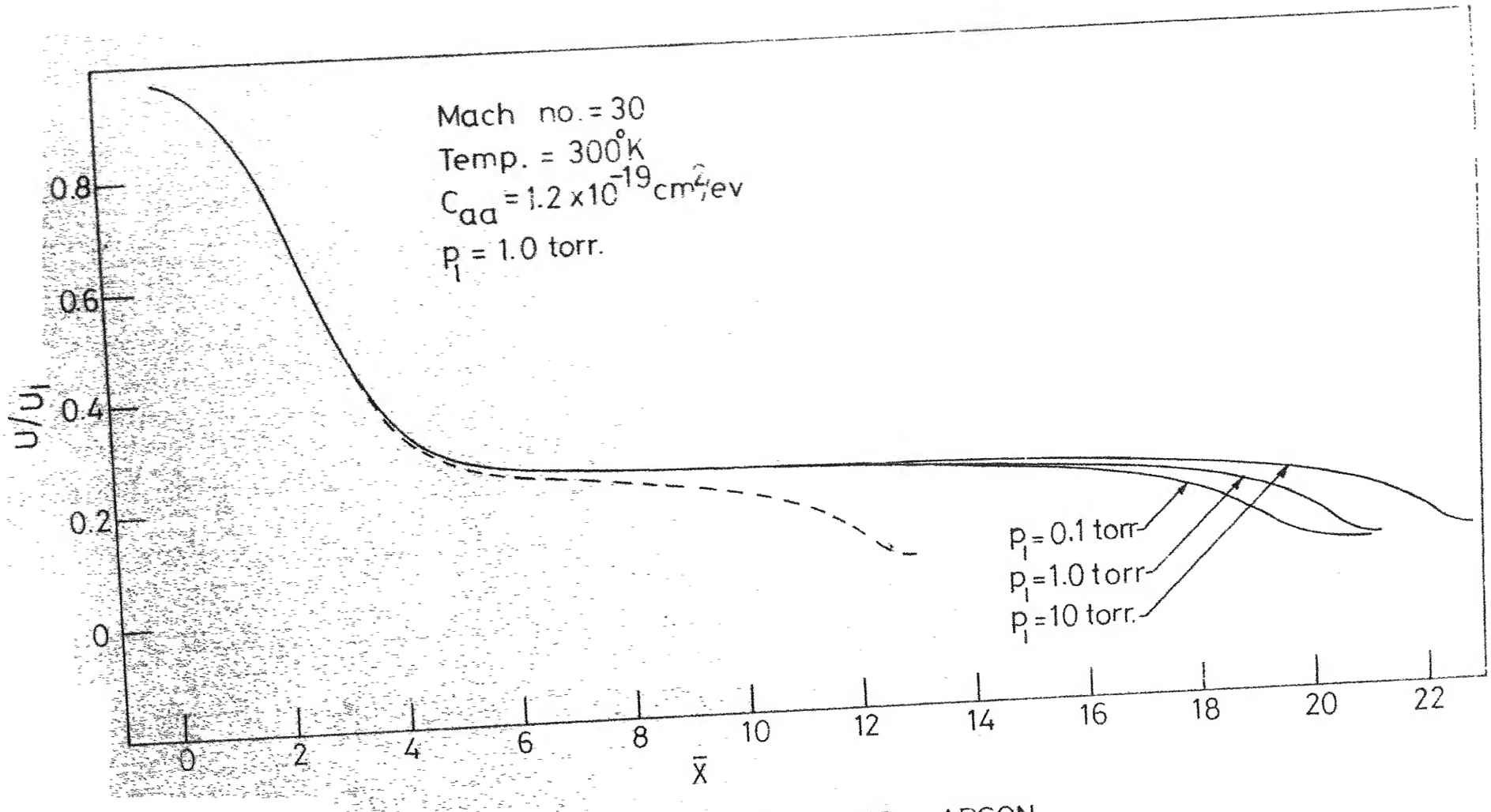

FIG. 6.9.1 VELOCITY PROFILES FOR ARGON

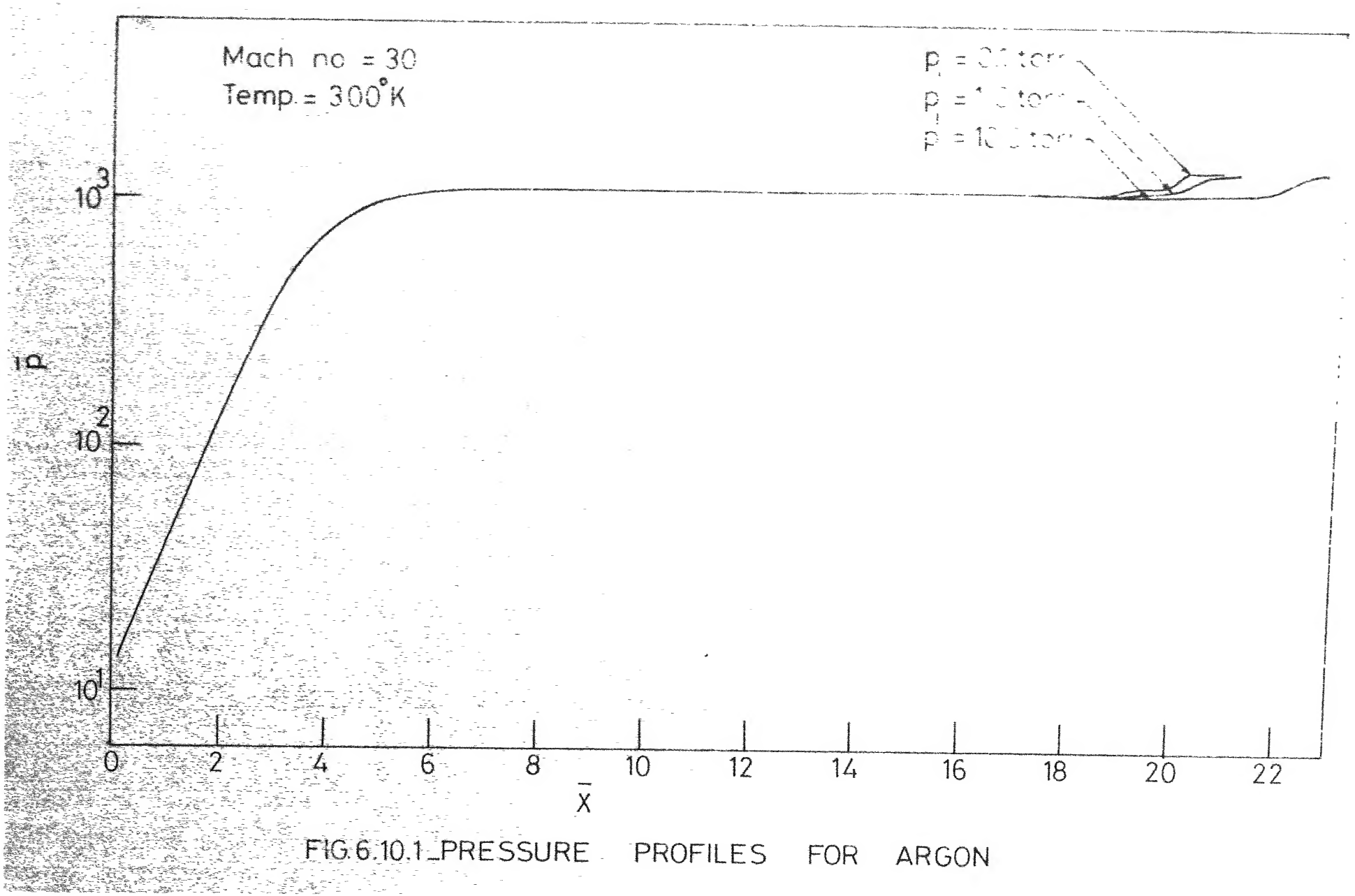

FIG.6.10.1_PRESSURE PROFILES FOR ARGON

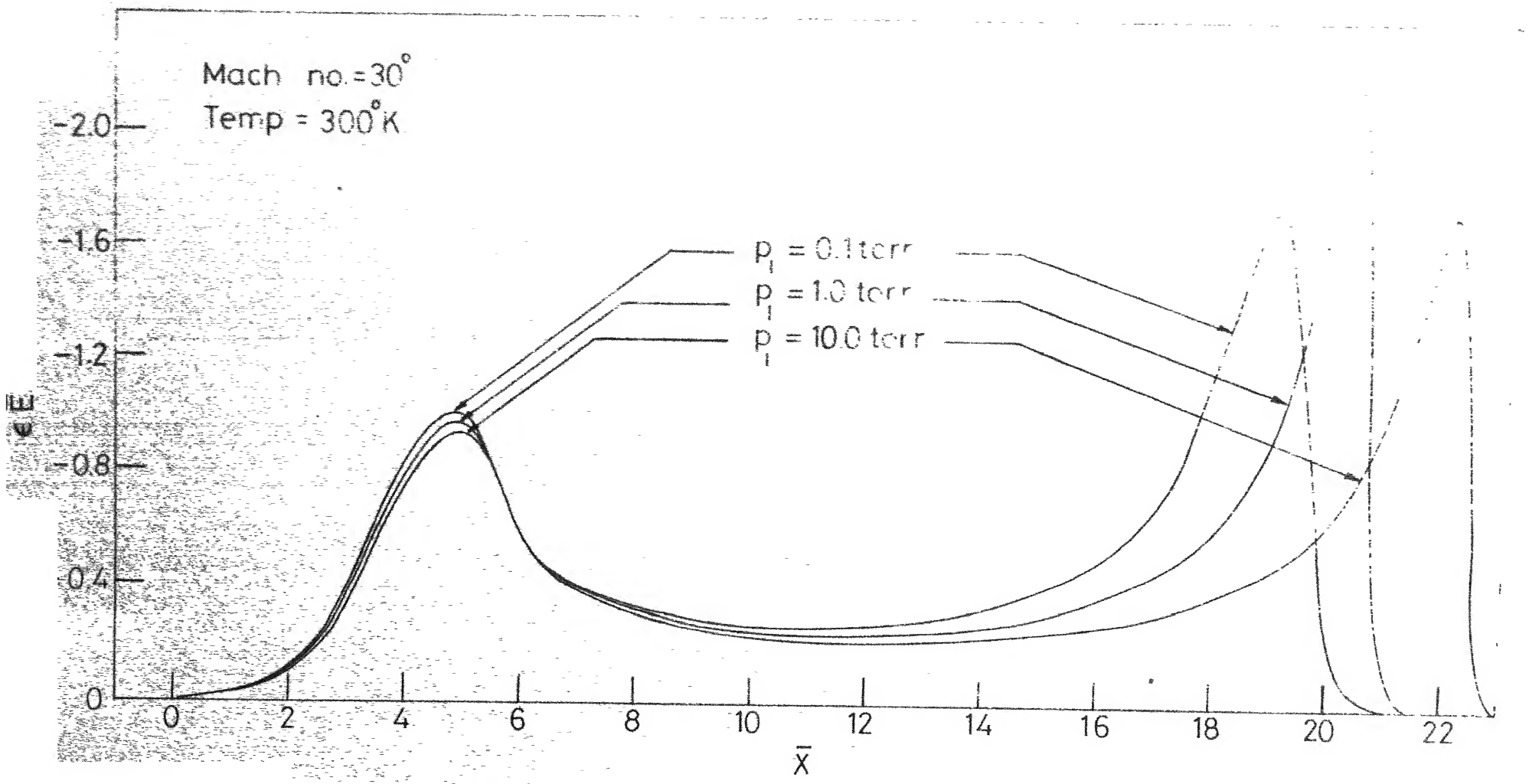

FIG. 6.11.1 ELECTRIC FIELD PROFILES FOR ARGON

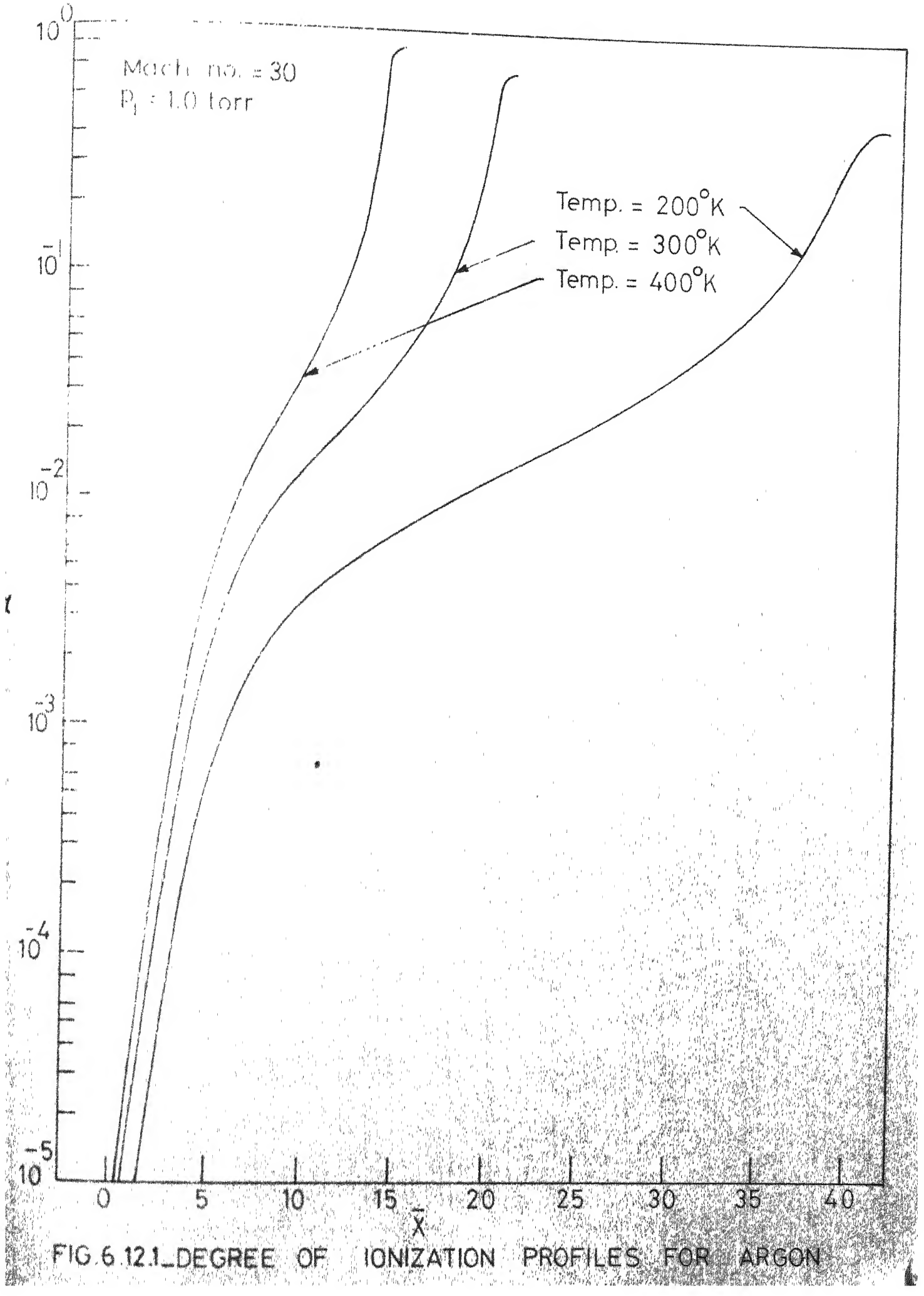

FIG. 6.12.1 DEGREE OF IONIZATION PROFILES FOR ARGON

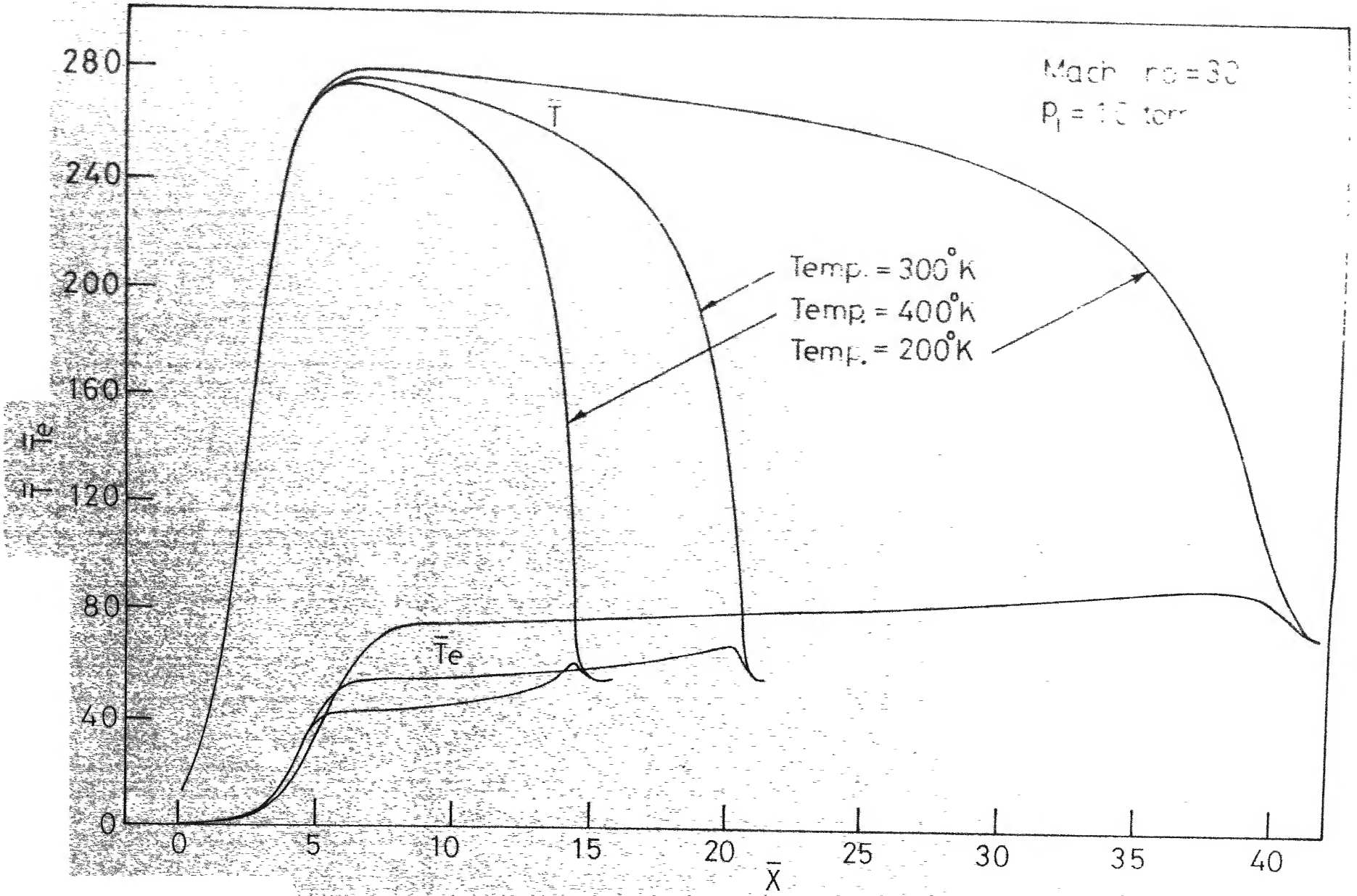

FIG. 6.12.2 TEMPERATURE PROFILES FOR ARGON.

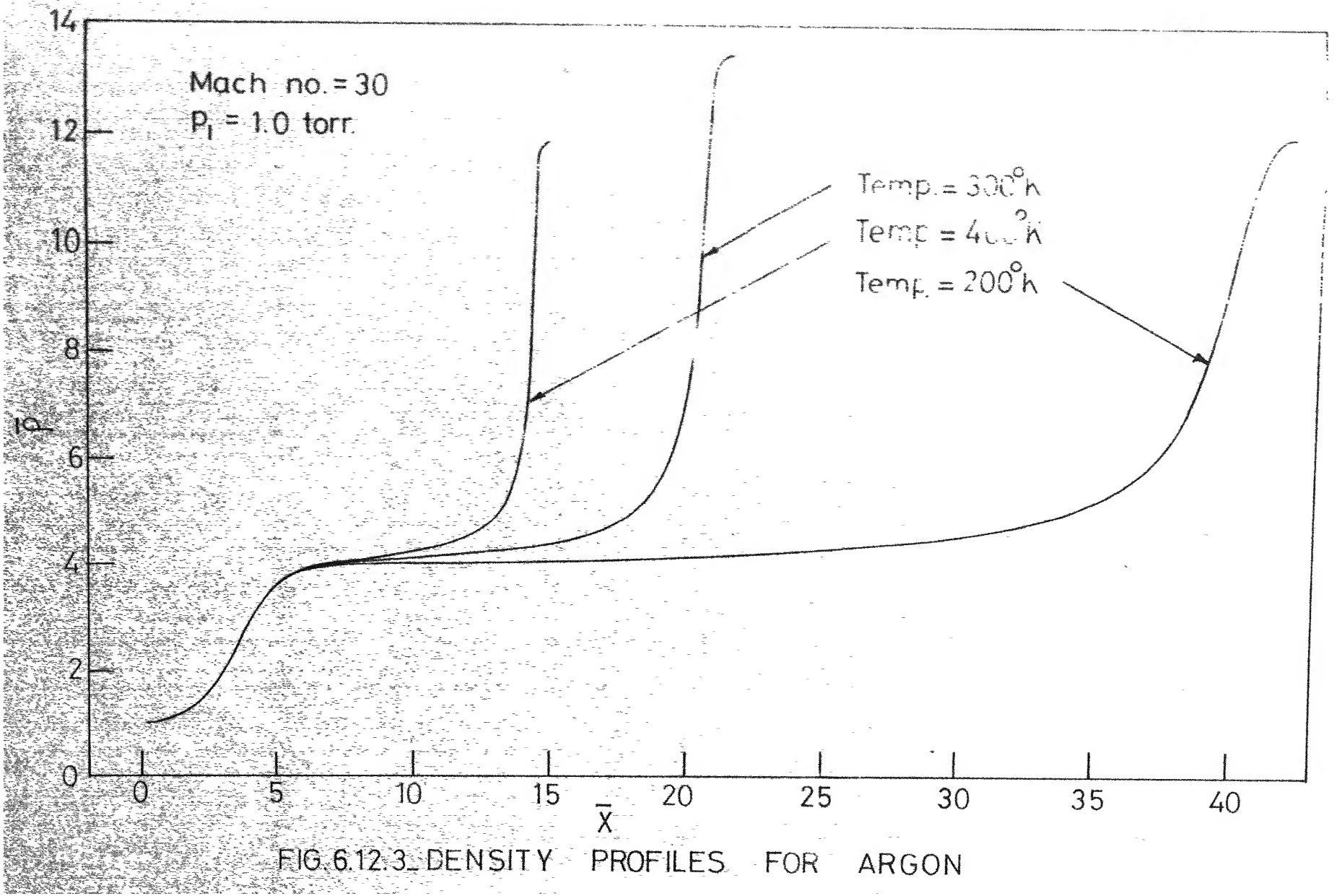

FIG. 6.12.3 DENSITY PROFILES FOR ARGON

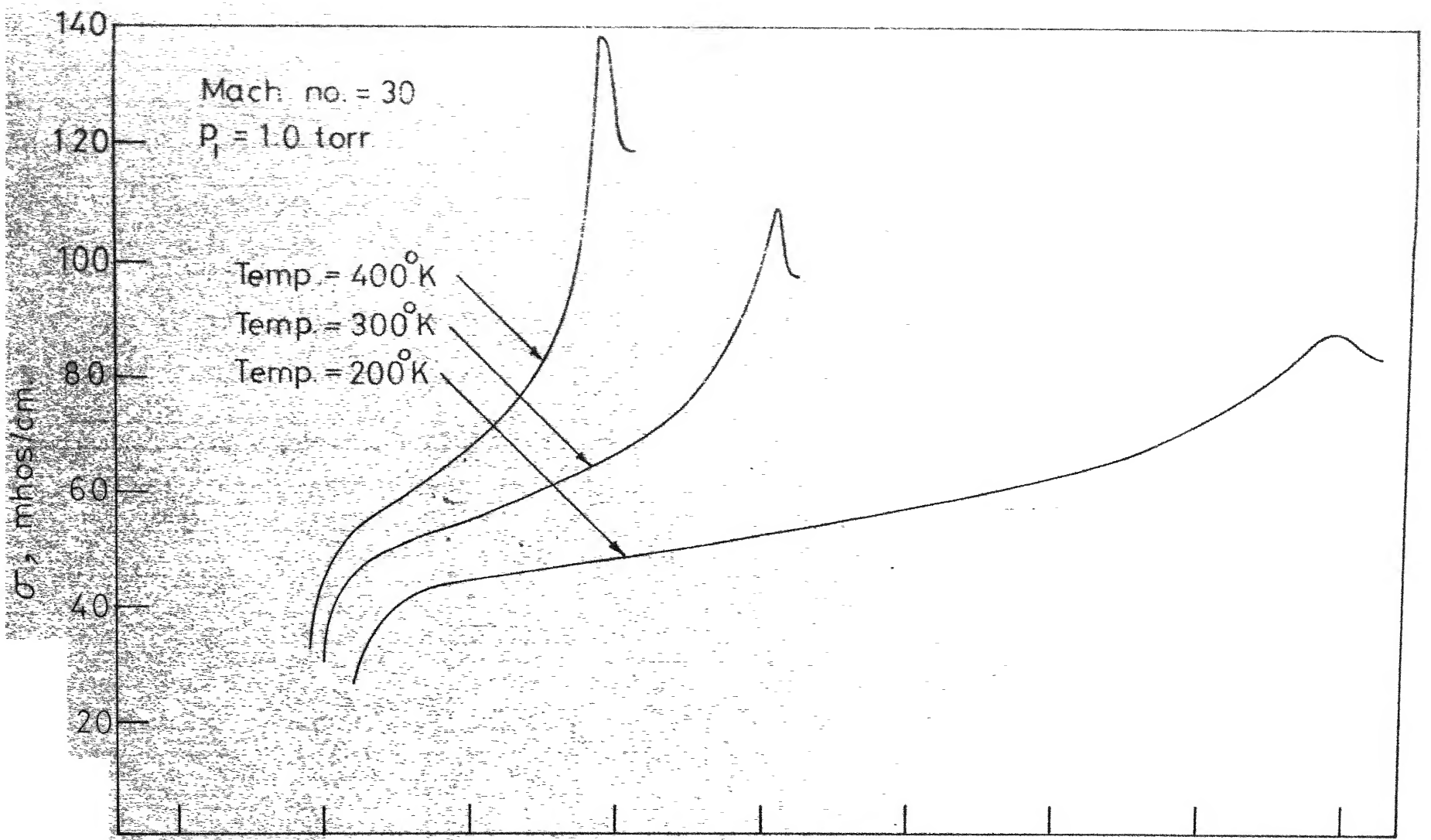

FIG. 6.12.4 ELECTRICAL CONDUCTIVITY PROFILES FOR ARGON

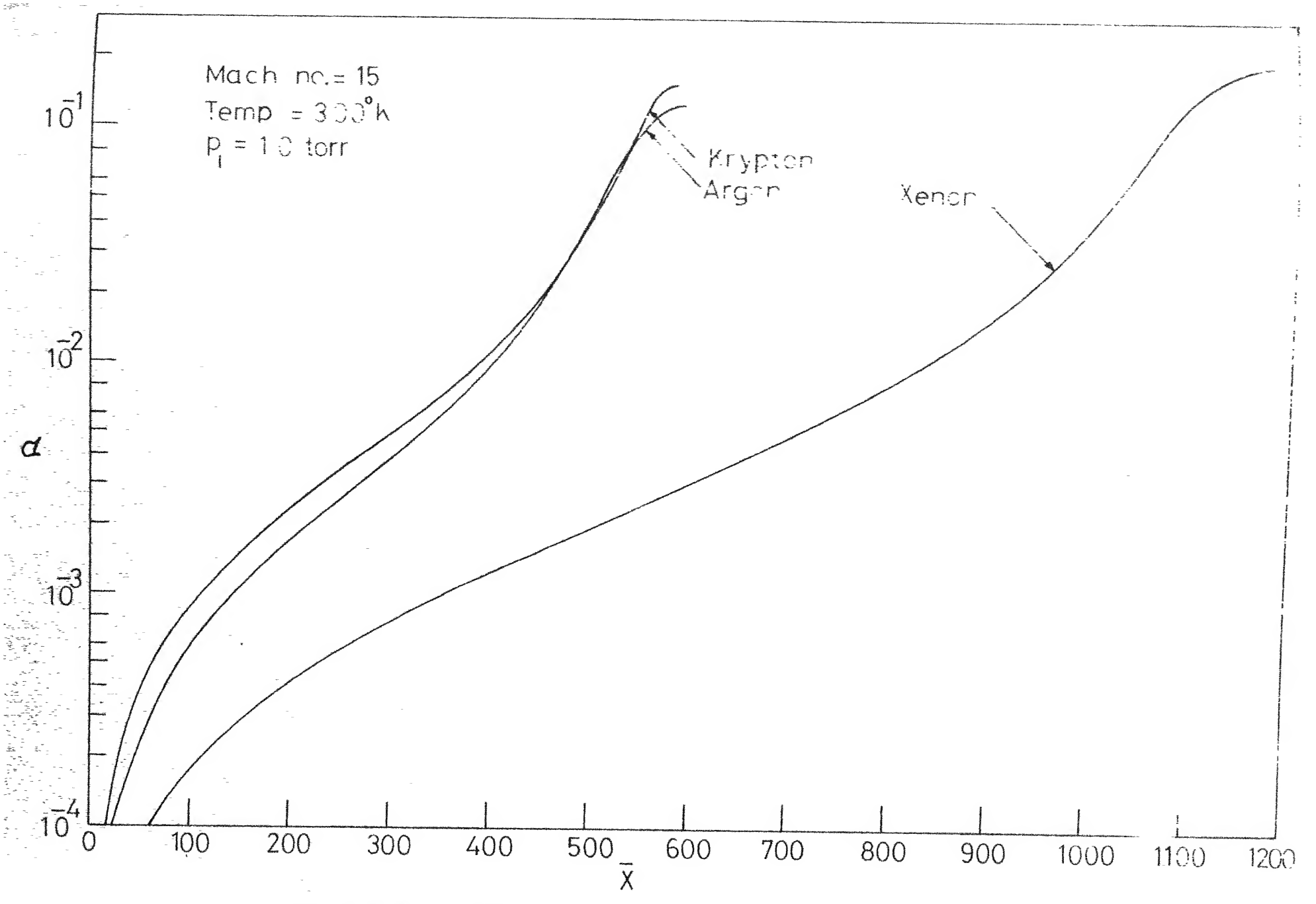

FIG.6.13.1_DEGREE OF IONIZATION PROFILES

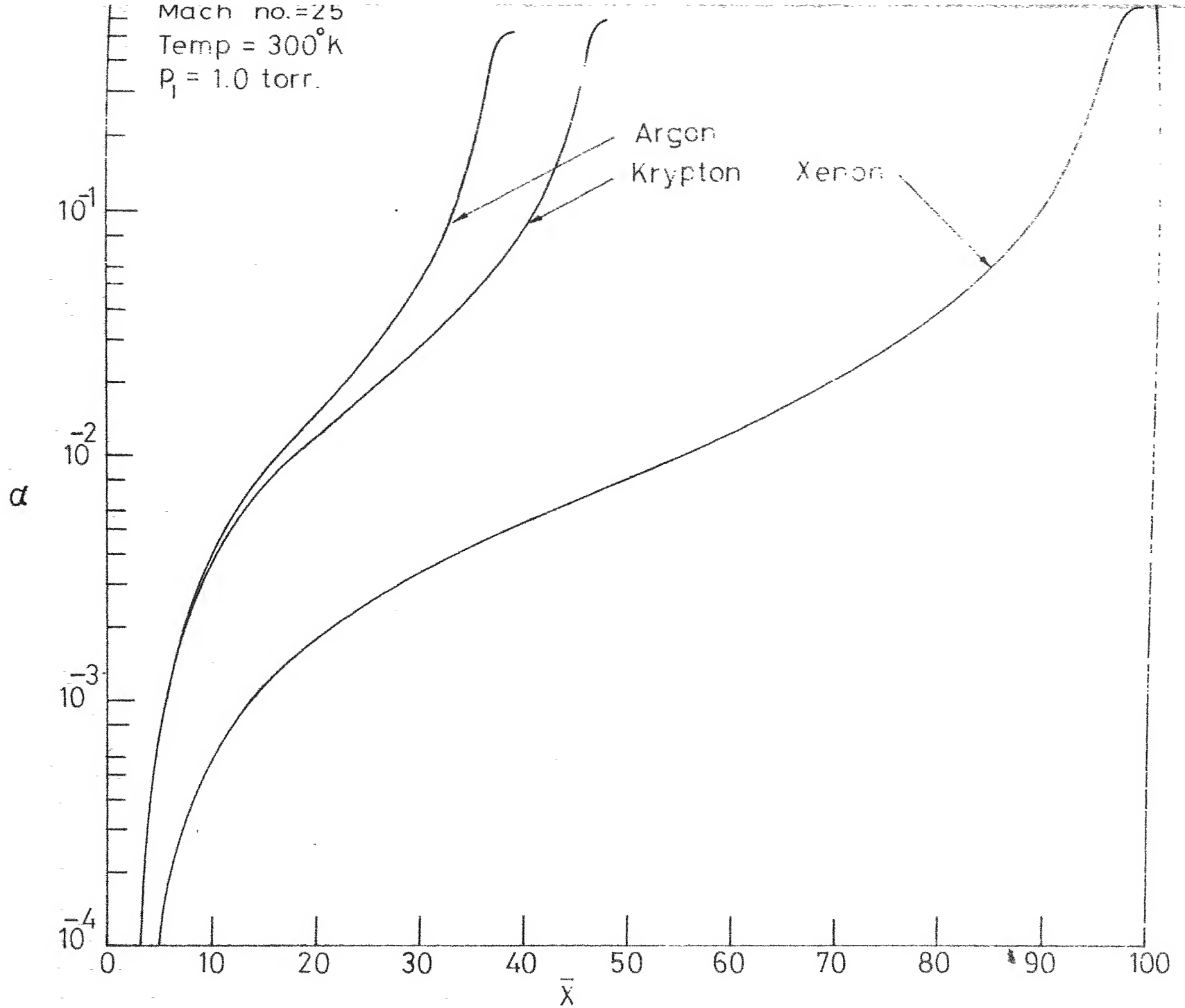

FIG.6.13.2.DEGREE OF IONIZATION

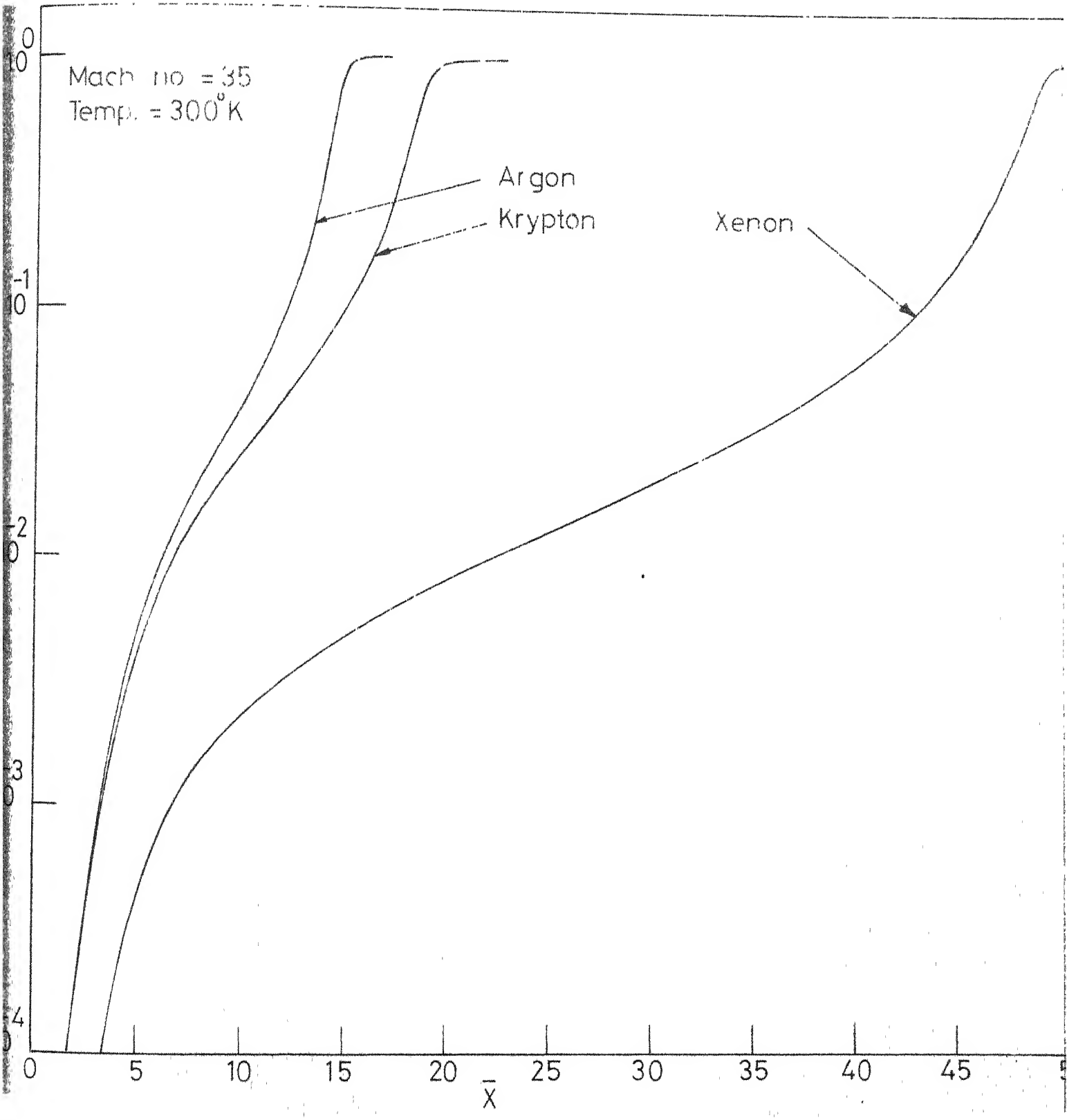

FIG.6.13.3 _ DEGREE OF IONIZATION PROFILES

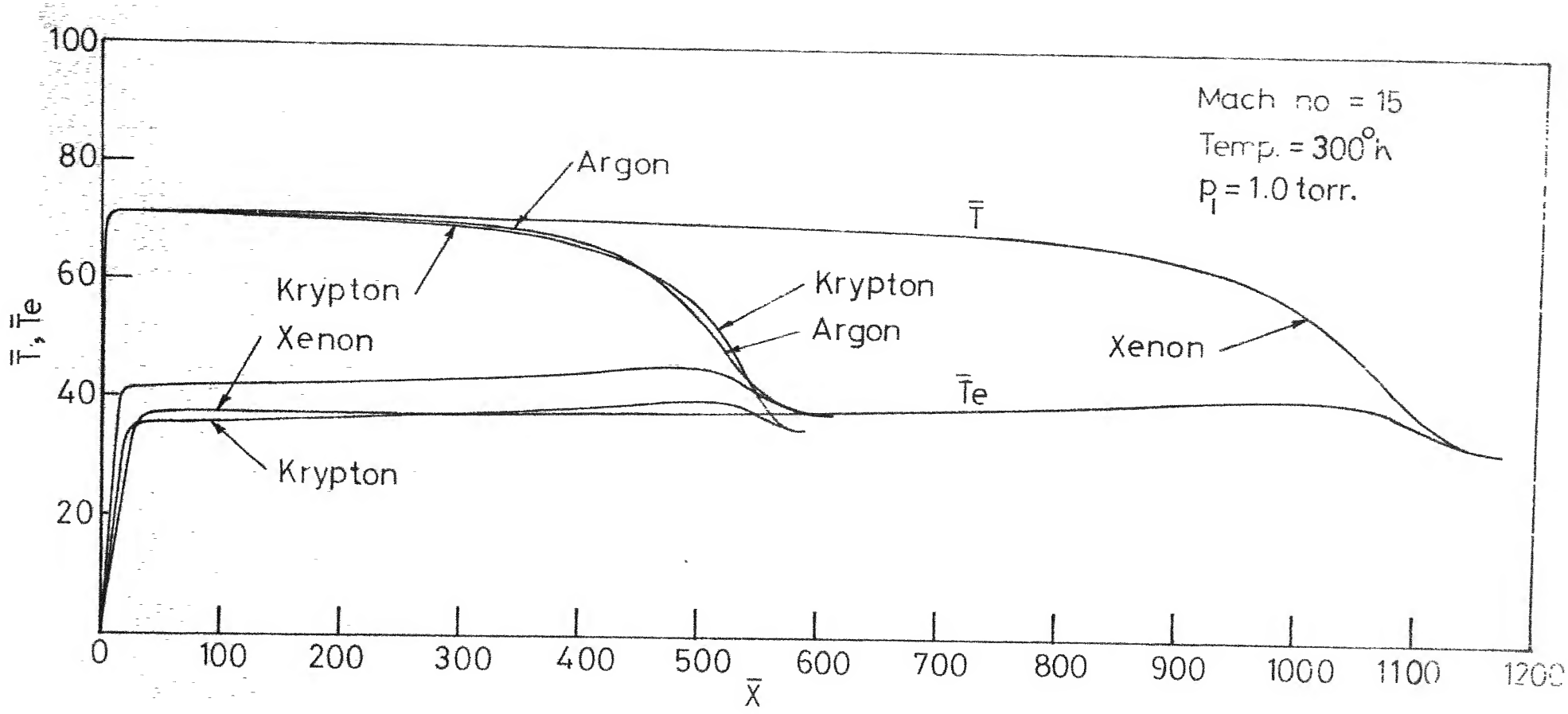

FIG. 6.14.1_TEMPERATURE PROFILES

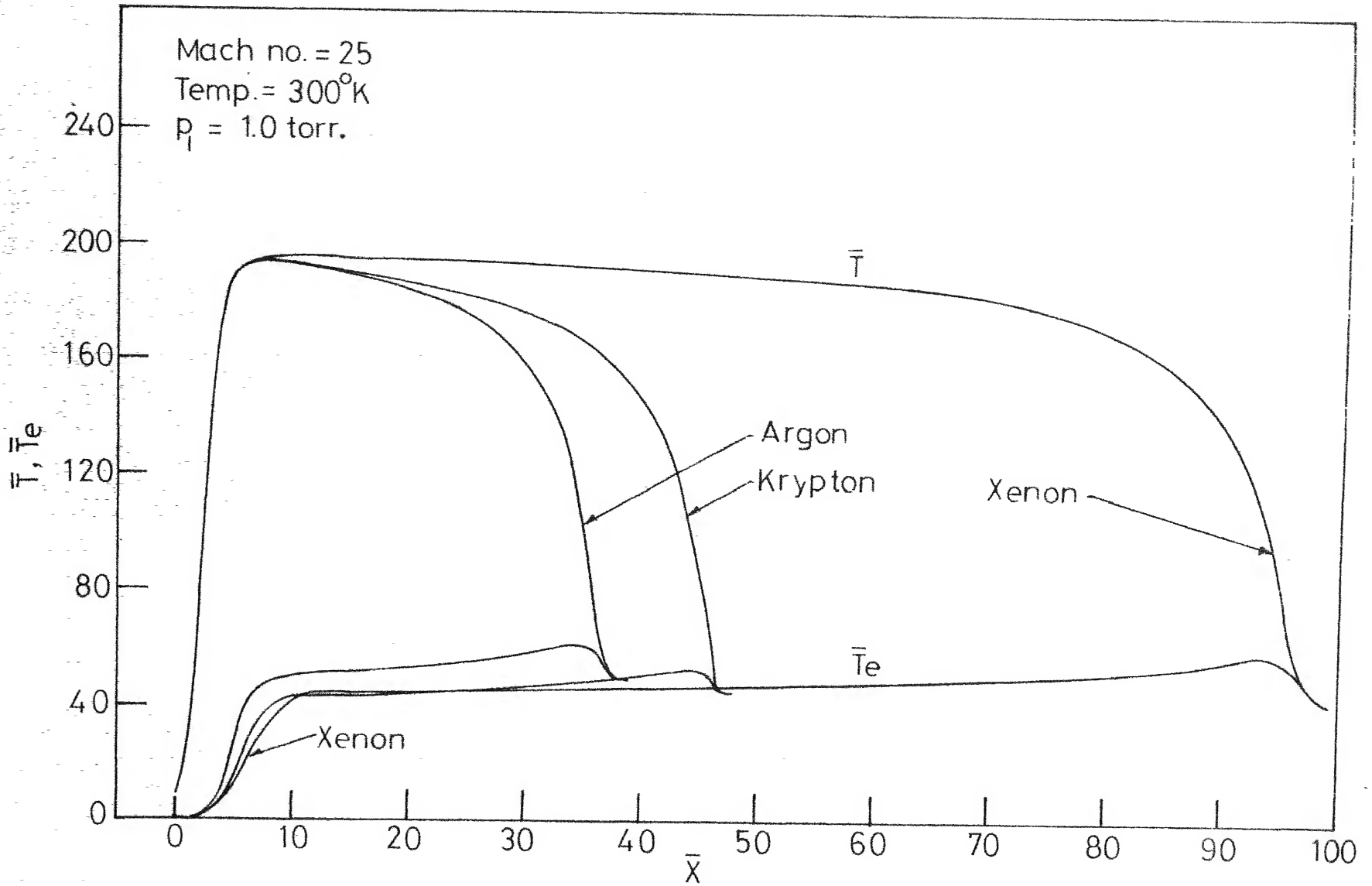

FIG 6.14.2_TEMPERATURE PROFILES

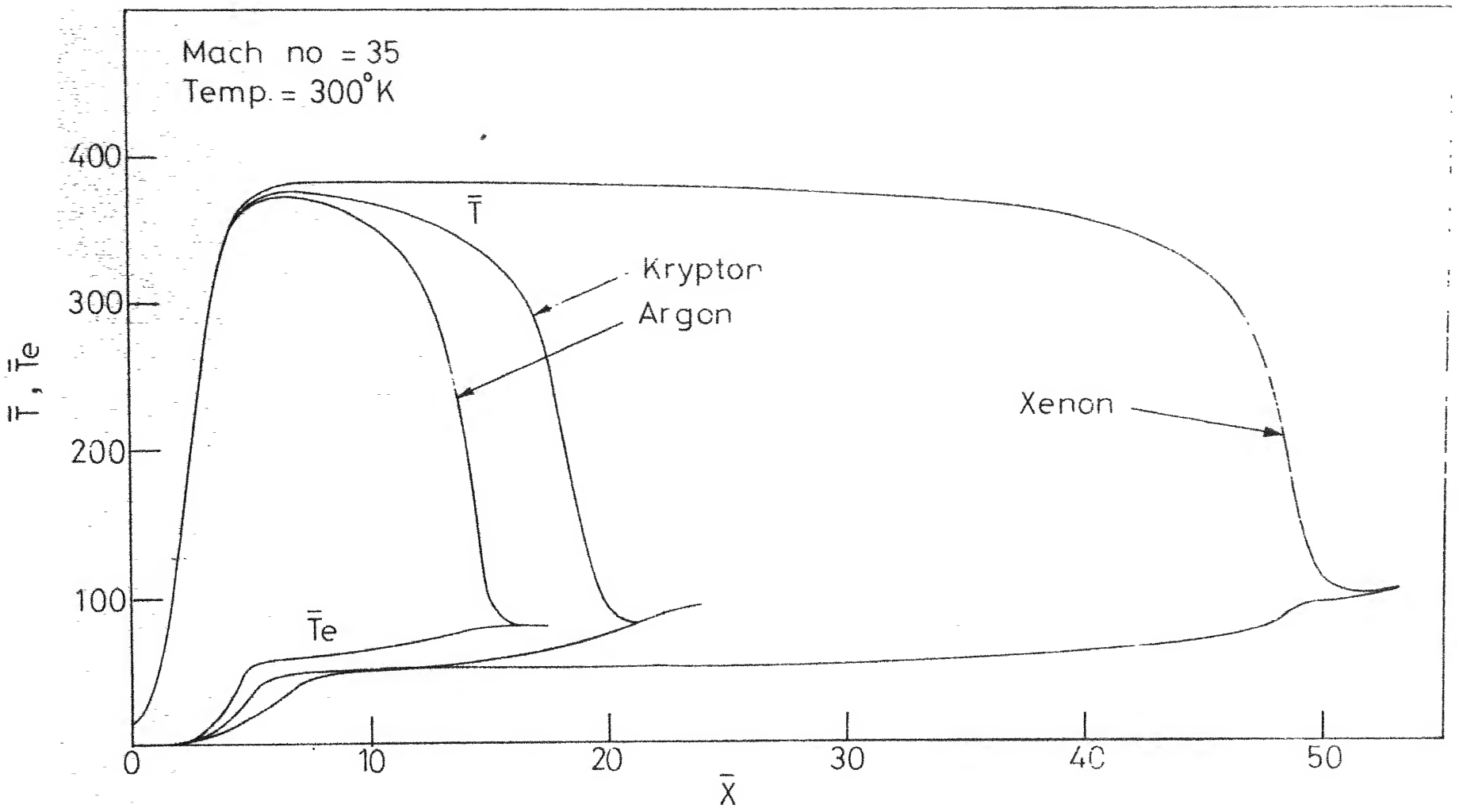

FIG. 6.14.3_TEMPERATURE PROFILES

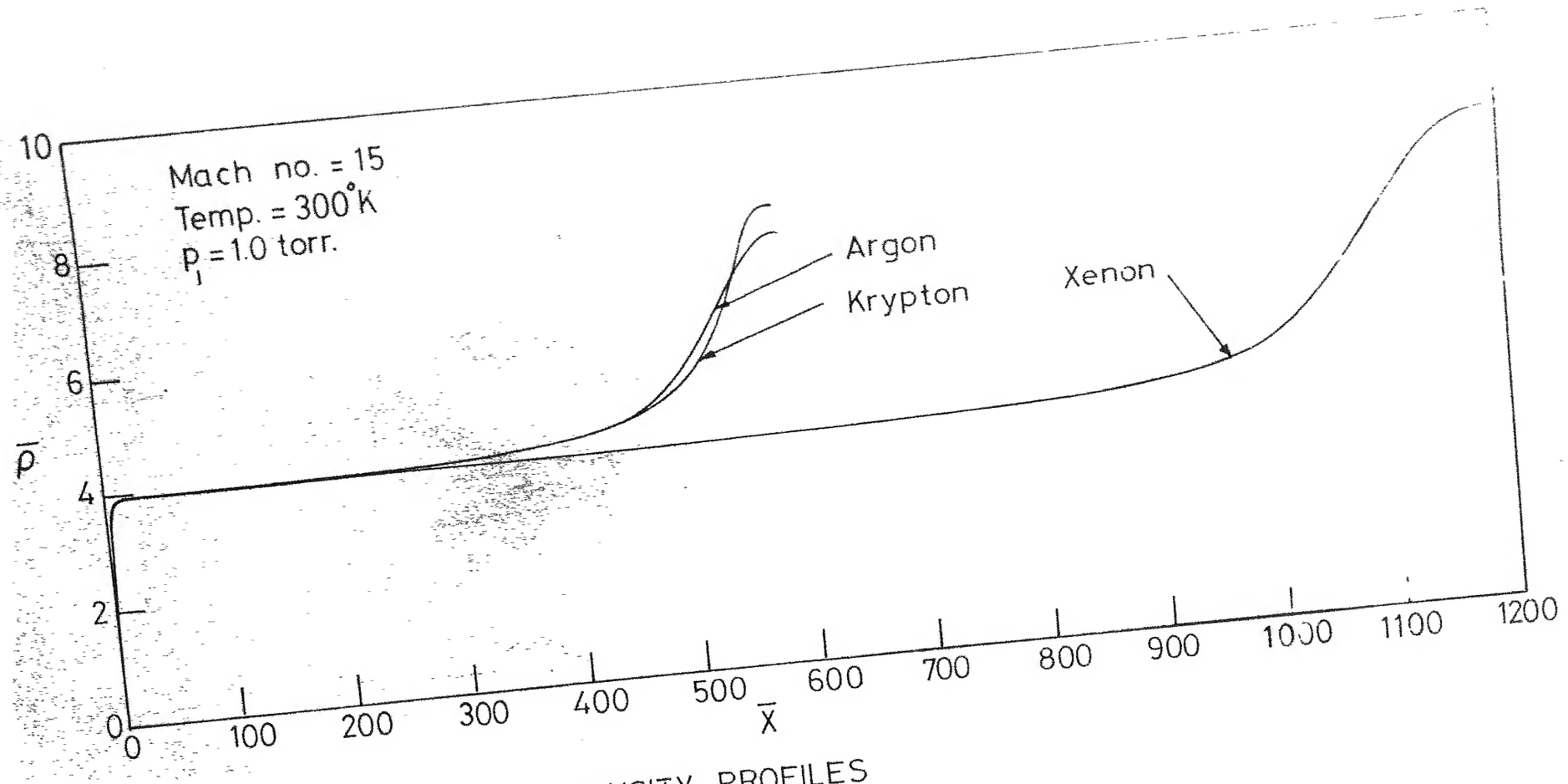

FIG.6.15.1_DENSITY PROFILES

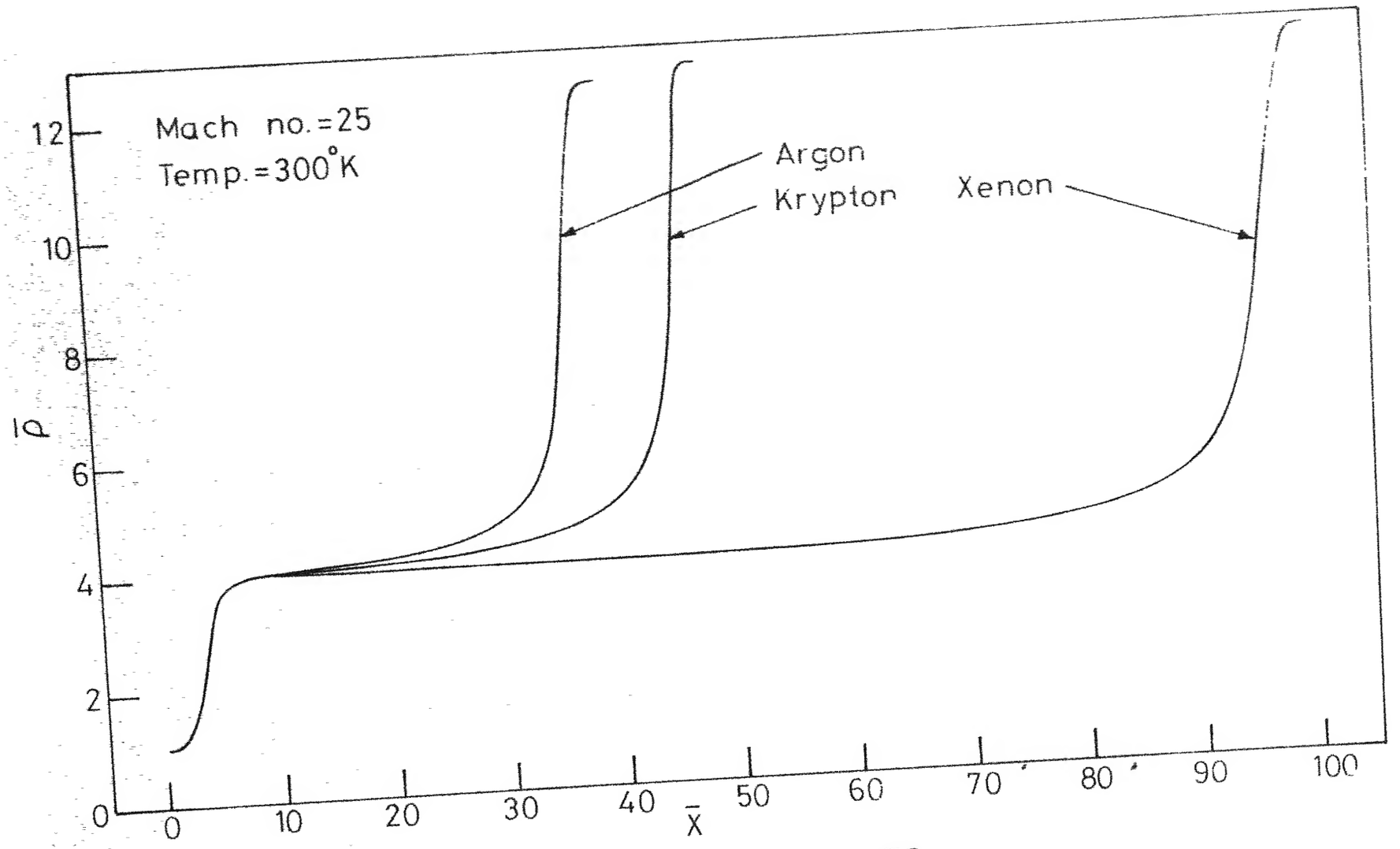

FIG. 6.15.2 _ DENSITY PROFILES

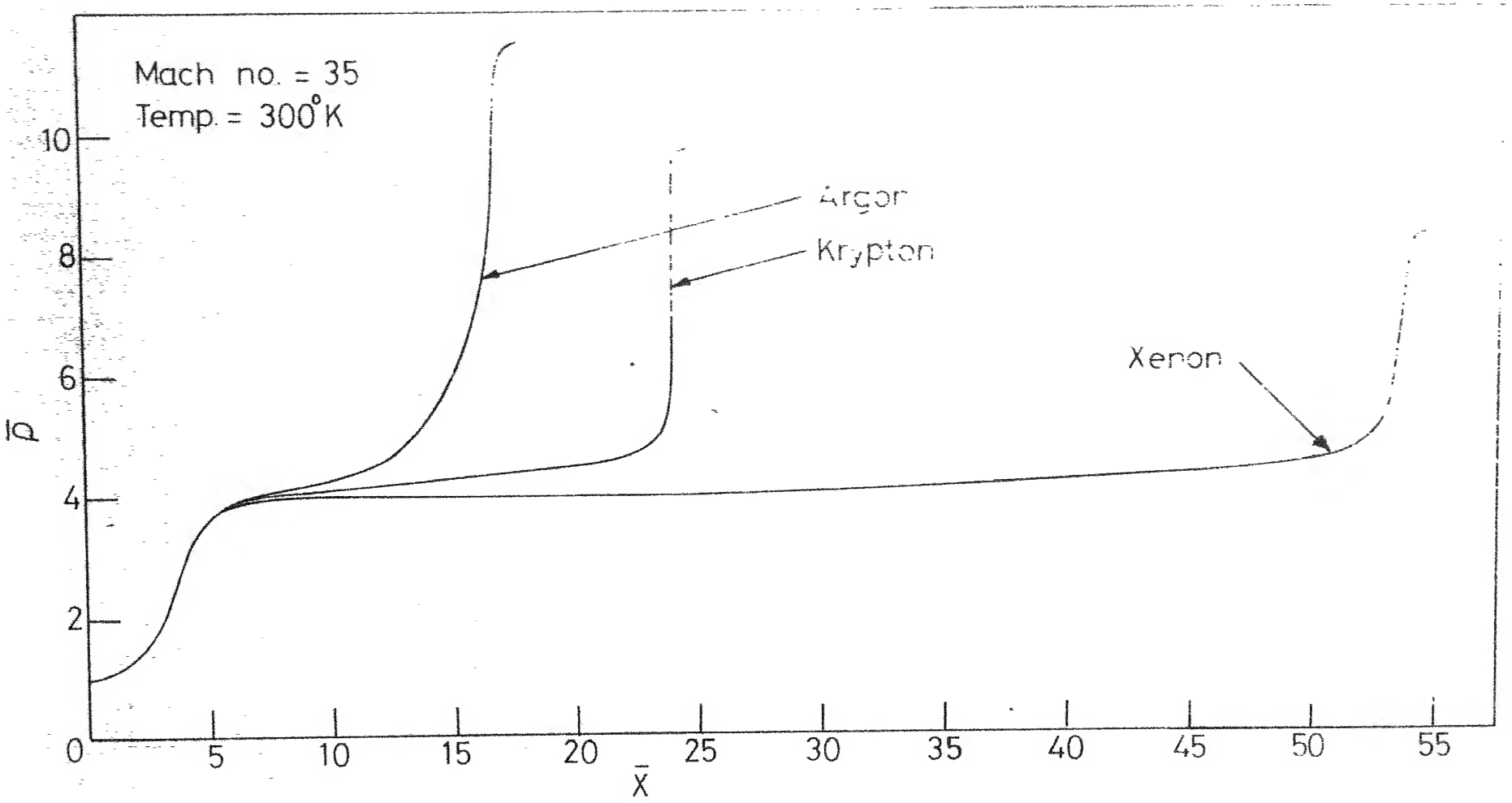

FIG. 6.15.3 _ DENSITY PROFILES

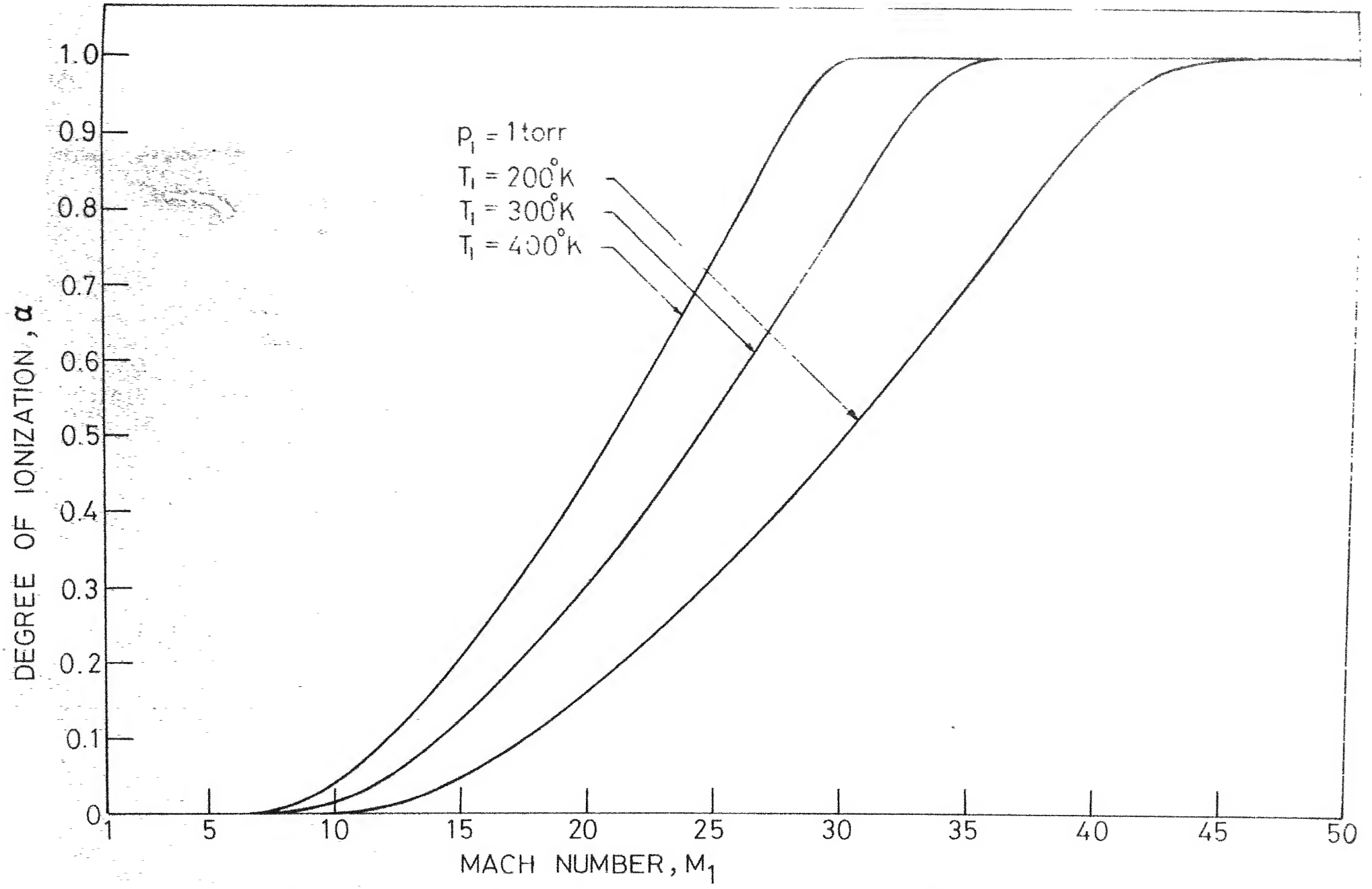

FIG. 6.16.1_EQUILIBRIUM DEGREE OF IONIZATION Vs MACH NUMBER FOR ARGON

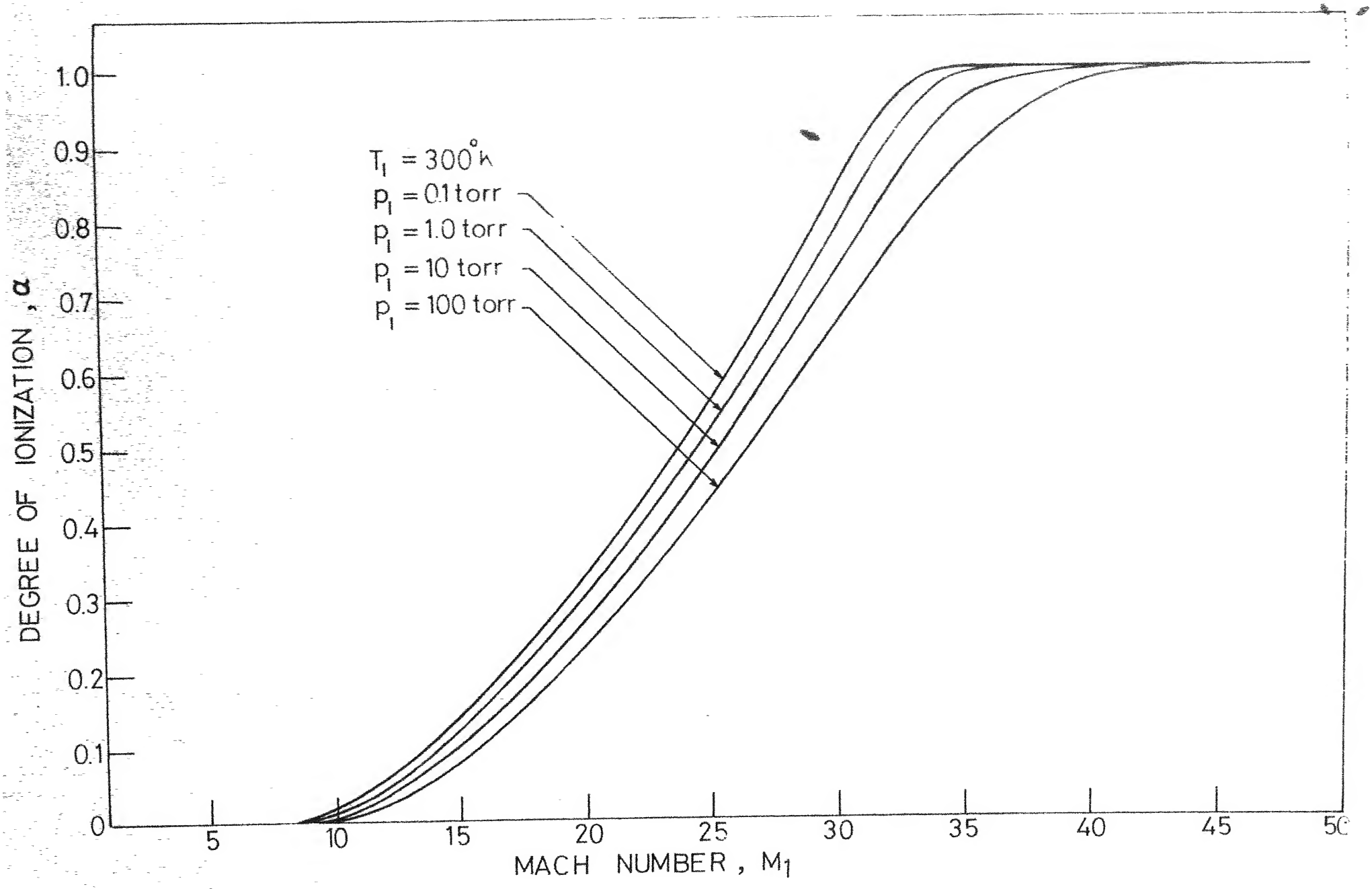

FIG.6.17.1_EQUILIBRIUM DEGREE OF IONIZATION Vs MACH NUMBER FOR ARGON

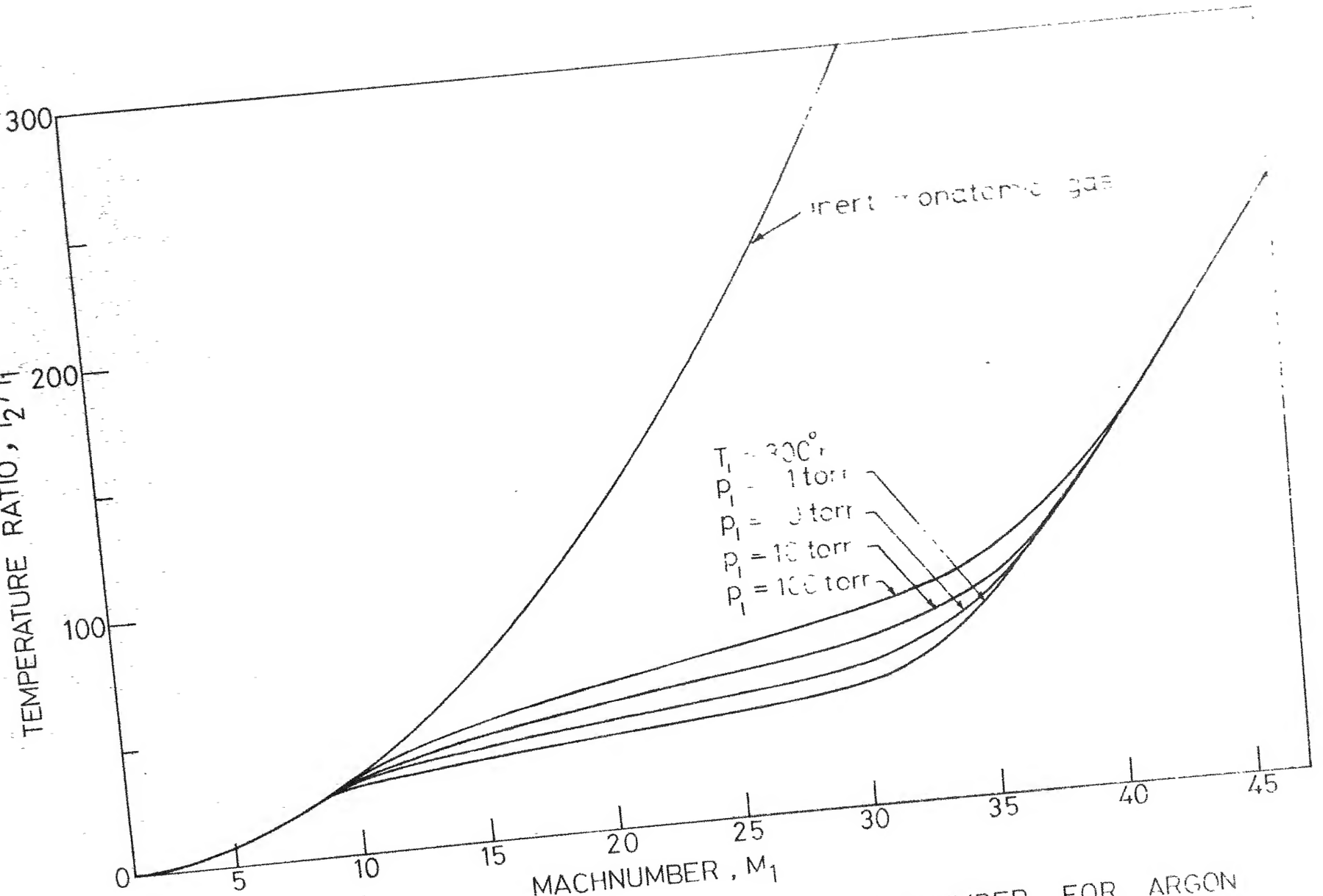

FIG.6.18.1_EQUILIBRIUM TEMPERATURE RATIO Vs MACHNUMBER FOR ARGON

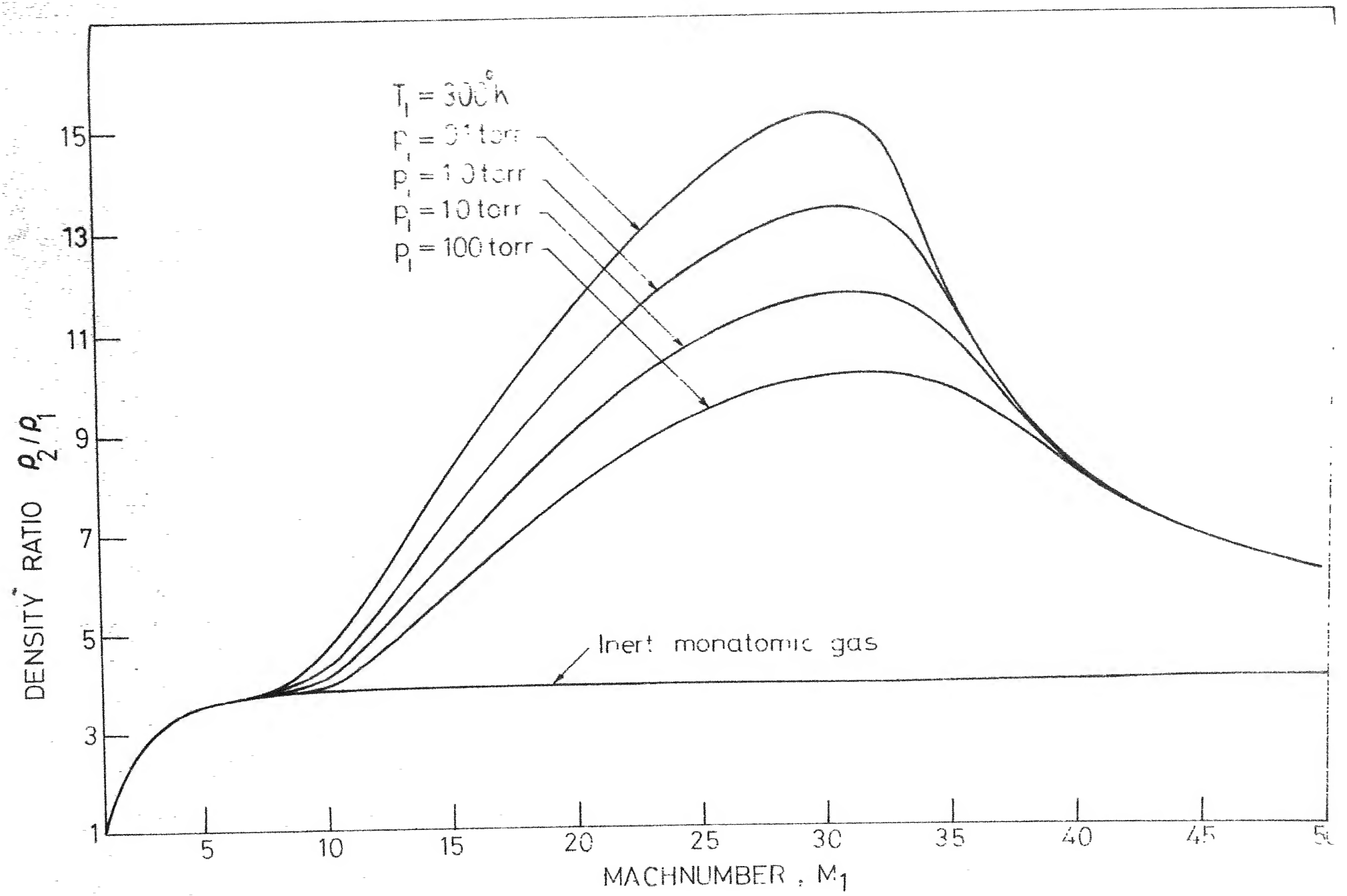

FIG. 6.19.1_EQUILIBRIUM DENSITY RATIO Vs MACHNUMBER FOR ARGON

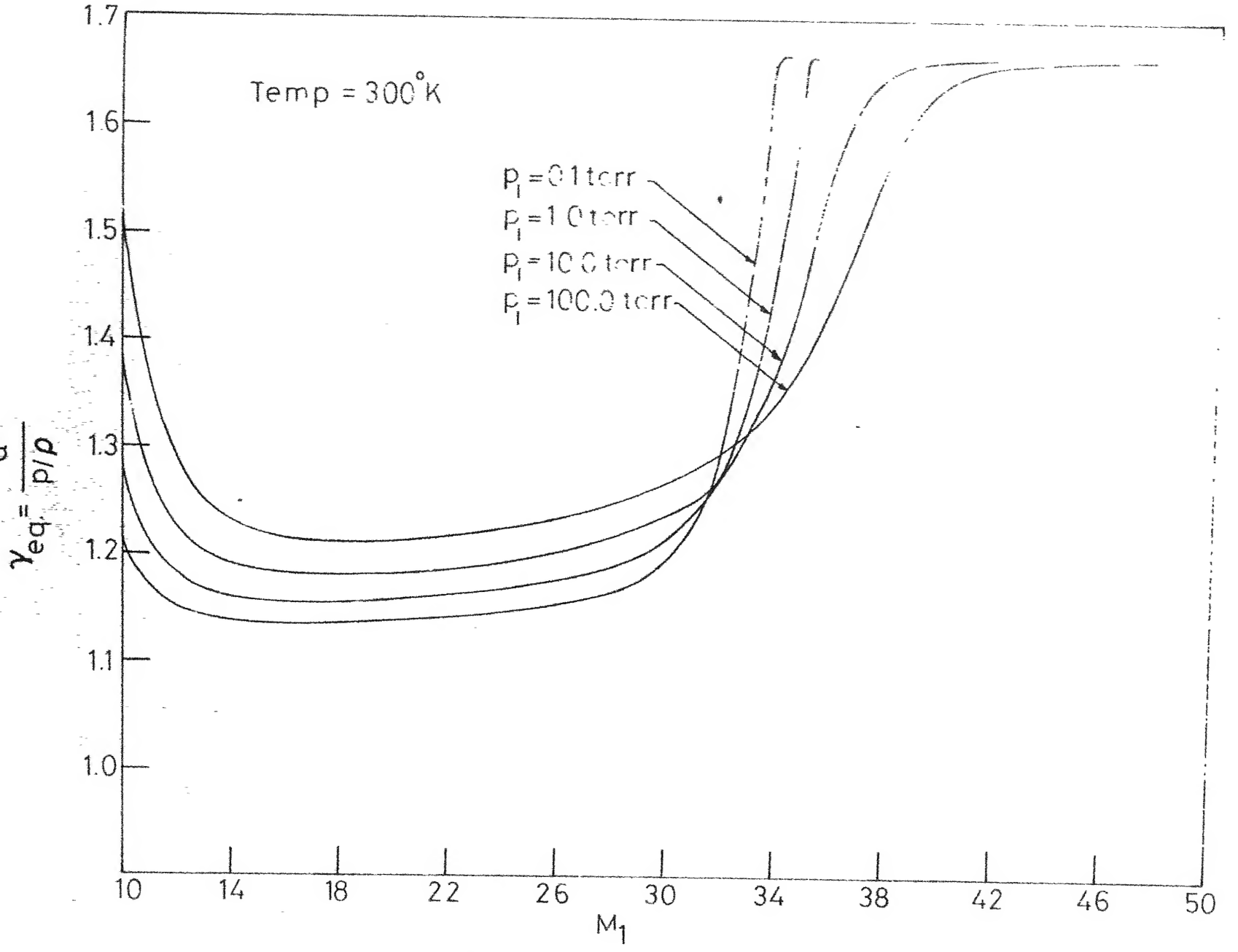

FIG. 6.20.1_EQIVALENT γ Vs FREE STREAM MACH NUMBER FOR ARGON.

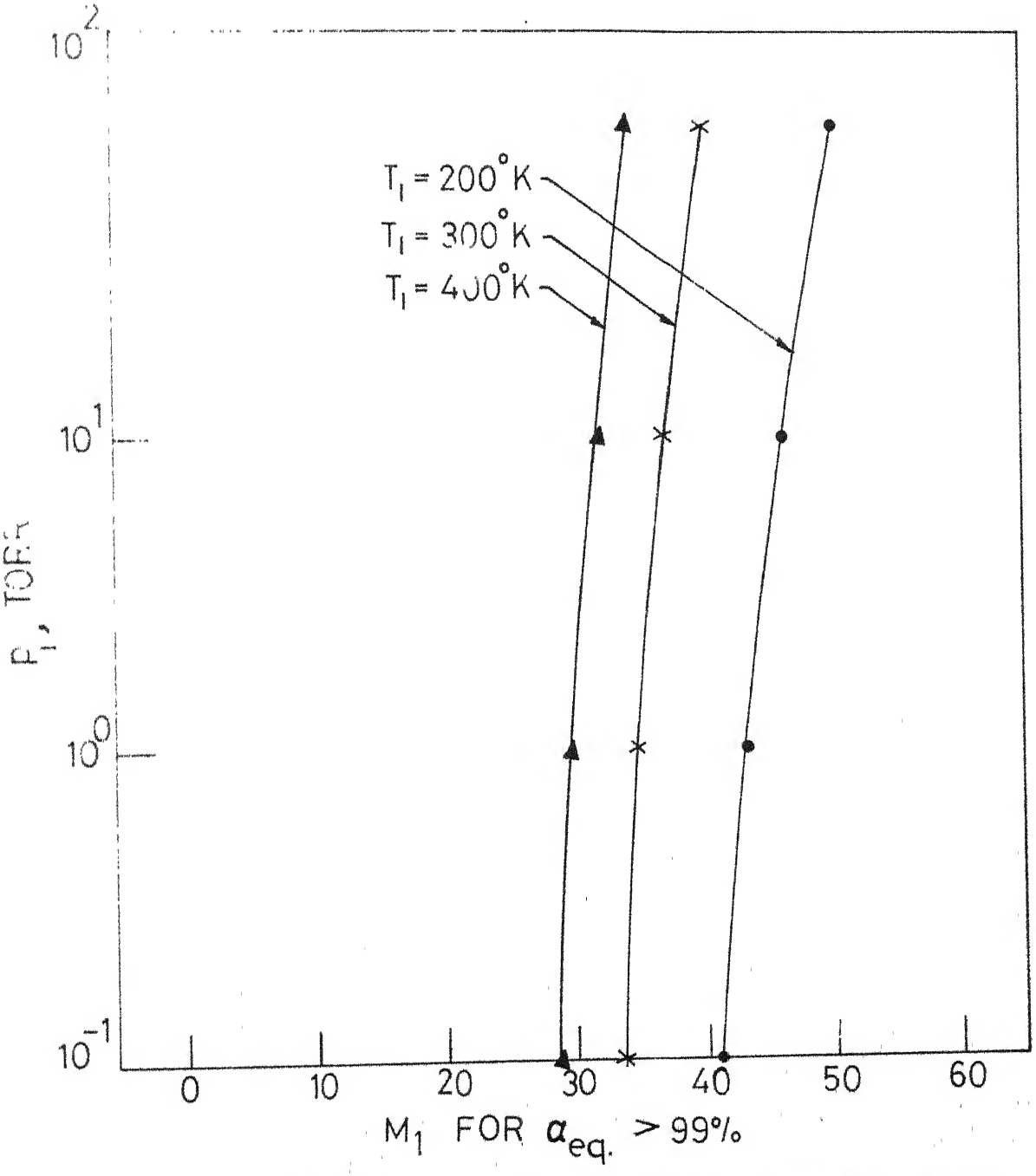

FIG. 6.21.1_FREE STEAM MACH NUMBER FOR $\alpha_{eq.} > 99\%$ Vs PRESSURE FOR ARGON

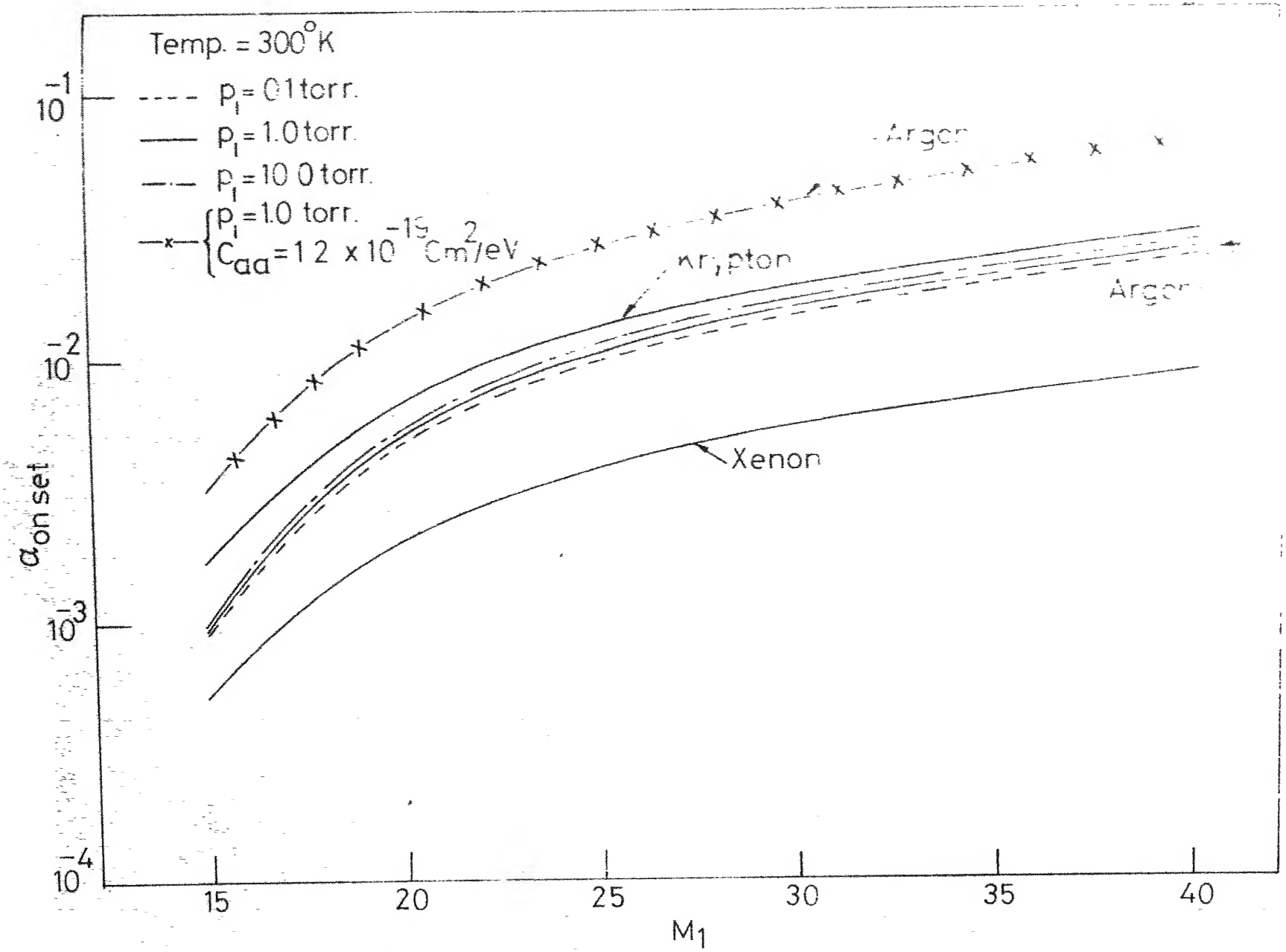

FIG.6.22.1_ONSET DEGREE OF IONIZATION Vs MACH NUMBER

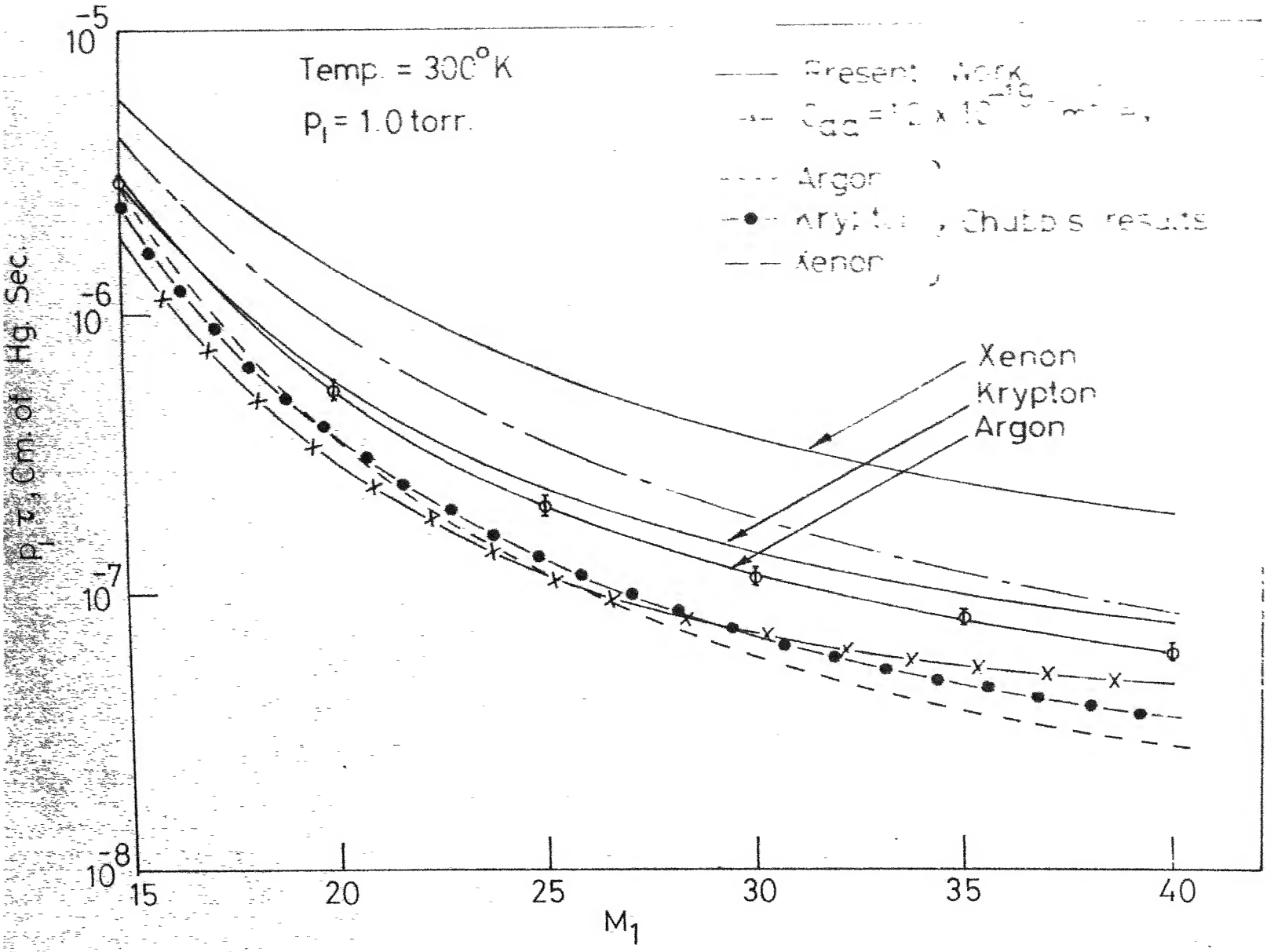

FIG. 6.23.1 _ THICKNESS PARAMETER Vs MACH NUMBER

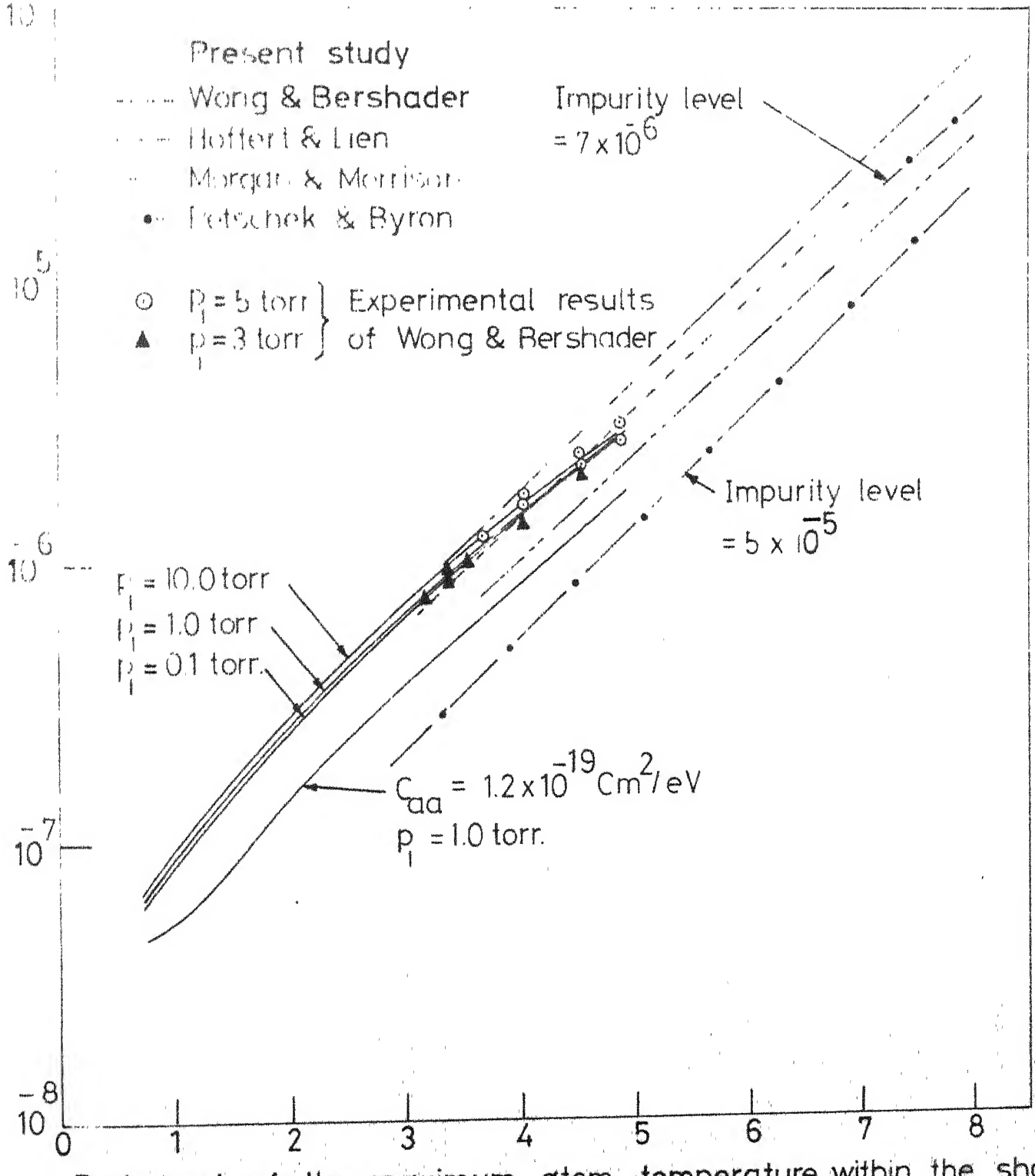

FIG. 6.24.1 – COMPARISON OF SHOCK THICKNESS PARAMETER FOR ARGON.

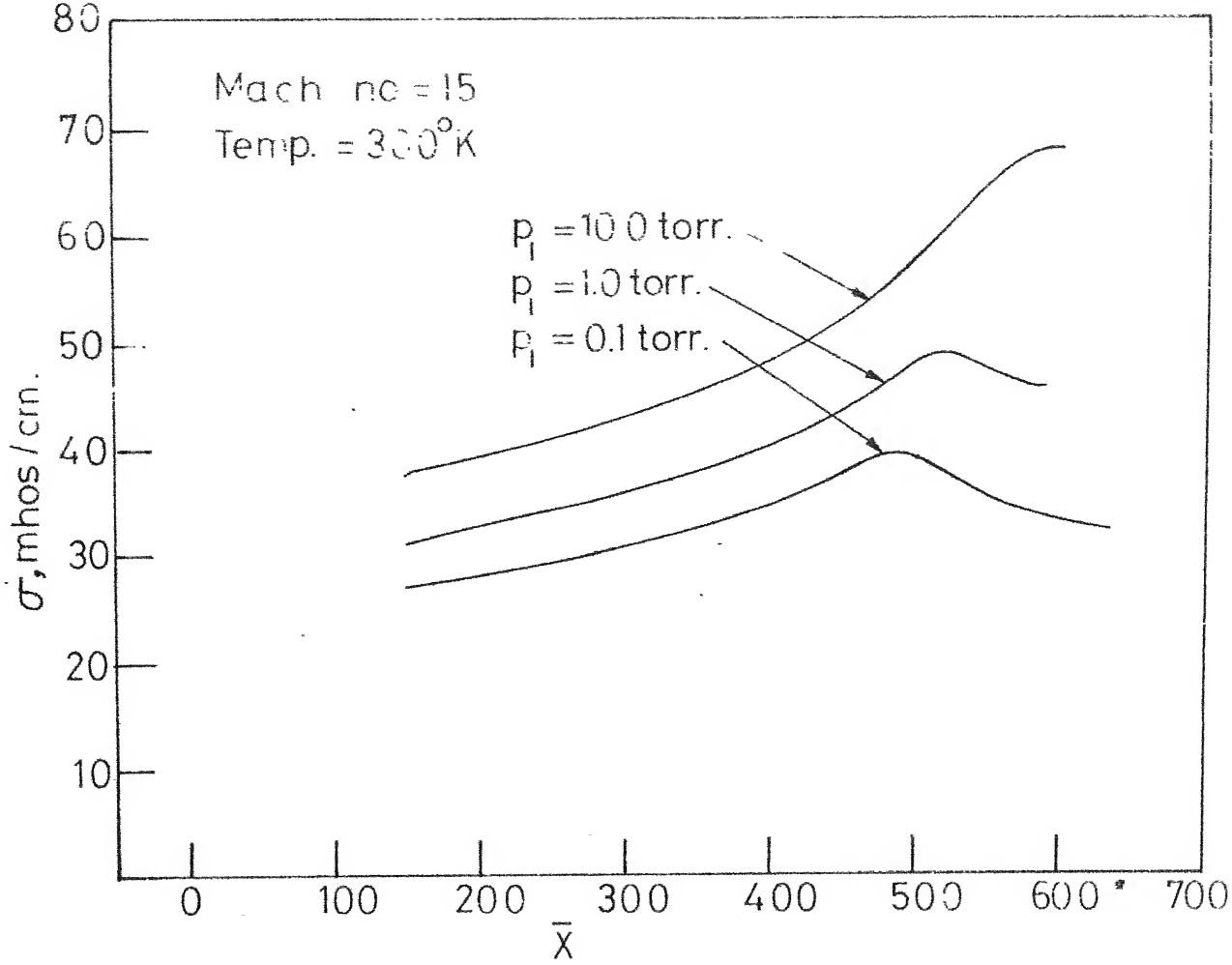

FIG. 6.4.1_ELECTRICAL CONDUCTIVITY PROFILES FOR ARGON

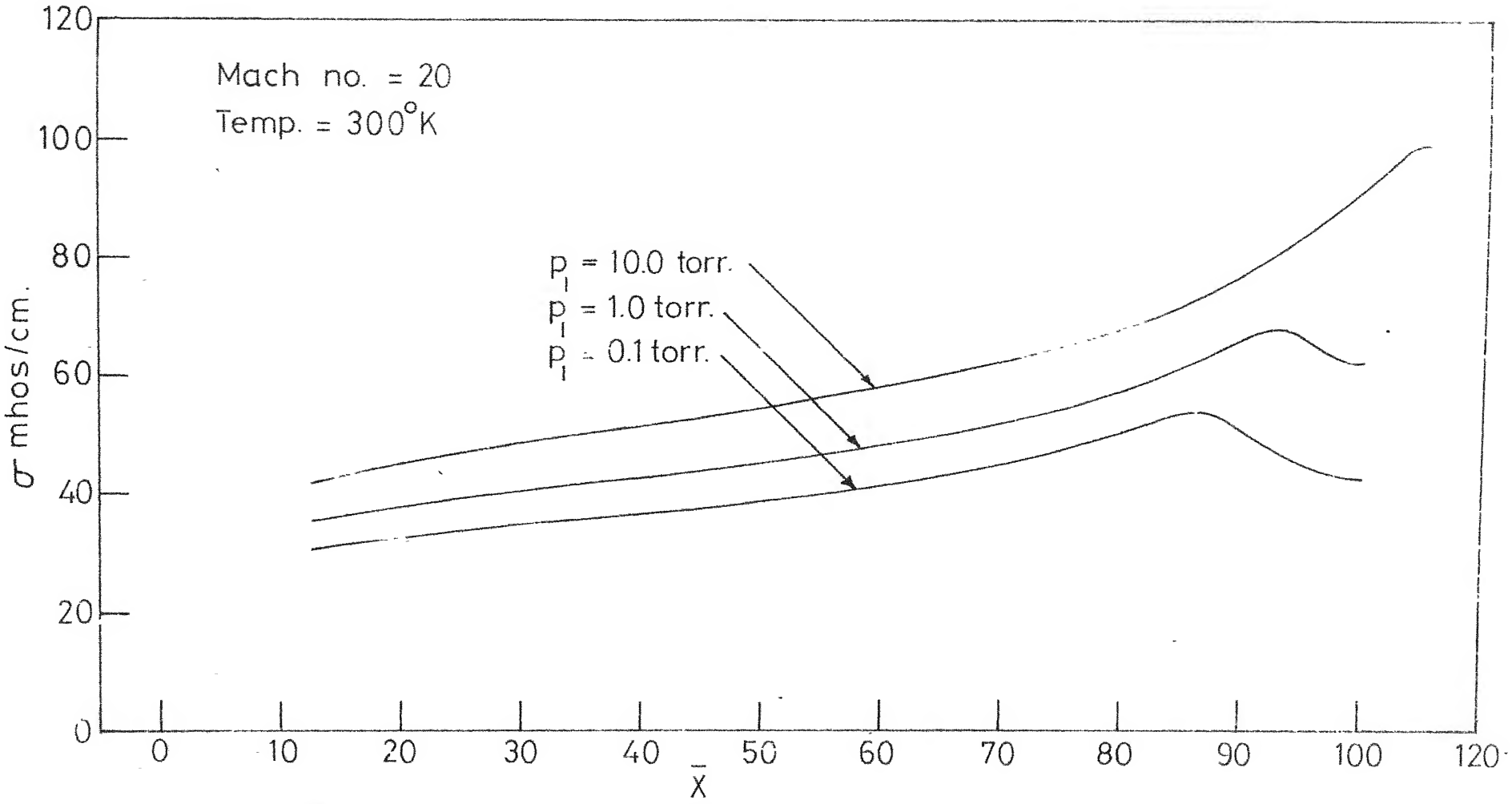

FIG.6.4.2 _ELECTRICAL CONDUCTIVITY PROFILES FOR ARGON

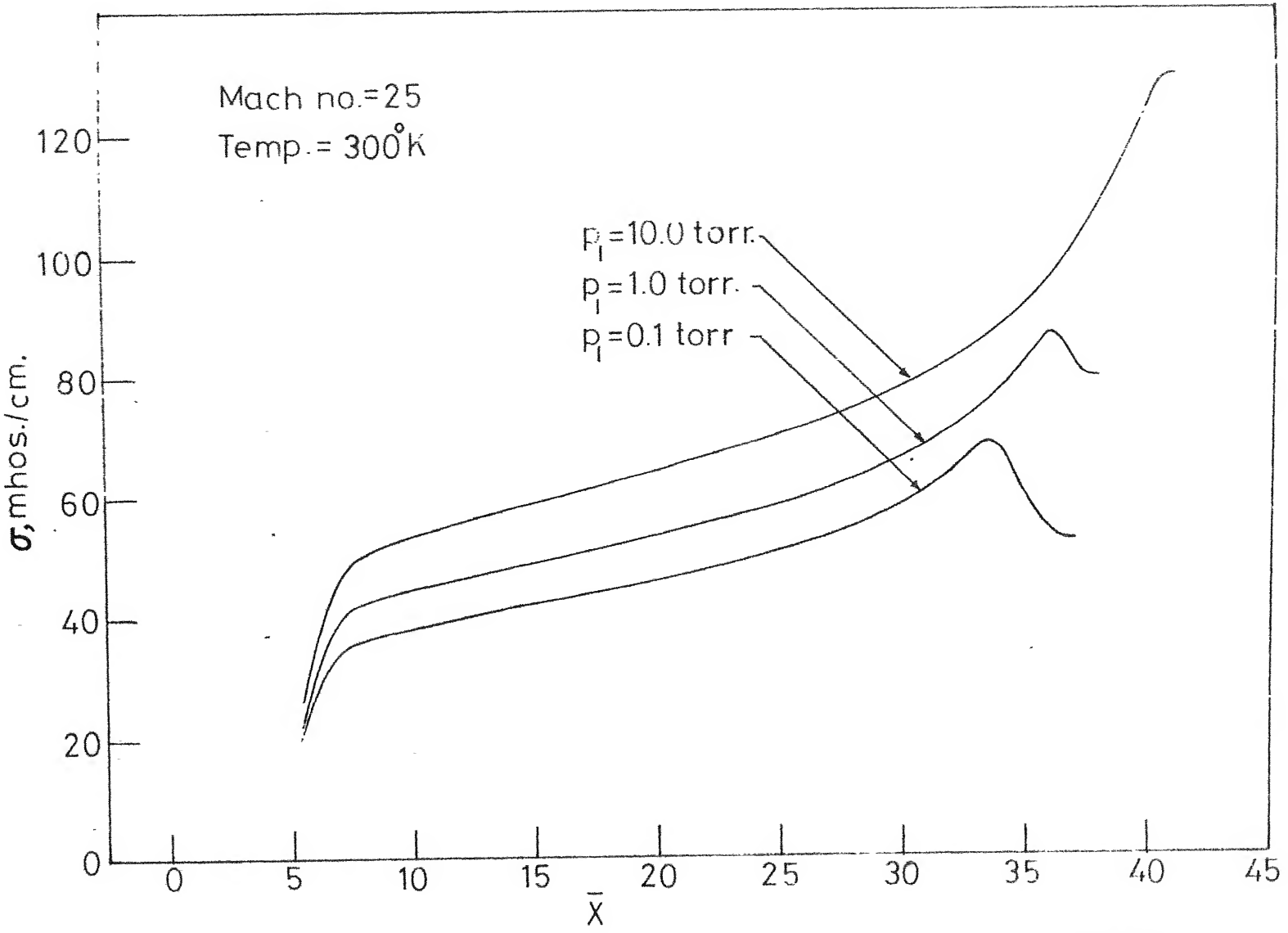

FIG.6.4.3. ELECTRICAL CONDUCTIVITY PROFILES FOR ARGON

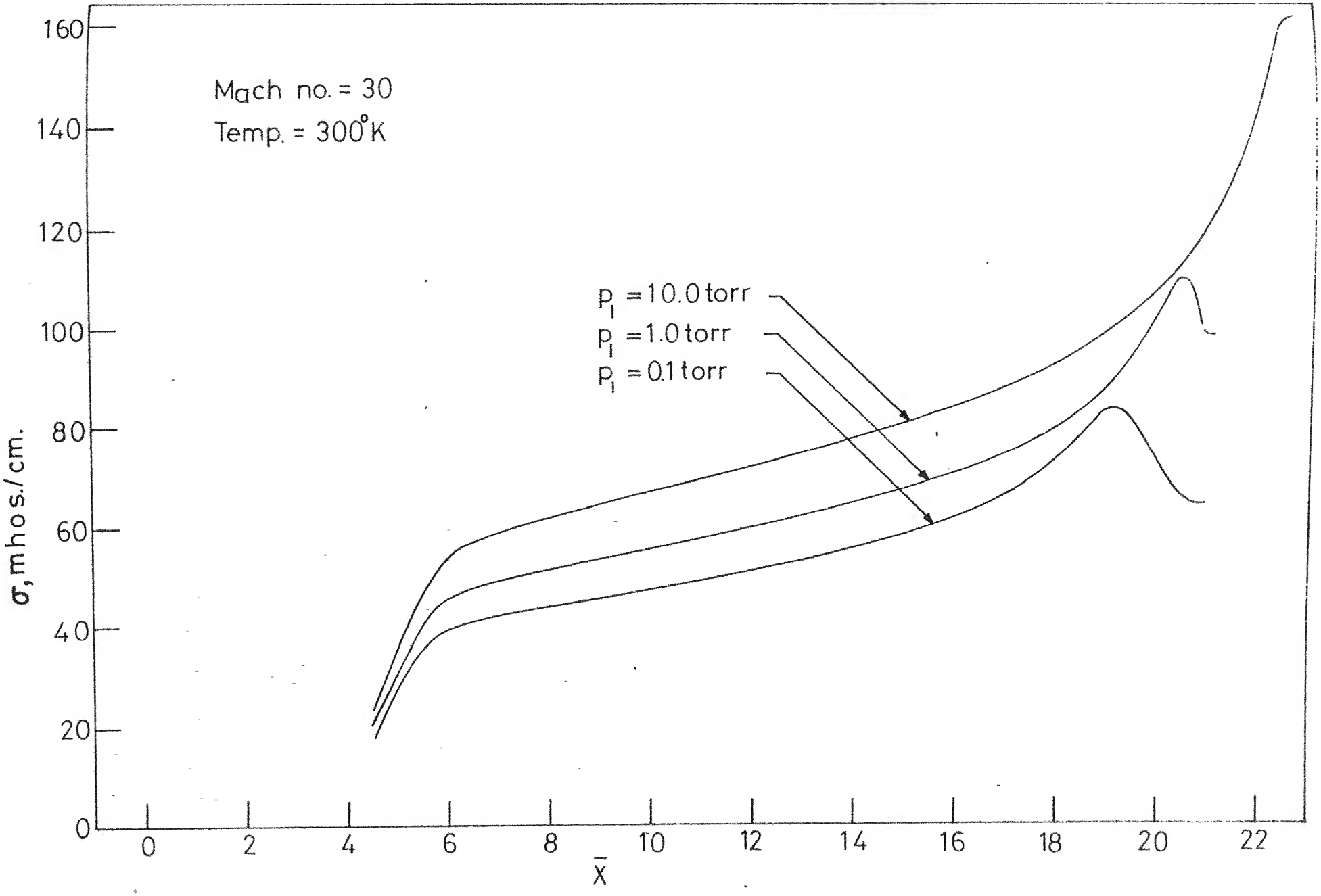

FIG.6.4.4.-ELECTRICAL CONDUCTIVITY PROFILES FOR ARGON

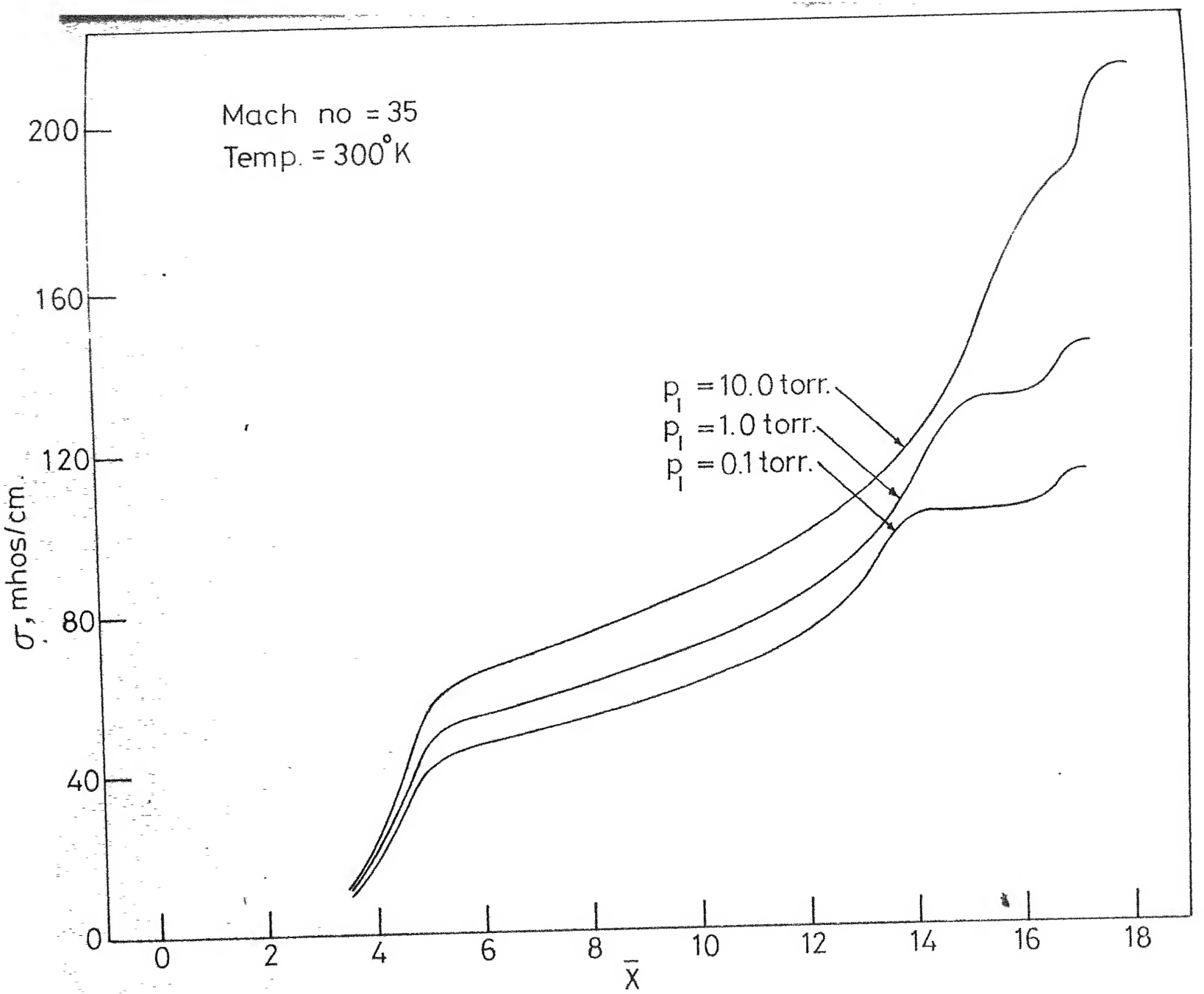

FIG.6.4.5_ELECTRICAL CONDUCTIVITY PROFILES FOR ARGON

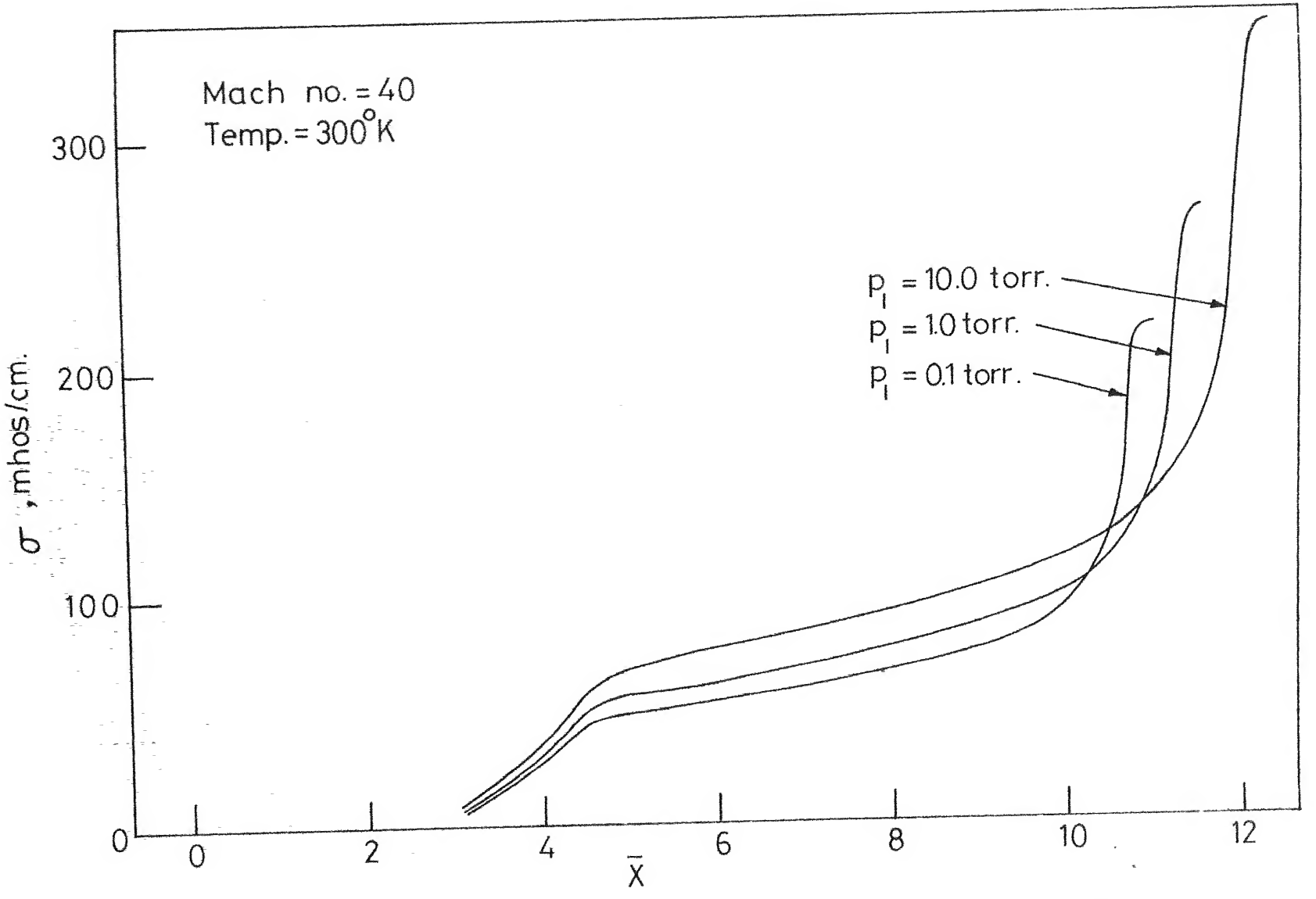

FIG.6.4.6_ELECTRICAL CONDUCTIVITY PROFILES FOR ARGON

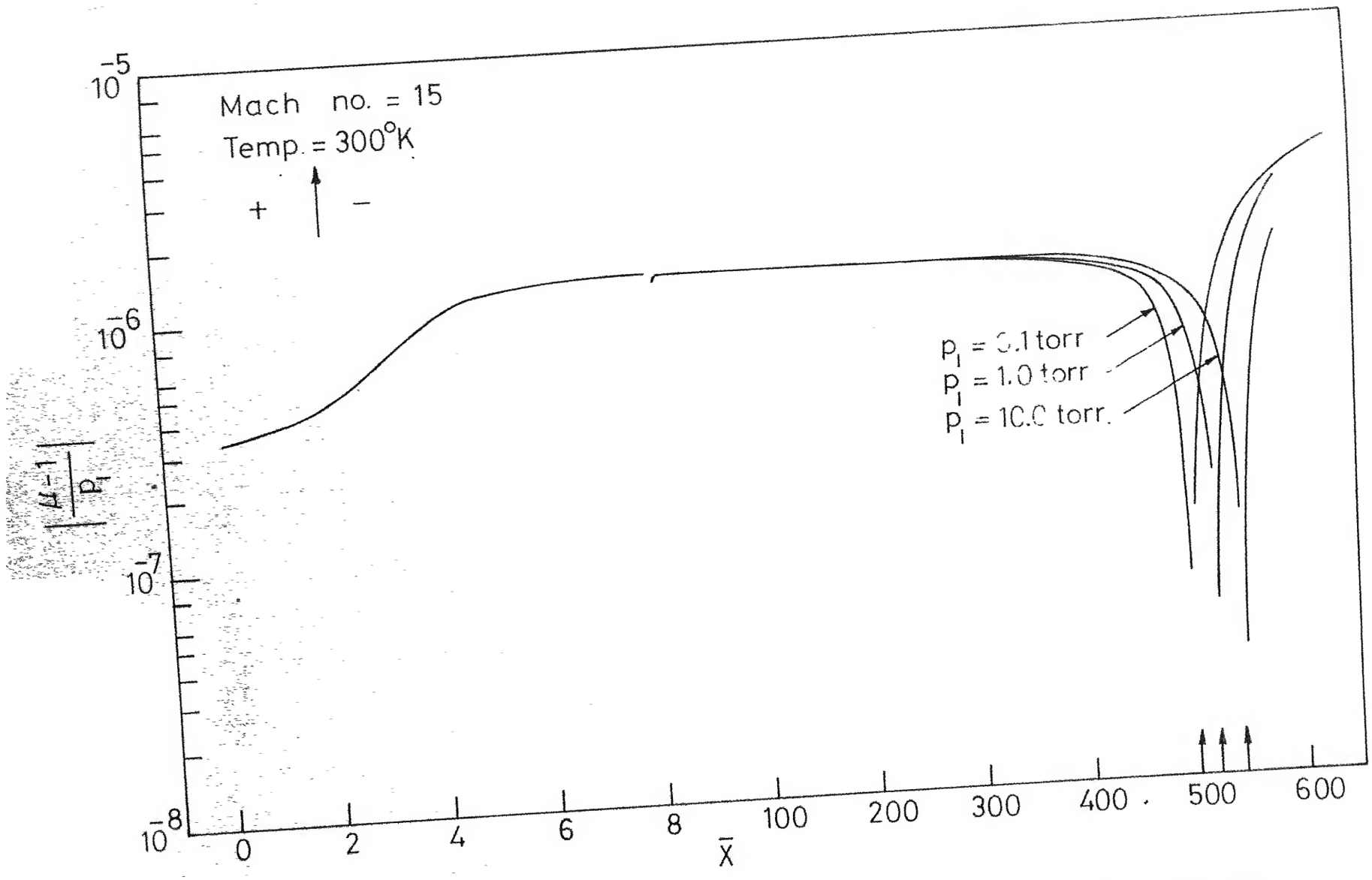

FIG.6.5.1_REFRACTIVE INDEX PROFILES FOR ARGON

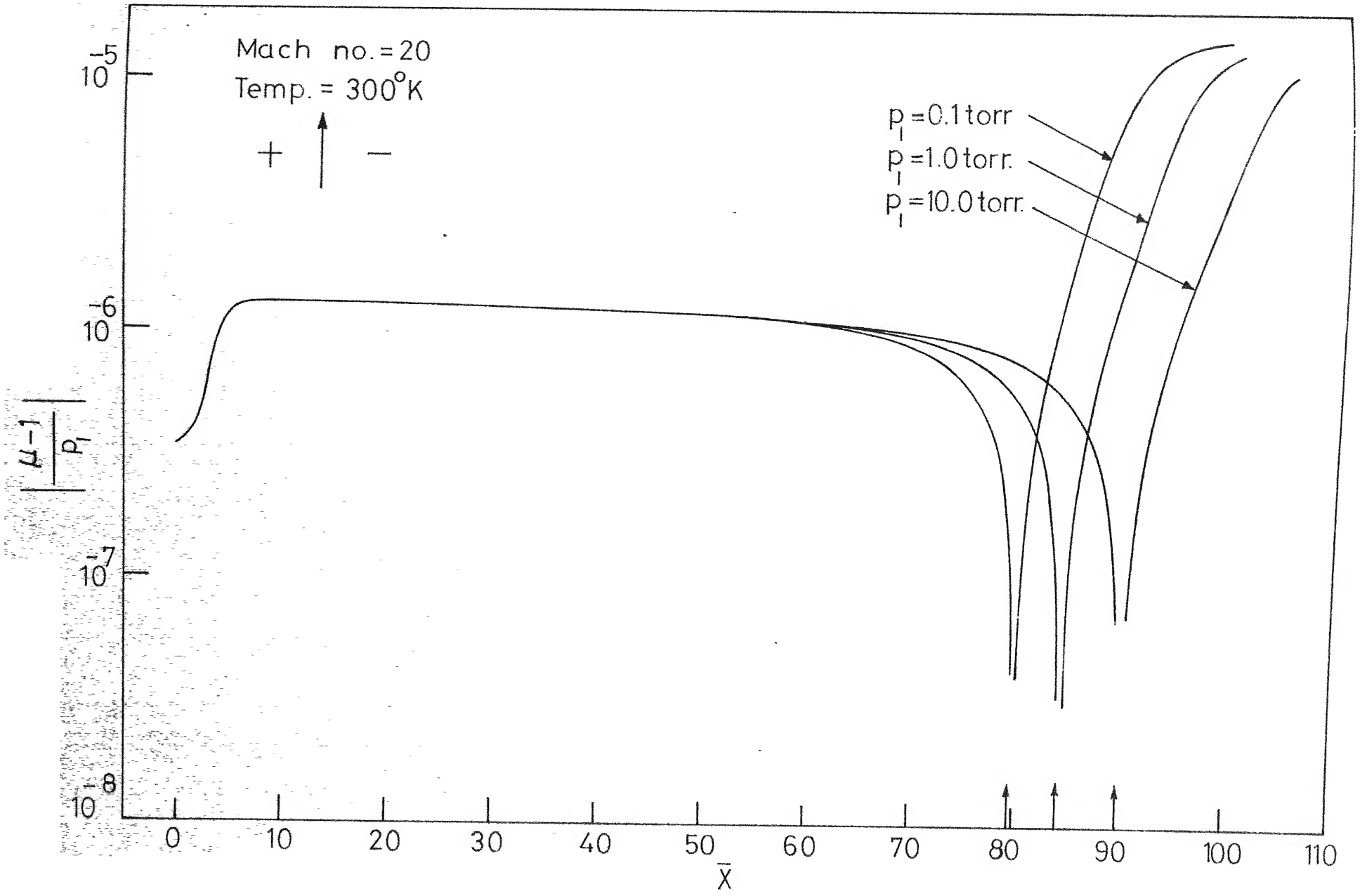

FIG. 6.5.2_REFRACTIVE INDEX PROFILES FOR ARGON

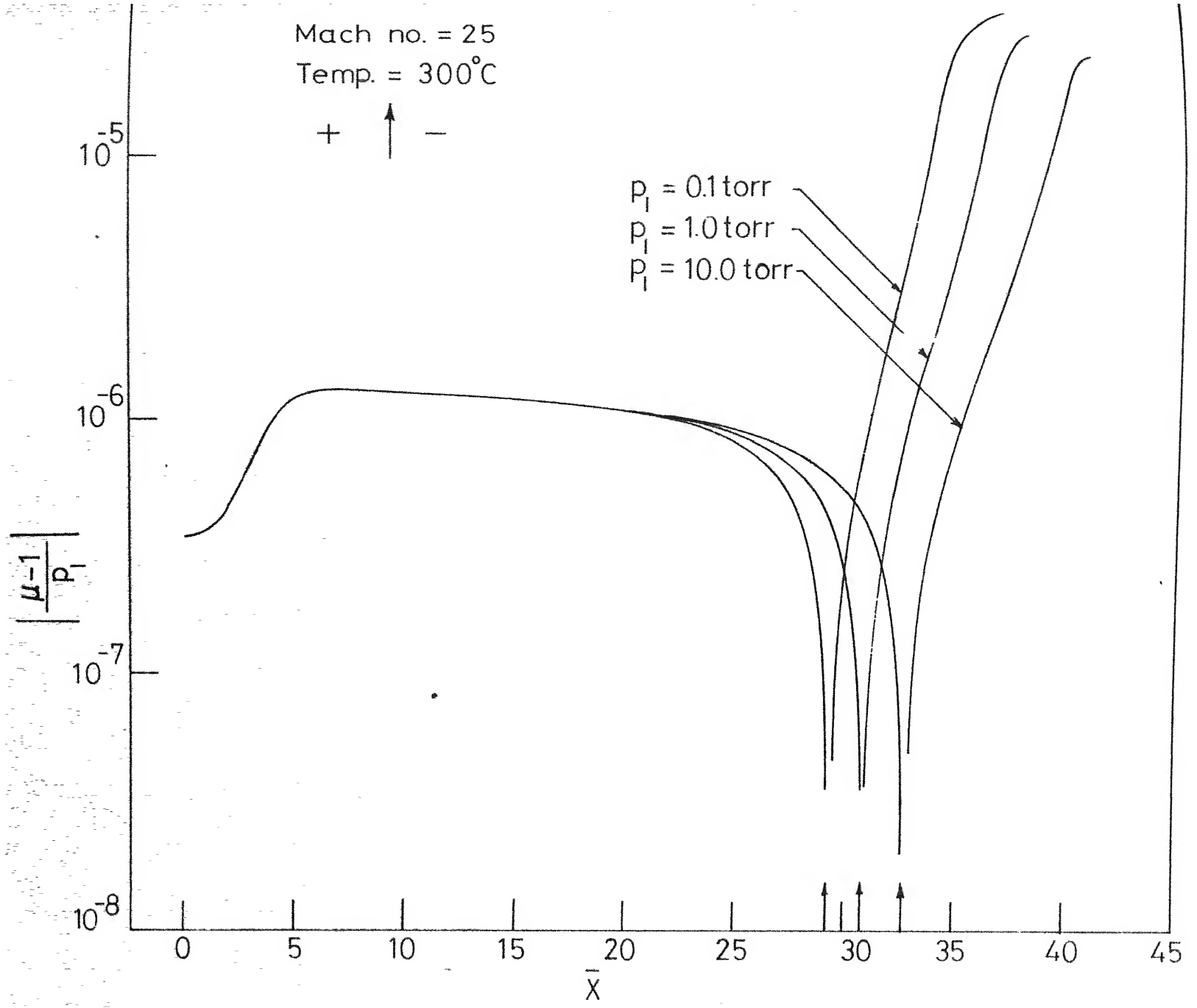

FIG. 6.5.3_REFRACTIVE INDEX PROFILES FOR ARGON

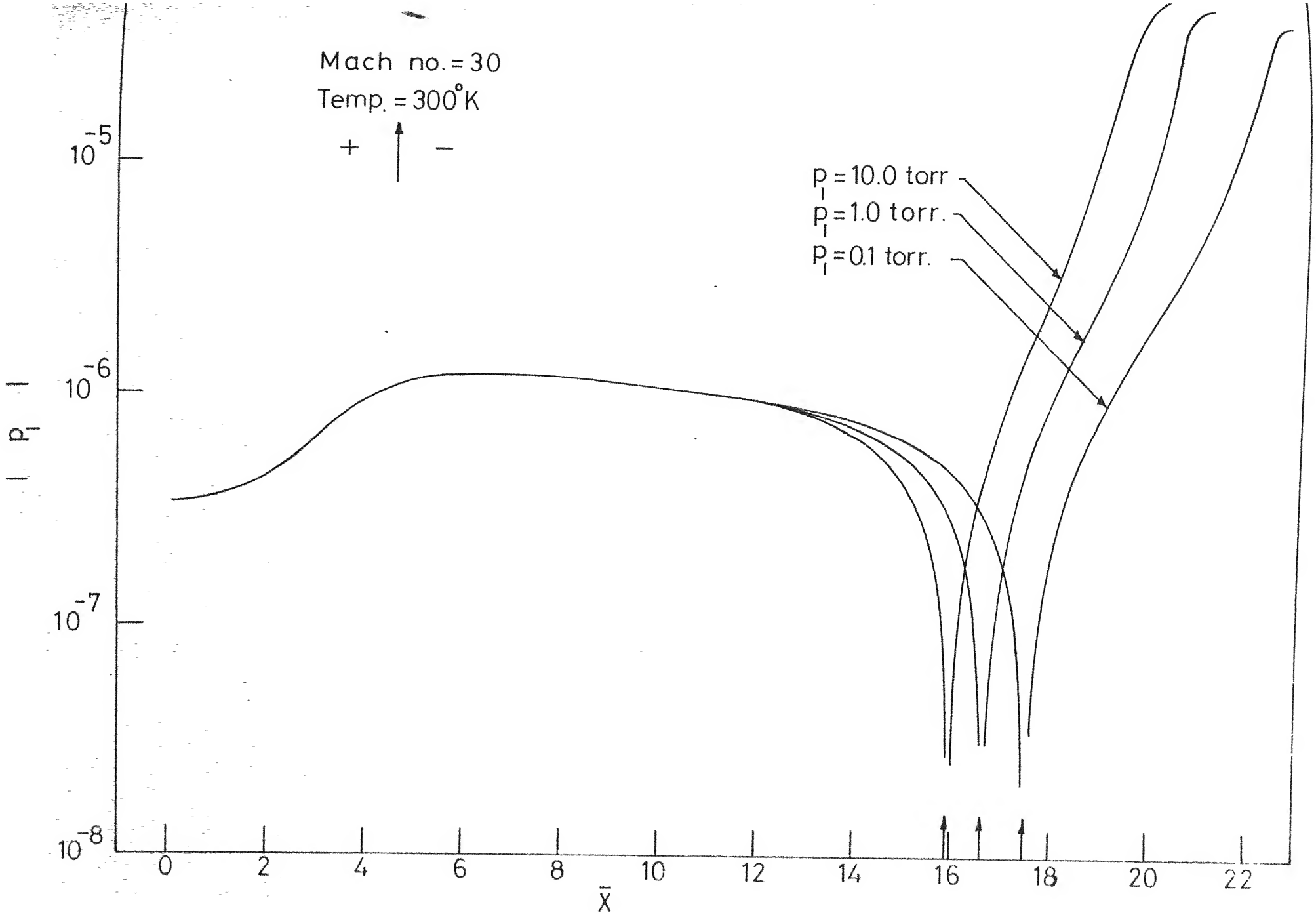

FIG. 6.5.4 – REFRACTIVE INDEX PROFILES FOR ARGON

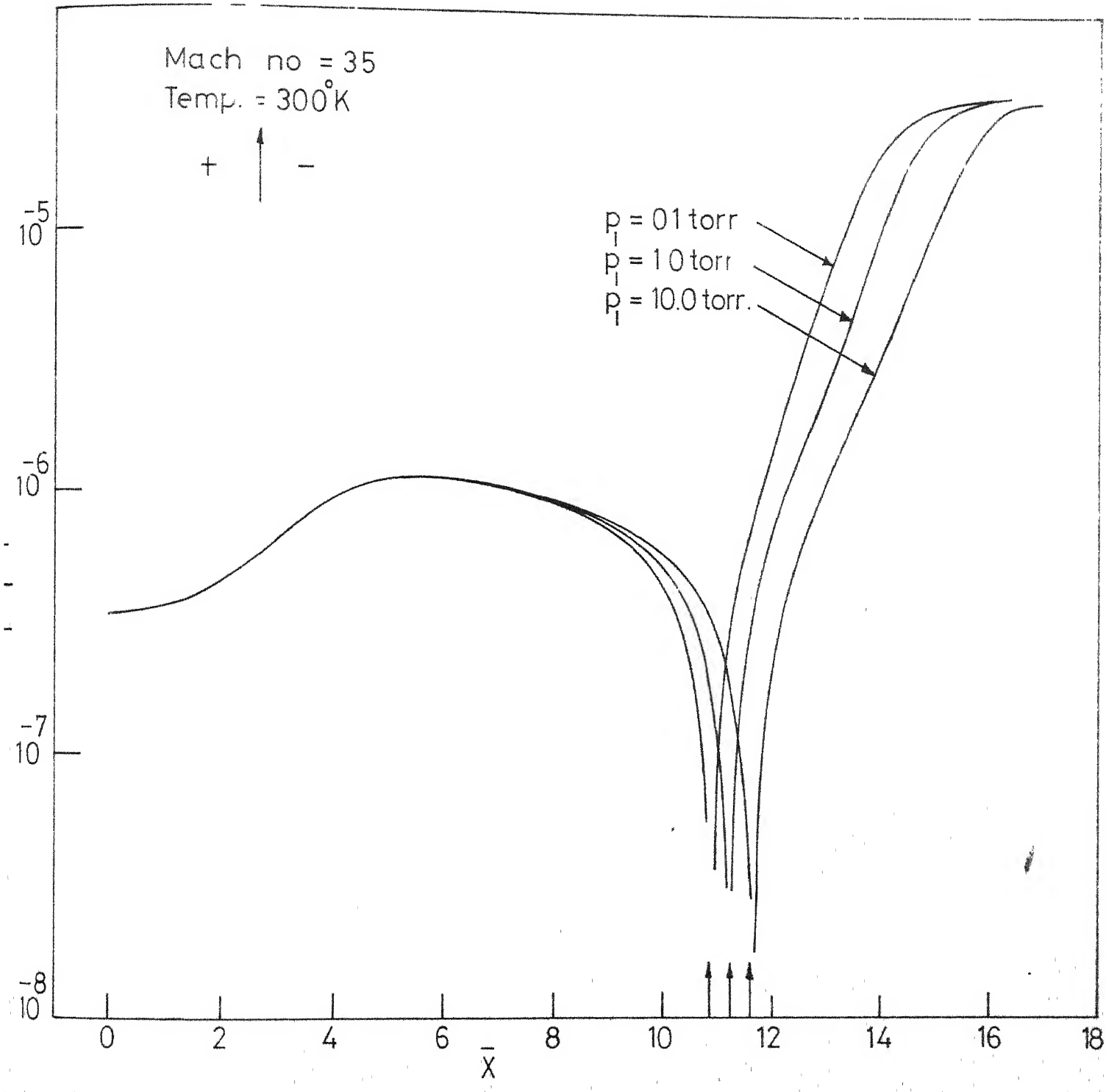

FIG.6.5.5_REFRACTIVE INDEX PROFILES FOR ARGON

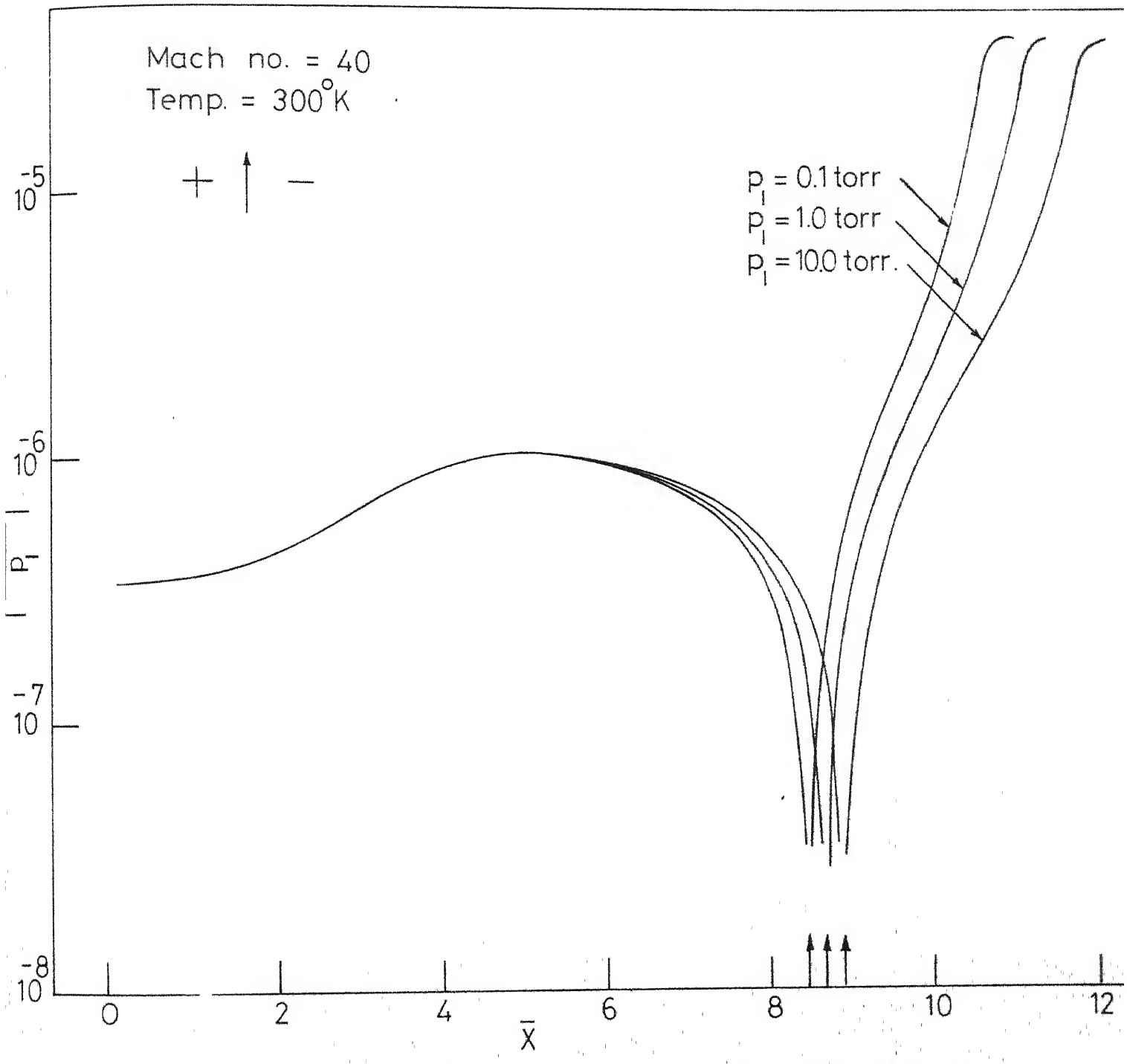

FIG.6.5.6_REFRACTIVE INDEX PROFILES FOR ARGON

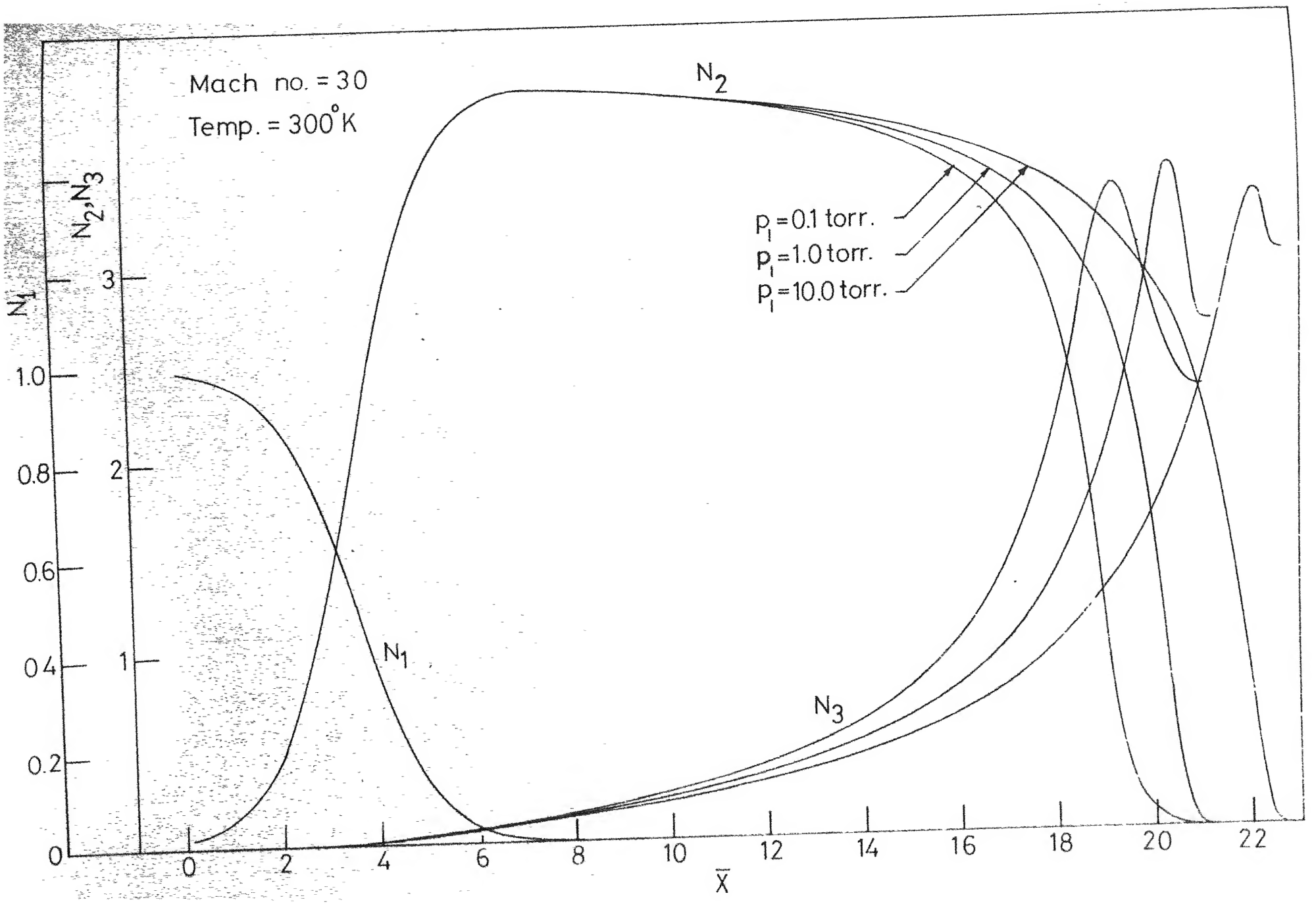

FIG. 6.6.2_TYPICAL PROFILES OF N_1, N_2, N_3, FOR ARGON

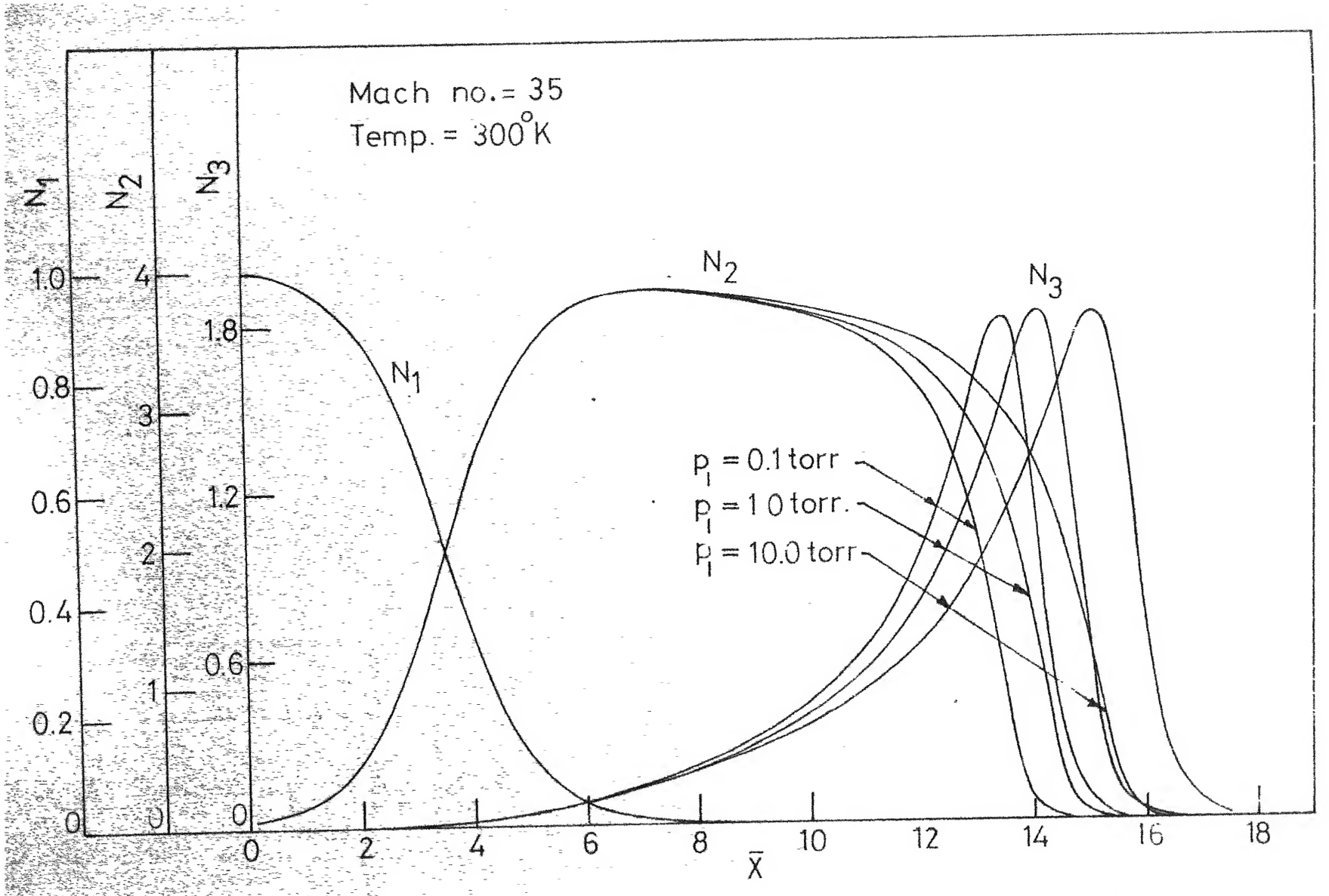

FIG.6.6.3_TYPICAL PROFILES OF N_1, N_2, N_3, FOR ARGON

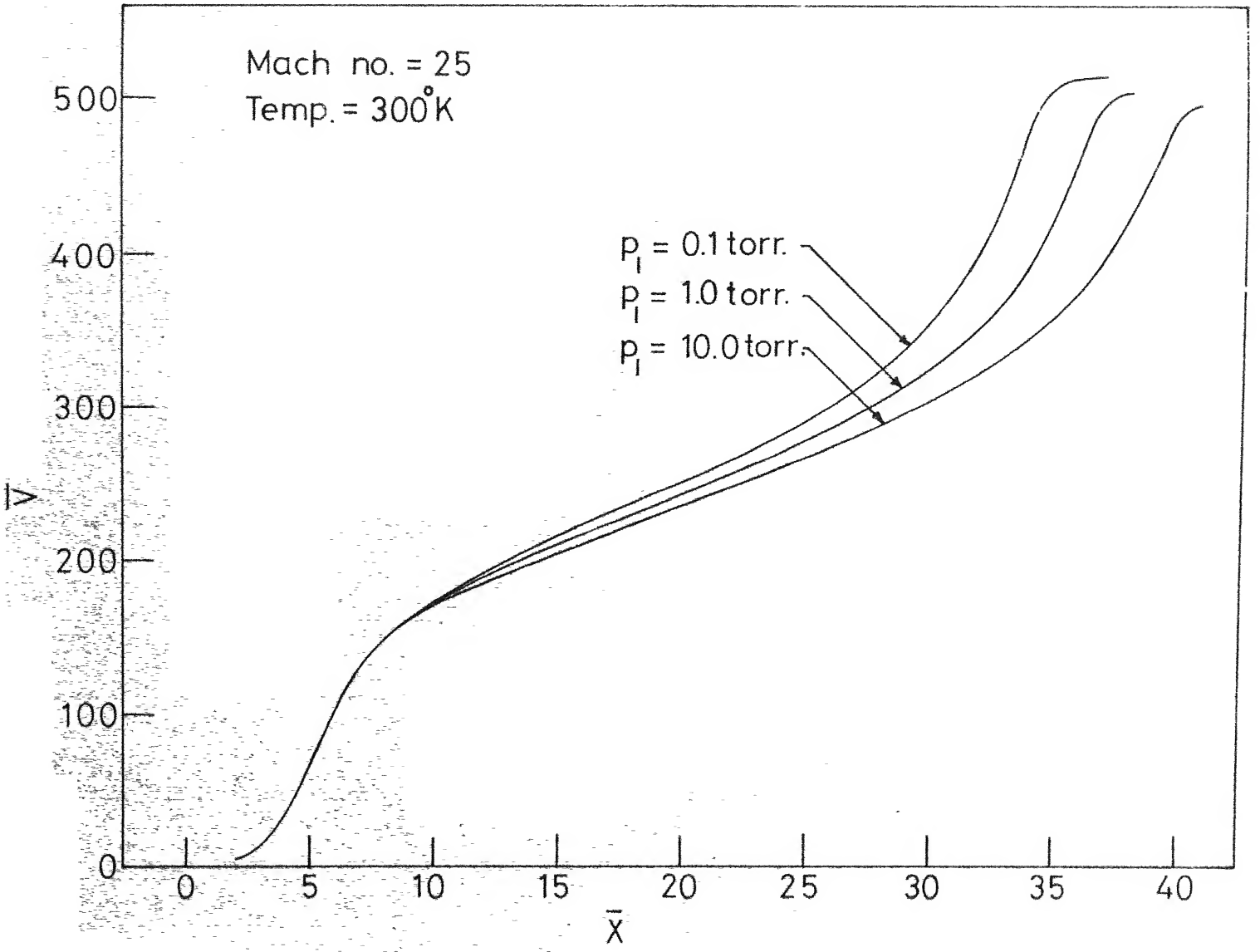

FIG. 6.7.1 ELECTRIC POTENTIAL PROFILES FOR ARGON.

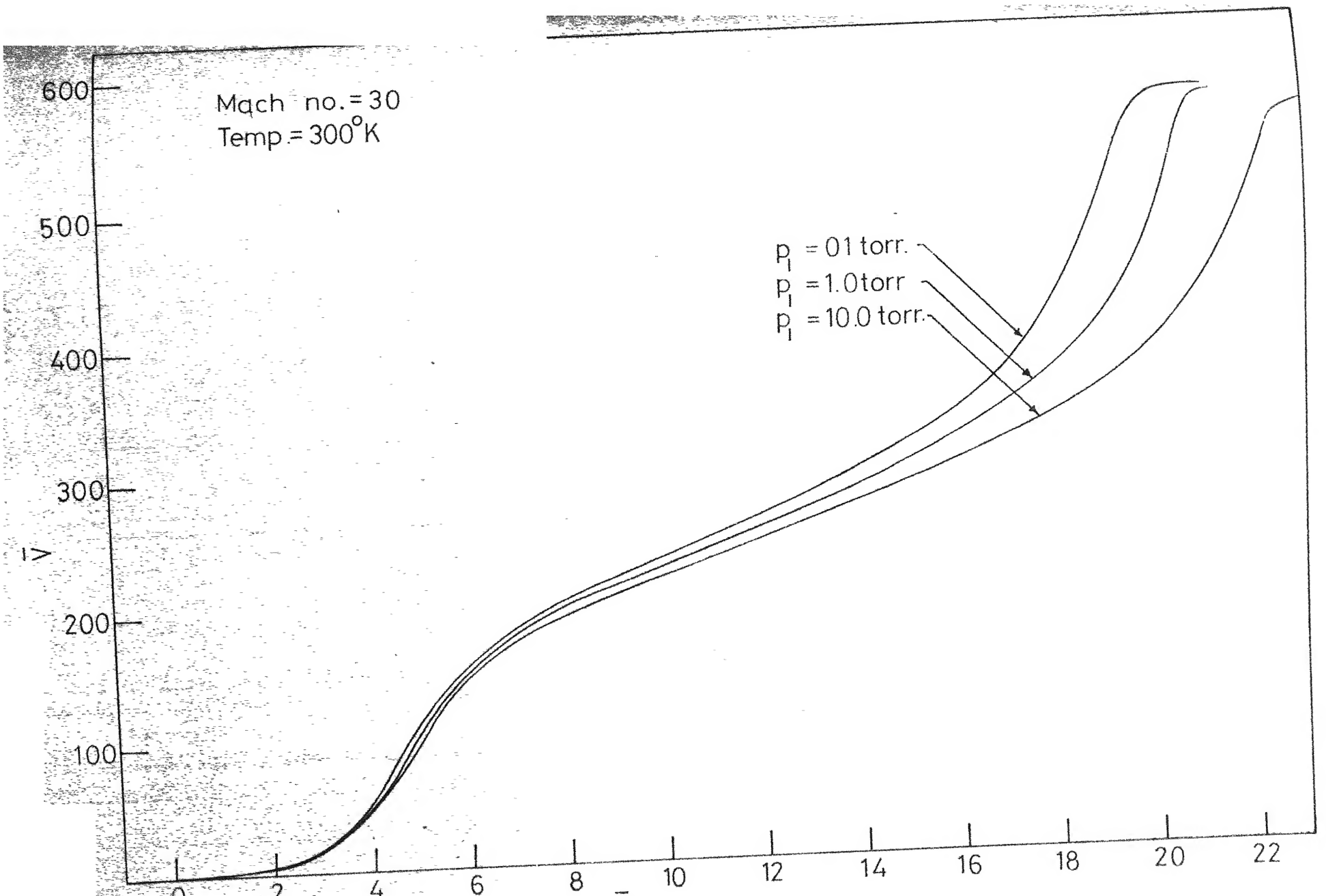

FIG. 6.7.2 ELECTRIC POTENTIAL PROFILES FOR ARGON

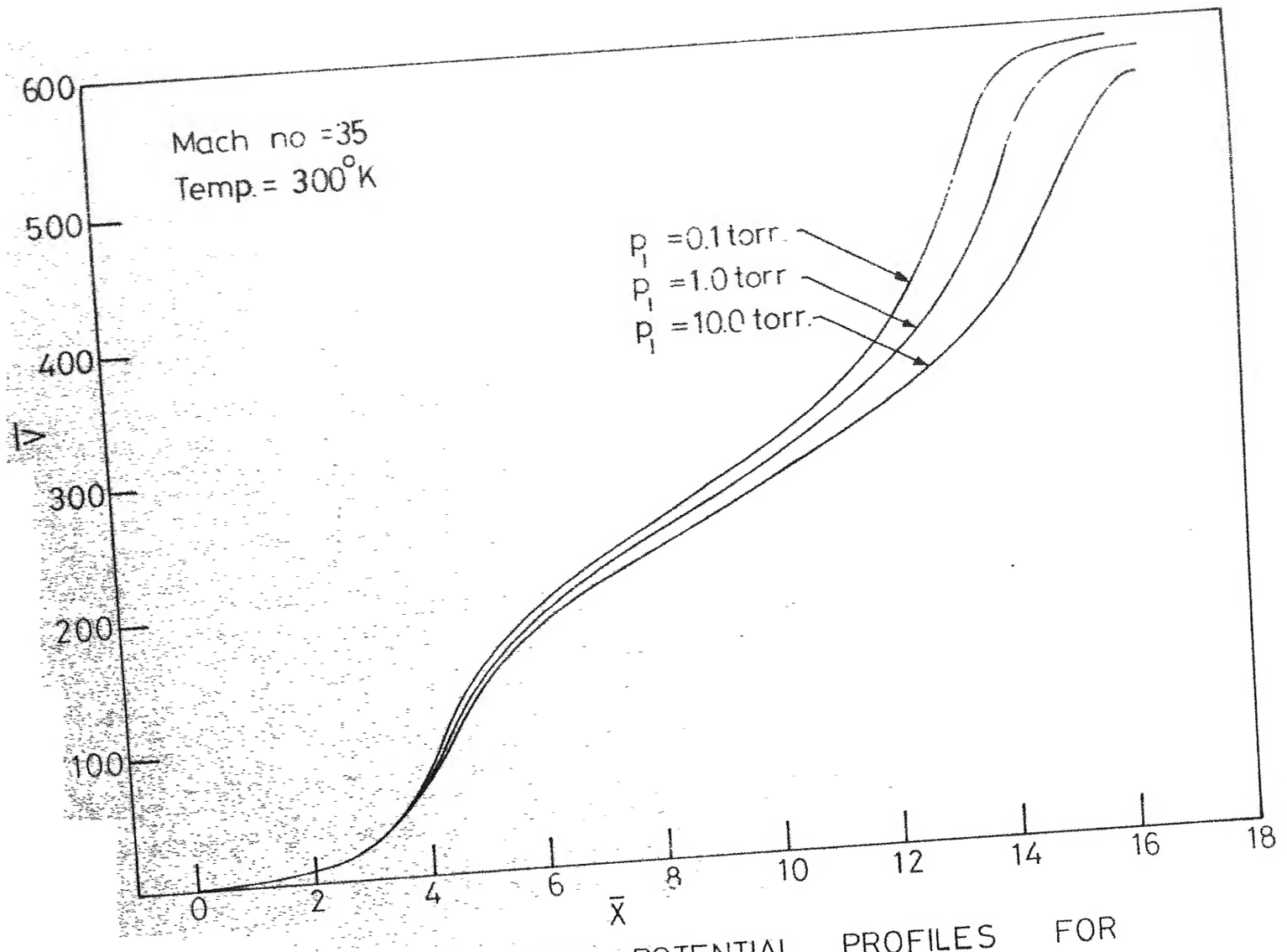

FIG.6.7.3_ELECTRIC POTENTIAL PROFILES FOR ARGON

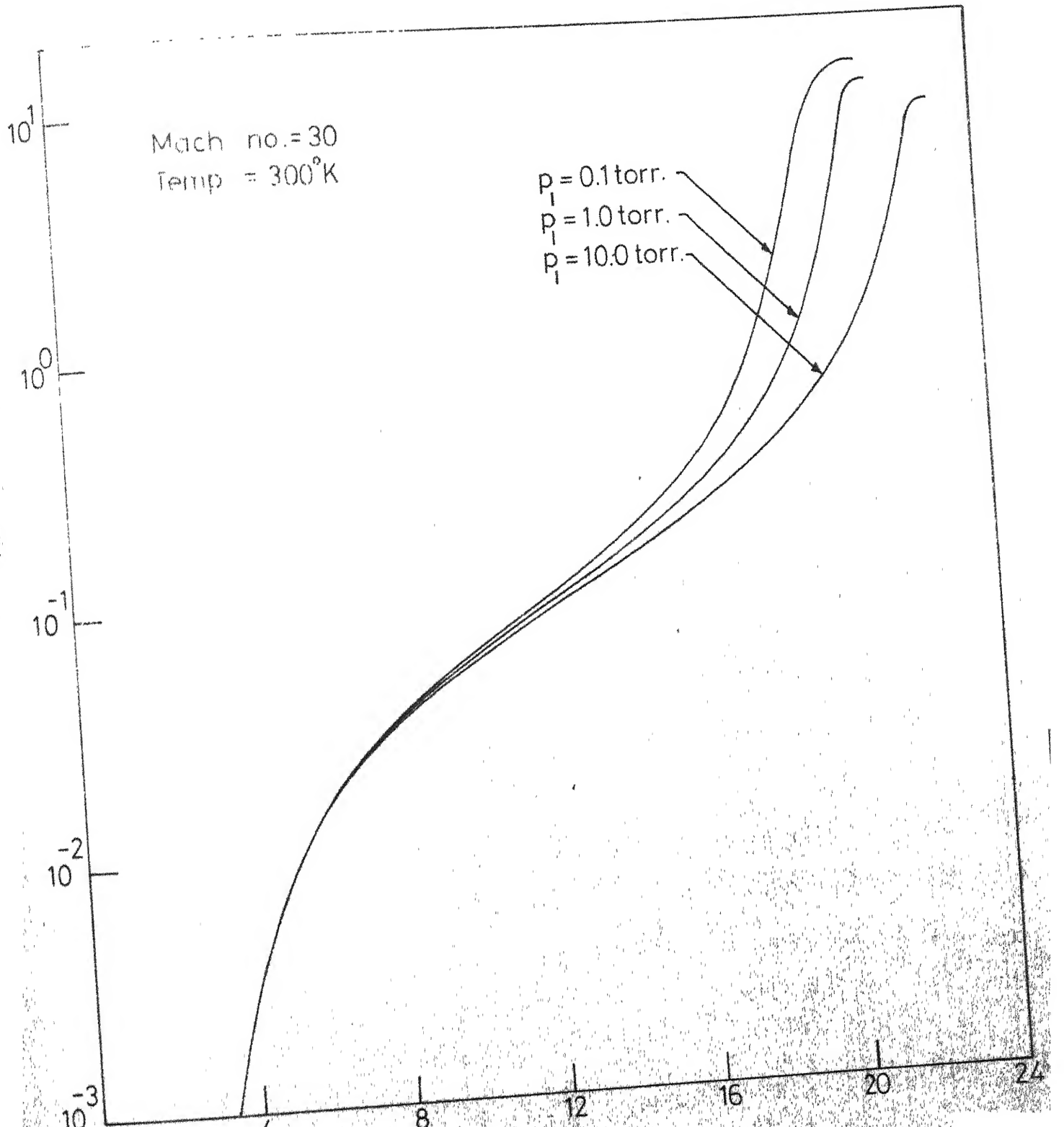

FIG.6.8.1–ELECTRON DENSITY PROFILES FOR ARGON.

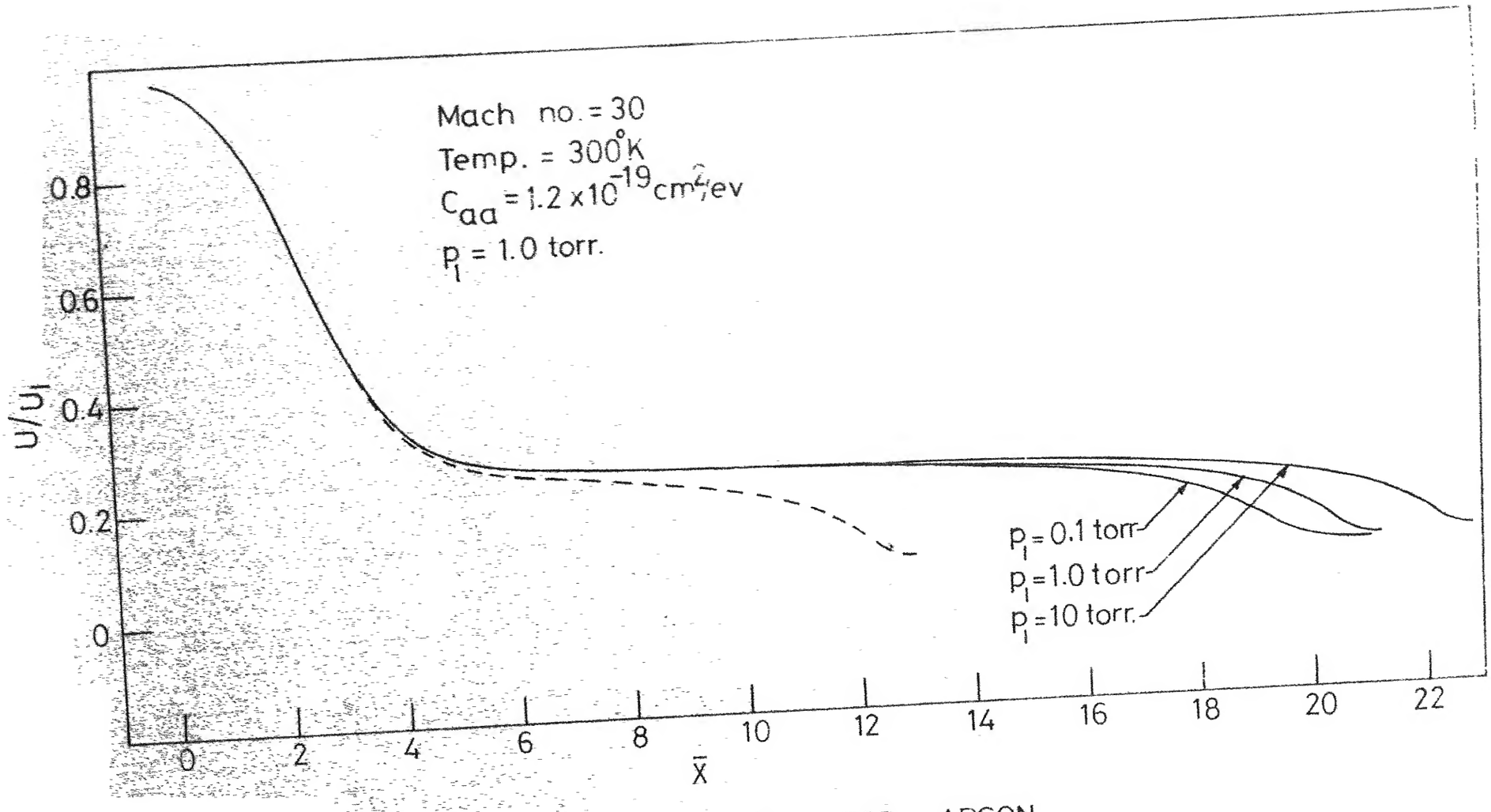

FIG. 6.9.1 VELOCITY PROFILES FOR ARGON

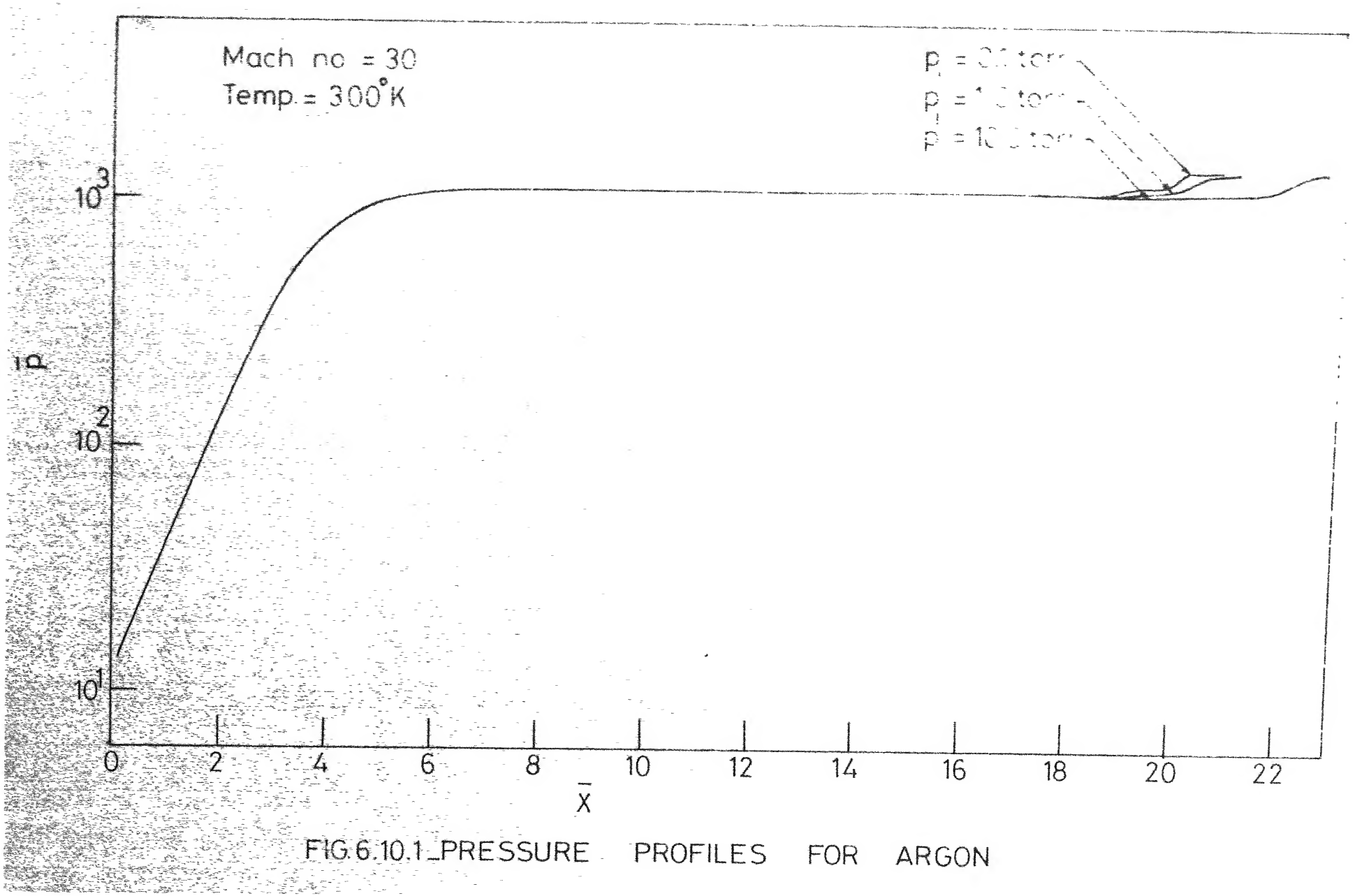

FIG.6.10.1_PRESSURE PROFILES FOR ARGON

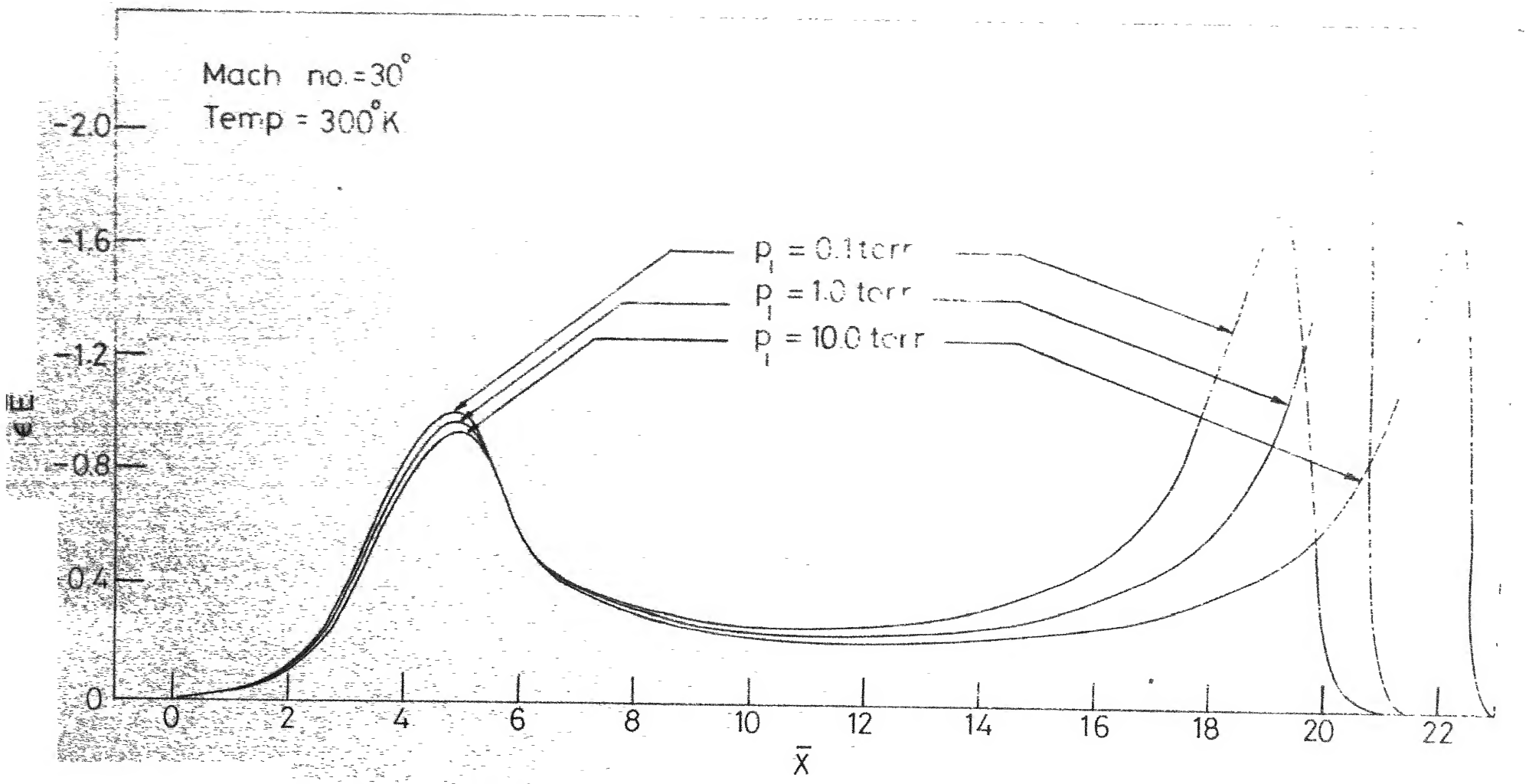

FIG. 6.11.1 ELECTRIC FIELD PROFILES FOR ARGON

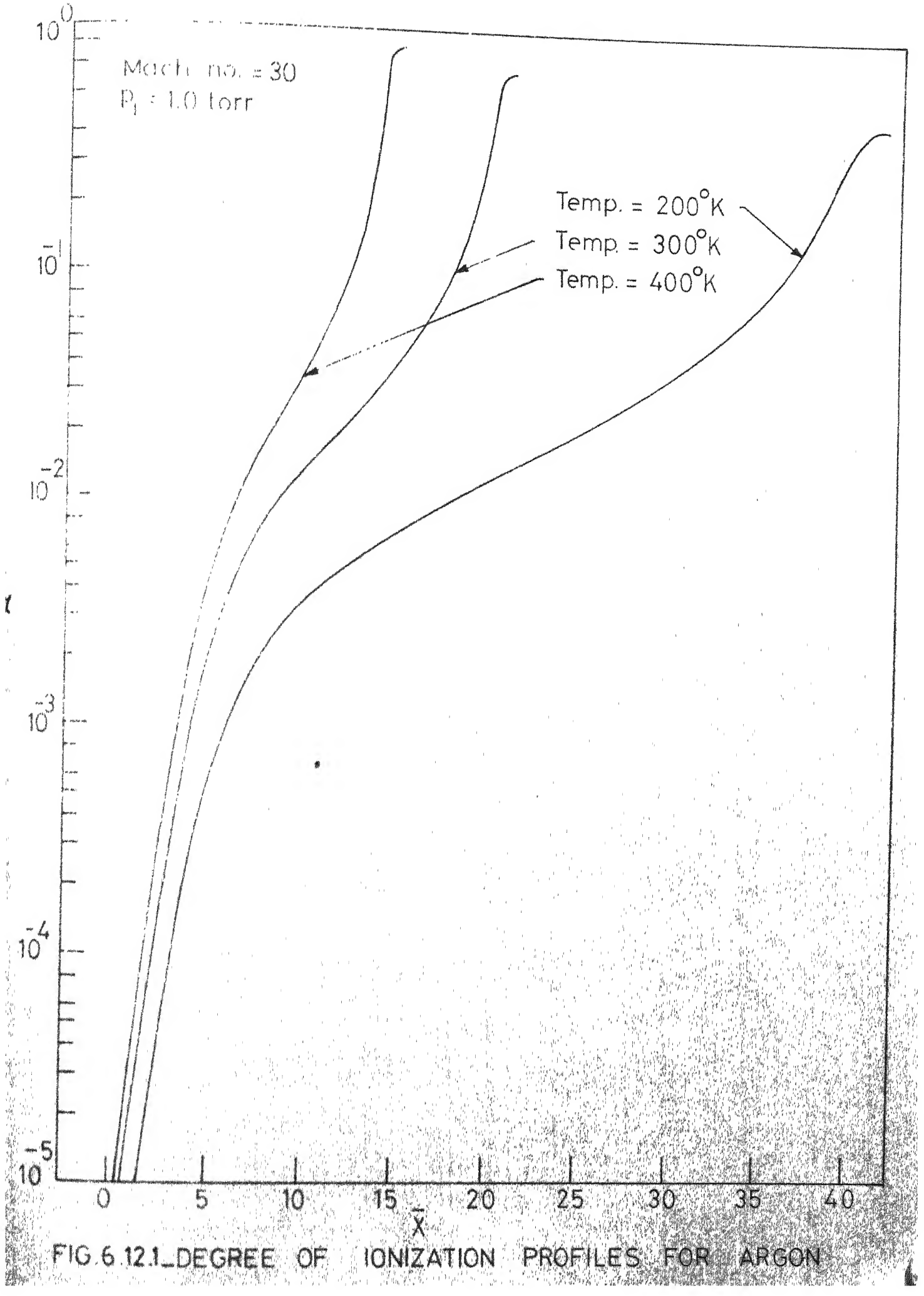

FIG. 6.12.1 DEGREE OF IONIZATION PROFILES FOR ARGON

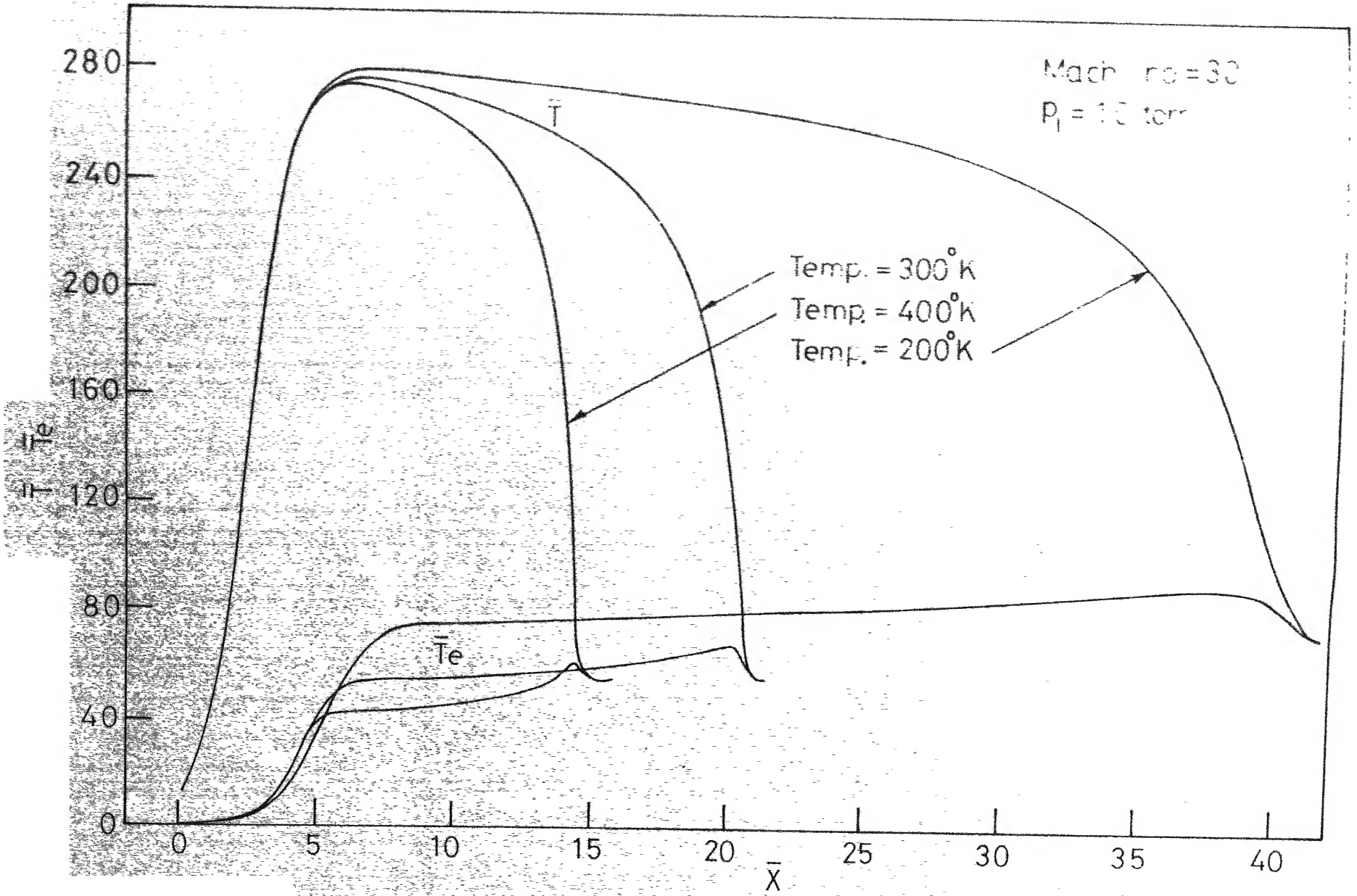

FIG. 6.12.2 TEMPERATURE PROFILES FOR ARGON.

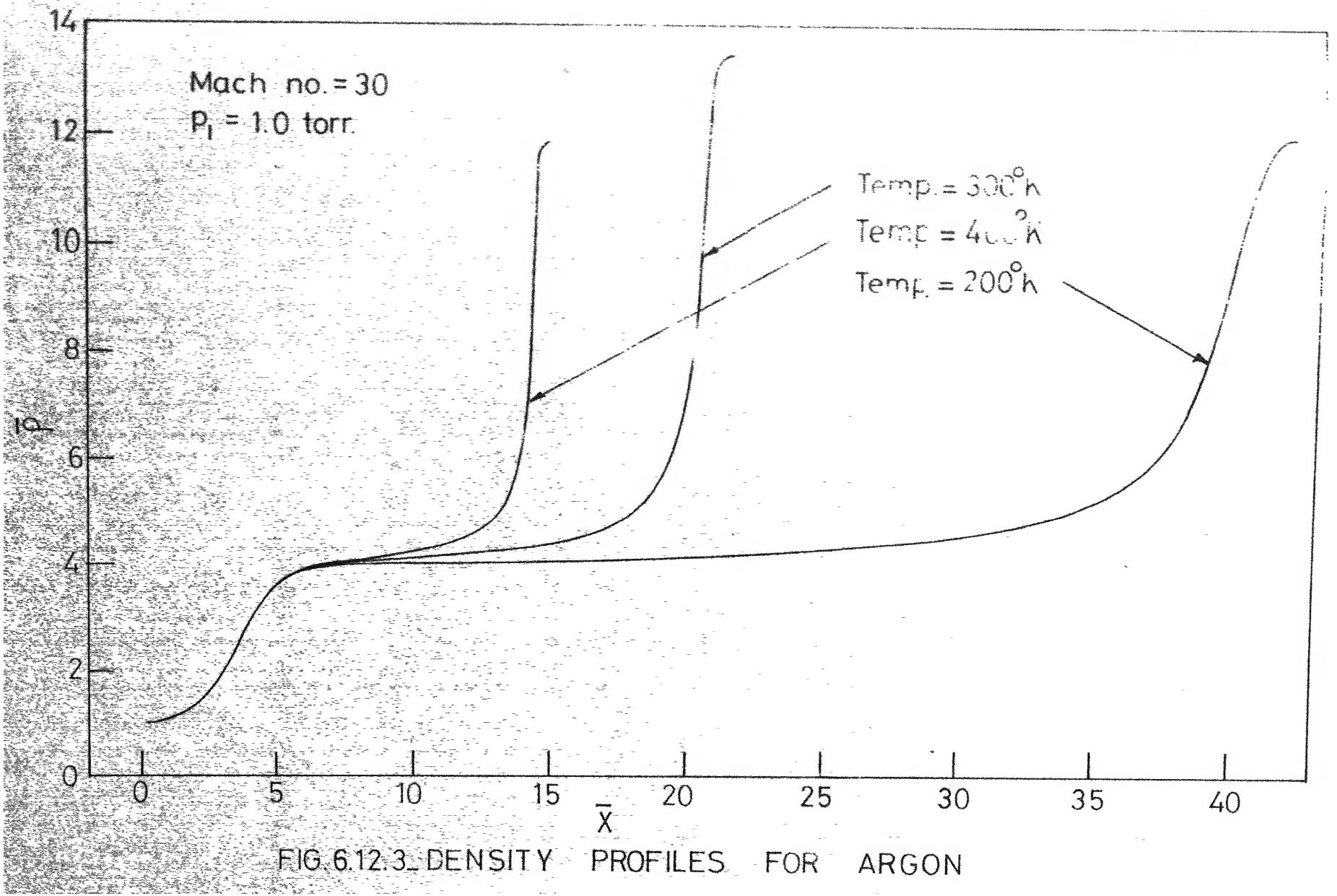

FIG. 6.12.3 DENSITY PROFILES FOR ARGON

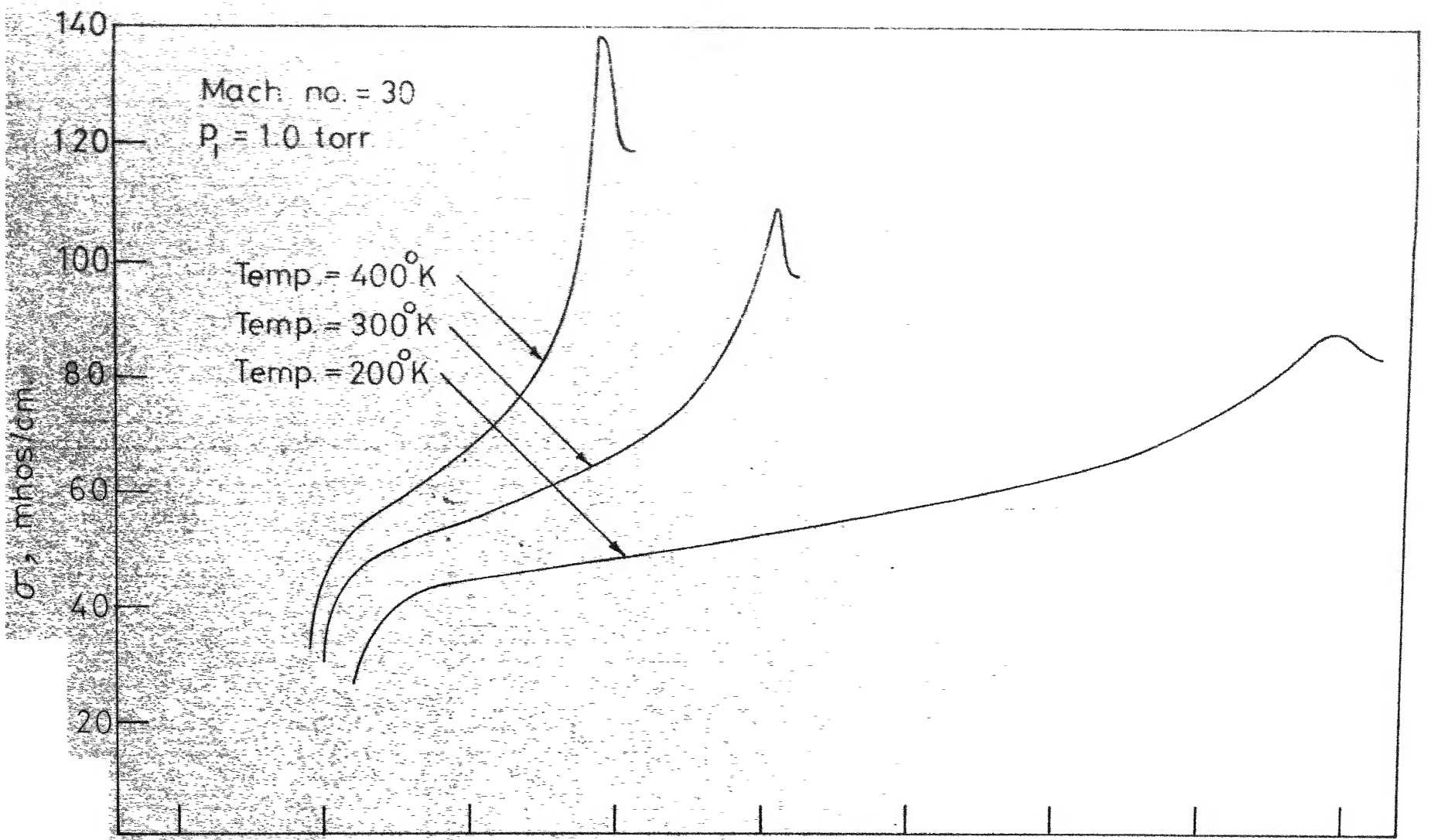

FIG. 6.12.4 ELECTRICAL CONDUCTIVITY PROFILES FOR ARGON

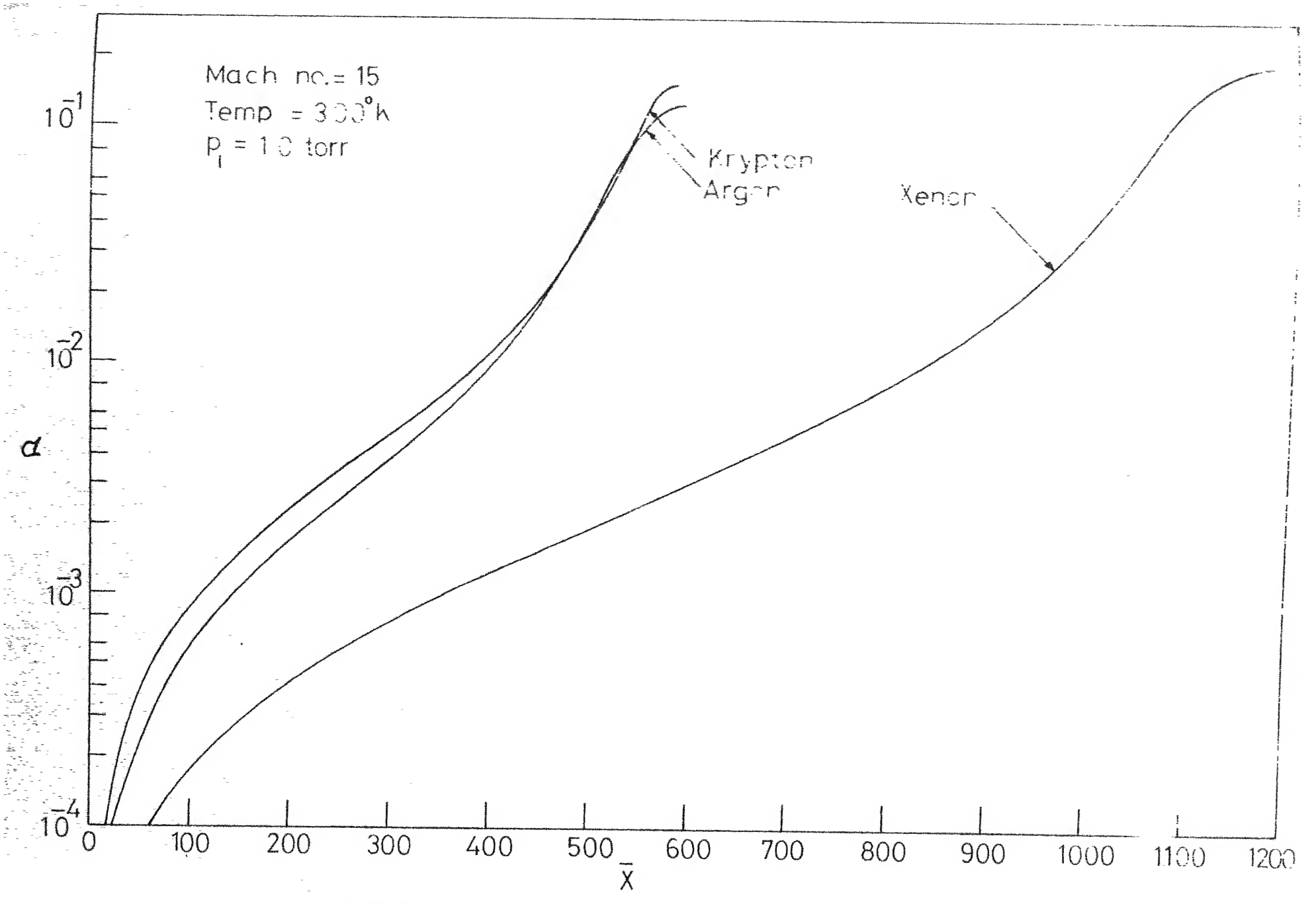

FIG.6.13.1_DEGREE OF IONIZATION PROFILES

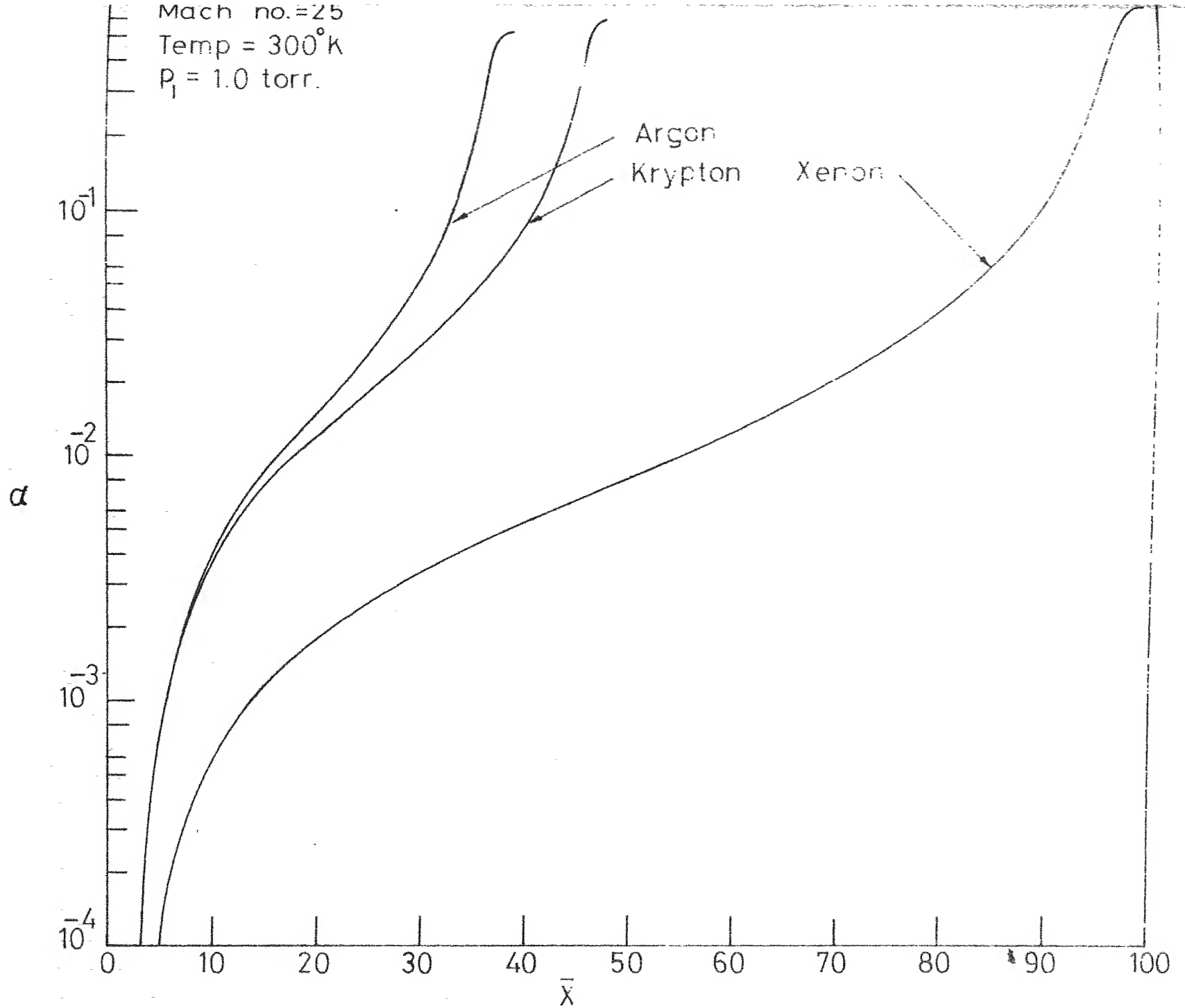

FIG.6.13.2.DEGREE OF IONIZATION

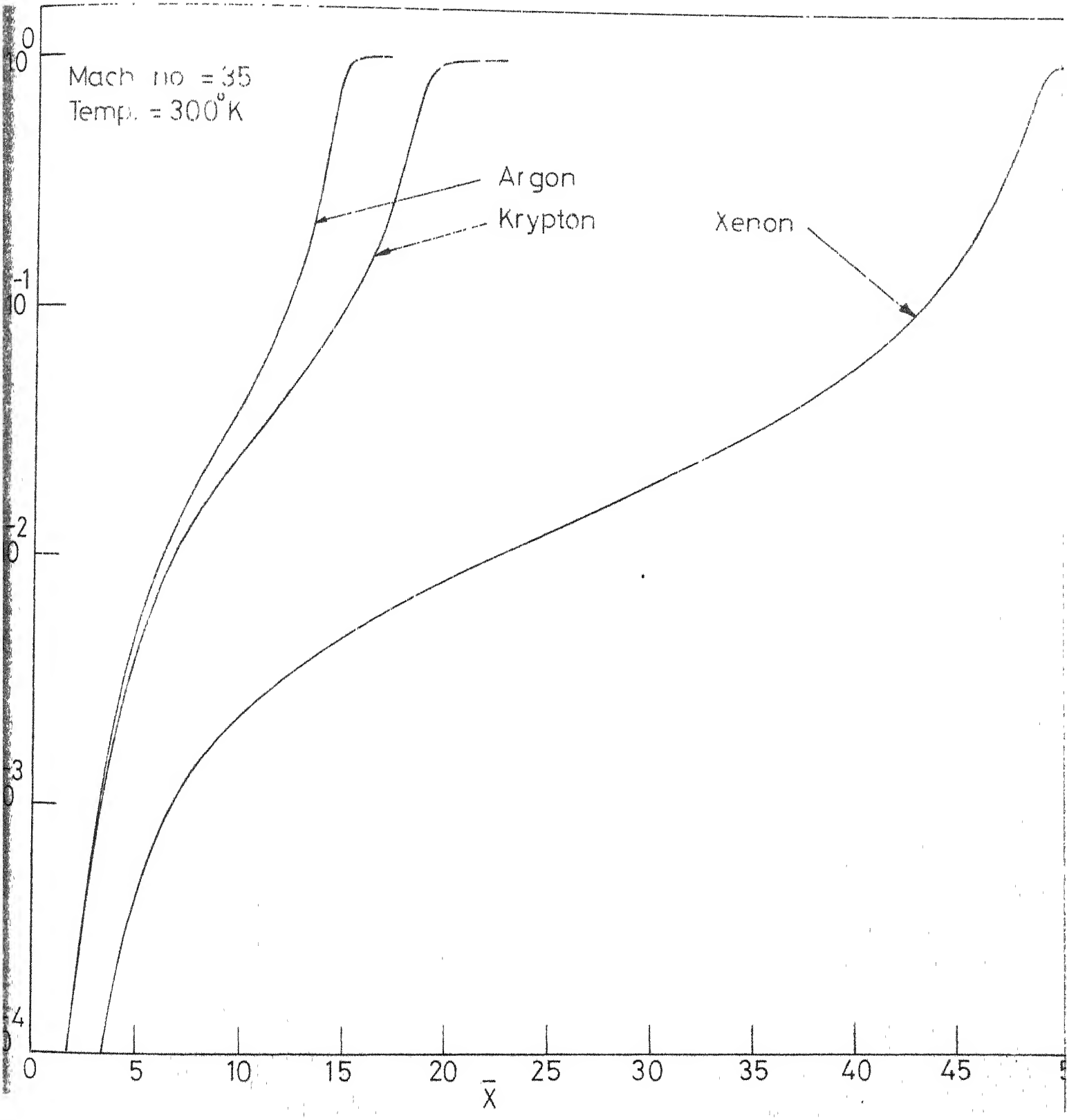

FIG.6.13.3 _ DEGREE OF IONIZATION PROFILES

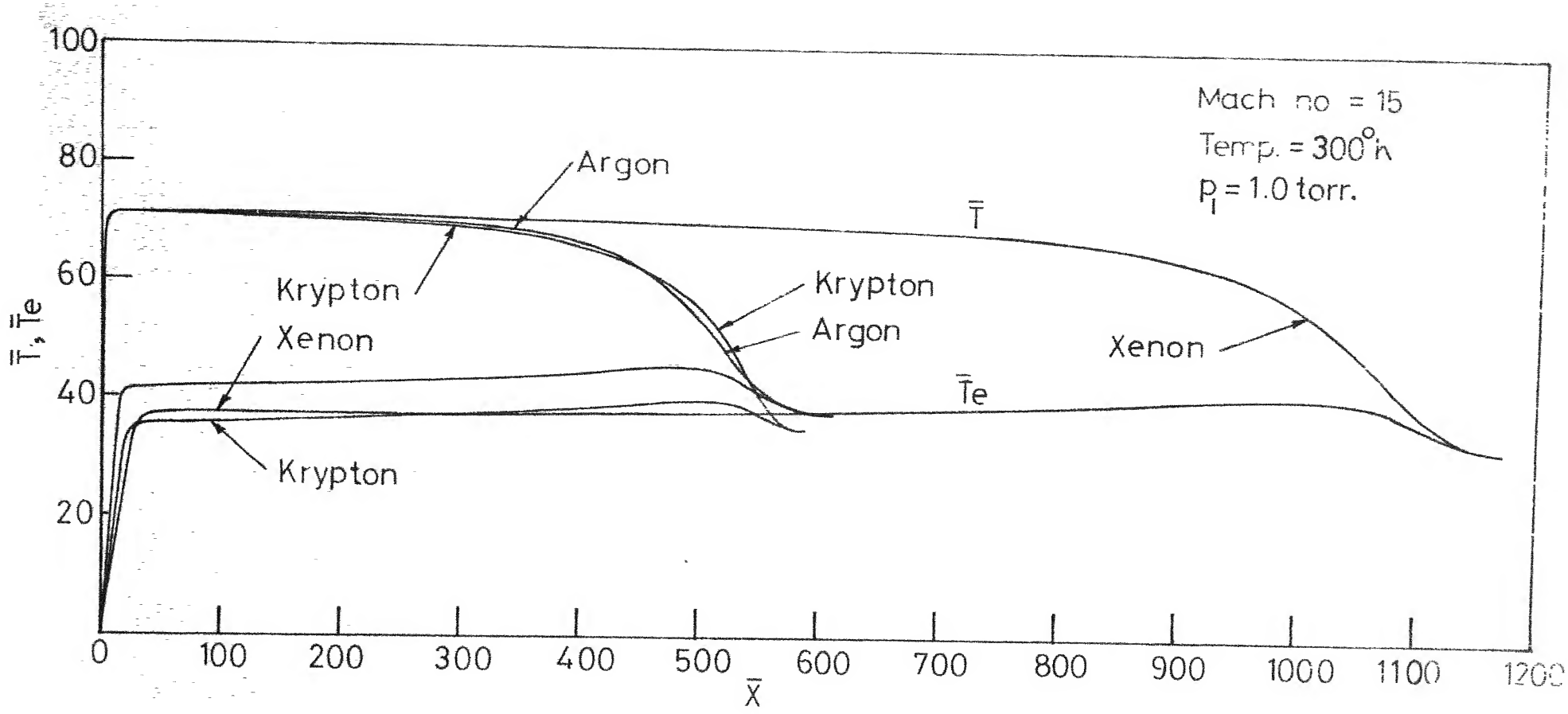

FIG. 6.14.1_TEMPERATURE PROFILES

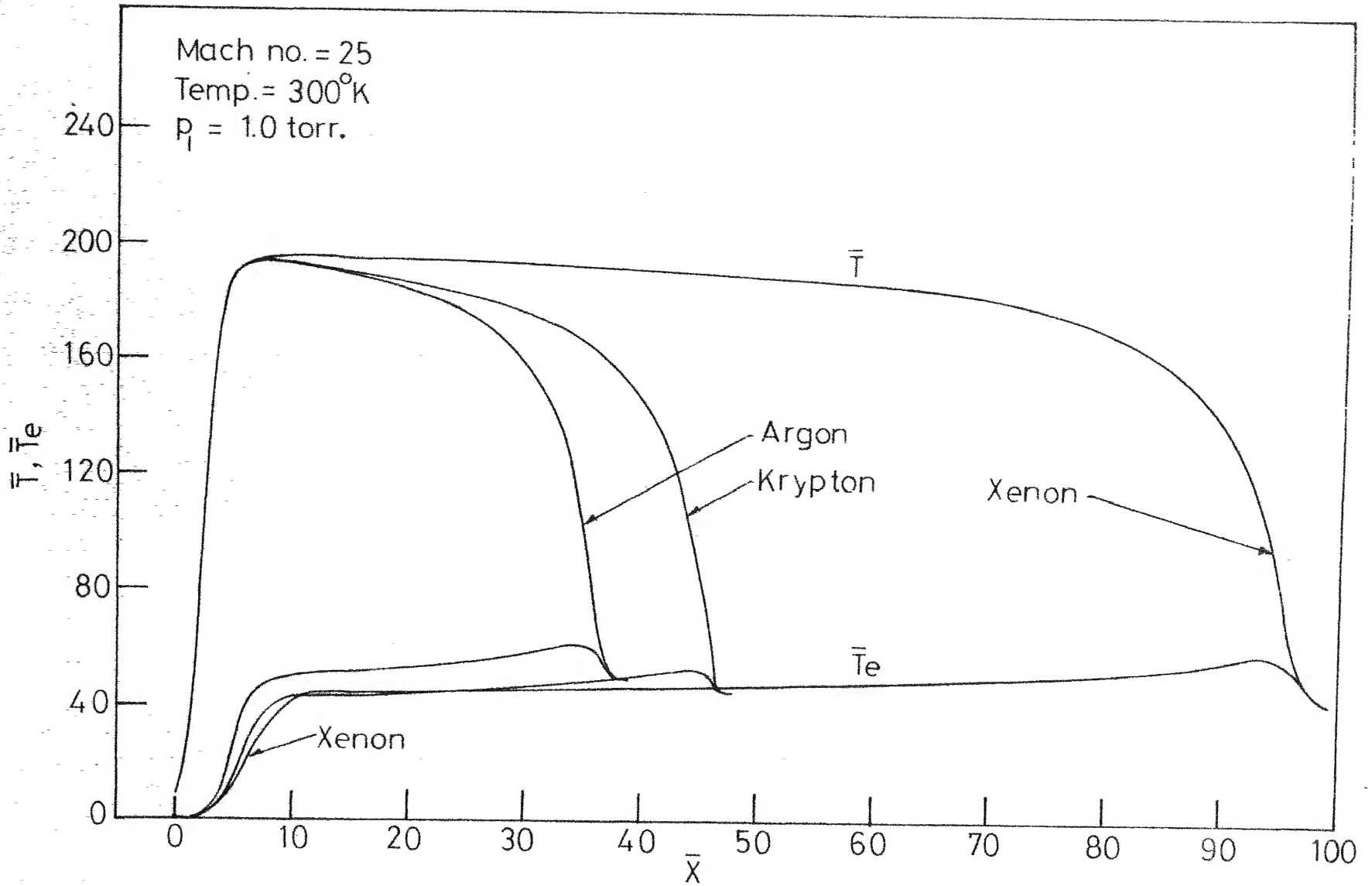

FIG 6.14.2_TEMPERATURE PROFILES

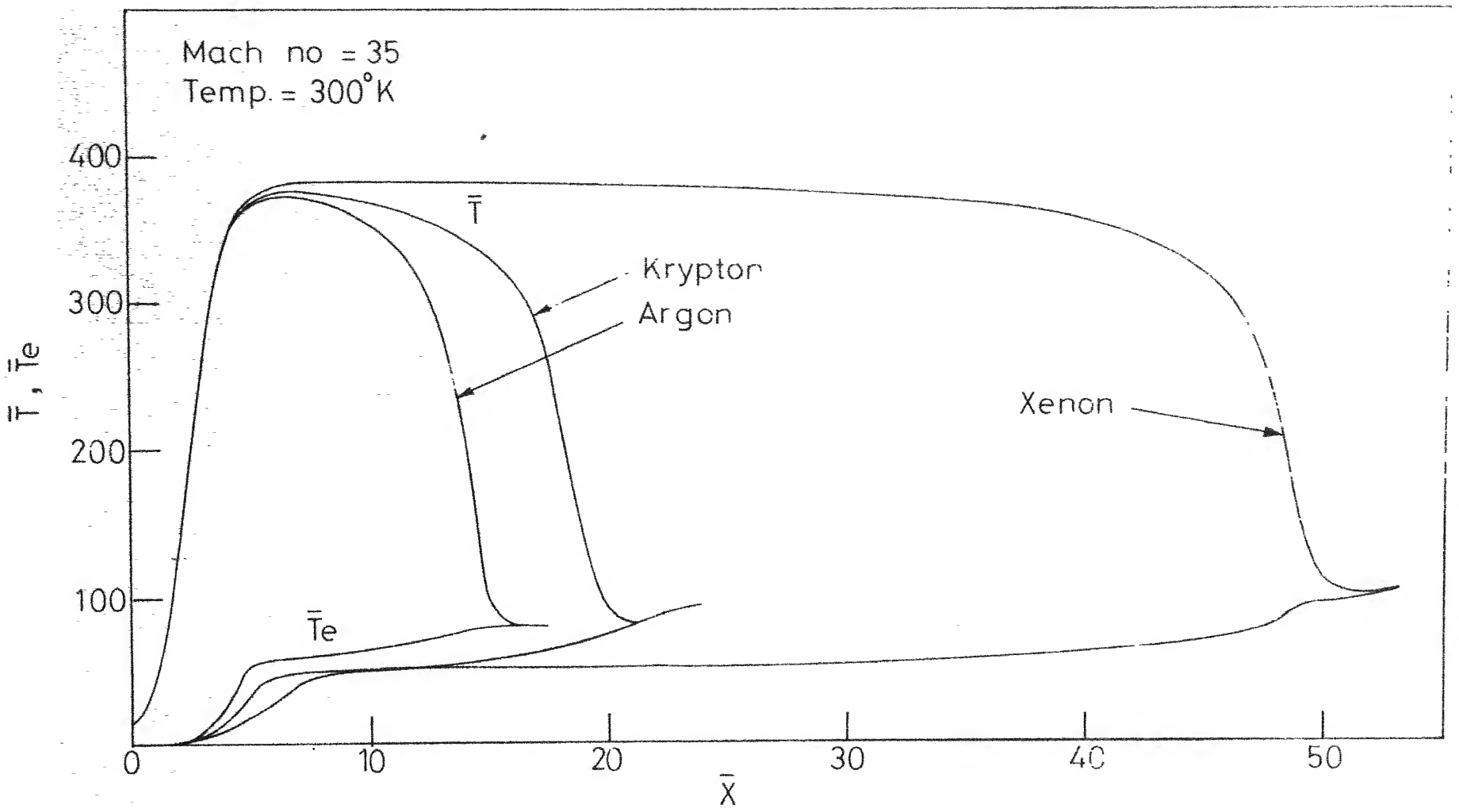

FIG. 6.14.3_TEMPERATURE PROFILES

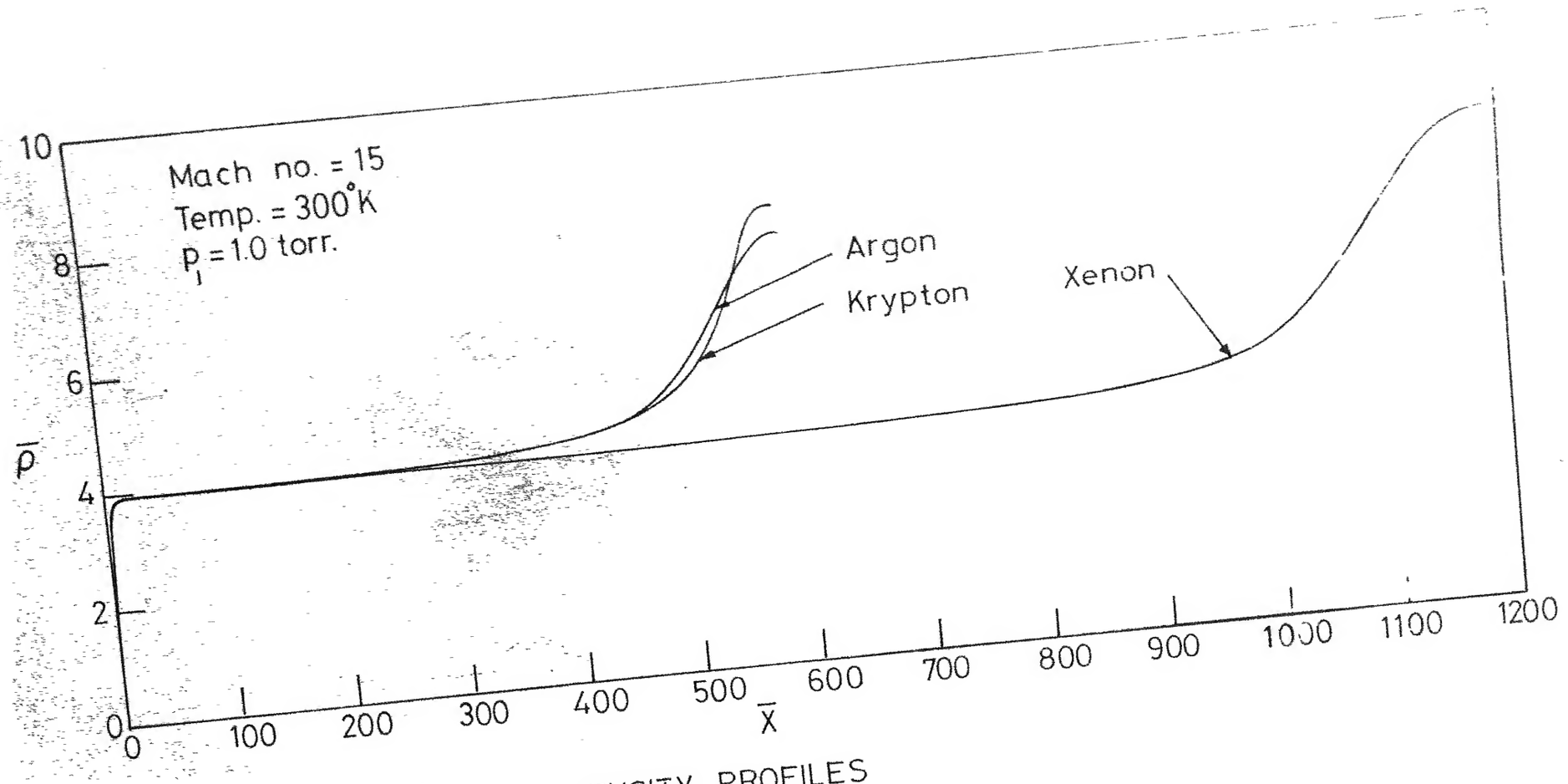

FIG.6.15.1_DENSITY PROFILES

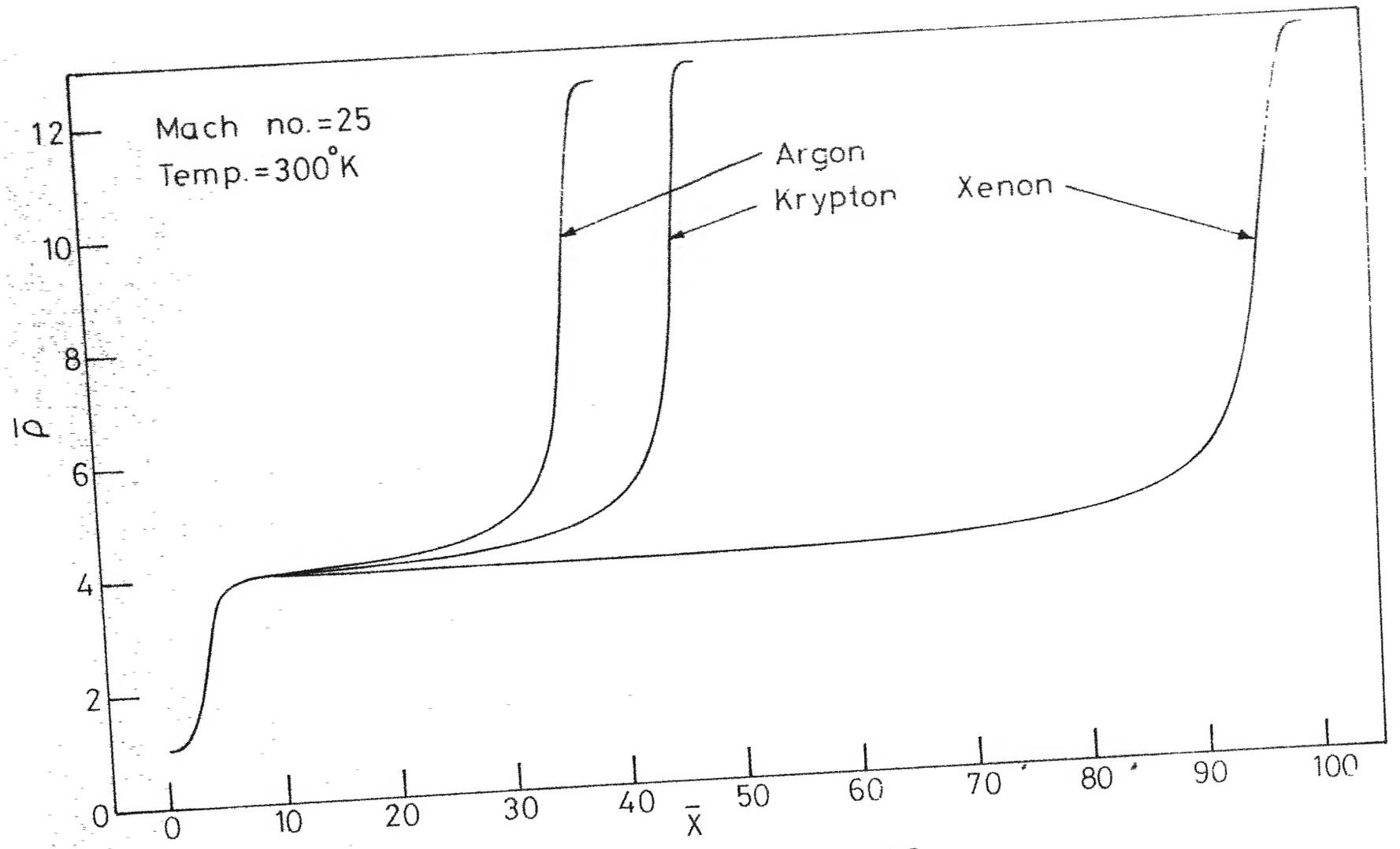

FIG. 6.15.2 _ DENSITY PROFILES

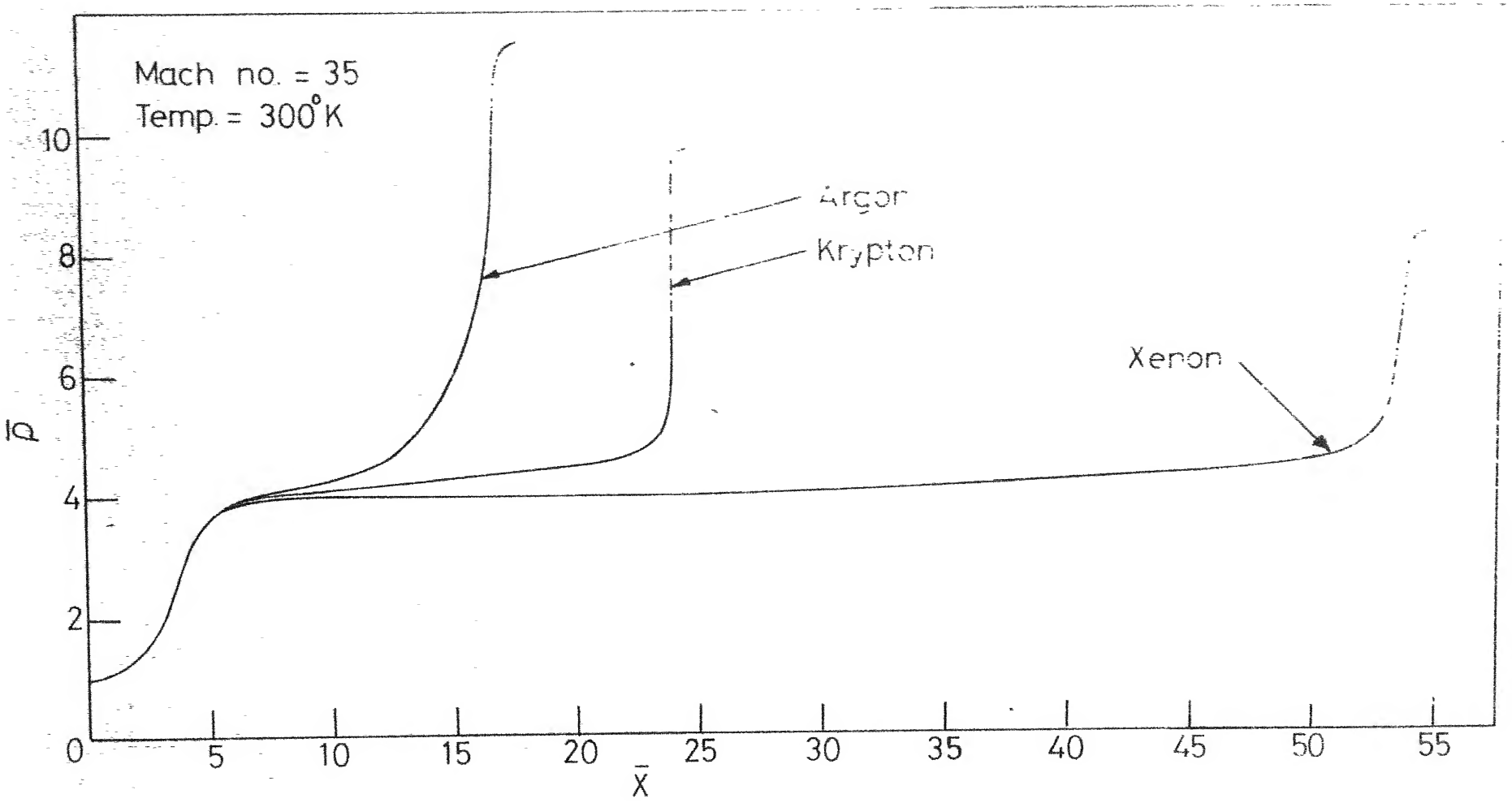

FIG. 6.15.3 _ DENSITY PROFILES

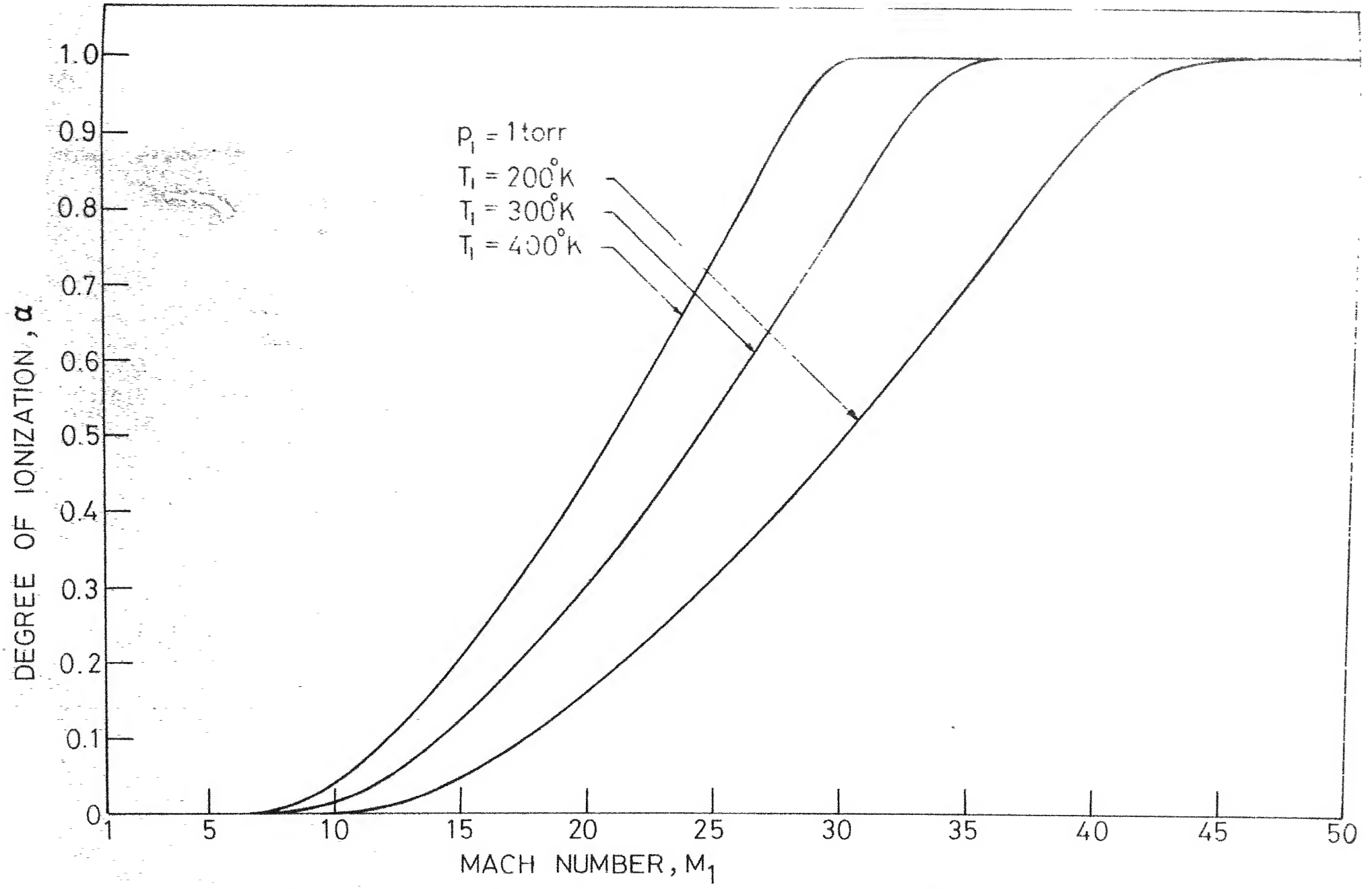

FIG. 6.16.1_EQUILIBRIUM DEGREE OF IONIZATION Vs MACH NUMBER FOR ARGON

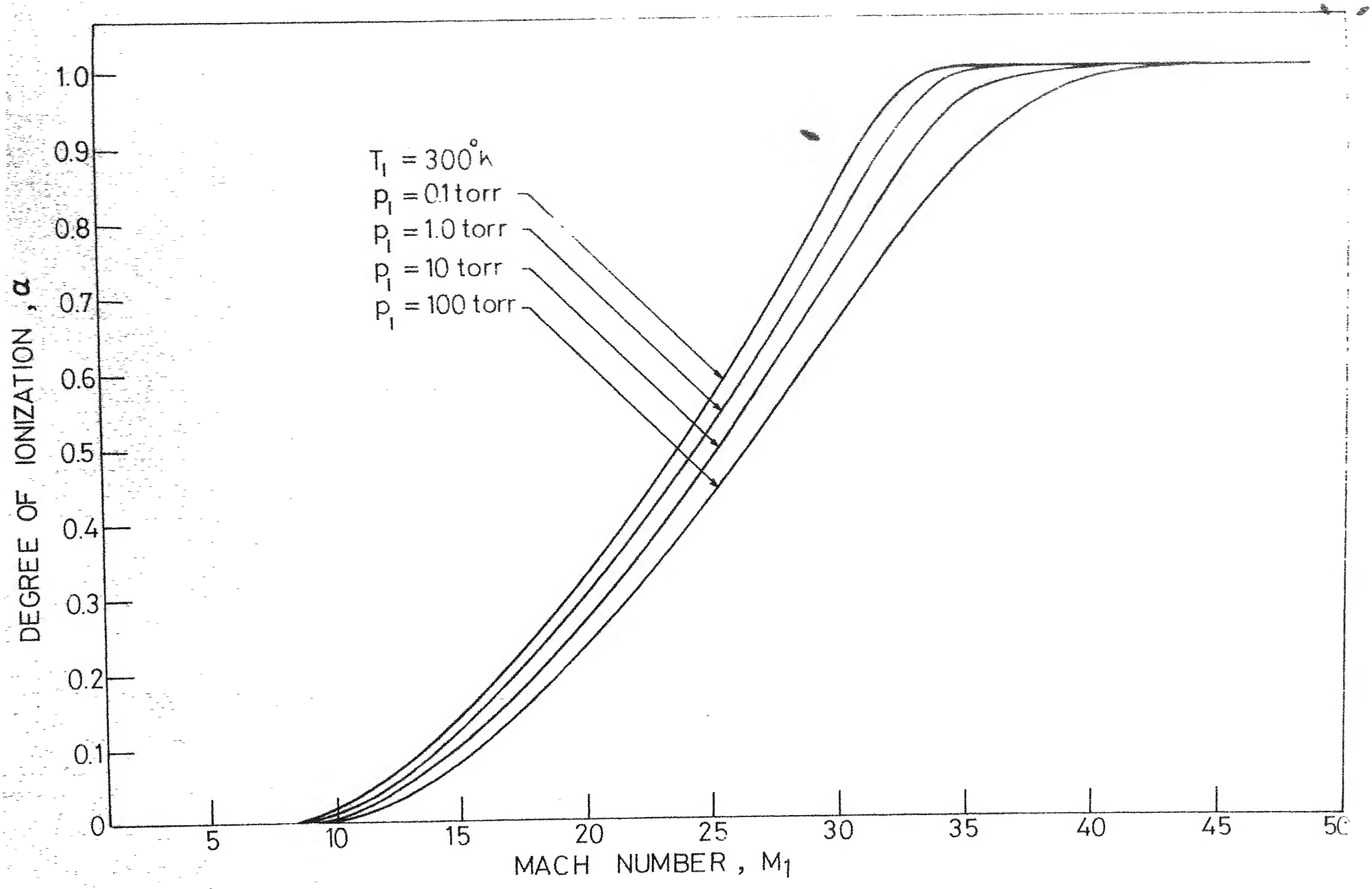

FIG.6.17.1_EQUILIBRIUM DEGREE OF IONIZATION Vs MACH NUMBER FOR ARGON

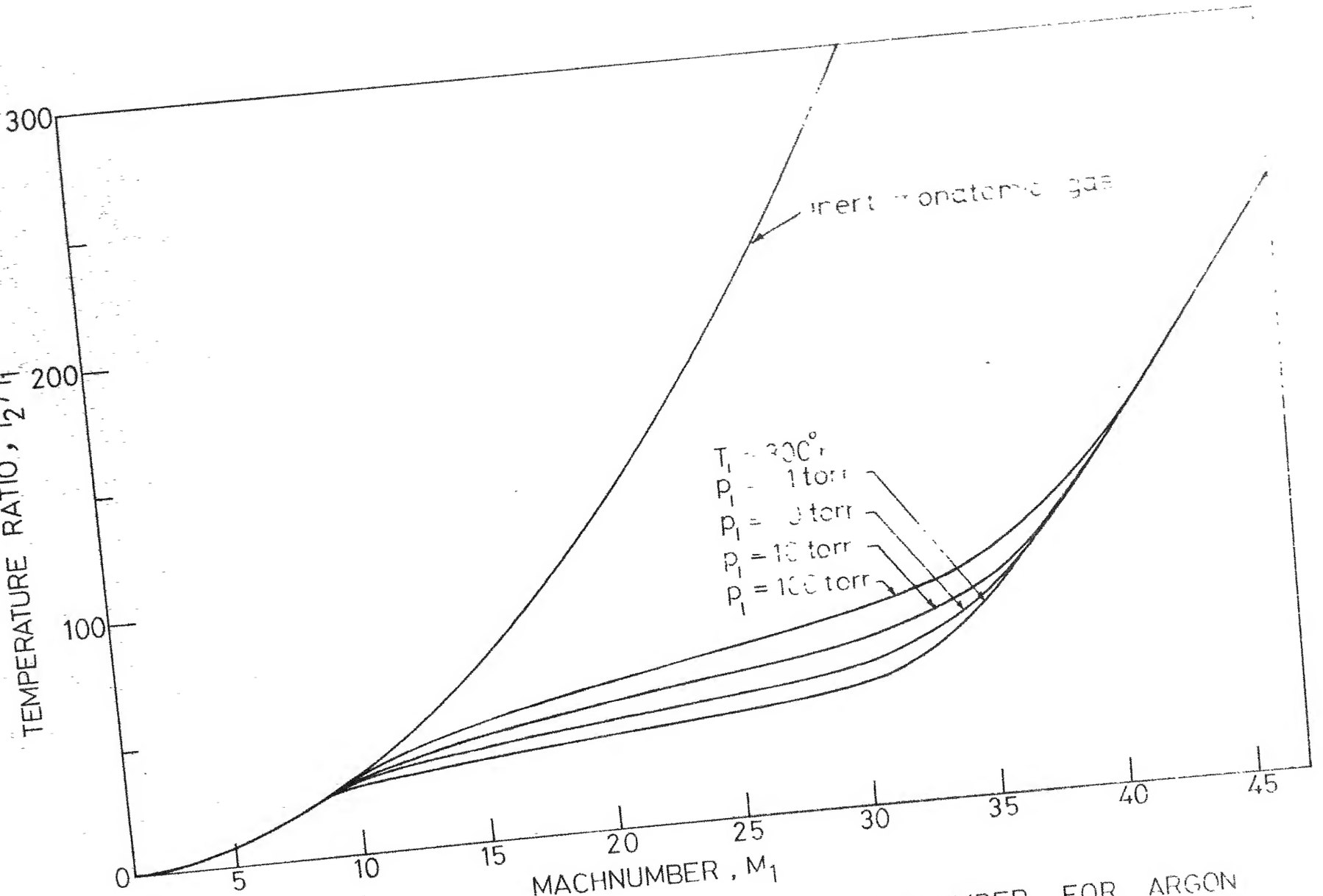

FIG.6.18.1_EQUILIBRIUM TEMPERATURE RATIO Vs MACHNUMBER FOR ARGON

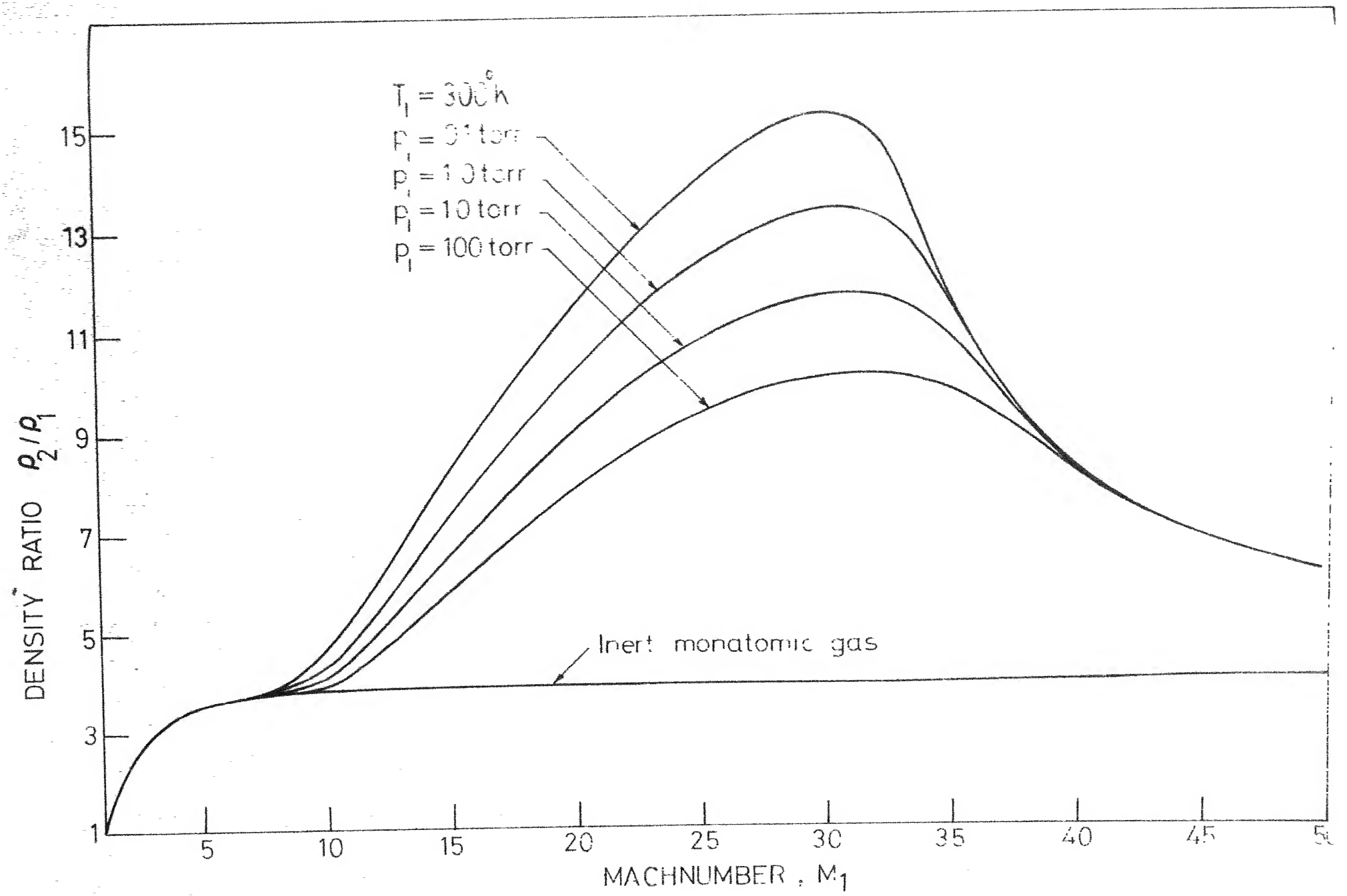

FIG. 6.19.1_EQUILIBRIUM DENSITY RATIO Vs MACHNUMBER FOR ARGON

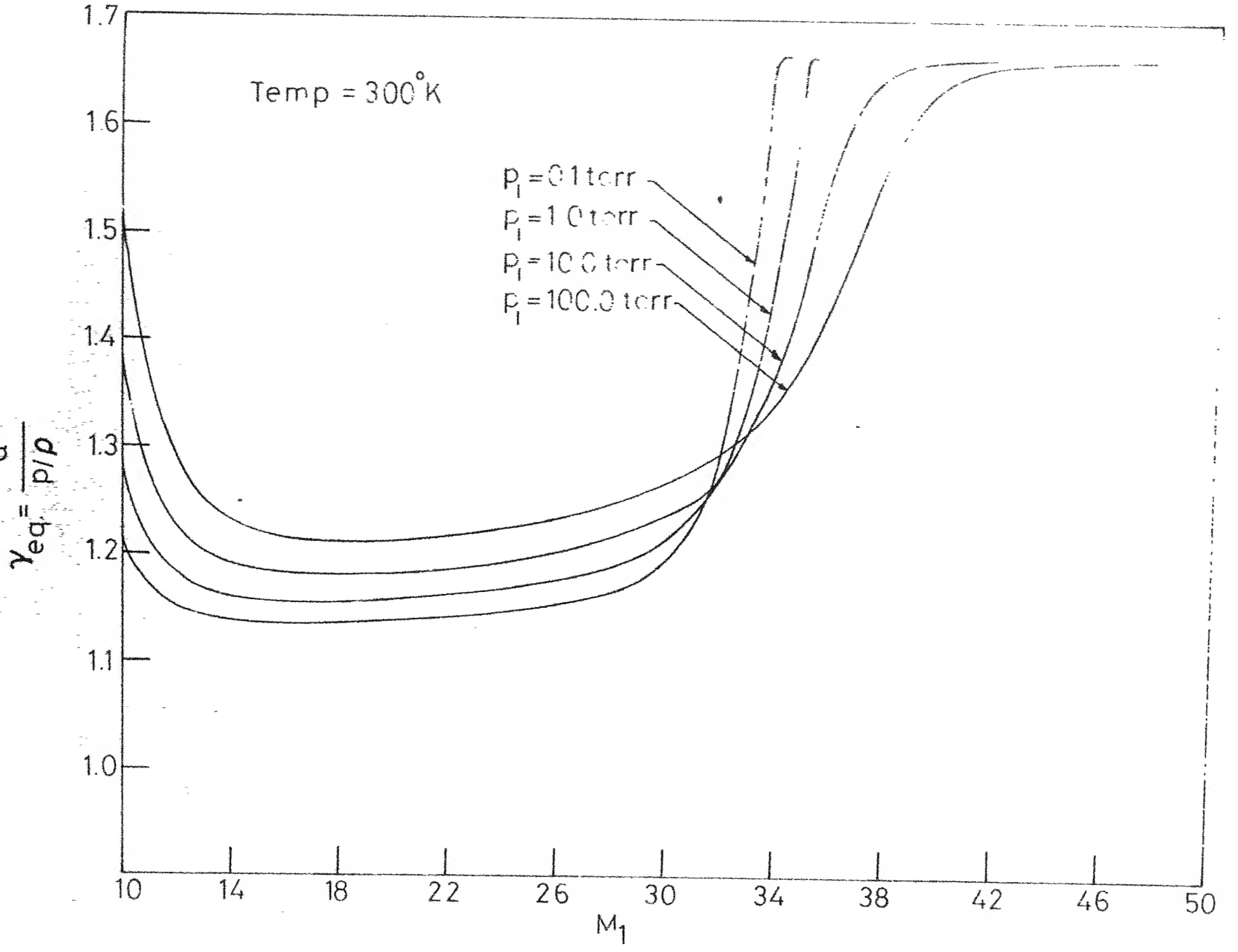

FIG. 6.20.1_EQIVALENT γ Vs FREE STREAM MACH NUMBER FOR ARGON.

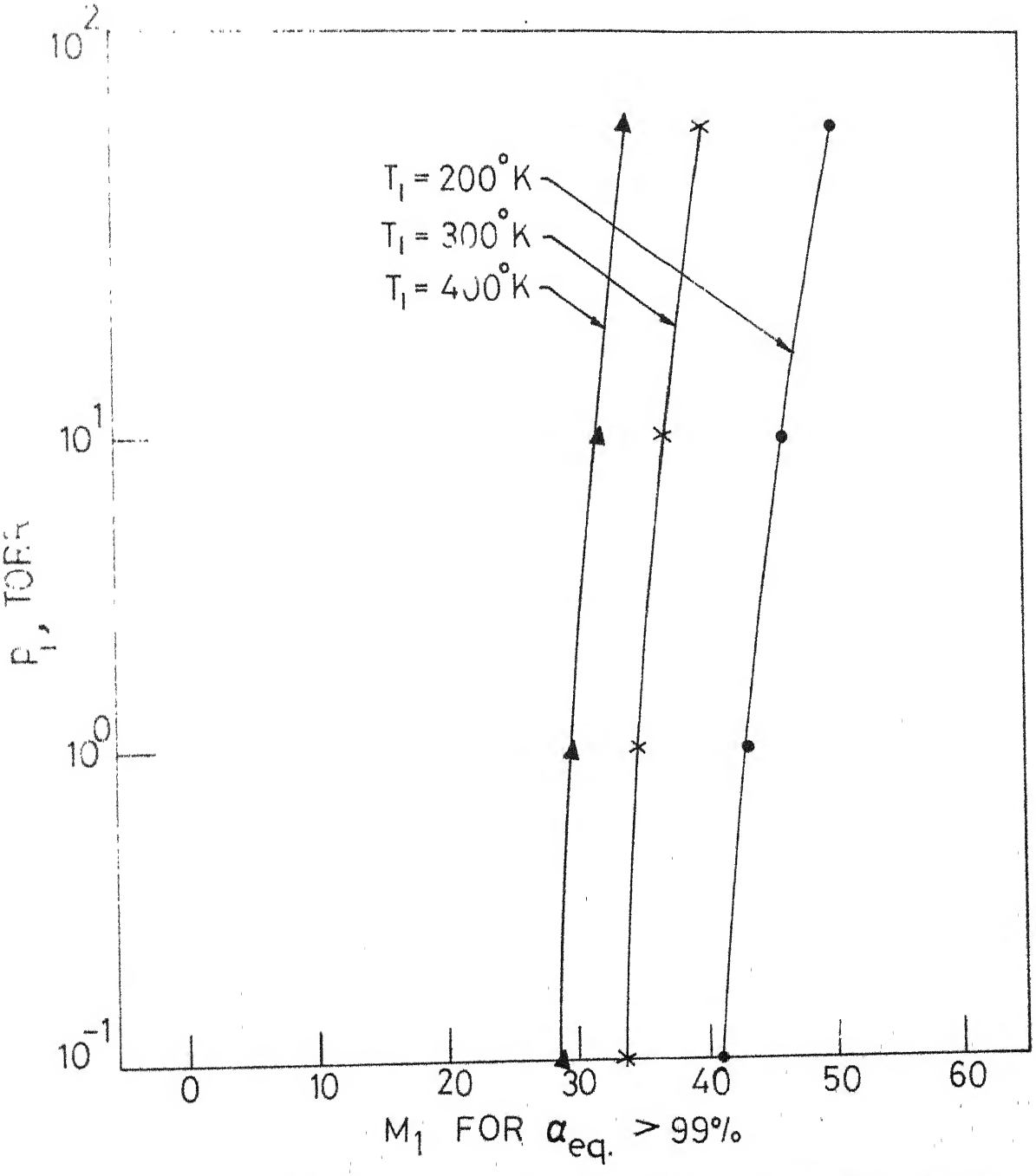

FIG. 6.21.1_FREE STEAM MACH NUMBER FOR $\alpha_{eq.} > 99\%$ Vs PRESSURE FOR ARGON

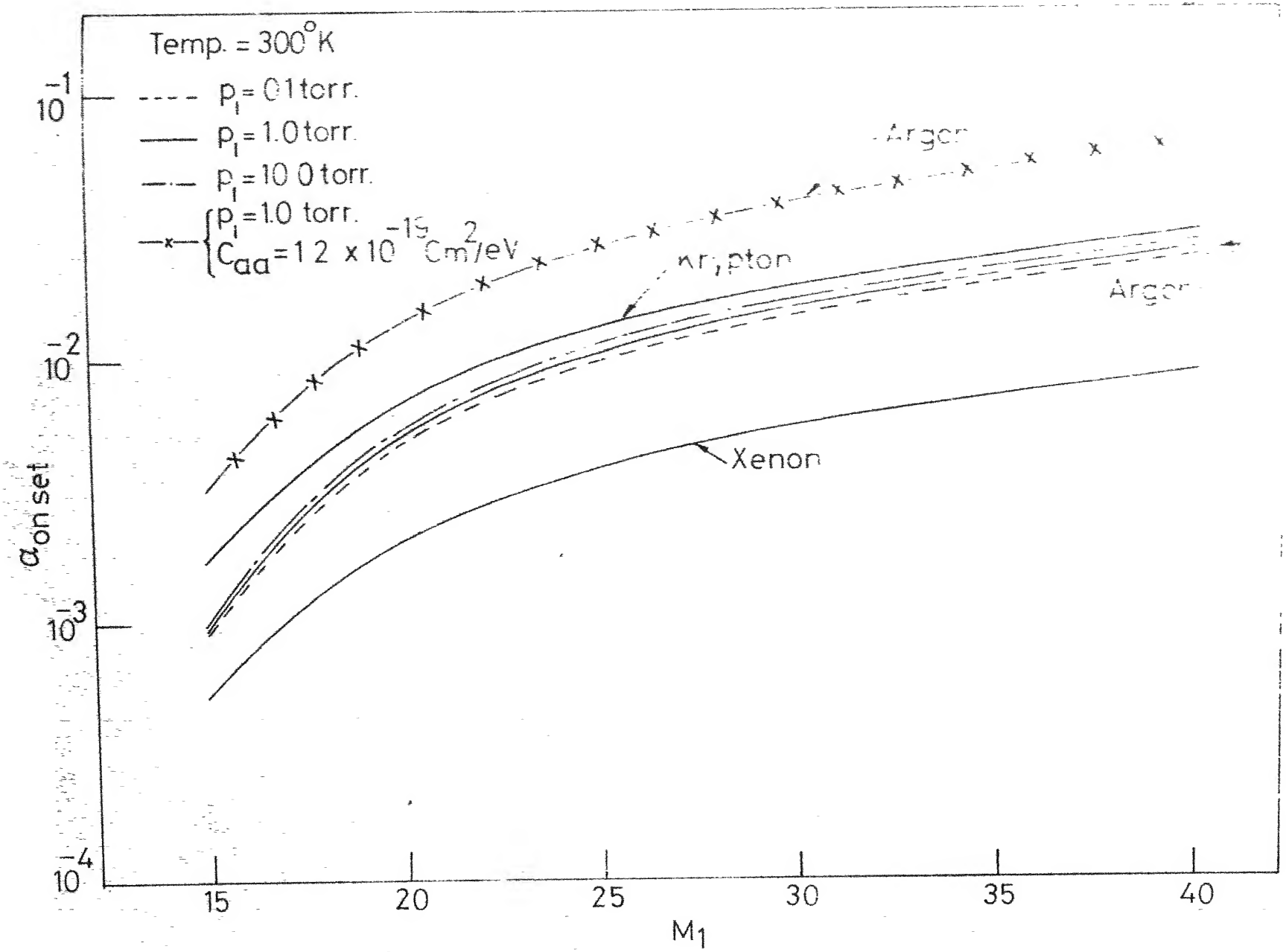

FIG.6.22.1_ONSET DEGREE OF IONIZATION Vs MACH NUMBER

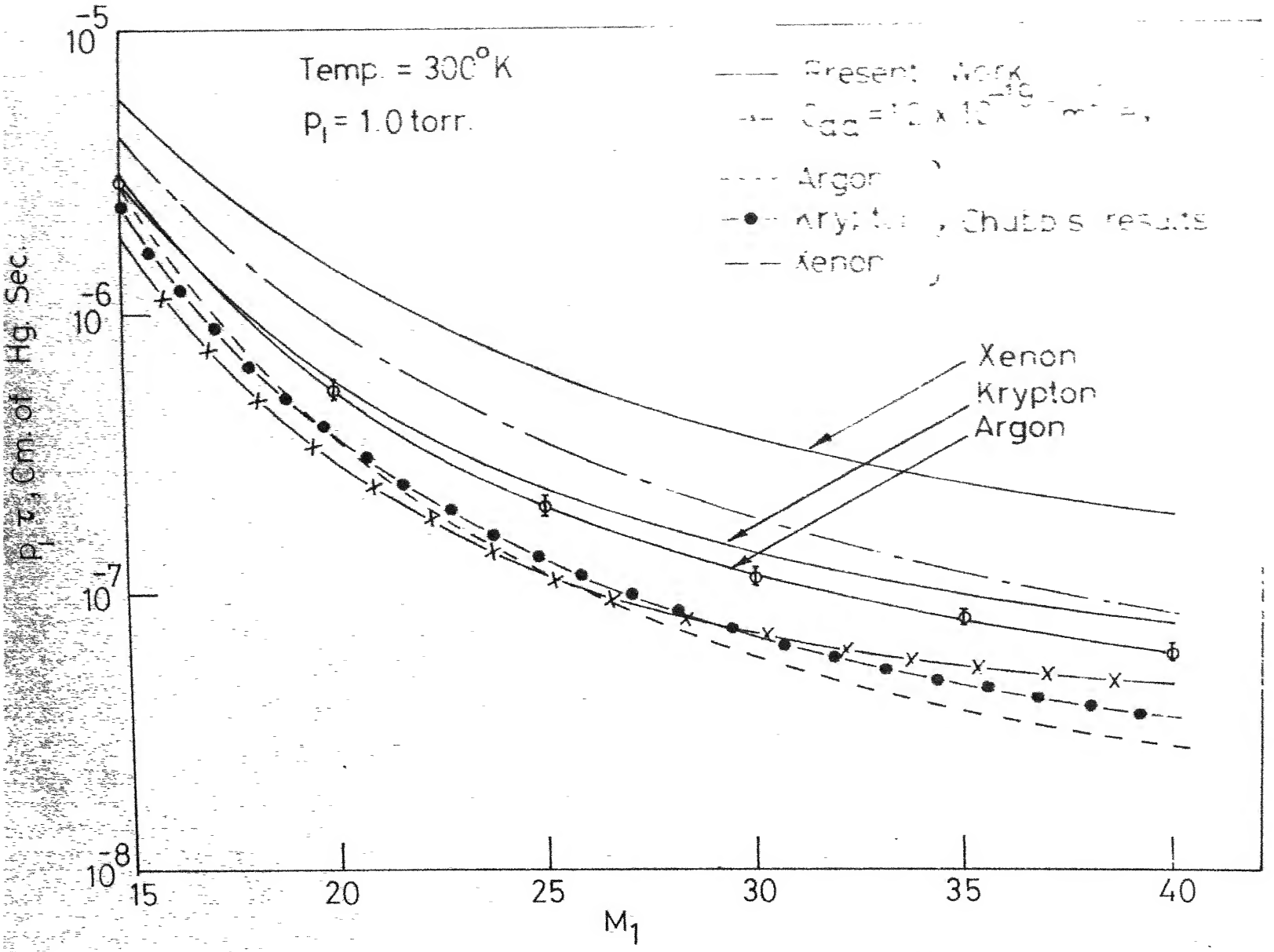

FIG. 6.23.1 _ THICKNESS PARAMETER Vs MACH NUMBER

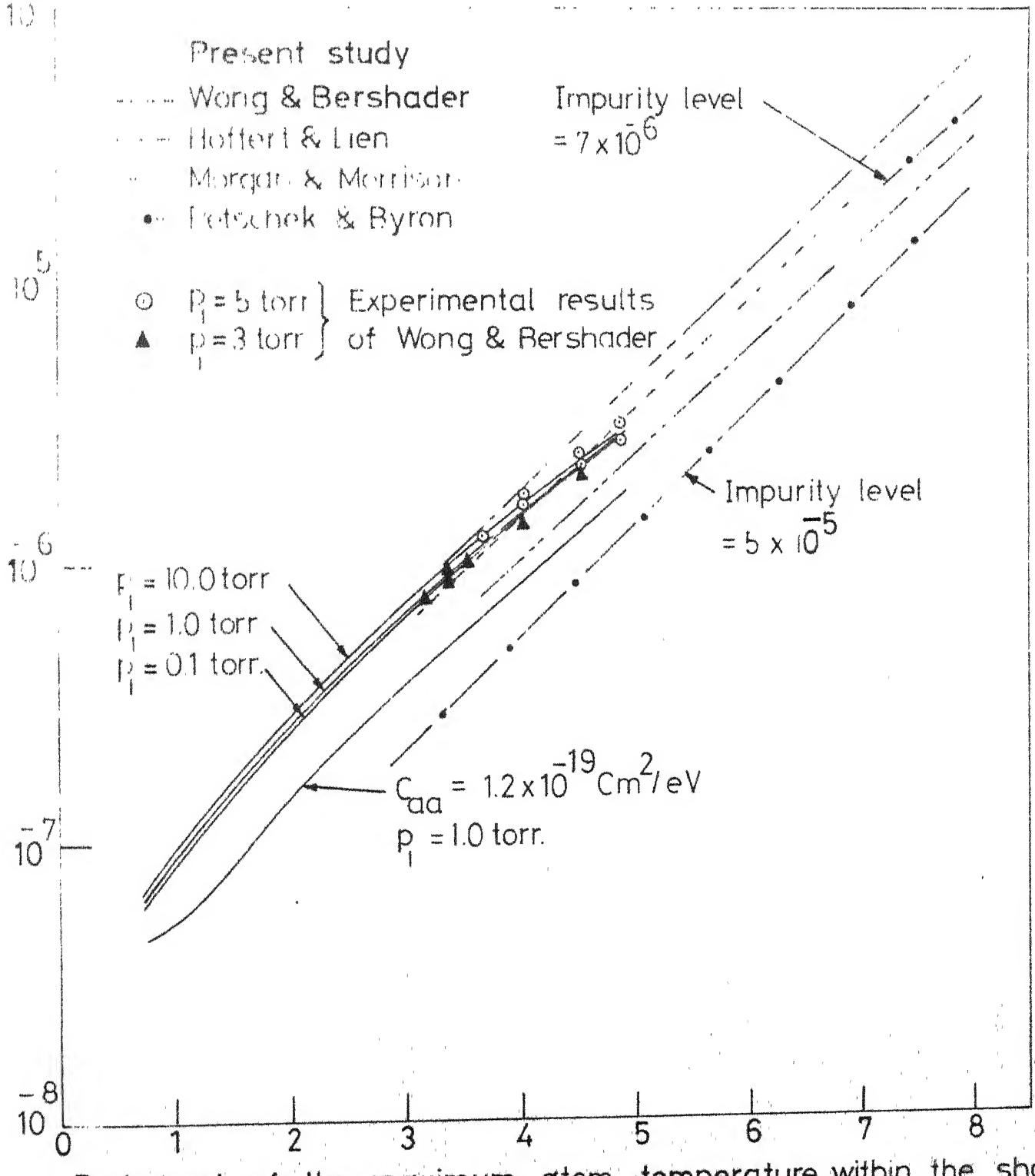

FIG. 6.24.1 – COMPARISON OF SHOCK THICKNESS PARAMETER FOR ARGON.